Physicochemical characterization of the interfacial behaviour of Janus nanoparticles

Miguel Ángel Fernández Rodríguez

Universidad de Granada

Diciembre 2015

Directores:
Dr. Roque Hidalgo Álvarez
Dr. Miguel Ángel Rodríguez Valverde
Grupo de Física de Fluidos y Biocoloides
Departamento de Física Aplicada

Programa de Doctorado en Física y Ciencias del Espacio

Editorial: Universidad de Granada. Tesis Doctorales
Autor: Miguel Angel Fernández Rodríguez
ISBN: 978-84-9125-376-1
URI: http://digibug.ugr.es/handle/10481/41244

Intellectual Property Rights

El doctorando, Miguel Ángel Fernández Rodríguez, y los directores de la tesis, Roque Hidalgo Álvarez, catedrático de universidad, y Miguel Ángel Rodríguez Valverde, profesor titular de universidad,

Garantizamos al firmar esta tesis doctoral, *Physicochemical characterization of the interfacial behaviour of Janus nanoparticles*, que el trabajo ha sido realizado por el doctorando bajo la dirección de los directores de la tesis. Y hasta donde nuestro conocimiento alcanza, en la realización del trabajo se han respetado los derechos de otros autores a ser citados, cuando se han utilizado sus resultados o publicaciones, así como que el doctorando ha disfrutado de una estancia en el extranjero, durante un periodo de tres meses, en el *Laboratory for Interfaces, Soft matter and Assembly* del *ETH-Zurich* (Suiza).

Granada, 22 de octubre de 2015.

Directores de la tesis | Doctorando

Fdo: Roque Hidalgo Álvarez | Fdo: Miguel Ángel Fernández Rodríguez

Fdo: Miguel Ángel Rodríguez Valverde

The pictures of third parties used in the front page are all under Creative Commons' licenses. They are hosted in Wikimedia Commons and Flickr.

A Leo, mi sol y mi estrella.

Defiende tu derecho a pensar, porque incluso pensar de manera errónea es mejor que no pensar.

Hipatia de Alejandría

Acknowledgements

Al finalizar la tesis, una de las tareas que uno se marca es escribir unos agradecimientos. Y es que al final de este camino tan fructífero, y en el que me lo he pasado francamente genial, no puedo dejar de pensar en todas aquellas personas que de alguna u otra manera me han hecho llegar a donde estoy ahora mismo.

Quiero mostrar mi profundo agradecimiento **a mis directores de tesis** oficiales, Roque Hidalgo Álvarez, del que tengo cierta envidia por no ser tan eterno aprendiz como él; y Miguel Ángel Rodríguez Valverde, que me ha mostrado con su incansable labor que después de trabajar y más trabajar lo que hay que hacer es seguir trabajando; y no oficiales, Miguel Ángel Cabrerizo Vílchez, que ha compartido conmigo su gran pasión por la divulgación de la Física Recreativa y la Física en general. Todos ellos han permitido que viernes a viernes avancemos en el trabajo que culmina en este texto. Con ellos me he sentido muy a gusto profesionalmente, pues han dejado que me expandiera como investigador con pensamiento independiente a la vez que han sabido encauzarme cuando la independencia iba a convertirse en catástrofe. A todos ellos les debo el éxito que considero que es este texto de por sí y lo satisfecho profesionalmente que me siento.

El grupo de Física de Fluidos y Biocoloides me ha enseñado, seminario a seminario y entre pasillos lo que es estar unidos en un gran departamento como es el de Física Aplicada, mención especial quiero hacer de los administrativos Miguel Heredia, Conrado y Belén que tantas y tantas papeletas burocráticas me han solucionado. Somos muchos, así que aquí os dejo mi gratitud hacia todos vosotros que en mayor o menor medida habéis contribuido a que este trabajo sea posible.

During my research stay at the Laboratory for Interfaces, Soft Matter and Self-Assembly at the ETH-Zurich, under supervision of Prof. Lucio Isa, I could experience a really nice working place in which I really felt like being back in Granada with my friends: Prof. Nick Spencer offered me all their facilities, equipment and fruitful advice; I really enjoyed Prof. Lucio Isa's supervision in which we could obtain really nice self-assembled patterns that are pretty awesome. Addrienne, Josephine, Shiva, Ella, Mohammad, Christian, Chengjun, Manjesh, Fabiana, Zita, Rebecca, Songbo and Ivo made the coffe breaks, the lab parties and in general

my living and working at the ETH-Zurich really nice. It was really amazing to see what it can be done when a government wants to invest in public research. I am really grateful with Prof. Lucio Isa because he invested a lot of time with my research stay and especially during the FreSCa measurements that were really marathons in which he worked a lot while I looked with wonder to his difficult but fruitful technique.

Quiero enmendar un error que me ha acompañado desde que me licencié en Física: en el discurso fin de carrera dije que mis padres me habían desaconsejado hacer Física y esto les dolió. Nada más lejos de la realidad, si estoy donde estoy es primero y principalmente por mis padres: mi madre, Blanca, que me enseñó desde que era un monicaco a estudiar y perseguir mis sueños (siempre recordaré las arrugas de tus codos de tanto estudiar por las noches) y mi padre, Pepe, que me inculcó el amor por la Ciencia y a apreciar los trabajos bien hechos (y por cierto, una máxima que me ha venido de perlas en todos estos años: *uno hace lo que uno buenamente puede*), mucha culpa tiene él de mi carácter y mis aficiones porque con él estuve asistiendo al instituto hasta que entré en la carrera. El siguiente en la lista de los culpables de que esté aquí es mi hermano Jose David, al que desde pequeño me pegaba como una lapa para escuchar sus cuentos de ciencia ficción y compartir su pasión por los ordenadores. Cuentan mis padres que si me razonaban algo siempre pedía el visto bueno de mi hermano antes de tomarlo por cierto. Elisa siempre me hace reír con sus dichos y hechos y junto a Jose David han traído a Isabel y a Jose para goce y disfrute de unos titos enamorados de sus sobrinos. Mi abuela “MamaCarmen” me enseñó la responsabilidad de las generaciones anteriores hacia las futuras, el sentido del avance social y del trabajo duro en pos de lo mejor para la familia. Mi abuelo “abuelito” me enseñó que no hay edad para aprender y que entender el pasado te hace entender el presente. Mi abuela “Tata” me rindió su cariño incondicional y me enseñó que casi todas las situaciones de la vida están contenidas en el refranero español, a través de ella pude conocer al que fuera mi díscolo y cariñoso abuelo. Mi tita MariCarmen y Antonio y mis primas me enseñaron que merece la pena convivir si el resultado es el cariño y el apego de la familia. Y mi tía Carmele me sirvió de referente intelectual y de las responsabilidades. Leonor, Serafín, Andrés y Ana se unieron después y me han enseñado lo mucho que se puede querer a alguien y lo tan en familia que se puede llegar a sentir uno cuando los que te rodean son puro amor y cariño. No puedo imaginar una familia “adoptiva” mejor que la que gozo y disfruto día a día. Sería imposible enumerar a todos los miembros de mi familia que me han influido de una u otra manera, como mis tíos Jose Miguel, Daniel y Ana o mis

primos más viejos y más nuevos, eso sin contar la innumerable familia que por parte y parte habita en los pueblos de Málaga y hasta en Inglaterra. Sirvan estas líneas para deciros que de volver a nacer y tener la oportunidad de escoger, os escogería a todos vosotros sin dudarlo.

Durante la carrera conocí a Leo y un 27 de abril me decidí a decirle cuánto me gustaba. Desde entonces estamos juntos, muy juntos y sin ganas de separarnos lo más mínimo. Es la persona con la que quiero estar hasta el fin de mis días. Su tenacidad, su cariño hasta niveles insospechados y su habilidad para hacer que todo sea más gustoso cuando estoy junto a ella es lo que me hace sentir mejor persona a su lado. Ella ha compartido penas y alegrías entorno a nuestras respectivas tesis, y ha sido el principal soporte emocional para llevar a buen puerto este trabajo.

Previo a la carrera y desde hace muchos años me acompaña una amistad perenne y muy preciada con Águeda, que siempre está ahí aunque yo me ausente. La carrera también me brindó una suerte de compañeros de los que guardaré para siempre, no en mi corazón, que también, sino para el día a día, esté donde esté. La lista también es interminable pero me atreveré a enumerar a algunos: Eme, quien me acompañó desde el minuto cero y que me ha enseñado a amar a los amigos como se ama a la familia; Miki, que quiso apoyarme en todo y darme los zascas necesarios para espabilar en la carrera; Jordi, que me enseñó a disfrutar de lo más grande y lo más pequeño dentro y fuera de la carrera; Juanpe, que me mostró que con pasión y vitalidad puedes llegar donde quieras; Fernando, que me enseñó como se ríe uno de verdad cuando está en buena compañía; Lourdes, con su encantador acento cordobés se nos fugó a Matemáticas; Germán (el viejo), que consiguió hacer reír al "tito Migue" siempre que tuvo ocasión; Laurita, que me soportó mucho tiempo y aun así no dejó de tratarme con cariño; Rafa, que me enseñó lo guapo y listo que hay que ser para cambiar a un heterosexual de gustos; Esperanza, que me enseñó que incluso en los gritos supersónicos hay amistad y buen rollo; Javibi, que compartió tantos momentos fisicoguitarriles conmigo; Brayan, mare mía lo que tienes ahí; Javi, que me hizo desear su intelecto y su cuerpo a partes iguales; MariCarmen, que me enseñó las risas que se puede echar uno a costa de la fauna universitaria; Alice y Ben, el dúo que no sé entender el uno sin el otro, italiano e inglés, pero de otro planeta y su secuaz Sebastiano; Germán nuevo, que aun con todo en su contra (su pachorra o sus ¿eh?) me hizo quererlo hasta límites insospechados; Álvaro, que nunca me hizo cascarón de huevo pero que compartió aficiones, secretos y por supuesto todas los madrugones de gimnasio (¡gracias!); Irene, que aunque se ponga pesada para que le escriba más lo único que va a conseguir es que le diga que su ritmo frenético y sus cariños y guiños son una delicia; Evil V, haciendo honor a su nombre; Paloma (a.k.a Pabloma), que derribó tantos estereotipos y me enseñó que la guerra de los sexos puede ser la guerra del sexo, o no; Jose Alberto, que me descubrió los placeres de discutir y luchar por lo que es mío; Jose Antonio, que me alegró con cada "va por ustedes";

Nico, que me cae muy bien por lo jodidamente majo que es; Adrián, que me hizo reír tanto con sus gifs y del que todavía espero un monólogo. Isi, PacoCordobés, María y toda la trupe de Priego, Almedinilla y Carcabuey (eh, Jony, eh, Davi, eh JoseAlberto, eh, Jospi, eh Juan'amón), ... Todos vosotros conformáis una gran familia que sé que no perderé aunque me aleje. Habéis hecho de mi periodo en la Universidad desde el primer día el más divertido y bonito de mi vida.

Durante el doctorado he conocido a gente muy variopinta, durante el Máster y sobre todo en la sala Π^f y anexos: los que tengo más manoseados son a Juan Pablo, el eterno fiestuqui; Azahara, qué ricos pasteles; Paola, diosa del cuero; Carmen, Felipe y Jesús Felipe, que me enseñaron el tesón con el que se trabaja cuando te guía el amor a tu familia; Diego, el papito bailongo; Marco, el insaciable en todo; Yadira, la abnegada AFM-ista; y las recientes incorporaciones: Inma, Keshvad, Elisa y Martín, que espero que se lo pasen tan bien como yo me lo he pasado estos años. También los más antiguos tienen aquí su lugar: Amelia, Efrén, Miguel Peláez, Miguel Wulff, César y Pablo, que veía como "viejos" y ahora resulta que el viejo soy yo. Este último, Pablo, fue quien me introdujo en la dimensión reivindicativa de la investigación y que desembocó en ser durante año y medio portavoz (coco-medios) de la FJI/Precarios y ser el actual presidente de ASI-Granada (más bien de lo que queda de ella). En esta dimensión pude rozarme con gente que me contagió sus ganas de hacer de esta profesión algo muy digno: Ester (sin hache), que compartió penurias de coco-medios; Javi, que muestra una increíble fuerza; Esther (con hache), que me metió en el buen rollo de la asociación; Juan, que sacó al inconformista que llevo dentro; Noe, que me inspiró en todo lo relativo a FJI/Precarios y Jose Manuel, que me sigue maravillando con su trabajo y compromiso diario; Ana Canda, los dos Xavis, las dos Elenas, Jose Manuel Félix, y tantos y tantos otros que siguen peleando en esta ardua tarea. Deseo lo mejor para las nuevas incorporaciones en ASI-Granada que son Verónica y Virginia.

Muchos de los que me conocen saben que mi memoria tiene fecha de caducidad y que más allá de dos o tres años solo recuerdo los acontecimientos y las personas por fotos e historias. Aunque esto no exime de quien pueda haber olvidado en estos agradecimientos, qué queréis que os diga, lo he intentado y mi corazón está con vosotros aunque sea en el pasado.

Katharine Burr Blodgett (1898-1979), demonstrating the Langmuir-Blodgett equipment in lab. Picture from the Smithsonian Institution from United States of America (Wikimedia Commons).

Contents

Consider again that dot. That's here. That's home. That's us. On it everyone you love, everyone you know, everyone you ever heard of, every human being who ever was, lived out their lives. The aggregate of our joy and suffering, thousands of confident religions, ideologies, and economic doctrines, [...] - on a mote of dust suspended in a sunbeam.

Carl Sagan

Abstract

Janus nanoparticles (JPs) are colloidal entities in which there are two differentiated spatial domains with different physicochemical properties. This anisotropy can lead to the spontaneous self-assembly of nanoparticles when exposed to an external stimulus such as a magnetic or electric field, pH or temperature gradients, etc. In particular, JPs with a wettability contrast between the two spatial domains are able to stabilize Pickering emulsions and provide the benefits from traditional molecular amphiphiles, e.g. the orientation of the hydrophobic and hydrophilic parts towards the oil and water phase in a water/oil interface, and the benefits of Pickering emulsions, e.g. the enhanced stabilization of foams and emulsions stabilized by nanoparticles due to the nanoparticles being in contact with each other and preventing the coalescence or the Ostwald ripening. Nevertheless, the different synthesis routes of JPs are costly and produce really small amounts of nanoparticles at the laboratory scale. Thus, it is important to verify if the JPs are better than the corresponding homogeneous nanoparticles (HPs), much easier to synthesize and already widely applied in the industry as foam and emulsion stabilizers. But the small amounts synthesized does not allow to perform easy tests in which a emulsion is formed with JPs and in this thesis we propose a collection of several techniques to characterize the interfacial activity of such JPs at water/air and water/oil interfaces. In the first chapter of introduction, we compile the state of the art regarding the JPs with interfacial activity through the following publication:

M.A. Fernandez-Rodriguez[†], M.A. Rodriguez-Valverde[†], M.A. Cabrerizo-Vilchez[†] and R. Hidalgo-Alvarez[†,*], **Surface activity of Janus particles adsorbed at fluid-fluid interfaces: Theoretical and experimental aspects**, Advances in Colloid and Interface Science, In Press, 2015, ISSN 0001-8686, DOI: 10.1016/j.cis.2015.06.002.

[†] *Biocolloid and Fluid Physics Group, Applied Physics Department, Faculty of Sciences, University of Granada, 18071 Granada (Spain)*

[*] *rhidalgo@ugr.es*

The interfacial activity characterization is performed by pendant drop tensiometry. With this technique, the interface area is of a few square millimeters and small amounts of sample are required in comparison with other interfacial tension measurements as the Langmuir balance with the Whihelmy plate or the Nouy ring. Moreover, in this work we deposit the nanoparticles from outside at the pendant drop water/air interface using a spreading solvent, requiring even less nanoparticles than if the nanoparticles are in the bulk of the pendant drop and have to reach the interface. When the spreading solvent is an organic solvent, the violent evaporation process also provides a significant amount of energy to the nanoparticles to become attached to the interface in case that there is an energy barrier to the adsorption. Thus, we monitor the surface or interfacial tension over time until the spreading solvent is fully evaporated, keeping the volume of the pendant drop constant. In usual conditions, the final interfacial tension is stable over time and decreases as the number of deposited nanoparticles is increased. After the solvent evaporation, the pendant drop is grown and shrinked several times at the lowest speed to obtain the surface or interfacial pressure against different area per particle of the pendant drop (i.e. different area of the pendant drop with a fixed amount of deposited nanoparticles per experiment). Combining the results of different runs with different amounts of deposited nanoparticles it is possible to build a piecewise-like compression isotherm, analogous to the usual compression isotherms obtained with the Langmuir balance. Moreover, the several growing and shrinking cycles gives extra information about the hysteresis of the process and the reproducibility of the measurements. When possible, we tried to fit the compression isotherms with different models as the hard disk model or the Frumkin model that have a geometric part, similar to the hard disk model, and an interaction part in which the lateral interaction between nanoparticles at interfaces is accounted. Finally, the pendant drop tensiometry experiments are enriched by the possibility to study the interfacial dilatational rheology through periodic variations of the volume of the pendant drop and computing the interfacial dilatational elastic and viscous moduli. The pendant drop technique was validated through the characterization of 2 nm-diameter gold HPs functionalized by hexanethiol and dispersed in tetrahydrofurane (THF), where the piecewise-like compression isotherm was fitted by a simply hard disk model for both water/air and water/decane interfaces:

M.A. Fernandez-Rodriguez[†], Y. Song[‡], M.A. Rodriguez-Valverde[†], S. Chen[‡], M.A. Cabrerizo-Vilchez[†] and R. Hidalgo-Alvarez[†,*], **Interfacial Activity of AuC6 Nanoparticles Using the Pendant Drop Technique**, Journal of Colloid Science and Biotechnology, Volume 3, Number 2, 2014, Pages 184-187, ISSN 2164-9634,

DOI: 10.1166/jcsb.2014.1084.
† *Biocolloid and Fluid Physics Group, Applied Physics Department, Faculty of Sciences, University of Granada, 18071 Granada (Spain)*
‡ *Department of Chemistry and Biochemistry, University of California, 1156 High Street, Santa Cruz, CA 95064 (USA)*
* *rhidalgo@ugr.es*

Several techniques were used to complement the interfacial activity characterization. The size and morphology of the nanoparticles were studied by high resolution TEM, cryo-SEM and dynamic light scattering (DLS) based devices as the Zetasizer Nano Z and the NanoSight (both from Malvern). In the former DLS device it is possible to obtain also the electrophoretic mobility which accounts for the electrostatic charge of the nanoparticles in bulk. All DLS measurements enable to characterize the the colloidal stability of the nanoparticles in bulk. The structured illumination microscopy also enabled to show the true Janus character of one of the studied JPs. Moreover, the interfacial microstructure was characterized by freeze fracture shadow casting cryo-SEM (FreSCa cryo-SEM), a technique developed by Prof. Lucio Isa and the measurements collected in this work where performed during the three months research stay at the Laboratory of Interfaces, Soft matter and Assembly in the ETH-Zurich. With this technique, it was possible to measure in a direct way the contact angle of the nanoparticles at the water/oil interface.

This work is focused on the interfacial activity characterization of JPs. Thus, each chapter in the Result and Discussion part is devoted to a different collection of JPs, synthesized by several international groups and enterprises. Each of these chapters is the result of an international collaboration. The interfacial activity of 3.5 nm-diameter HPs functionalized by hexanethiol and true JPs half functionalized by hexanethiol and half by 2-(2-mercapto-ethoxy)ethanol (MEE) was characterized by pendant drop tensiometry, resulting in a clear improvement of the interfacial activity of JPs compared to HPs for both water/air and water/decane interfaces. Although the hard disk model fitted the HPs piecewise-like compression isotherms, it underestimated the interfacial activity of the JPs. These results are published in:

M.A. Fernandez-Rodriguez[†], Y. Song[‡], M.A. Rodriguez-Valverde[†], S. Chen[‡], M.A. Cabrerizo-Vilchez[†] and R. Hidalgo-Alvarez[†,*], **Comparison of the Interfacial Activity between Homogeneous and Janus Gold Nanoparticles by Pendant Drop Tensiometry**, Langmuir, Volume 30, Issue 7, 2014, Pages 1799-1804, ISSN 0743-7463, DOI: 10.1021/la404194e. Cited by 7.

† *Biocolloid and Fluid Physics Group, Applied Physics Department, Faculty of Sciences, University of Granada, 18071 Granada (Spain)*
‡ *Department of Chemistry and Biochemistry, University of California, 1156 High Street, Santa Cruz, CA 95064 (USA)*
* *rhidalgo@ugr.es*

The interfacial activity and collective behaviour of 100 nm-diameter silver Janus-like nanoparticles functionalized in a one-pot method by 11-mercaptoundecanoic acid and 1-undecanthiol ligands and dispersed in methanol was studied at the water/air interface. The interfacial activity was analogous to that of the molecular amphiphiles but with larger nanoparticles and the piecewise-like compression isotherm was fitted by the Frumkin model in which apart from the hard disk part it is included a term regarding the lateral interactions between nanoparticles at the interface. The interfacial dilatational rheology showed an elastic shell behaviour that point out these nanoparticles as good emulsion stabilizers. These results are published in:

M.A. Fernandez-Rodriguez†, M.A. Rodriguez-Valverde†, M.A. Cabrerizo-Vilchez† and R. Hidalgo-Alvarez†,*, **Surface activity and collective behaviour of colloidally stable Janus-like particles at the air-water interface**, Soft Matter, Volume 10, Issue 19, 2014, Pages 3471-3476, ISSN 1744-683X, DOI: 10.1039/C3SM52624K. Cited by 5.
† *Biocolloid and Fluid Physics Group, Applied Physics Department, Faculty of Sciences, University of Granada, 18071 Granada (Spain)*
* *rhidalgo@ugr.es*

PMMA-HPs (119 nm-diameter) dispersed in water, silica functionalized nanoparticles (silica-FPs) with methacryloxypropyltrimethoxysilane (181 nm-diameter) dispersed in water, and the aforementioned silver JPs (Ag-JPs) were characterized at the water/decane interface. The direct contact angle (CA) was obtained by FreSCa cryo-SEM. Although the CA was similar for both silica-FPs and Ag-JPs, the interfacial activity was much higher for the Ag-JPs, needing 100-times more particle concentration to match the interfacial activity of Ag-JPs with silica-FPs or PMMA-HPs. This points out to the importance of the physicochemical properties of the capping ligands and the Janus structure to design nanoparticles with enhanced interfacial activity. These results are published in:

M.A. Fernandez-Rodriguez†, J. Ramos‡,§, L. Isa‖, M.A. Rodriguez-Valverde†,

M.A. Cabrerizo-Vilchez[†] and R. Hidalgo-Alvarez[†,*], **Interfacial Activity and Contact Angle of Homogeneous, Functionalized, and Janus Nanoparticles at the Water/Decane Interface**, Langmuir, Volume 31, Issue 32, 2015, Pages 8818-8823, ISSN 0743-7463, DOI: 10.1016/acs.langmuir.5b02137.

[†] *Biocolloid and Fluid Physics Group, Applied Physics Department, Faculty of Sciences, University of Granada, Granada, Spain*

[‡] *POLYMAT, Bionanoparticles Group, Applied Chemistry Department, UFI 11/56, Faculty of Chemical Sciences, University of País Vasco UPV/EHU Donostia-San Sebastián, Spain*

[∥] *Laboratory for Interfaces, Soft matter and Assembly, ETH Zürich, Vladimir-Prelog-Weg 5, 8093 Zürich, Switzerland*

[§] *Department of Materials, Department of Bioengineering, and the Institute for Biomedical Engineering, Imperial College London, London SW7 2AZ, United Kingdom*

[*] *rhidalgo@ugr.es*

The importance of the election of the capping ligands was studied by comparing the aforementioned gold JPs half covered by MEE with similar JPs but covered by a shorter and more hydrophilic capping ligand than MEE, the 1,2-mercaptopropanediol (MPD). Apart from the hydrophilic capping ligand, both JPs were dispersed in THF and were similar in fabrication process, hydrophobic capping ligand, wettability contrast, size and charge. Nevertheless, the JPs with MPD were clearly much more interfacial active than the JPs with MEE. These results are published in:

M.A. Fernandez-Rodriguez[a], L. Chen[b], C.P. Deming[b], M.A. Rodriguez-Valverde[a], S. Chen[b], M.A. Cabrerizo-Vilchez[a], and R. Hidalgo-Alvarez[a,*], **A simple strategy to improve the interfacial activity of true Janus gold nanoparticles: a shorter hydrophilic capping ligand**, Soft Matter, Accepted Manuscript, 2015, ISSN 1744-683X, DOI: 10.1039/C5SM01908G.

[a] *Biocolloid and Fluid Physics Group, Applied Physics Department, Faculty of Sciences, University of Granada, Granada, Spain.*

[b] *Department of Chemistry and Biochemistry, University of California, 1156 High Street, Santa Cruz, CA 95064, USA.*

[*] *rhidalgo@ugr.es*

The role of capping ligands and spreading agent on the interfacial activity of gold JPs (of 13 nm and 23 nm-diameter) half functionalized by polystyrene (PS) and half by polyethylene glycol (PEG) was analyzed at water/air and water/decane interfaces. The HPs exhibited no interfacial activity compared to the JPs, pointing out the ability of the later JPs as foam stabilizers. The spreading

agents tested were water, a mixture of water/$CHCl_3$ and the better resulted to be the pure $CHCl_3$. In these conditions, the water/air interface behaved as an elastic shell which pointed out also the ability of these JPs as foam stabilizers. The interfacial activity was near zero when the pendant drops were immersed in decane probably due to an irreversible aggregation of the nanoparticles in decane. This work was carried out thank to the following collaboration:

M.A. Fernandez-Rodriguez[1], A.M. Percebom[2,3,4], J.J. Giner-Casares[3], M.A. Rodriguez-Valverde[1], M.A. Cabrerizo-Vilchez[1], L.M. Liz-Marzán[3] and R. Hidalgo-Alvarez[1,*], **Interfacial activity of gold nanoparticles coated by a polymeric Janus shell and the role of spreading agents**.

[1] *Biocolloid and Fluid Physics Group, Applied Physics Department, Faculty of Sciences, University of Granada, Granada, Spain.*

[2] *Department of Physical Chemistry, Institute of Chemistry, University of Campinas - UNICAMP, P.O. Box 6154, 13084-862 Campinas, SP, Brazil.*

[3] *CIC biomaGUNE, Paseo de Miramón 182, 20009 Donostia-San Sebastián, Spain.*

[4] *Department of Chemistry, Pontifical Catholic University of Rio de Janeiro (PUC-Rio), Rua Marquês de São Vicente 225, Gávea, 22451-900, Rio de Janeiro, RJ, Brazil.*

[*] *rhidalgo@ugr.es*

A completely different route of synthesis, without inorganic core and capping ligands, was explored with polymethylmethacrylate/polytert-butylmethacrylate (PMMA/PtBMA) JPs (in the range of 160-200 nm-diameter) fabricated by Electrohydrodynamic Co-Jetting and dispersed in water. The true Janus character was demonstrated by super-resolution imaging in which the two spatial domains appear separated. Although there was a trend of the JPs being more interfacial active than the HPs, the cationic character of these nanoparticles resulted in easy pollution of the samples and irreproducibility in the measurements. Moreover, the interfacial dilatational rheology of JPs showed an elastic shell behavior that also might point out to the ability of these particles as emulsifiers. This work was carried out thank to the following collaboration:

M.A. Fernandez-Rodriguez[1], S. Rahmani[2,3,6], C.K.J. Yu[2,5], M.A. Rodriguez-Valverde[1], M.A. Cabrerizo-Vilchez[1], C.A. Michel[2,4], J. Lahann[2−6] and R. Hidalgo-Alvarez[1,*]**Synthesis and interfacial activity of PMMA/PtBMA Janus and homogeneous nanoparticles at water/oil interfaces: the difficulties of using cationic nanoparticles**.

[1] *Biocolloid and Fluid Physics Group, Applied Physics Department, Faculty of Sciences, University of Granada, 18071 Granada, Spain.*

[2] *Biointerfaces Institute, University of Michigan, Ann Arbor, MI 48109, USA.*
[3] *Biomedical Engineering, University of Michigan, Ann Arbor, MI 48109, USA.*
[4] *Chemical Engineering, University of Michigan, Ann Arbor, MI 48109, USA.*
[5] *Material Science & Engineering, University of Michigan, Ann Arbor, MI 48109, USA.*
[6] *Institute of Functional Interfaces (IFG), Karlsruhe Institute of Technology (KIT), 76131 Karlsruhe, Germany.*
[*] *rhidalgo@ugr.es*

Finally, we found some issues when we tried to fit the compression isotherms to the model proposed by Aveyard et al. in "Compression and Structure of Monolayers of Charged Latex Particles at Air/Water and Octane/Water Interfaces" (Langmuir 2000; 16(4), 1969-1979). We explain the problems found in the following manuscript:

M.A. Fernandez-Rodriguez[†], M.A. Rodriguez-Valverde[†], M.A. Cabrerizo-Vilchez[†] and R. Hidalgo-Alvarez[†,*], **Comment on the Compression and Structure of Monolayers of Charged Latex Particles at Air/Water and Octane/Water Interfaces**.

[†] *Biocolloid and Fluid Physics Group, Applied Physics Department, Faculty of Sciences, University of Granada, 18071 Granada (Spain)*
[*] *rhidalgo@ugr.es*

After all the results obtained through the different collaborations and works produced in this thesis, we are able to state that in general, JPs present greater interfacial activity than the corresponding HPs. Furhter, The characterization techniques, such as pendant drop tensiometry and FreSCa cryo-SEM are a successful way to explore small samples of JPs.

Considera de nuevo ese punto. Eso es aquí. Eso es nuestra casa. Eso somos nosotros. Todas las personas que has amado, conocido, de las que alguna vez oíste hablar, todos los seres humanos que han existido, han vivido en él. La suma de todas nuestras alegrías y sufrimientos, miles de ideologías, doctrinas económicas y religiones seguras de sí mismas [...] - en una mota de polvo suspendida en un rayo de sol.

Carl Sagan

Resumen

Las nanopartículas Janus (JPs, del inglés Janus nanoparticles) son entidades coloidales con dos dominios espaciales diferenciados con diferentes propiedades fisicoquímicas. Esta anisotropía puede conducir al auto-ensamblaje espontáneo de dichas nanopartículas cuando se exponen a un estímulo externo, como un campo magnético o eléctrico, o ante un gradiente de pH o de temperatura, etc. En particular, las JPs con un contraste de mojabilidad, entre los dos dominios espaciales, son capaces de estabilizar emulsiones de Pickering y proporcionan los beneficios de los anfífilos moleculares tradicionales (esto es, los surfactantes), como por ejemplo la reorientación de la parte hidrófoba e hidrófila hacia las fases aceite y agua, respectívamente, en una interfaz agua/aceite, y los beneficios de las emulsiones de Pickering, como por ejemplo la mayor estabilización de espumas y emulsiones debido a que las nanopartículas entran en contacto entre sí previniendo la coalescencia o la maduración de Ostwald. Sin embargo, las diferentes rutas de síntesis de las JPs son costosas y producen realmente pequeñas cantidades de nanopartículas a escala de laboratorio. Por lo tanto, es importante verificar si las JPs son mejores que las nanopartículas homogéneas correspondientes (HPs, del inglés homogeneous nanoparticles), mucho más fáciles de sintetizar y aplicadas ampliamente en la industria como estabilizadores de espumas y emulsiones. Sin embargo, las pequeñas cantidades sintetizadas no permiten realizar pruebas sencillas en las que se forma una emulsión con JPs. En esta tesis se propone una colección de varias técnicas para caracterizar la actividad interfacial de tales JPs en las interfaces agua/aire y agua/aceite. En el primer capítulo de introducción, compilamos el estado del arte respecto a las JPs con actividad interfacial en la siguiente publicación con título "Actividad superficial de nanopartículas Janus adsorbidas en interfaces fluido-fluido: aspectos teóricos y experimentales":

M.A. Fernandez-Rodriguez[†], M.A. Rodriguez-Valverde[†], M.A. Cabrerizo-Vilchez[†] and R. Hidalgo-Alvarez[†,*], **Surface activity of Janus particles adsorbed at fluid-fluid interfaces: Theoretical and experimental aspects**, Advances in Colloid and Interface Science, In Press, 2015, ISSN 0001-8686, DOI:

10.1016/j.cis.2015.06.002.
† *Biocolloid and Fluid Physics Group, Applied Physics Department, Faculty of Sciences, University of Granada, 18071 Granada (Spain)*
* *rhidalgo@ugr.es*

La caracterización de la actividad interfacial se realiza por tensiometría de gota pendiente. Con esta técnica, el área de la interfase es de unos pocos milímetros cuadrados y se requieren pequeñas cantidades de muestra en comparación con otras mediciones de tensión interfacial como la balanza de Langmuir con la placa de Whihelmy o el anillo de Nouy. Además, en este trabajo depositamos las nanopartículas desde fuera en la interfaz agua/aire de la gota pendiente utilizando un agente de extensión, lo que requiere aún menos nanopartículas para cubrir la interfaz que si las nanopartículas están dispersas en el seno de la gota pendiente y tienen que alcanzar la interfaz. Cuando el agente de extensión es un disolvente orgánico, el proceso de evaporación violento también proporciona una cantidad significativa de energía para que las nanopartículas se adsorban en la interfaz agua/aire, en caso de que exista una barrera de energía a la adsorción. Así, hacemos un seguimiento de la tensión superficial o interfacial a lo largo del tiempo hasta que el agente de extensión se evapora totalmente, manteniendo el volumen de la gota pendiente constante. En condiciones normales, la tensión interfacial final es estable en el tiempo y disminuye a medida que se incrementa el número de nanopartículas depositadas. Después de la evaporación del disolvente, la gota pendiente se somete a ciclos de inyección y extracción de volumen a la velocidad más baja posible para obtener la presión superficial o interfacial versus el área por partícula de la gota pendiente (es decir, áreas diferentes de la gota pendiente para una cantidad fija de nanopartículas depositadas por experimento). Combinando los resultados de diferentes experimentos con diferentes cantidades de nanopartículas depositadas, es posible construir una isoterma de compresión a trozos, de manera análoga a las isotermas de compresión habituales obtenidas con la balanza de Langmuir. Por otra parte, los ciclos de inyección/extracción dan información adicional sobre la histéresis del proceso y la reproducibilidad de las medidas. Cuando ha sido posible, hemos tratamos de ajustar las isotermas de compresión con diferentes modelos como el modelo de disco duro o el modelo de Frumkin que tiene una parte geométrica, similar al modelo de disco duro, y una parte de interacción en el que se tiene en cuenta la interacción lateral entre las nanopartículas adsorbidas en una interfaz. Por último, los experimentos de tensiometría de gota pendiente se enriquecen con la posibilidad de estudiar la reología interfacial dilatacional a través de variaciones periódicas del volumen de la gota pendiente y el cálculo de los módulos interfaciales dilatacionales de elasticidad y viscosidad. La técnica de gota pendiente fue validada a través de la caracterización de HPs de oro de 2 nm de diámetro funcionalizadas con hexanotiol

y dispersadas en tetrahidrofurano (THF), donde la isoterma de compresión a trozos fue ajustada por un modelo de disco duro simple tanto para interfaces agua/aire como agua/decano, en el trabajo titulado "Actividad interfacial de nanopartículas AuC6 usando la técnica de la gota pendiente":

M.A. Fernandez-Rodriguez[†], Y. Song[‡], M.A. Rodriguez-Valverde[†], S. Chen[‡], M.A. Cabrerizo-Vilchez[†] and R. Hidalgo-Alvarez[†,*], **Interfacial Activity of AuC6 Nanoparticles Using the Pendant Drop Technique**, Journal of Colloid Science and Biotechnology, Volume 3, Number 2, 2014, Pages 184-187, ISSN 2164-9634, DOI: 10.1166/jcsb.2014.1084.

[†] *Biocolloid and Fluid Physics Group, Applied Physics Department, Faculty of Sciences, University of Granada, 18071 Granada (Spain)*

[‡] *Department of Chemistry and Biochemistry, University of California, 1156 High Street, Santa Cruz, CA 95064 (USA)*

[*] *rhidalgo@ugr.es*

Se utilizaron varias técnicas para complementar la caracterización de la actividad interfacial de las JPs. El tamaño y la morfología de las nanopartículas fueron estudiados por TEM de alta resolución, crio-SEM y dispersión de luz dinámica (DLS, del inglés dynamic light scattering) mediante dispositivos basados en DLS como el Zetasizer Nano Z y el NanoSight (ambos de Malvern). En el primer dispositivo de DLS es posible obtener también la movilidad electroforética que representa la carga electrostática de las nanopartículas en el seno del agua. Las mediciones DLS de tamaño y movilidad electroforética permiten caracterizar la estabilidad coloidal de las nanopartículas en el seno del agua. La microscopía de iluminación estructurada también permitió demostrar el verdadero carácter Janus de una de las JPs estudiadas. Por otra parte, la microestructura interfacial se caracterizó mediante una técnica consistente en vitrificar la interfaz agua/decano con un chorro de propano muy frío y la posterior fractura de la interfaz, dejando visible las nanopartículas en la interfaz y los huecos que estas dejan en la otra interfaz. Se cubre con una capa de tungsteno formando 30° con la interfaz y las nanopartículas hacen de máscaras, impidiendo el recubrimiento con tungsteno y generando una "sombra". Esta sombra se puede medir en un crio-SEM y así se puede estimar el ángulo de contacto de cada nanopartícula en la interfaz. Esta técnica, Fresca cryo-SEM (del inglés freeze fracture shadow casting cryo-SEM) fue desarrollada por el Profesor Lucio Isa en el Laboratorio de Interfases, de la Materia Blanda y el Ensamblaje en el centro de investigación ETH-Zurich. Las medidas recogidas en este trabajo se realizaron durante la estancia de investigación de tres meses en su laboratorio bajo su supervisión. Con esta novedosa técnica, fue posible medir de forma directa el ángulo de contacto de las nanopartículas en la

interfaz agua/aceite.

En este trabajo nos centramos en la caracterización de la actividad interfacial de distintas JPs. Por lo tanto, cada capítulo de la parte de Resultado y Discusión está dedicado a una colección diferente de JPs, sintetizadas por varios grupos y empresas internacionales. Cada uno de estos capítulos son el resultado de dichas colaboraciones internacionales. El primer sistema estudiado involucrando JPs fue caracterizar la actividad interfacial de HPs de oro de 3.5 nm de diámetro funcionalizadas con hexanotiol y JPs reales funcionalizadas en una mitad con hexanotiol y la otra mitad con 2-(2-mercapto-etoxi)etanol (MEE) mediante tensiometría de gota pendiente. El resultado fue una clara mejora de la actividad interfacial de las JPs en comparación con las HPs, tanto para interfaces agua/aire como agua/decano. Aunque el modelo de disco duro ajustó para las isotermas de compresión a trozos de las HPs, este modelo subestimaba la actividad interfacial de las JPs. Estos resultados están publicados en el trabajo con título "Comparación de la actividad interfacial entre nanopartículas de oro homogéneas y Janus mediante tensiometría de gota pendiente":

M.A. Fernandez-Rodriguez[†], Y. Song[‡], M.A. Rodriguez-Valverde[†], S. Chen[‡], M.A. Cabrerizo-Vilchez[†] and R. Hidalgo-Alvarez[†,*], **Comparison of the Interfacial Activity between Homogeneous and Janus Gold Nanoparticles by Pendant Drop Tensiometry**, Langmuir, Volume 30, Issue 7, 2014, Pages 1799-1804, ISSN 0743-7463, DOI: 10.1021/la404194e. Cited by 7.

[†] *Biocolloid and Fluid Physics Group, Applied Physics Department, Faculty of Sciences, University of Granada, 18071 Granada (Spain)*

[‡] *Department of Chemistry and Biochemistry, University of California, 1156 High Street, Santa Cruz, CA 95064 (USA)*

[*] *rhidalgo@ugr.es*

La actividad interfacial y el comportamiento colectivo de nanopartículas de plata de 100 nm de diámetro al estilo Janus (Janus-like en inglés) fueron estudiadas en la interfaz agua/aire. Se dicen que son Janus-like porque fueron funcionalizadas en un método de un solo recipiente con los ligandos ácido 11-mercaptoundecanoico y 1-undecanotiol y dispersos en metanol y se supuso una separación espontánea de los ligandos en la interfaz. La actividad interfacial medida fue análoga a la de los anfífilos moleculares pero con nanopartículas más grandes y la isoterma de compresión a trozos fue ajustada por el modelo de Frumkin mencionado anteriormente. La reología interfacial dilatacional mostró un comportamiento de "cáscara" elástica de la gota pendiente que señala a estas nanopartículas como buenas estabilizadoras de emulsiones. Estos resultados están

publicados en el trabajo titulado "Actividad superficial y comportamiento colectivo de partículas al estilo Janus coloidalmente estables en la interfaz agua/aire":

M.A. Fernandez-Rodriguez[†], M.A. Rodriguez-Valverde[†], M.A. Cabrerizo-Vilchez[†] and R. Hidalgo-Alvarez[†,*], **Surface activity and collective behaviour of colloidally stable Janus-like particles at the air-water interface**, Soft Matter, Volume 10, Issue 19, 2014, Pages 3471-3476, ISSN 1744-683X, DOI: 10.1039/C3SM52624K. Cited by 5.

[†] *Biocolloid and Fluid Physics Group, Applied Physics Department, Faculty of Sciences, University of Granada, 18071 Granada (Spain)*

[*] *rhidalgo@ugr.es*

HPs de PMMA (de 119 nm de diámetro) dispersas en agua, nanopartículas de sílice funcionalizadas homogéneamente con metacriloxipropiltrimetoxisilano (de 181 nm de diámetro) dispersas en agua, y las JPs de plata antes mencionadas se caracterizaron en la interfaz agua/decano. El ángulo de contacto de las nanopartículas en la interfaz se obtuvo mediante la técnica Fresca cryo-SEM anteriormente mencionada. Aunque el ángulo de contacto fue similar para las partículas de sílice y las JPs de plata, la actividad interfacial fue mucho mayor para la JPs de plata, necesitando 100 veces más concentración de partículas de sílice o de PMMA para alcanzar la actividad interfacial de las JPs de plata. Esto apunta a la importancia de las propiedades fisicoquímicas de los ligandos que forman parte de las nanopartículas y la estructura Janus para diseñar nanopartículas con mayor actividad interfacial. Estos resultados están publicados en el trabajo titulado "Actividad interfacial y ángulo de contacto de nanopartículas homogéneas, funcionalizadas y Janus en la interfaz agua/decano":

M.A. Fernandez-Rodriguez[†], J. Ramos[‡,§], L. Isa[‖], M.A. Rodriguez-Valverde[†], M.A. Cabrerizo-Vilchez[†] and R. Hidalgo-Alvarez[†,*], **Interfacial Activity and Contact Angle of Homogeneous, Functionalized, and Janus Nanoparticles at the Water/Decane Interface**, Langmuir, Volume 31, Issue 32, 2015, Pages 8818-8823, ISSN 0743-7463, DOI: 10.1016/acs.langmuir.5b02137.

[†] *Biocolloid and Fluid Physics Group, Applied Physics Department, Faculty of Sciences, University of Granada, Granada, Spain*

[‡] *POLYMAT, Bionanoparticles Group, Applied Chemistry Department, UFI 11/56, Faculty of Chemical Sciences, University of País Vasco UPV/EHU Donostia-San Sebastián, Spain*

[‖] *Laboratory for Interfaces, Soft matter and Assembly, ETH Zürich, Vladimir-Prelog-Weg 5, 8093 Zürich, Switzerland*

[§] *Department of Materials, Department of Bioengineering, and the Institute for Biomedical*

Engineering, Imperial College London, London SW7 2AZ, United Kingdom
* *rhidalgo@ugr.es*

La importancia de la elección de los ligandos con los que se funcionalizan las nanopartículas se estudió mediante la comparación de las JPs de oro mencionadas anteriormente cubiertas en una mitad por MEE con JPs similares pero funcionalizadas con un ligando más corto y más hidrófilo que el MEE, el 1,2-mercaptopropanediol (MPD). Aparte de la diferencia en el ligando hidrófilo, ambas JPs se dispersaron en THF y fueron similares en proceso de fabricación, ligando hidrófobo, contraste de mojabilidad, tamaño y carga. Sin embargo, las JPs con MPD fueron claramente mucho más activas interfacialmente que las JPs con MEE. Estos resultados están publicados en el trabajo titulado "Una estrategia simple para mejorar la actividad interfacial de nanopartículas Janus de oro reales: un ligando más corto e hidrófilo":

M.A. Fernandez-Rodriguez[a], L. Chen[b], C.P. Deming[b], M.A. Rodriguez-Valverde[a], S. Chen[b], M.A. Cabrerizo-Vilchez[a], and R. Hidalgo-Alvarez[a,*], **A simple strategy to improve the interfacial activity of true Janus gold nanoparticles: a shorter hydrophilic capping ligand**, Soft Matter, Accepted Manuscript, 2015, ISSN 1744-683X, DOI: 10.1039/C5SM01908G.
[a] *Biocolloid and Fluid Physics Group, Applied Physics Department, Faculty of Sciences, University of Granada, Granada, Spain.*
[b] *Department of Chemistry and Biochemistry, University of California, 1156 High Street, Santa Cruz, CA 95064, USA.*
* *rhidalgo@ugr.es*

Analizamos el papel de los ligandos y el agente de extensión en la actividad interfacial de JPs de oro (de 13 nm y 23 nm de diámetro) funcionalizadas en una mitad con poliestireno (PS) y en la otra mitad con polietilenglicol (PEG) en interfaces agua/aire y agua/decano. Las HPs no exhibieron actividad interfacial en comparación con las JPs, señalando la capacidad de estas JPs como estabilizadores de espumas. Los agentes de extensión probados fueron agua, una mezcla de agua/cloroformo ($CHCl_3$) y el mejor resultado fue obtenido cuando fue usado $CHCl_3$ puro como agente de extensión. En estas condiciones, la interfaz agua/aire se comportó como una "cáscara" elástica que pone de manifiesto también la capacidad de estas JPs como estabilizadores de espumas. Por otro lado, la actividad interfacial fue cercana a cero cuando las gotas pendientes se sumergieron en decano probablemente debido a la agregación irreversible de estas en decano. Este trabajo se llevó a cabo gracias a la siguiente colaboración

titulada “Actividad interfacial de nanopartículas de oro cubierta por una corteza polimérica Janus y el rol de los agentes de extensión”:

M.A. Fernandez-Rodriguez[1], A.M. Percebom[2,3,4], J.J. Giner-Casares[3], M.A. Rodriguez-Valverde[1], M.A. Cabrerizo-Vilchez[1], L.M. Liz-Marzán[3] and R. Hidalgo-Alvarez[1,*], **Interfacial activity of gold nanoparticles coated by a polymeric Janus shell and the role of spreading agents**.

[1] *Biocolloid and Fluid Physics Group, Applied Physics Department, Faculty of Sciences, University of Granada, Granada, Spain.*

[2] *Department of Physical Chemistry, Institute of Chemistry, University of Campinas - UNICAMP, P.O. Box 6154, 13084-862 Campinas, SP, Brazil.*

[3] *CIC biomaGUNE, Paseo de Miramón 182, 20009 Donostia-San Sebastián, Spain.*

[4] *Department of Chemistry, Pontifical Catholic University of Rio de Janeiro (PUC-Rio), Rua Marquês de São Vicente 225, Gávea, 22451-900, Rio de Janeiro, RJ, Brazil.*

[*] *rhidalgo@ugr.es*

Una ruta completamente diferente de síntesis sin un núcleo inorgánico y funcionalización con ligandos se exploró con JPs enteramente hechas de polimetilmetacrilato/polytert-metacrilato de butilo (PMMA/PtBMA) (en el intervalo de 160-200 nm de diámetro) fabricadas por co-eyección electrohidrodinámica y dispersas en agua. El verdadero carácter Janus fue demostrado por imágenes de super-resolución en la que los dos dominios espaciales de cada polímero aparecen separados. Aunque hubo una tendencia de las JPs a ser más activas interfacialmente que las HPs, el carácter catiónico de estas nanopartículas dio como resultado que fuesen contaminadas fácilmente y por tanto, hubo irreproducibilidad en las medidas. Por otra parte, la reología interfacial dilatacional de las JPs mostró un comportamiento de “cáscara” elástica que también señala la capacidad de estas partículas como emulsionantes. Este trabajo se llevó a cabo gracias a la siguiente colaboración titulada “Síntesis y actividad interfacial de nanopartículas homogéneas y Janus de PMMA/PtBMA en interfaces agua/aceite: las dificultades de usar nanopartículas catiónicas”:

M.A. Fernandez-Rodriguez[1], S. Rahmani[2,3,6], C.K.J. Yu[2,5], M.A. Rodriguez-Valverde[1], M.A. Cabrerizo-Vilchez[1], C.A. Michel[2,4], J. Lahann[2−6] and R. Hidalgo-Alvarez[1,*]**Synthesis and interfacial activity of PMMA/PtBMA Janus and homogeneous nanoparticles at water/oil interfaces: the difficulties of using cationic nanoparticles**.

[1] *Biocolloid and Fluid Physics Group, Applied Physics Department, Faculty of Sciences, University of Granada, 18071 Granada, Spain.*

[2] *Biointerfaces Institute, University of Michigan, Ann Arbor, MI 48109, USA.*
[3] *Biomedical Engineering, University of Michigan, Ann Arbor, MI 48109, USA.*
[4] *Chemical Engineering, University of Michigan, Ann Arbor, MI 48109, USA.*
[5] *Material Science & Engineering, University of Michigan, Ann Arbor, MI 48109, USA.*
[6] *Institute of Functional Interfaces (IFG), Karlsruhe Institute of Technology (KIT), 76131 Karlsruhe, Germany.*
[*] *rhidalgo@ugr.es*

Por último, encontramos algunos problemas al intentar ajustar de las isotermas de compresión con el modelo publicado por Aveyard y colaboradores en "Compresión y estructura de monocapas de partículas cargadas de látex en interfaces aire/agua y agua/octano" (Langmuir 2000; 16 (4), 1969 a 1979). Exponemos estos problemas en el siguiente trabajo titulado "Comentario sobre el trabajo titulado Compresión y estructura de monocapas de partículas cargadas de látex en interfaces aire/agua y agua/octano"::

M.A. Fernandez-Rodriguez[†], M.A. Rodriguez-Valverde[†], M.A. Cabrerizo-Vilchez[†] and R. Hidalgo-Alvarez[†,*], **Comment on the Compression and Structure of Monolayers of Charged Latex Particles at Air/Water and Octane/Water Interfaces**.
[†] *Biocolloid and Fluid Physics Group, Applied Physics Department, Faculty of Sciences, University of Granada, 18071 Granada (Spain)*
[*] *rhidalgo@ugr.es*

Después de todos los resultados obtenidos a través de las diferentes colaboraciones internacionales y los diferentes trabajos de esta tesis, estamos en condiciones de afirmar que las JPs presentan en general mayor actividad interfacial que las HPs correspondientes. Las técnicas de caracterización utilizadas, como la tensiometría de gota pendiente y FreSCa cryo-SEM son un medio eficaz para caracterizar JPs cuando son tan escasas en su producción a escala de laboratorio.

Introduction

Somewhere, something incredible is waiting to be known.
Carl Sagan

1 Surface activity of Janus particles adsorbed at fluid-fluid interfaces: Theoretical and experimental aspects

Published in Advances in Colloid and Interface Science, In Press, 2015, ISSN 0001-8686, DOI: 10.1016/j.cis.2015.06.002

M.A. Fernandez-Rodriguez[†], M.A. Rodriguez-Valverde[†], M.A. Cabrerizo-Vilchez[†] and R. Hidalgo-Alvarez[†,*]

[†] *Biocolloid and Fluid Physics Group, Applied Physics Department, Faculty of Sciences, University of Granada, 18071 Granada (Spain)*
[*] *rhidalgo@ugr.es*

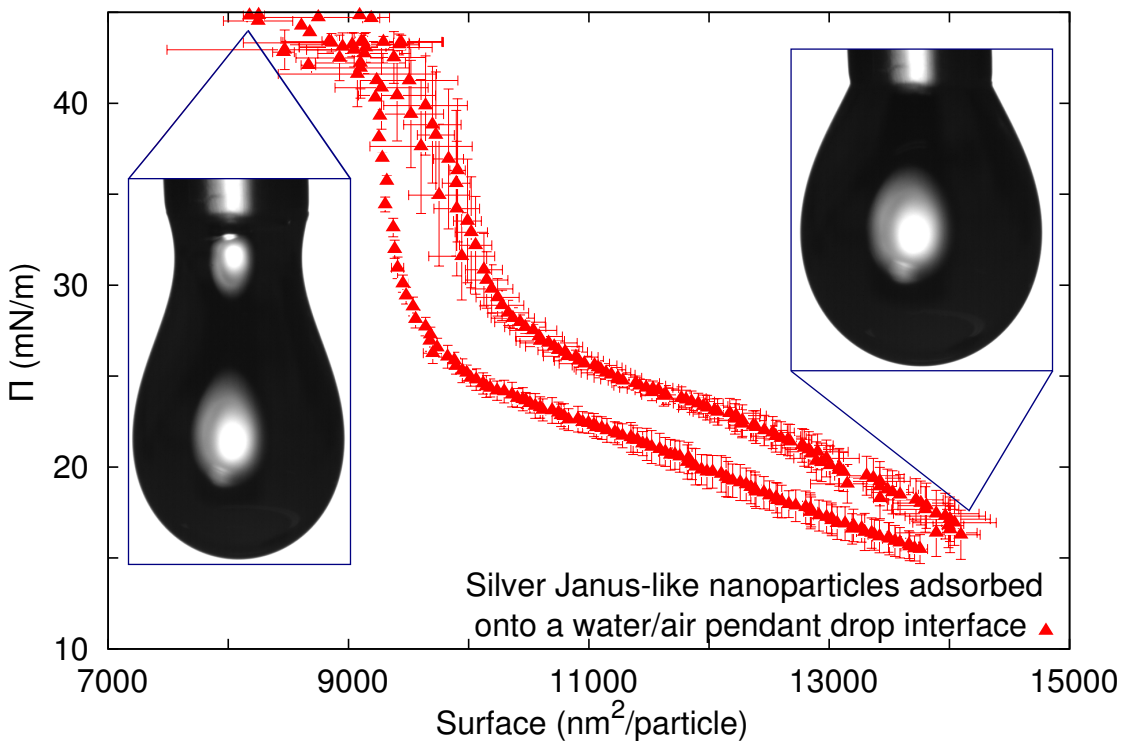

Figure 1.1: Graphical abstract.

Highlights

- Janus particles exhibit surface activity at fluid-fluid interfaces.
- Physical properties of Janus particle-laden interfaces are studied.
- Shape and wettability of Janus particles affect their arrangement at fluid-fluid interfaces.
- Surface activity of Janus particles is explored using pendant drop tensiometry.

Abstract

Since de Gennes coined in 1992 the term Janus particle (JP), there has been a continued effort to develop this field. The purpose of this review is to present the most relevant theoretical and experimental results obtained so far on the surface activity of amphiphilic JPs at fluid interfaces. The surface activity of JPs at fluid-fluid interfaces can be experimentally determined using two different methods: the classical Langmuir balance or the pendant drop tensiometry. The second method

requires much less amount of sample than the first one, but it has also some experimental limitations. In all cases collected here the JPs exhibited a higher surface or interfacial activity than the corresponding homogeneous particles. This reveals the significant advantage of JPs for the stabilization of emulsions and foams.

Keywords: Janus particles; Surface and interfacial activity; Fluid-fluid interfaces; Particle-laden interfaces; Pendant drop tensiometry.

1.1 Introduction

Janus Particles (JPs), named after the double-faced Roman god, are anisotropic colloids with two spatial domains of different physicochemical properties [1]. The contrast between the spatial domains can induce spontaneous self-assembly of the nanoparticles and be responsive to external stimuli such as magnetic or electric fields, pH or temperature gradients [2–4]. Depending on the particular Janus character of the nanoparticles, they cover a wide range of applications such as biosensors, drug-delivery and immunotherapy [5–9], water-repellent textile [10], photonic micro-scale elevator [11] or nanoparticles that become aligned by an external electric or magnetic field [12–19].

In recent years, there is an increasing interest in the design and synthesis of JPs and their self-assembly and physical properties in particle-laden interfaces [20–28]. The JPs are being developed to be used in electronic paper, asymmetrical carriers for catalysis, sensing and drug delivery, nanoscale machinery in the conversion of solar energy into electrical current, colloidal surfactants [29]. More explicitly the JPs laden-interfaces have currently applications as artificial antigen-presenting cells for T-cell activation [30], and in the fabrication of superhydrophobic surfaces formed by micropillars with hydrophobic sidewalls and hydrophilic tops, which are Janus micropillars [10].

One of the most fascinating applications of JPs is the stabilization of multiphasic fluid mixtures such as emulsions and bubbles because these particles are adsorbed to the interfaces more efficiently than their homogeneous counterparts [25, 31–33]. To develop these applications it is mandatory to evaluate properly the colloidal stability in bulk and the interfacial activity of JPs and their interplay. However, there are a few woks devoted to study these properties. Glaser et al. were the first to measure the interfacial activity of JPs (composed of gold and an iron oxide moiety) at liquid-liquid interfaces (water-hexane) by using pendant drop tensiometry [28]. Casagrande et al. [25] performed the first experiments on the behavior of JPs at water-oil interfaces, but they only focussed their experiments on the position of particles at that interface. Most recently, Ruhland et al. [34] have performed the first study on the self-assembly behavior of Janus cylinders at liquid-liquid interfaces using pendant drop technique and microscopic imaging. Kumar et al. [26] have published a review on amphiphilic JPs at fluid interfaces where they survey the recent development in the use of these particles as colloidal surfactants to stabilize multiphasic mixtures such as emulsions. They also discuss on the importance of controlling the shape of JPs, which has a significant impact on their behavior at fluid interfaces. Obviously, the area occupied by the JPs at the interface changes drastically as they aggregate because they lose their original size and shape. Ruhland et al. [34] were

the first in describing an experimental study on the self-assembly of Janus cylinders at liquid interfaces. These authors found significant differences in the structures formed at the interface. More recently, the same authors have studied again the influence of JP shape on their interfacial behavior at liquid-liquid interfaces [35]. More specifically they investigated the self-assembly behavior of JPs with different geometries (spheres, cylinders and discs) trapped at an oil-water interface.

JPs with wettability anisotropy can be used to stabilize Pickering emulsions during longer periods of time and under experimental conditions more stressing (temperature changes or shear effects, for instances) than with homogeneous particles (HPs). Unlike HPs, amphiphilic JPs can exhibit high interfacial activity regardless of the degree of amphiphilicity, due to the spatial separation of the different wettability regions [31]. Thus, amphiphilic Janus-like gold nanoparticles functionalized with thiol-terminated polyethylene glycol chains and short alkane-thiols have been used as water/oil emulsion stabilizers because the authors state that the domains rearrange when the JPs are placed at the interface [36]. However, recently Reguera et al. [37] found that the capping ligands of gold nanoparticles functionalized with 1-octanethiol and 6-mercapto-1-hexanol did not rearrange when placed at a fluid-fluid interface. Moreover, gold JPs half functionalized with polydopamine show that the electrostatic repulsion between nanoparticles determine the resulting particle self-assembly at water/oil interfaces as a result of the hydrophilic polydopamine and hydrophobic gold faces of each particle [38]. In addition, micrometer-sized gold-silica JPs have been found to stabilize water/oil emulsions for longer than one year, compared to 2 h of demulsification when homogeneous silica nanoparticles were used [39]. Importantly, not only the wettability contrast of the JPs rules the interfacial activity, their morphology also controls the interfacial activity at a given water/oil interface, which determines the packing behavior of the JPs [35]. Thereby, nonspherical drops of emulsion have been obtained by using asymmetrical JPs [40].

There are different synthesis strategies involving bulk methods in which the JPs are synthesized in a solvent, usually one-pot method [13, 36, 41]. On the other hand, in other strategies the particles are trapped at a given liquid interface to be functionalized [27, 42], usually resulting in noticeably lower amount of JPs than in bulk methods. It should be noted that the details on the synthesis of JPs are out of focus of the aims of this review. Recently, some reviews on the JP synthesis have been published [24, 25].

Characterization of the surface activity of JPs is of fundamental interest as they represent a completely new class of Pickering surfactants [26]. The surface characterization of colloidal monolayers formed by JPs becomes a difficult task [43, 44]. To explore the surface activity of spherical JPs at fluid interfaces, the following factors are crucial: the colloidal stability of the particles in bulk, the presence of traces of the surface-active reagents used in the particle synthesis and of the spreading agent typically employed to prepare colloidal monolayers. These factors may hinder the effect of the interface area on the surface pressure due exclusively to the presence of JPs. The extremely low colloidal stability of JPs is a serious limitation in their utilization as colloidal surfactants. Park et al. [45] have studied the self-assembly behavior of JPs at fluid interfaces in detail. These authors found that JPs form a fractal-like aggregate structure spontaneously, which means that their interactions are predominantly attractive. The formation of aggregates at fluid interfaces makes unrealizable the study of colloidal monolayers, because these aggregates lead to multi-

layers or unresolved monolayers. Nie et al. [46] found that amphiphilic polymeric JPs assembled into supermicelles. Chen et al. [47] found that JPs with a hydrophobic hemisphere and a negatively charged hemisphere aggregate in supracolloidal objects ranging from spherical clusters to fibrillar triple helices. Furthermore, it has been reported that metallo-dielectric JPs form fibrillar-like shapes under external electric or magnetic fields [12–18]. Yu et al. [48] found similar fibers external field but by preferential wetting of the hemispheres of silica and gold JPs. Shah et al. [49] reported that the fibers formed by metallo-dielectric Janus ellipsoids under AC electric field kept a shape-memory of the state before the external field is applied. From simulations, Beltran-Villegas et al. [50] found that Janus spheres under sedimentation form lamellar structures. Instead, as reported by Luo et al. [51], a stable colloidal monolayer can be formed with electrically charged JPs. Simulations performed by Hong et al. [52] on the assembly of charged Janus spheres showed that the charge asymmetry of a single JP is preserved in the cluster acting as a larger charged JP.

From theoretical calculations, an amphiphilic JP, half hydrophobic and half hydrophilic, can be up to three times more active at the interface than the corresponding HP [31]. In these energetic calculations, the JPs are not aggregated, which is rather difficult to achieve experimentally if the particles exhibit a strong wettability contrast between both hemispheres. One way to avoid the aggregation of the JPs is to functionalize the particle surface with hydrophobic and hydrophilic ligands [27, 43]. The electrical charge of the hydrophilic ligand plays a decisive role in the stabilization of JPs and the hydrocarbon chain of the hydrophobic ligand also introduces a steric effect between particles. A combination of both effects is expected to stabilize metallic particles through an electrosteric mechanism [27, 43]. As reported by Garbin et al. [44], capping ligands play a prominent role in determining both interparticle interactions and the particle-fluid interactions. The simplest model to describe the interfacial arrangement of particles is the hard disk model in which the particles are represented by hard entities placed at the interface. These particles do not interact when there is enough room for every nanoparticle, but they become close-packed when the area per particle is sufficiently low [53]. However, when the particles are functionalized with large polymers, Monte Carlo simulations and experimental data show a complex behavior compared to hard objects at liquid/liquid interfaces [54].

The direct deposition of the nanoparticles dispersed in a spreading solvent at the interface requires lower amount of nanoparticles than adsorption from the bulk. From the growing and shrinking of the pendant drop the interfacial activity of the nanoparticles can be evaluated and compared within a wide range of area per particle. Glaser et al. [28] observed that the self-assembly of JPs at the water-hexane interface resulted in a significant decrease in the interfacial tension. Furthermore, they demonstrated an adequate control over the interfacial activity by tuning the particles' amphiphilicity via ligand exchange reactions. Liu et al. [55] simulated JPs with capping ligands of different length confined in a fluid-fluid interface and stretched the available area. The nanoparticle arrangement exhibited a reversible transition between random and long-ranged configurations that could be effectively controlled by various structural parameters of the Janus morphology and the applied pressure. They revealed that conformational entropy effect of the capping ligands and capping ligand differences dominated the collective nanoparticle organization in the mechanical response.

1.2 Adsorption of Janus particles at fluid-fluid interfaces: theoretical aspects

Janus particles in particle-laden interfaces are being extensively studied due to their promising properties for applications in biotechnology, nanotechnology, electronics, and clean energy [56]. Particles larger than a few nanometers can be permanently attached to interfaces (e.g. water/oil) as the interfacial tension and the contact angle, which can result in large adsorption energy, E_{ads}:

$$E_{ads} = \pi r^2 \gamma_{12} \left(1 \pm \cos\theta_{12}\right)^2 \tag{1.1}$$

where r is the particle radius, γ_{12} is the interfacial tension between the fluids and θ_{12} is the three-phase contact angle. It should be noted that the interfacial tension (γ_{12}) between both fluids strictly exists only when the particle size is small (smaller than $100\,nm$). For larger particle sizes, however, three phases are present and the interfacial tension is not defined. In this case, what is rigorously defined is the change of interfacial Gibbs energy, and it should be referred to as apparent interfacial tension. The sign $\pm$ inside the bracket is negative for removal from the water phase, and positive for removal from the air or oil phase. To get an idea about the order of magnitude of the adsorption energy, we assume a HP of r = 10-8 m adsorbed at the water/toluene interface ($\gamma_{12} = 0.036\,N/m$) with $\theta_{12} = 90°$ and according to Eq. 1.1, E_{ads} is $2750\,k_BT$ [23]. Above or below $90°$, E_{ads} decreases rapidly such that for θ_{12} between $0°$ and $20°$ or between $160°$ and $180°$ this energy is relatively small ($< 10\,k_BT$). One consequence of the very high energy of adsorption of particles with $\theta_{12} = 90°$, relative to the thermal energy, is that these particles once placed at the interface are effectively irreversibly adsorbed. Therefore, we can say that colloidal particles spontaneously adsorbed at the interface between two immiscible fluids to minimize the interfacial area between the two phases. Nevertheless, the shape and wettability of particles have a strong influence on their configuration and interactions at fluid-fluid interfaces. For that reason, we will consider in this review both aspects: particle shape and wettability.

Binks and Fletcher [31] performed a theoretical comparison between the desorption energy of spheres of uniform wettability (HPs) and JPs adsorbed at an oil-water interface as the amphiphilicity is tuned from zero to the maximum value. In comparing the adsorption of HPs and JPs, it is useful to distinguish between surface activity and amphiphilicity. A surface-active particle shows a tendency to adsorb at interfaces, whereas an amphiphilic particle possesses a diblock structure in which the two domains have different affinities for each fluid phase. HPs for which the contact angle at the oil-water interface is around $90°$ are strongly surface active although they are not amphiphilic. Instead, JPs are both surface active and amphiphilic [31]. The amphiphilicity of JPs can be tuned through variation of both the angle α (parameterizing the relative areas of the polar and apolar domains, see Fig. 1.2) and the magnitude of the difference between θ_A and θ_P, the equilibrium contact angles of the two domains of the particle adsorbed at the oil-water interface. Zero amphiphilicity (corresponding to HPs) corresponds to either $\alpha = 0°/180°$ or $(\theta_A - \theta_P) = 0°$. The strongest amphiphilicity is expected when $\alpha = 90°$ and $|\theta_A - \theta_P| = 180°$. The total

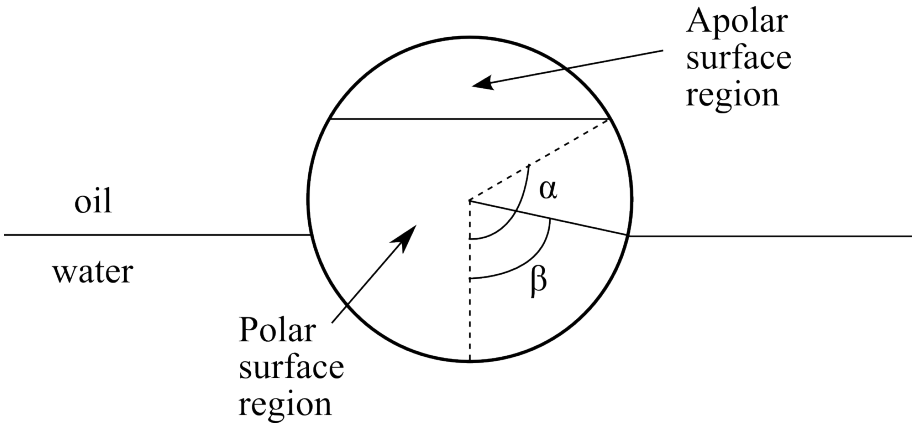

Figure 1.2: Geometry of a Janus particle within an oil-water interface. The relative areas of the polar and apolar particle surface regions are parameterized by the angle α. The immersion depth of the particle in the oil-water interface is parameterized by the angle β. Reprinted with permission from [31]. Copyright (2001) American Chemical Society.

surface free energy E of a JP at an oil-water interface as a function of the angle β (characterizing the immersion depth of the particles, see Fig. 1.2) are given by:
for $\beta \leq \alpha$

$$E(\beta) = 2\pi r^2 \left[\gamma_{AO}(1+\cos\alpha) + \gamma_{PO}(\cos\beta - \cos\alpha) + \gamma_{PW}(1-\cos\beta) - \frac{1}{2}\gamma_{OW}(\sin^2\beta)\right] \tag{1.2}$$

and for $\beta \geq \alpha$

$$E(\beta) = 2\pi r^2 \left[\gamma_{AO}(1+\cos\beta) + \gamma_{AW}(\cos\alpha - \cos\beta) + \gamma_{PW}(1-\cos\alpha) - \frac{1}{2}\gamma_{OW}(\sin^2\beta)\right] \tag{1.3}$$

where r is the particle radius and γ_{AO}, γ_{PO}, γ_{AW}, γ_{PW} and γ_{OW} are the interfacial tensions of the apolar-oil, polar-oil, apolar-water, polar-water, and oil-water interfaces, respectively. Eqs. 1.2 and 1.3 are valid under conditions such that the radius of curvature of the oil-water interface is negligible relative to the particle radius and are applicable to the case in which micrometer-sized liquid drops are coated with nanometer-sized particles. For the case of nanoparticles considered by Binks and Fletcher [31] where their density is not too different to that of the bulk oil and water phases, the oil-water interface shape is not significantly deformed by particle buoyancy effects. It is further assumed that the JPs are oriented with the apolar region all or mostly in the oil phase and the polar region all or mostly in the water. In addition, effects of the line tension associated with the liquid-solid perimeter line around the particle were neglected. The desorption energies for different particle radii and interfacial tension scale as the product $\gamma_{OW} \cdot r^2$.

The contact angles θ_A and θ_P correspond to the equilibrium angles given by the Young's equation as follows:

$$\cos\theta_A = \frac{\gamma_{AW} - \gamma_{AO}}{\gamma_{OW}} \tag{1.4}$$

$$\cos\theta_P = \frac{\gamma_{PW} - \gamma_{PO}}{\gamma_{OW}} \tag{1.5}$$

The average contact angle of the JP is weighted by the relative areas of the polar and apolar domains as follows:

$$\theta_{average} = \frac{\theta_A(1+\cos\alpha) + \theta_P(1-\cos\alpha)}{2} \tag{1.6}$$

The immersion angle β corresponding to the minimum surface energy configuration of the JPs depends on the relative magnitudes of α, θ_A and θ_P. The three possibilities are listed here:

$$\begin{aligned} \text{For } \alpha < \theta_A < \theta_P, \text{ then } \beta = \theta_A \\ \text{For } \theta_A < \alpha < \theta_P, \text{ then } \beta = \alpha \\ \text{For } \theta_A < \theta_P < \alpha, \text{ then } \beta = \theta_P \end{aligned} \tag{1.7}$$

Eqs. 1.2 and 1.3 together with the inequalities in Eq. 1.7 allow the calculation of the minimum surface energy of the adsorbed particle, E_{ads}. The surface energy of the particle located entirely in either the bulk oil (E_{oil}) or water (E_{water}) is given by Eqs. 1.2 and 1.3 with β set to either $0°$ (for the particle in oil) or $180°$ (for the particle in water). The surface activity of the particle was calculated by Binks and Fletcher [31] as the desorption energy, which is defined as the free energy required to desorb the particle from the interface into either the bulk oil or water phase, $(E_{oil} - E_a ds)$ or $(E_{water} - E_a ds)$, whichever is the lowest.

Fig. 1.3 shows the variation of particle desorption energy in units of $k_B T$ per particle for different values of the angle $\Delta\theta$ (defined as $|\theta_A - \theta_P|/2$). For this series, α, r, and γ_{OW} were set to constant values of $90°$, $10\,nm$, and $36\,mN/m^{-1}$, respectively. According to the different selected contact angles, the appropriate combinations of surface energies were obtained by solution of Eqs. 1.4 and 1.5.

For this series at constant α, the particle amphiphilicity is tuned by changing $\Delta\theta$. The case $\Delta\theta = 0°$ corresponds to a HP with zero amphiphilicity, $\Delta\theta = 90°$ corresponds to the maximum possible amphiphilicity in which the polar region of the particle is completely wetted by water and the apolar region is completely wetted by oil.

As can be seen in Fig. 1.3, as increasing the particle amphiphilicity through $\Delta\theta$, the strength of particle adsorption increases up to a maximum of 3-fold for $\theta_{average}$ of $90°$. In addition, the JPs maintain strong adsorption with average contact angles near $0°$ or $180°$, where the surface activity of the HPs is low.

The most important conclusions that may be drawn of the study made by Binks and Fletcher [31] are: first, desorption energies may be increased 3-fold by maximizing the amphiphilicity of JPs; second, unlike HPs, JPs retain their strong adsorption even for average contact angles of $0°$ and $180°$.

In relation to the stability of symmetric JPs (where the two different surface domains are of equal area) at fluid-fluid interfaces, Cheung and Bonn [57] demonstrated using

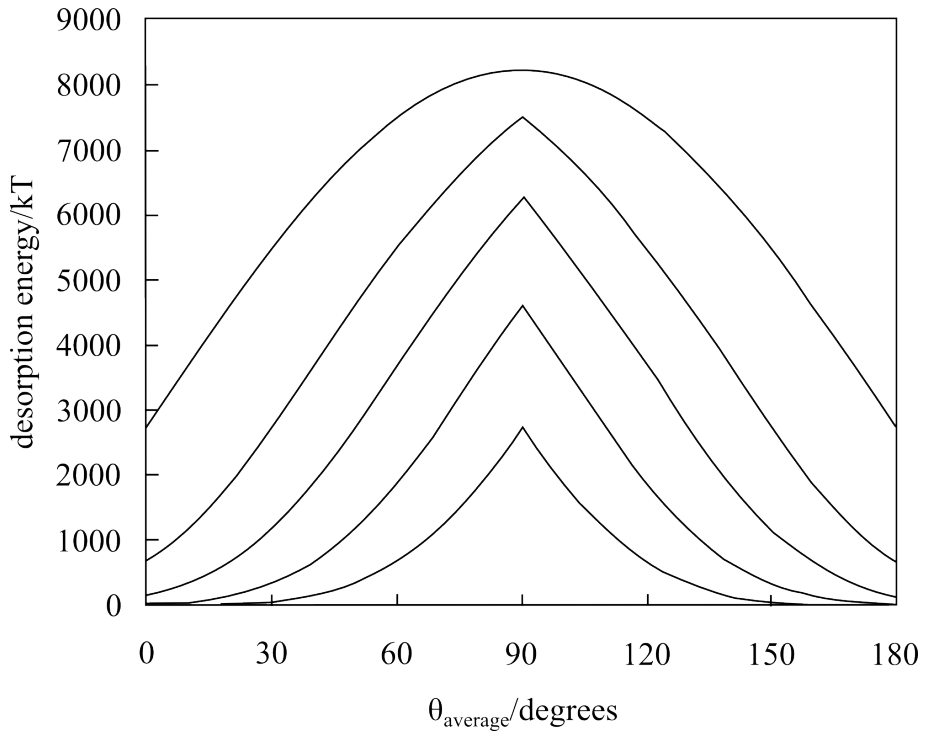

Figure 1.3: Variation of particle desorption energy with area-weighted average contact angle for particles of radius $10\,nm$ and $\alpha = 90°$. The oil-water tension was set to $36\,mN \cdot m^{-1}$. In order of increasing desorption energies, the curves refer to $\Delta\theta = 0°$ (the homogeneous particle case), 20, 40, 60 and $90°$. Reprinted with permission from [31]. Copyright (2001) American Chemical Society.

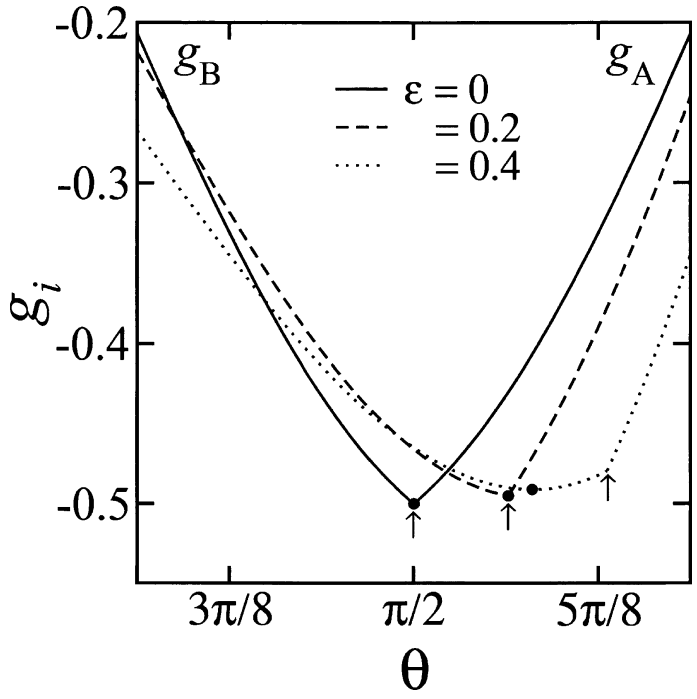

Figure 1.4: The dimensionless adsorption energy g_i as a function of the contact angle θ for $\epsilon = 0$ (solid line), $\epsilon = 0.2$ (dashed line), and $\epsilon = 0.4$ (dotted line). The other parameters are $\alpha = \pi/2$, $\gamma_A = \dfrac{\gamma_{1A} - \gamma_{2A}}{\gamma_{12}} = -0.25$, and $\gamma_B = \dfrac{\gamma_{1B} - \gamma_{2B}}{\gamma_{12}} = 0.25$. The minimum denoted by the filled circle coincides with the anchoring angle (indicated by an arrow) when $\epsilon = 0$ and 0.2, while it is given by Young's equation for $\epsilon = 0.4$. Reprinted with permission from [32]. Copyright [2007], AIP Publishing LLC.

Monte Carlo simulations that the presence of the particle at the interface became more stable as increasing the difference in affinity of the two faces with the respective liquid phase.

Hirose et al. [32] investigated the effect of the interface curvature on the JP adsorption and showed that although the equilibrium contact angle is determined by the classical Young's equation (being independent of the curvature), the adsorption energy is affected by the interfacial curvature. Fig. 1.4 shows the dimensionless adsorption energy ($g_i(\theta, \epsilon)$, in Eq. 1.8 as a function of the contact angle θ and $\epsilon = r/R$ (r and R are the JP and the liquid drop radii, respectively), for a flat interface ($\epsilon = 0$) and two curved interfaces ($\epsilon = 0.2$ and 0.4).

$$g_i(\theta, \epsilon) = \frac{w_i}{2\pi r^2 \gamma_{12}} - \gamma - \tau \cos\alpha - \frac{r(p_1 + p_2)}{3\gamma_{12}} \tag{1.8}$$

If the JP is divided into two parts as an angle α: A (hydrophilic) and B (hydrophobic), w_i ($i = A, B$) is the corresponding interfacial energy, 1 and 2 are the two fluid phases

of the interface, γ_{12} is the interfacial tension between both fluids, $\gamma = \frac{\gamma_{1A} + \gamma_{2B}}{\gamma_{12}}$, $\tau = \frac{\gamma_{1A} - \gamma_{2B}}{\gamma_{12}}$, p_1 and p_2 are the pressures in each fluid.

Recently, the chance of to stabilize thermodynamically Pickering emulsions using JPs has been theoretically addressed by Aveyard [58]. The key-point is how the magnitude of the adsorption free energy of JPs can affect the emulsion formation with negative changes in its free energy. In the lateral interactions between particles adsorbed at drop surfaces the electrical, hydration and van der Waals forces were taken into account. Following a simple approach, Aveyard showed that emulsions stabilized by JPs are thermodynamically stable because the large adsorption energy of these particles can overcome the free energy increase for the formation of a bare oil-water interface. Furthermore, Aveyard found that the long-range electrostatic repulsion can play a prominent role in the stabilization of Pickering emulsions with JPs and the van der Waals attraction appears to be negligible in all cases. A theoretical study performed by Tu et al. [59] confirmed that the Pickering emulsions can be stabilized by using amphiphilic Janus dumbbells, which are nonspherical particles made of two partially fused spherical particles of opposite wettability. To the best of our knowledge, there is not yet experimental evidence of these theoretical predictions.

Recently, there is a growing interest in the study of non-spherical JPs and particularly in ellipsoidal particles with different aspect ratio adsorbed at liquid-liquid interfaces [49, 60–63]. This type of JP has an additional degree of freedom in tuning the particle characteristics, for example, Janus paramagnetic ellipsoids have been shown to exhibit unique response to a rotating magnetic field [64]. Park and Lee [60] theoretically studied the equilibrium orientation of nonspherical JPs adsorbed at an oil-water interface. The equilibrium orientation of a Janus nanoparticle at this interface is the result of two competing driving forces: (1) the minimization of the unfavorable water-oil interactions, which is obtained when the Janus nanoparticle occupies as much interfacial area as possible, and (2) the minimization of Janus nanoparticle-solvent interactions, which is obtained when the polar beads on the Janus nanoparticle interact preferentially with water beads. Two types of particles were considered: Janus ellipsoids and Janus dumbbells. The equilibrium orientation was calculated on the basis of a minimum condition in the adsorption energy as a function of the orientation angle respect to the oil-water interface. In general, it was found that this type of JPs adopts the upright orientation (i.e., the major axis of the ellipsoid or dumbbell is perpendicular to the interface) if the difference in the wettability of the two regions is large or if the particle aspect ratio is close to 1. Otherwise, the nonspherical JPs would tend to have a tilted orientation at equilibrium. Another important conclusion of this theoretical study is that the interaction potential between Janus dumbbells showed only a primary energy minimum indicating that these particles prefer always to be in a single orientation, whereas Janus ellipsoids, under appropriate conditions, can be kinetically trapped in a metastable state due to the presence of a secondary energy minimum. In consequence, as Park and Lee affirm, the orientation of nonspherical JPs likely will have important influence on their ability to stabilize emulsions and modify the rheological properties of fluid interfaces. Whereas Park and Lee [60] found theoretically that in some cases it is possible that an ellipsoidal JP at a liquid-liquid interface adopts two well-defined orientations (one is representative of the equilibrium orientation,

while the second one represents a local minimum in the free-energy landscape), Luu et al. [61] using dissipative particle dynamics simulations found that the ellipsoidal JP has one preferential orientation although they oscillate around it. The same conclusion was reached when the ellipsoidal JPs were assembled at spherical oil-water interfaces [63]. It is possible that the temperature of simulated systems provide sufficient fluctuations that the JPs escape the local minima discussed by Park and Lee [60]. Concerning to interfacial tension, Luu et al. [61] found that the ellipsoidal JPs reduce the decane-water interfacial tension more efficiently than spherical ones, provided that the nanoparticle surface density is high. For a given nanoparticle shape, the interfacial tension reduction becomes more significant as the percent of nonpolar beads on the nanoparticle surface increases. Analysis of simulation results suggested that prolate and oblate nanoparticles are more effective than spherical particles in reducing the interfacial tension because of the larger excluded volume, which increases when the nanoparticle orient their longer axis parallel to the interface. These results are consistent with experimental data obtained by Ruhland et al. [34] with Janus cylinder.

Although in literature there is none comparative study of the self-assembly and rheological behavior between ellipsoidal Janus and homogeneous particles, there are good experimental data with ellipsoidal homogeneous particles [65–67]. However, theoretically we know that in the study of the interactions of ellipsoidal JPs at an oil-water interface unlike homogeneous ellipsoids with quadrupolar deformations, Janus ellipsoids induce a hexapolar interface shape due to the change in meniscus sign by crossing the Janus boundary. The overlapping of such distortions for neighboring particles leads to long-ranged capillary interactions [62].

Gao et al. [68] have also studied using molecular dynamics simulations the influence of shape of JPs on their orientation and interface activity at fluid-fluid interfaces. Three types of JPs were considered: spheres, rods and discs. In the simulations, Gao et al. considered four types of beads: JPs constructed by lumping Lennard-Jones (LJ) beads with different types at one of the two halves of the JP surface. Two "atomic" types of LJ beads modeled the immiscible fluids.

The beads interacted with each other through a shifted-force Lennard-Jones potential. A linear term was added so that the force smoothly went to zero at cut-off distance in Eqs. 1.9 and 1.10.

$$U(rij) = \begin{cases} 4\epsilon \left[\left(\dfrac{\sigma}{r_{ij}} \right)^{12} - \alpha ij \left(\dfrac{\sigma}{r_{ij}} \right)^{6} \right] + \Delta U(r_{ij}) & r_{ij} < r_c \\ 0 & r_{ij} \geq r_c \end{cases} \tag{1.9}$$

and

$$\Delta U = -\left(r_{ij} - r_c\right) \frac{\partial U_{LJ}}{\partial r_{ij}} \left(r_c\right) \tag{1.10}$$

Here, r_{ij} is the distance between two beads, σ is the bead size, ϵ is the interaction potential well depth, and the potential is cut-off at $r_c = 2.5\sigma$. For simplicity, all the beads in the system had the same size σ and mass m. The symmetric coefficient matrix $\alpha_{ij} = \alpha_{ji}$

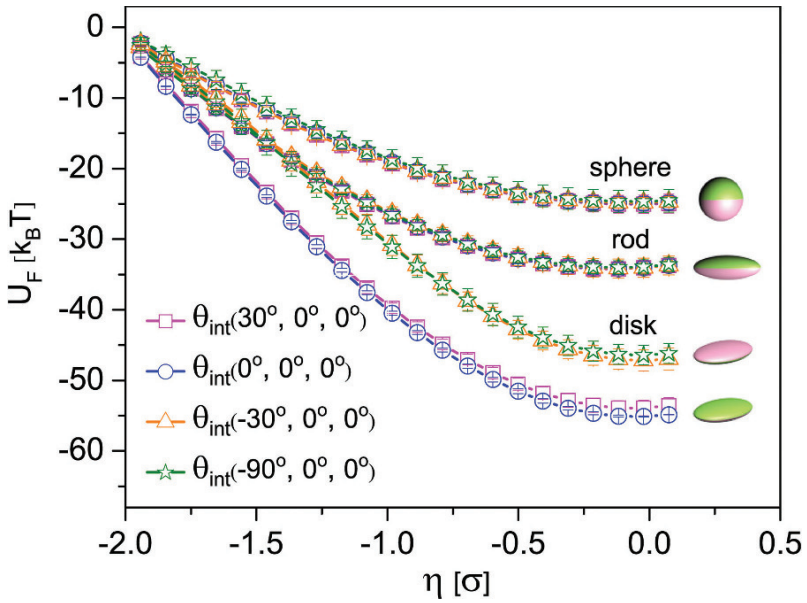

Figure 1.5: Free energy U_F as a function of the particle distance from the interface at different θ_{int} with the parameter $\beta = 0.08$ for Janus spheres, Janus rods, and Janus discs. The schematics of Janus particles show their final orientations at the fluid-fluid interface. The error bars represent one standard deviation from the average. The aspect ratio of Janus particles is 1, 3.3, and 0.3 for Janus sphere, rod, and disk, respectively. Reprinted with permission from [68]. Copyright [2014], AIP Publishing LLC.

($0 \leq \alpha \leq 1$) controls the attraction between beads of different types in the simulations, which in turn determined the wetting properties.

The free energy profiles for the different morphologies Janus spheres, Janus rods and Janus discs transferring from a fluid phase to the interface are shown in Fig. 1.5. In this scheme, θ_{int} corresponds to the initial orientation angle between the JP and the planar interface and $\beta = \alpha_0 - \alpha_1$ ($0 \leq \beta \leq 1$) the index of amphiphilicity, being α_0 and α_1 a measure of the surface wettability of the JP by the two fluids. For Janus spheres and rods, they had a free energy minimum at the interface, irrespective of the initial orientation of the JPs. Therefore, there is one equilibrium orientation for both Janus spheres and Janus rods at the fluid-fluid interface. In comparison, upon contact to the interface, Janus discs with different initial orientation angles follow different pathways ending up in two different final orientations, corresponding to forward orientation and reverse orientation, respectively. The existence of two different orientations of the Janus discs at the fluid-fluid interface indicates that some Janus discs can be kinetically trapped in a metastable orientation, and the initial orientations of Janus discs have a great impact on their final orientation. Apparently, Janus discs are the most efficient to stabilize a fluid interface. But this interface may be metastable depending on the orientation of the Janus discs at the interface.

The fluid-fluid interfacial tension, γ, was calculated from the difference in the diagonal

components of the pressure tensor (a planar interface was assumed in the simulations) averaged over the entire interface as follows:

$$\gamma = \frac{1}{2}\left\langle L_z\left(P_{zz} - \frac{P_{xx}+P_{yy}}{2}\right)\right\rangle \tag{1.11}$$

where L_z is the box length in z direction (i.e., normal to the planar interface), and P_{ii} is the diagonal component of the viral tensor ($i = x$, y or z). Fig. 1.6 shows the time evolution of interfacial tension of fluid-fluid interface by adsorbing, respectively, Janus spheres, Janus rods, and Janus discs with different β at a particle volume fraction of 0.13. The interfacial tension showed a rapid decrease at early stages of adsorption for all types of JPs, which leveled off and reached a stable value. A change in shape of the JPs led to different adsorption behavior at the interface. As can be seen in Fig. 1.6, Janus spheres are not so efficient to decrease the interfacial tension; in contrast Janus rods most efficiently reduced the interfacial tension. Janus discs with smaller values of β showed similar efficiency on interfacial tension reduction, but increasing β will decrease the ability of Janus discs to reduce the interfacial tension. These results clearly demonstrated that anisotropy in the shape of JPs, as earlier indicated by Park and Lee [60], leads to a decisive influence on the surface activity. It should be noted that for Janus spheres and Janus rods the interfacial tension reduction was independent on β, while for Janus discs the interfacial tension reduction became more significant as β decreased. These simulated results of interfacial tension are in a reasonable agreement with the experimental data of interface activity measured by Ruhland et al. [35] with JPs of similar geometries to those used by Gao et al. [68].

1.3 Surface activity and interfacial behavior of Janus particles adsorbed at fluid-fluid interfaces: experimental data

1.3.1 Experimental studies performed using a Langmuir balance

The Langmuir film balance technique is very used to characterize the interfacial activity and arrangement of nanoparticles at water/air and water/oil particle-laden interfaces [27, 43, 69–71].

To the best of our knowledge, Sashuk et al. [43] were the first ones to experimentally study the surface activity of Janus-type nanoparticles at the water/air interface using a Langmuir balance. The aim of this study, however, was to develop a simple method to obtain close-packed and charged colloidal monolayers of well-defined surface charge at the air-water interface, which can be easily transferred onto solid substrates. This method is based on the fact that ligands forming the protecting layer around noble metal nanoparticles exhibit ability to arrange at the nanoparticles surface [72, 73]. Sashuk et al. demonstrated that if the protecting layer is composed of a mixture of hydrophobic

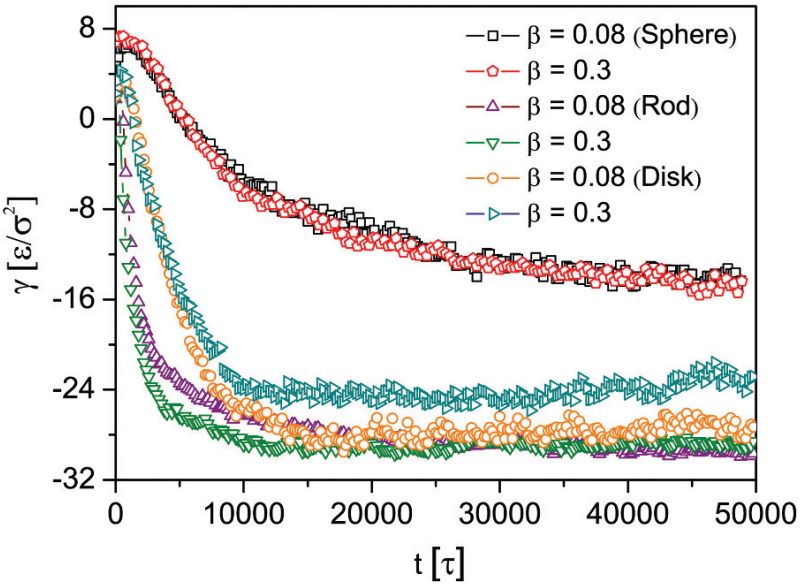

Figure 1.6: Time evolution of interfacial tension γ for Janus particles with different shapes and different β. In these simulations, the aspect ratio of Janus particles is 1, 3.3, and 0.3 for Janus sphere, rod, and disk, respectively. Reprinted with permission from [68]. Copyright [2014], AIP Publishing LLC.

(1-undecanethiol (UDT)) and hydrophilic charged ligands (11-mercaptoundecanoic acid (MUA) and N,N,N-trimethyl (11-mercaptoundecyl) ammonium chloride (TMA), for the negatively silver and positively gold charged nanoparticles, respectively) in appropriate proportions ($10-15\%$ of the hydrophilic ligand), the nanoparticle becomes Janus-like with a contrast of wettability between both hemispheres of the particle. The surface pressure-area ($\Pi - A$, where $\Pi = \gamma_0 - \gamma$, with γ_0 the surface tension without JPs and γ the measured surface tension with JPs) isotherm recorded by Sashuk et al. for the colloidal monolayer composed of positively charged gold containing 10% of TMA in the protecting layer (10 Au +) is shown in Fig. 1.7. As can be seen in this figure, the compression proceeded without any noticeable change in Π down to $\simeq 200\,nm^2$/nanoparticle. Below this point (the gas-liquid transition), a steep rise in the surface pressure was observed. The threshold value of about $200\,nm^2$/nanoparticle corresponds to the average surface-surface distance between the nanoparticles of about $3\,nm$, which can serve as a rough estimate of the Debye screening length in the aqueous phase. The presence of electric charge allowed compressing the colloidal monolayer up to a relatively high surface pressure of about $40\,mN/m$. Further compression resulted in the collapse of the colloidal monolayer. At the collapse point, the area occupied by a single nanoparticle was about $100\,nm^2$, which is very close to the value found for a hexagonally close-packed monolayer, $117.5\,nm^2$/nanoparticle assuming a radius of $5.42\,nm$ per particle.

The hysteresis displayed by the $\Pi - A$ isotherm in Fig. 1.7 was mostly due to migration of a small fraction of 10 Au + nanoparticles into the aqueous phase. From thermodynamics point of view, the existence of hysteresis cycles is always interpreted as an experimental

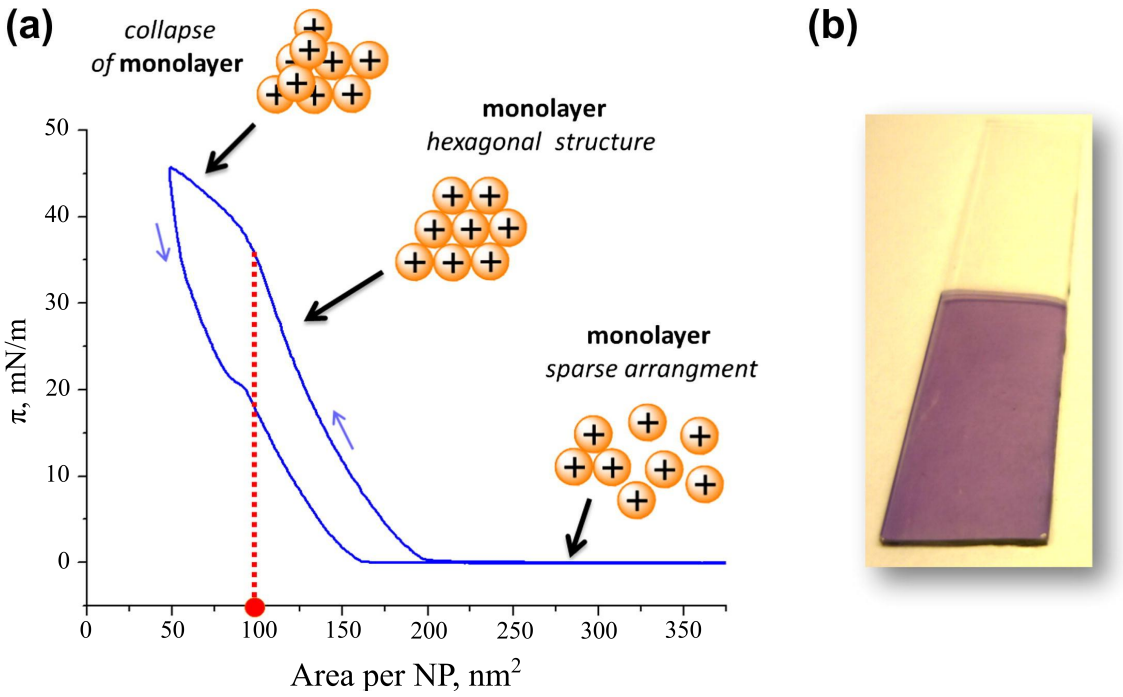

Figure 1.7: The $\Pi - A$ isotherm of a monolayer of 10 Au (+) NPs. The monolayer is compressed at $\sim 100\, nm^2$/NP. This point (marked in red) corresponds to the close-packed hexagonal structure. (b) Photograph of a glass slide covered with 10 Au (+) NPs using the up-stroke deposition method. Reprinted from [43], Copyright (2012), with permission from Elsevier.

evidence of lack of equilibrium.

The contact angles of both hemispheres were $(91.5\pm2)^\circ$ and $(80.5\pm1.5)^\circ$, which proved that the two hemispheres of the nanoparticles presented different hydrophilicity. Also, data obtained with FTIR spectroscopy suggested that the Janus structure was formed during the ligand exchange process but the ligands only rearranged when the nanoparticles were brought at the water/air interface.

Recently, Reguera et al. [37] have presented an experimental approach based on Neutron Reflectivity (NR) that allows in-situ measurements of the contact angles of nanoparticles (NPs) adsorbed at fluid interfaces. They used two sets of gold nanoparticles, one coated by a single ligand, perdeuterated 1-octanethiol (d-OT) and the other one coated by two ligands, perdeuterated 1-octanethiol and 6-mercapto-1-hexanol (d-OT:MHol $1:1$). In the first set of NPs, the experimental value of contact angle was $119.5\pm5.5^\circ$, which was in good agreement with 121° determined from simulation. Concerning to the d-OT:MHol $1:1$ sample of NPs, the value of contact angle was $85\pm10^\circ$, which is much lower than that of d-OT NPs as expected due to the presence of hydrophilic ligands. The most important conclusion of this comprehensive study on the contact angle measurement is that the Janus structure was not present in their NPs because the ligands were uniformly distributed on the gold surface, suggesting that the capping ligands did not rearrange in Janus-like form when the NPs were placed at the interface. This would imply that the one-pot method might be in fact a wrong strategy for synthesis of JPs. Nevertheless, nanoparticles synthesized by one-pot method and that involves the sequential functionalization of the particle surface with thiol-terminated polyethylene glycol (PEG) chains and short alkane-thiol molecules have demonstrated to be highly effective emulsifying agents. This emulsification effect is due to the strong adsorption of this type of particles at oil-water and air-water interfaces, although they must not be considered as JPs [36].

1.3.2 Experimental studies performed using pendant drop tensiometry

Pendant drop tensiometry is an extensively employed method for measuring surface and interfacial tension of liquids [74]. The surface tension of JPs can be measured using pendant drop tensiometry. As Ruhland et al. [34] state, an elegant way of determining the influence of particles at liquid-liquid interfaces is to analyze the interfacial tension of a dispersion of the desired material via the pendant drop method. This technique enables to measure the surface or interfacial tension of colloidal monolayers using a much smaller amount of particles than that the well-established technique of Langmuir balance, where the particles are spread on a fluid subphase from a volatile solvent to form the monolayer [44]. Instead, the colloidal monolayer is formed onto the surface of a pendant drop with a few microliters of solution. This is very important because for the JPs synthesis simple strategies are still being developed for the preparation of large amounts of JPs [24].

A typical set-up is composed of a CMOS camera interfaced with a computer-based data acquisition system, which is used to capture the image of an equilibrium drop [75]. Then edge-detecting software is used to fit the drop shape to the Young-Laplace equation using the Axisymmetric Drop Shape Analysis Profile (ADSA-P) [74]. Real time drop images are

processed at each step of volume variation and the drop area and surface tension are calculated [74]. It is strongly required for the reference system of two fluids that the drop phase and the particle solution are immiscible. An initially relatively high interfacial tension is additionally beneficial to produce a large driving force for the JPs to assemble at the interface. Furthermore, the density of the liquid forming the drop needs to be higher than the surrounding dispersion liquid in order to ensure the development of a hanging drop at the end of the syringe needle. To the best of our knowledge, Kwok et al. [76] were the first in using the axisymmetric drop shape analysis (ADSA) as a film balance. They studied the surface behavior of an octadecanol monolayer.

Although the quantity of nanoparticles required is much lower than that necessary for a standard Langmuir film balance experiment, a certain amount of nanoparticles is still necessary for the experiments that involve the adsorption of JPs at the interface of a pendant drop from the bulk [25, 34, 42, 77]. When the sample amount is insufficient to study the adsorption from the bulk to the interface of the pendant drop, the direct deposition of the nanoparticles onto the drop interface from a volatile solvent allows the study of the interfacial activity. Moreover, solvent evaporation is a violent and rapid process, which helps the nanoparticles to be adsorbed at the interface of the pendant drop, faster than the diffusion from the bulk [44]. This methodology enables to control the amount of nanoparticles deposited at the interface, contrary to the diffusion from bulk experiments in which the control parameter is the initial concentration of particles in the bulk. Nevertheless, neither method presents the possibility to know a priori the exact amount or microstructure of the particles that finally are placed onto the interface.

a) Water/hexane.

Glaser et al. [28] were the first in presenting experiments on the interfacial activity of JPs (gold and an iron oxide moiety) at fluid-fluid interfaces, where the JPs were diffusing from the hexane phase onto the water pendant drop interface. The aim of this study was to provide an experimental confirmation of Binks' theoretical prediction whereby the stabilization of Pickering emulsions should be considerably improved when JPs instead of HPs are used [31]. The JPs were made of an Au and Fe_3O_4 part following the protocol of Yu et al. [78]. The mean diameter of the gold particle was around $4\,nm$ and the diameter of iron oxide was about $10\,nm$, resulting in an overall diameter of about $14\,nm$.

To establish the effect of the Janus character of the particles on their interfacial activity, HPs of both gold and iron oxide of comparable sizes were synthesized as well, 10 and $7\,nm$ in diameter, respectively. Oleic acid and oleylamine were used as ligands for the homogeneous iron oxide nanoparticle as well as the iron oxide part of the JPs. To increase the amphiphilic character of the JPs further, dodecanethiol (DDT) and octadecanethiol (ODT) molecules were attached to the gold part via ligand exchange. The excess thiol and ligands at the iron oxide part were properly removed. This cleaning process is crucial to obtain meaningful values of interfacial tension using pendant drop tensiometry because the desorption of any ligand from the JP greatly can affect to the interfacial tension. For quantitative comparison, the homogeneous gold nanoparticles were also capped with DDT following the same procedure as for the JPs.

The concentration of nanoparticles in solution was about $1.2 \cdot 10^{-4}\,mmol/L$ (i.e., $7 \cdot$

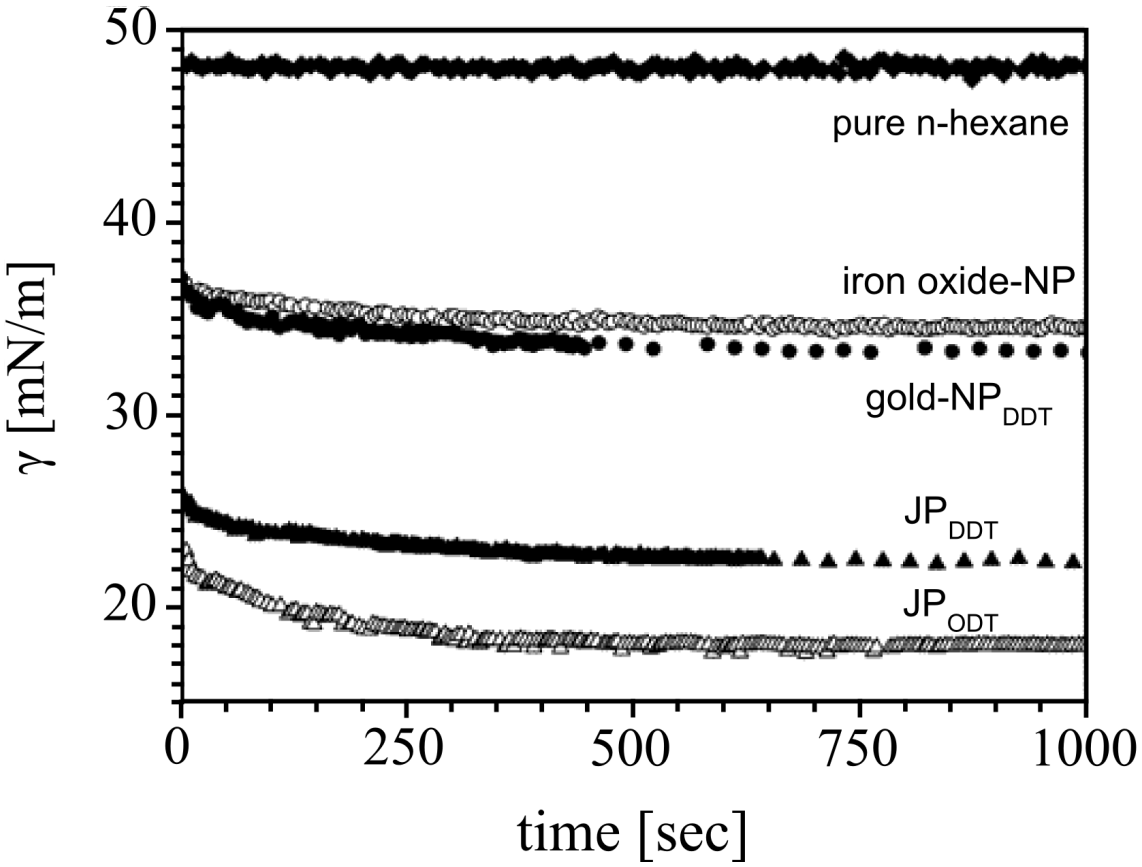

Figure 1.8: Interfacial tension in terms of time. Water was used as the drop phase, and n-hexane was used as the ambient phase in which the nanoparticles were diluted. (NP: homogeneous nanoparticles; JP: Janus particles. The gold moieties were modified using dodecanethiol (DDT) or octadecanethiol (ODT).). Reprinted with permission from [28]. Copyright (2006) American Chemical Society.

10^16 nanoparticles$/L$). As can be seen in Fig. 1.8, as soon as the water drop is formed, the water/n-hexane interfacial tension begins to decrease as the particles adsorb at the interface. For the homogeneous particles, similar values of the interfacial tension were found after $1000\,s$ (Fe_3O_4: $34.5\,mN/m$; Au: $33\,mN/m$). These values were lower than for the water/hexane interface, which was around $48\,mN/m$ in the absence of surface-active agents.

For the JPs modified with DDT (JP_{DDT}) the interfacial tension dropped up to $22.5\,mN/m$. This decrease in the interfacial tension of the JPs in comparison with the HPs confirmed that the JPs are considerably more effective to reduce the interfacial tension as expected and according to the Binks' theoretical prediction [31]. It can be concluded that the JPs orient at the liquid-liquid interface. Because of its nonpolar character, the hydrocarbon ligand-covered gold part should point to the hexane phase, and the polar iron oxide should be (partially) immersed in the water phase (see scheme in Fig. 1.9).

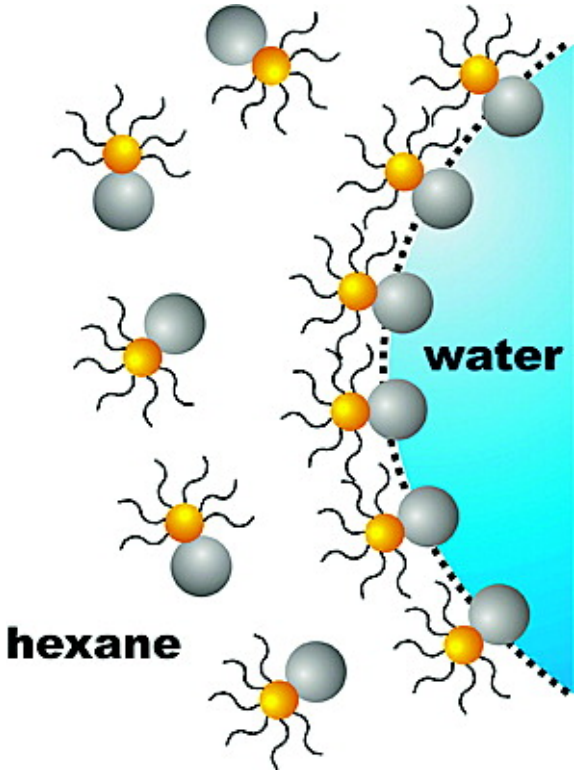

Figure 1.9: Schematic representation of Janus particles at the hexane-water interface (red: gold part; gray: iron oxide part). Reprinted with permission from [28]. Copyright (2006) American Chemical Society. (For interpretation of the references to color in this figure legend, the reader is referred to the web version of this article.)

If ODT ($C_{18}H_{37}SH$) replaces DDT ($C_{12}H_{25}SH$) then the interfacial tension reached a minimum value of $18\,mN/m$. Obviously, the particle concentration of JP_{DDT} in hexane plays an important role in the decreasing of the interfacial tension and the lowest value of the interfacial tension measured was around $12\,mN/m$ at a JP_{DDT} concentration of $3.9 \cdot 10^{-4}\,mmol/L$. This value of concentration is approximately 4 orders of magnitude lower than for typical surfactant, e.g., AOT. This reveals the significant advantages of JPs in the stabilization of emulsions and foam.

b) Perfluorinated oil-dioxane and perfluorinated oil-dimethyl sulfoxide interfaces.

Ruhland et al. [34] were the pioneers in the study of the self-assembly of Janus cylinders at liquid-liquid interfaces. The Janus cylinders were characterized by a phase separation along the major axis into two hemicylinders of different wettability. They used the pendant drop tensiometry and microscopic imaging to characterize the adsorption behavior and self-assembly of Janus cylinders at perfluorinated oil-dioxane and perfluorinated

oil-dimethyl sulfoxide interfaces. The key difference between spherical and anisotropic particles is the number of transitions in interfacial tension that can be encountered during concentration changes.

The synthetic pathway to obtain cylindrical Janus structures was based on a template-assisted synthesis, involving cross-linking of a microphase-segregated lamellar-cylinder morphology of a bulk film of polystyrene-block-polybutadiene-block-poly-(methyl methacrylate) (SBM) block terpolymer, followed by a sonication treatment. This process resulted in the formation of core-crosslinked cylinders, possessing a polybutadiene (PB) core and two hemicylinders of PS and PMMA. The PB cylinder had an average diameter of approximately $23\,nm$ with a surrounding corona, leading to a total diameter of the cross section of $80\,nm$. They chose perfluorooctane (PFO) as the drop phase and dimethyl sulfoxide (DMSO) and dioxane as solvents in order to get sufficiently high interfacial tensions with values of 21.7 (PFO/DMSO) and $10.7\,mN/m$ (PFO/dioxane), respectively.

In a first series of experiments, they assessed the influence of different length of the Janus cylinder on the interfacial tension of liquid-liquid interfaces for the two systems. Fig. 1.10 displays a series of pendant drop tensiometer measurements for cylinders with number of average lengths of 2300, 1600, 800 and $350\,nm$, dissolved in dioxane at a concentration of $1\,g/L$. As can be seen in Fig. 1.10, the interfacial tension decreased with time and approached quasi-equilibrium. At early stages of adsorption, the interfacial tension decreased rapidly. Subsequently, the decrease in interfacial tension slowed down, and finally, it approached a plateau, where the maximum coverage of the interface with cylinders was obtained. After reaching the plateau value, the Janus cylinders were located and arranged at the interface. An increase of the average length of the Janus cylinders led to an enhanced adsorption at the interface, and the plateau was reached earlier. The differences observed in Fig. 1.10c are probably due to the lower viscosity of dioxane ($1.37\,mPa \cdot s$) compared to DMSO ($2.24\,mPa \cdot s$), which affects obviously to the diffusion coefficients and the adsorption kinetics of cylinders onto liquid interfaces.

Presumably, the Janus cylinders are orientated parallel to the liquid-liquid interface and their interfacial assembly is evidently determined by a minimization of the free energy. Hence, the longest Janus cylinders had most influence on the interfacial tension and the highest surface activity (see Fig. 1.10). Considering the values of solubility parameters of the various polymers, it has sense to assume that PS is preferably orientated towards the PFO phase and the PMMA side chains towards the external solute phase (dioxane or DMSO). If we compare the interfacial tension isotherms of the uncrosslinked polymer (SBM) and the Janus cylinders (see Fig. 1.10), we can conclude that the block terpolymer provides a minor reduction of around 10% of the interfacial tension for both solvents, however, the Janus cylinders showed a significantly stronger decrease, i.e., an up to 5-fold better performance for the PFO-dioxane solvent system and up to 4-fold better performance for PFO-DMSO. These results indicate that Janus cylinders are more efficient stabilizing agents for the nanostructuration of interfaces than the block terpolymers.

Concerning to the mechanism of cylinder adsorption, Ruhland et al. [34] found that the adsorption took place following three different stages (see Fig. 1.11). First, there was free cylinder diffusion to the interface (I). Therefore, the number of particles at the interface increased rapidly, the cylinders packed closer, and the decrease in interfacial tension slowed down (II). Furthermore, similar to phase II a closer cylinder organization

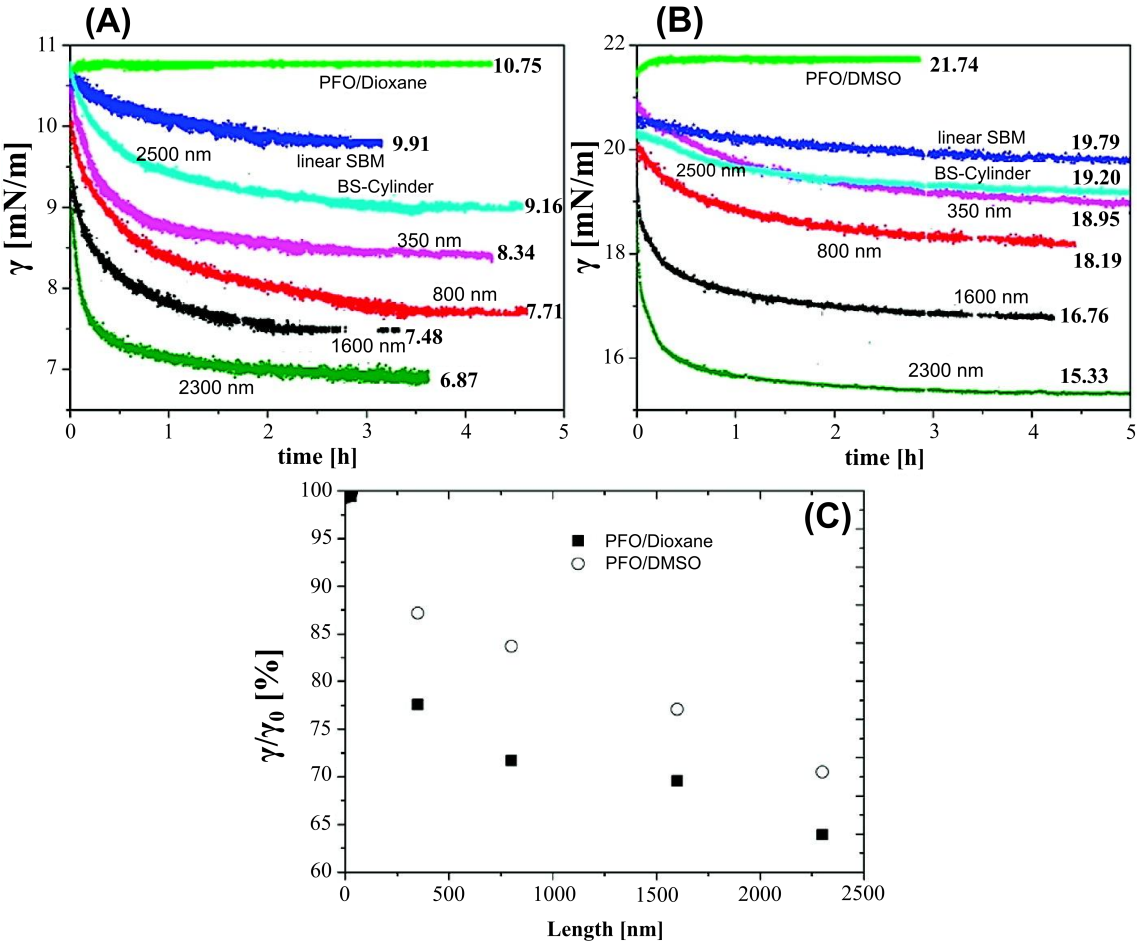

Figure 1.10: Influence of the length of Janus cylinders on the interfacial tension. (A) Interfacial tension isotherms of solutions of Janus cylinders in dioxane at the PFO/dioxane interface and (B) in DMSO at the PFO/DMSO interface ($c = 1\,g/L$). Interfacial tension isotherms for uncrosslinked SBM and homogeneous BS core-shell cylinders are included. (C) Relative decrease of quasi-equilibrium interfacial tensions as a function of the cylinder length for both solvent systems. Reprinted with permission from [34]. Copyright (2011) American Chemical Society.

played an important role in order to get more cylinders to the interface (III). Here, the adsorption of new Janus cylinders came along with a rearrangement and better ordering of already adsorbed cylinders at the interface. These microscopic arrangements of the Janus cylinders at the interface were confirmed by ex-situ TEM images (see Fig. 1.11).

c) Toluene-water interface.

Recently, Ruhland et al. [35] have again studied the influence of JP shape (spheres, cylinders and discs) on their interfacial behavior at liquid-liquid interfaces, but now using the toluene-water interface. As previously, the synthetic pathway to obtain JPs was based on a template-assisted synthesis, involving cross-linking of a bulk terpolymers and a subsequent sonication treatment. The block terpolymer precursors used in the preparation of cylinders and spheres JPs were: the two polystyrene-block-polybutadiene-block-poly(methyl methacrylate) block terpolymers $S_{41}B_{41}M_{45}$ and $S_{44}B_8M_{48}$, respectively. Whereas, the polystyrene-block-polybutadiene-block-poly(tert-butyl acrylate) block terpolymer $S_{42}B_{10}T_{48}$ was the block terpolymer precursor of the Janus discs. The geometries of JPs synthesized by Ruhland et al. [35] are shown in Fig. 1.12.

Pendant drop tensiometry isotherms of the interfacial tension at the toluene/water interface ($\gamma = 34\,mN/m$) were measured on a Krüss DSA100 tensiometer at room temperature. The measurements were performed with a degassed Milli-Q-water droplet saturated with toluene immersed in a toluene solution of the JPs saturated with water. The interfacial tension was measured as a function of time (see Fig. 1.13). Different adsorption dynamics for spheres, cylinders, and discs were observed. The addition of Janus cylinder resulted in the maximum reduction in the equilibrium interfacial tension, from 34 to ca. $14\,mN/m$. In comparison, Janus spheres showed a moderately lower surface activity with an intermediate γ_{inf} value of ca. $17.5\,mN/m$. Janus discs provided the smallest amount of effective interfacial tension reduction, from 34 to ca. $19\,mN/m$. Additionally, the Janus discs showed a different trend of adsorption dynamics, which clearly pointed towards a change in the packing of the Janus discs at the interface with time due to the anisotropic shape.

As pointed out by the authors of this very interesting comparative study on the self-assembly behavior of JPs with different geometries at the toluene/water interface, one reason for the different adsorption kinetics is the size of the JPs. The Janus spheres were $50\,nm$ in diameter, whereas the cylinders had a length of $2300\,nm$ and the discs were around $300\,nm$. Smaller sizes led to higher diffusion coefficients and thus faster adsorption kinetics, however, the particle shape is also a determining factor of the quasi-equilibrium state and the final value of the interfacial tension. The ability for stabilization slightly decreases from Janus cylinders to Janus spheres to Janus discs. Ruhland et al. [35] simulated the free energy change upon adsorption of the various types of JPs to get a better understanding of the adsorption behavior and kinetics of JPs at liquid-liquid interfaces. The free energy of adsorption for the particles at the interface was calculated similarly to the method used by Pieranski [79] at a series of rotations and translations through the interface from the Eq. 1.12.

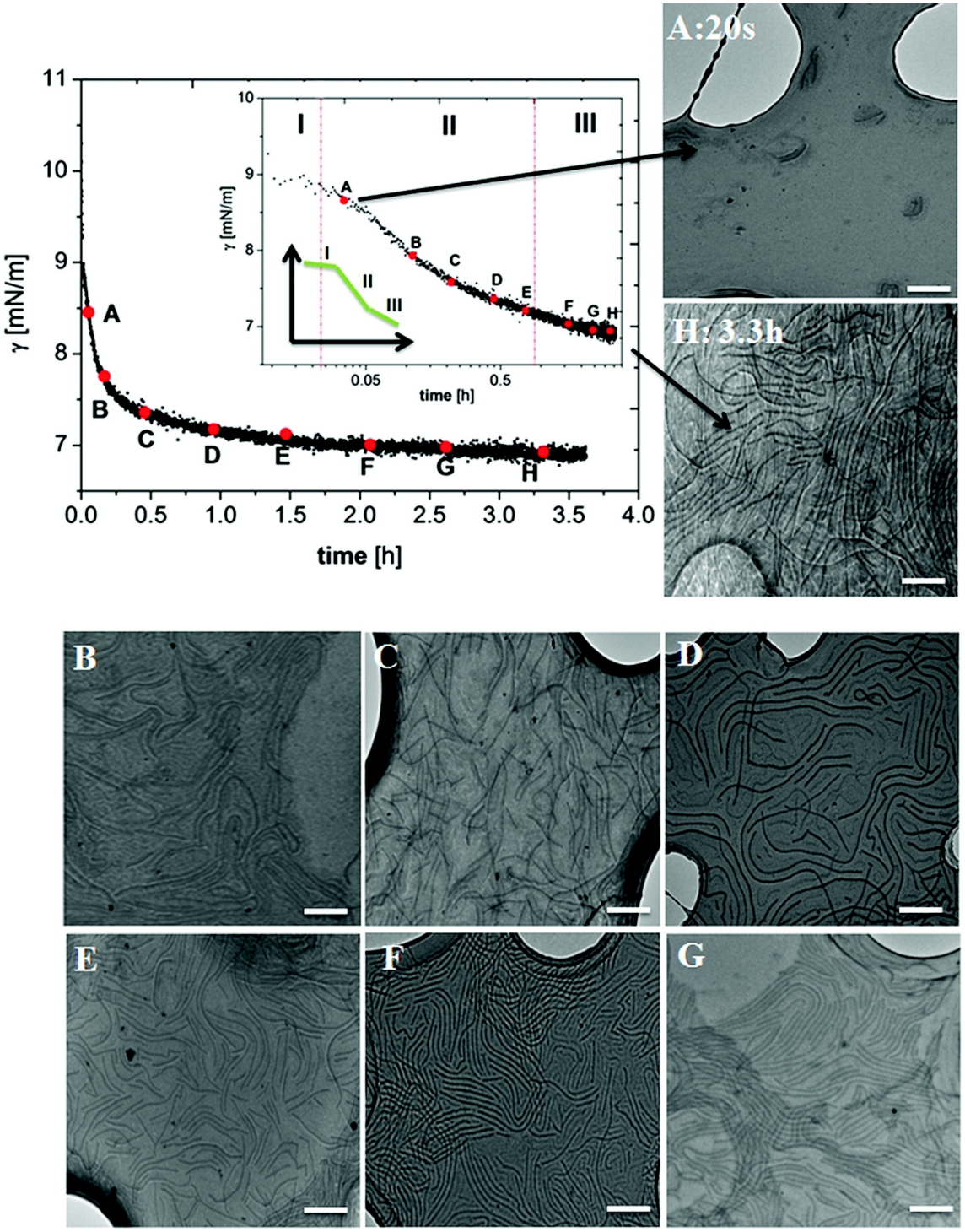

Figure 1.11: Left top: adsorption curves in linear and logarithmic presentation. (A-H) Series of TEM images (obtained from Lacey grids) of $2300\,nm$ Janus cylinders ($1\,g/L$) adsorbing at the PFO/dioxane interface at different times as noted in the interfacial isotherms (scale bars: $1\,\mu m$). Reprinted with permission from [34]. Copyright (2011) American Chemical Society.

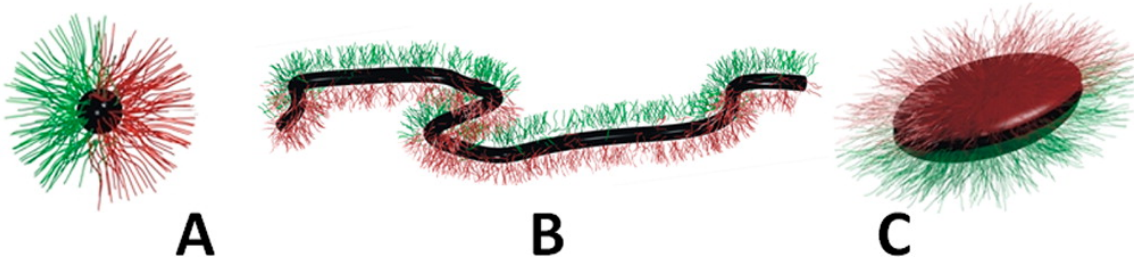

Figure 1.12: Overview of possible janus particle architectures: (A) spheres, (B) cylinders, and (C) discs. Reprinted with permission from [35]. Copyright (2013) American Chemical Society.

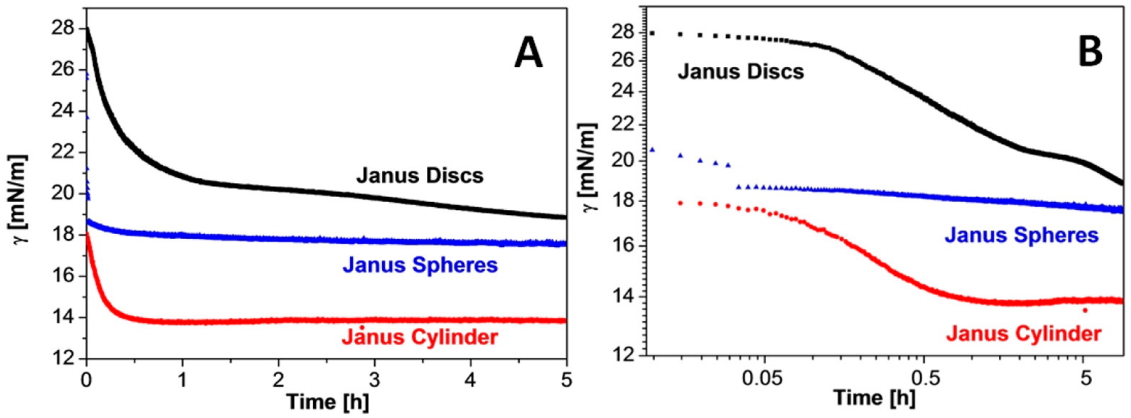

Figure 1.13: Influence of the Janus particle shape on the interfacial tension. (A) Interfacial tension isotherms of solutions of Janus particles in toluene at a water/toluene interface. (B) Logarithmic representation of the data in (A). Reprinted with permission from [35]. Copyright (2013) American Chemical Society.

$$\Delta G_{ad} = \sum_{P} A_{P1}\gamma_{P1} + \sum_{P} A_{P2}\gamma_{P2} - A_{12}\gamma_{12} \tag{1.12}$$

where A_{ij} represents the area and γ_{ij} the interfacial tension with the subscripts $P1$, $P2$ and 12 for the polymer phase in liquid 1, the polymer phase in liquid 2, and the fluid-fluid interface, respectively. The values of the areas were calculated by simply summing the area of triangles of the PMMA or PS phase in the corresponding liquid phase. The interfacial tension values used in the calculations were: water-toluene, $34\,mN/m$; PS-toluene, $6.5\,mN/m$; PS-water, $32\,mN/m$; PMMA-toluene, $11.4\,mN/m$; PMMA-water $16\,mN/m$. The simulation method was the same used by Morgan et al. [80] to evaluate the adsorption energy of hematite particles at a liquid interface. On the basis of calculated data, these authors found a favored orientation of PS to the toluene phase and PMMA side chains to the water phase. The energy barrier for the removal an isolated Janus sphere from the interface is $\simeq 5 \cdot 10^5\, k_B T$. In comparison, the energy profile of Janus discs showed two energy minima and therefore predicted the existence of two different orientations, which correspond to the global and local minimum energies, of the Janus discs at the toluene-water interface. The energy barriers were $\simeq 1.5 \cdot 10^6\, k_B T$ and $5 \cdot 10^5\, k_B T$, respectively. The Janus cylinders had one energy global minimum of $1 \cdot 10^6\, k_B T$ with an orientation parallel to the interface. On the basis of the experimental data and simulation results, Ruhland et al. [35] were able to describe the fundamental aspects of adsorption kinetics of the JPs at liquid-liquid interfaces, which depend not only of the particle size but also of the geometrical shape of particles. Whereas the adsorption kinetics of spheres and cylinders can be described by three different adsorption stages, the discs require of four stages (see Fig. 1.13).

d) Water/air and water/decane interfaces.

Park et al. [45] have studied the behavior of JPs (gold-coated polystyrene particles-AuPS) at an oil-water interface formed between decane (superphase) and an aqueous subphase with $2\,wt.\%$ of Gellan (Gellan gum is a water-soluble anionic polysaccharide produced by the bacterium Sphingomonas elodea), JPs were inserted at the interface with a spreading solvent (isopropanol). The spreading agent plays a crucial role in the formation of well-structured colloidal monolayers, although the effects that cause on the colloidal stability of particles and the surface tension of the fluid-fluid interfaces are not very well understood yet [81]. To investigate the effect of the wettability of the gold hemisphere on the interfacial behavior of JP, the gold surface was modified using 1-dodecanethiol (DDT), 1-octadecanethiol (ODT) and 3-mercaptopropionic acid (MPA). The water contact angles of a water drop on a un-modified and thiol-modified gold (Au) were: Au $(119 \pm 5)^\circ$, DDT-Au $(139 \pm 3)^\circ$, ODT-Au $(152 \pm 2)^\circ$ and MPA-Au $(62 \pm 2)^\circ$.

The behavior of the amphiphilic JPs at the decane-water interface was completely different from that of un-modified PS particles (PS, diameter $2.9\,\mu m$). Whereas the un-modified PS particles and MPA-Au-PS are organized into a stable hexagonal lattice, Au-PS JPs, ODT-Au-PS, and DDT-Au-PS immediately are aggregated giving rise to fractal structures. This observation suggested to Park et al. [45] that the formation of stable colloidal monolayers was the result of long-range electrostatic dipolar repulsions between

the electrically charged particles [79] and that the attractive interaction associated with the uncharged JPs and the formation of fractal structures was due to capillary interactions provoked by an undulating contact line around the particle surface [82]. A simpler explanation could be that the weakly charged colloidal particles coagulate easily when they are placed at fluid interfaces [83]. Hong et al. have experimentally found the formation of clusters of charged Janus spheres [52]. The cluster shapes were analyzed by combined epifluorescence microscopy and Monte Carlo computer simulations with excellent agreement. The most interesting result obtained in that work was that the charge asymmetry of individual JPs was preserved in the clusters. The low colloidal stability of the most JPs explains why the fluid-like, glass-like and hexagonal solid structures are not present at the JPs laden-interfaces, whereas these microstructures appear very often at the homogeneous particles laden-interfaces [84, 85]. On the contrary, the amphiphilic JPs tend to form supermicelles because they behave like surfactants [46]. In this context, Beltran-Villegas et al. [50] have recently simulated using Brownian dynamics the equilibrium phase behavior of Janus colloids by implementing a sedimentation equilibrium approach, but the obtained information is not applicable to the possible microstructures at JPs laden-interfaces. Furthermore, Tran et al. [86] recently found the coexistence of multiple stable mesophases for JPs based on lipids and stabilized by Pluronic F127 surfactant.

On the other hand, Fernandez-Rodriguez et al. have made a comparative study between gold and Janus gold particles behavior at air-water and water-decane [87]. Homogeneous gold nanoparticles ($AuC6$) capped with hexanethiol (HPs) were synthesized following the Brust protocol [88]. Janus gold nanoparticles (JPs) were synthesized by functionalizing a hemisphere of the HPs with 2-(2-mercapto-ethoxy)ethanol (MEE) using the Chen protocol [27, 71]. In some cases the hydrophilic MEE was substituted by the 3-mercaptopropane-1,2-diol (MPD). The terminal groups were -CH3 and -OH for the hexanethiol and MEE or MPD functionalized hemispheres, respectively. Both nanoparticles were redispersed separately in tetrahydrofuran as a spreading agent (THF). The JPs diameter quantified from isolated nanoparticles in High Resolution TEM (HRTEM) pictures was $(3.5 \pm 0.9)\, nm$. The amphiphilic character of the Janus gold particles was examined by contact angle measurements. The hydrophobic side showed an average contact angle of $(63.3 \pm 2.7)^\circ$ (using MPD) or $(56.1 \pm 1.8)^\circ$ (using MEE), whereas it decreased up to $(53.4 \pm 2.9)^\circ$ (MPD) or $(49.0 \pm 1.3)^\circ$ (MEE) into the hydrophilic side. The wettability differences between -CH3 and -OH terminal groups suggested a surface activity of the JPs. Atomic Force Microscopy (AFM) confirmed the amphiphilic nature of these Janus gold particles [89]. The mean value of the adhesion force between the Janus gold particles and a modified gold surface was found to be $(31.5 \pm 10.0)\, nN$, whereas this force diminished up to $(27.5 \pm 4.5)\, nN$ when homogeneous ($AuC6$) particles were used. This latter value of adhesion force was very close to the mean value estimated for the direct contact between the AFM tip and the modified gold surface ($C6$ self-assembled monolayer surface). In any case, Perro et al. have pointed out that the direct visualization of the surface dis-symmetry of the JPs is not a simple task, as the difference between the two hemispheres is at the molecular level [21]. In addition to the AFM characterization of the structural details of the JPs, Nuclear Overhauser Enhancement Spectroscopy (NOESY) has also been used [71]. This is a two-dimensional phase-sensitive NMR technique that detects the distance-dependent nuclear Overhauser effect between proton spins. This spectroscopy technique

also confirmed that the gold JPs prepared by Chen's method exhibited segregated distribution of the two kinds of ligands, supporting the amphiphilic structural model of these JPs prepared using the Langmuir-Blodgett technique. Nevertheless, it must be pointed out that because of the anisotropic characteristics and absence of electric charges on the JP surface, extensive aggregation was also observed in selected solvent media (THF) [87]. The low colloidal stability of these JPs is a serious drawback for a proper characterization of their interfacial behavior or surface activity.

Fernandez et al. [87] used the pendant drop tensiometry to precise change and control the volume and therefore the area of a MilliQ water pendant drop using a microinjector. The growing and shrinking of the pendant drop volume forced different nanoparticle arrangements, once a fixed amount of nanoparticles was adsorbed at the pendant drop interface. First, they deposited a given amount of the HPs or JPs dispersed in THF onto a MilliQ water pendant drop in air with a microsyringe and a micropositioner and waited until full evaporation of the spreading solvent. As stated before, the evaporation of the spreading solvent ensured that the nanoparticles had enough energy to adsorb at the interface, compared with the slow process of adsorption from the bulk [44]. In Fig. 1.14, it can be observed the surface tension evolution over time after different amounts of HPs and JPs deposited at the pendant drop. The surface tension decreased as the nanoparticle concentration increased at the pendant drop surface. This decrease was greater for JPs than for HPs, suggesting enhanced interfacial activity of the Janus nanoparticles as compared to the homogeneous equivalents.

Next, for each particle concentration the shrinking and growing experiment enabled to build a piecewise-like compression isotherm with the pendant drop in air or immersed in decane (see Fig. 1.15). Given that the adsorption energy of the nanoparticles at the interface is of the order of k_BT when the nanoparticle diameter is in the range of a few nanometers [77], the $3.5\,nm$-diameter HPs and JPs were expected to desorb from the pendant drop interfaces due to thermal fluctuations. However, both HPs and JPs exhibited a significant and stable effect on the surface tension after the THF evaporation and low hysteresis during the growing and shrinking experiments, suggesting that there were nanoparticles at the interface and that they did not desorb from the pendant drop interface over time. Once again, the JPs showed higher interfacial activity than the HPs. Furthermore, the hard disk model (Eq. 1.13) fitted the HPs compression isotherm and underestimated the JPs results.

$$\Pi(A_p) = \frac{k_BT}{A_p\left(1 - \frac{\pi d^2}{4A_p}\right)} \tag{1.13}$$

Eq. 1.13 is written in terms of the surface pressure Π for a given area per particle at the interface A_p, where k_B is the Boltzmann constant, T is the temperature and d is the hard disk diameter.

Finally, Fernandez-Rodriguez [90] examined the surface activity and the collective behavior of colloidally stable silver Janus-like particles synthesized following the Sashuk et al. protocol [43] deposited at the water/air interface. The capping ligands were 11-mercaptoundecanoic acid and 1-undecanethiol, hydrophilic and hydrophobic, respectively. They showed an average particle diameter of $(100 \pm 40)\,nm$ and were dispersed in

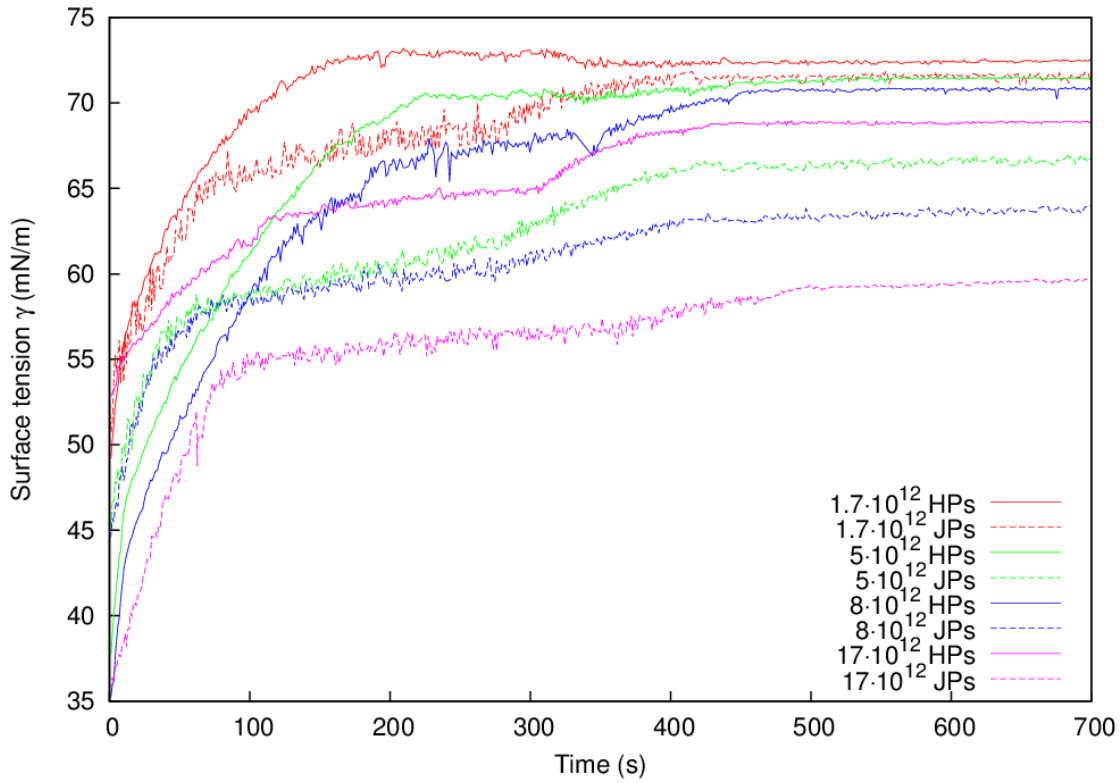

Figure 1.14: Surface tension evolution over time after depositions of gold HPs and JPs at the surface of an initial $5\,\mu L$ MilliQ water pendant drop and subsequent growing at a $0.08\,\mu L/s$ rate up to $20\,\mu L$. Each line corresponds to different depositions with different number of HPs or JPs. After the solvent evaporation, the surface tension remained stable. Reprinted with permission from [87]. Copyright (2014) American Chemical Society.

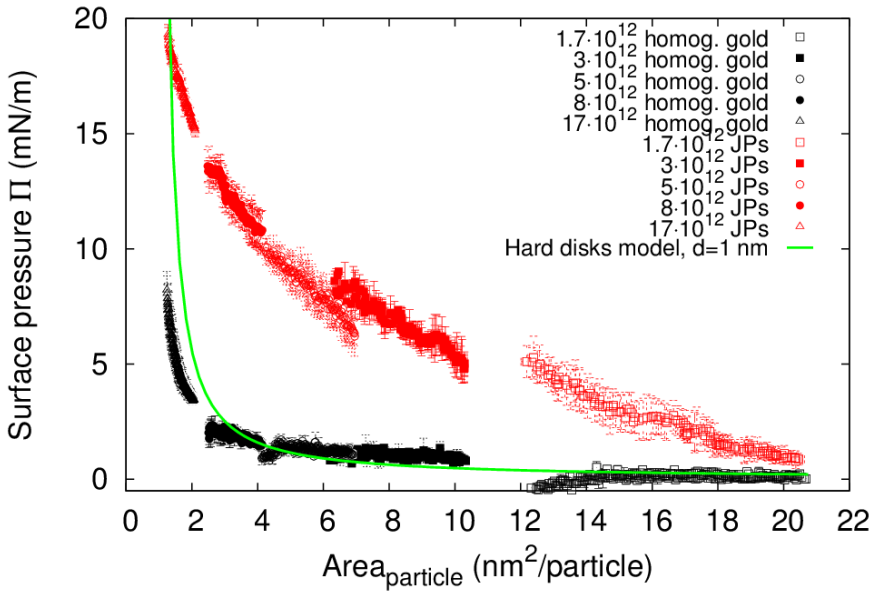

(a) Water/air interface

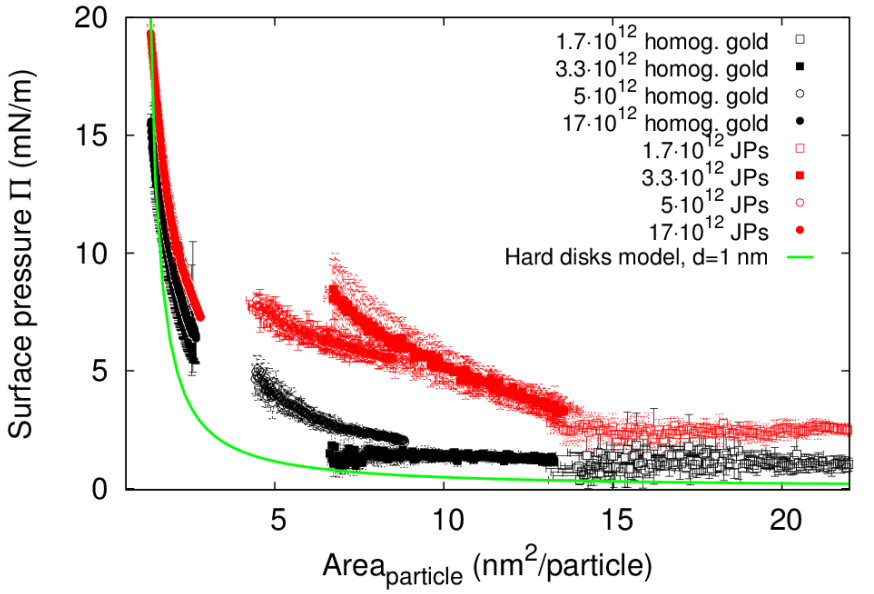

(b) Water/decane interface

Figure 1.15: Surface pressure against the area per particle for different number of gold JPs (red dots) and HPs (black dots) deposited at the interface. Each black or red symbol corresponds to a single JP or HP deposition at the interface of the pendant drop. The solid line is the hard disks model (Eq. 1.13) for disks of $1\,nm$ diameter. Reprinted with permission from [87]. Copyright (2014) American Chemical Society. (For interpretation of the references to color in this figure legend, the reader is referred to the web version of this article.).

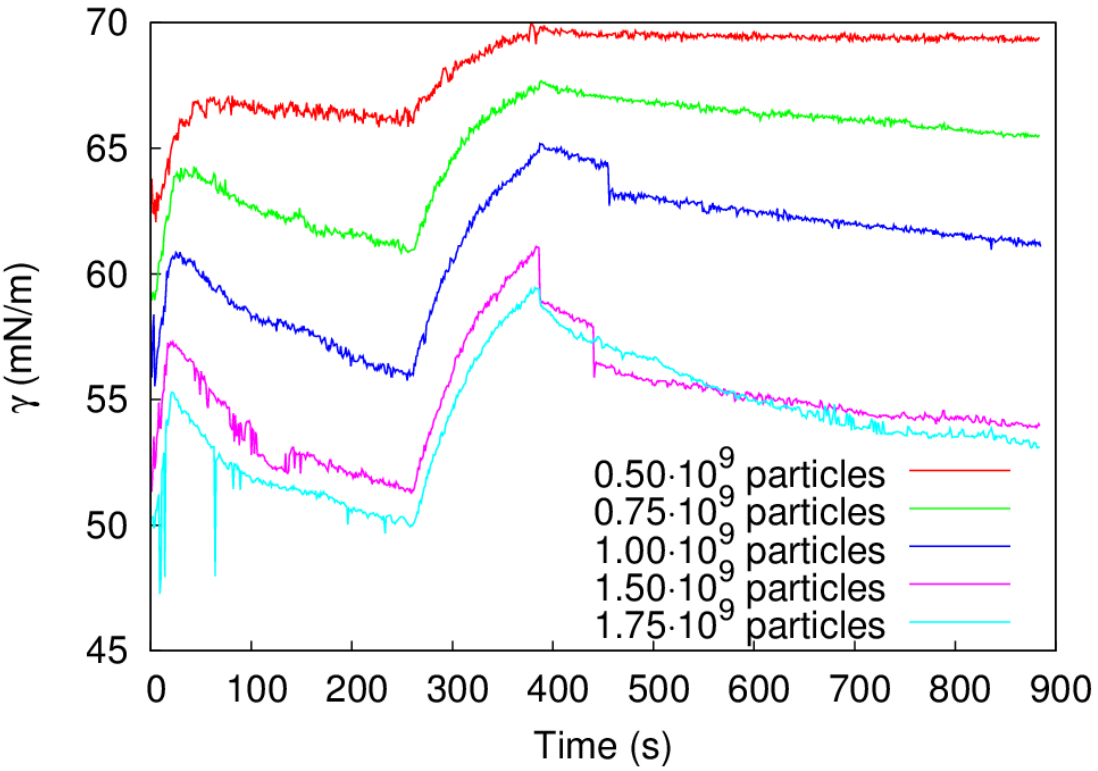

Figure 1.16: Surface tension γ as a function of time for different silver Janus-like particle concentrations during the formation of the pendant drop and the subsequent deposition of the monolayer [90]. Reproduced by permission of The Royal Society of Chemistry.

methanol or a mixture of methanol and 2-propanol. The JPs in aqueous media showed colloidal stability at pH values above 5. All experiments of surface activity and collective behavior were performed at $pH \sim 6$.

Using pendant drop tensiometry, they measured the surface tension of JP monolayers as a function of time, as the spreading solvent was evaporating at different particle surface concentrations and the corresponding adsorption isotherms from the growing and shrinking cycles (surface pressure as a function of area per particle) in a similar way as their previous work [87].

After the evaporation of the spreading solvent, the final surface tension decreased as increasing amounts of JPs were deposited at the interface. As can be seen in Fig. 1.16, the final surface tension decreased $15\,mN/m$ when the amount of JPs deposited was increased 3.5 times.

They found that the mixture of 2-propanol and methanol as spreading solvent resulted in higher interfacial activity than the methanol alone. This might be due to the formation of complexes between the methanol, 2-propanol and water as reported by Grossmann and Ebert [91].

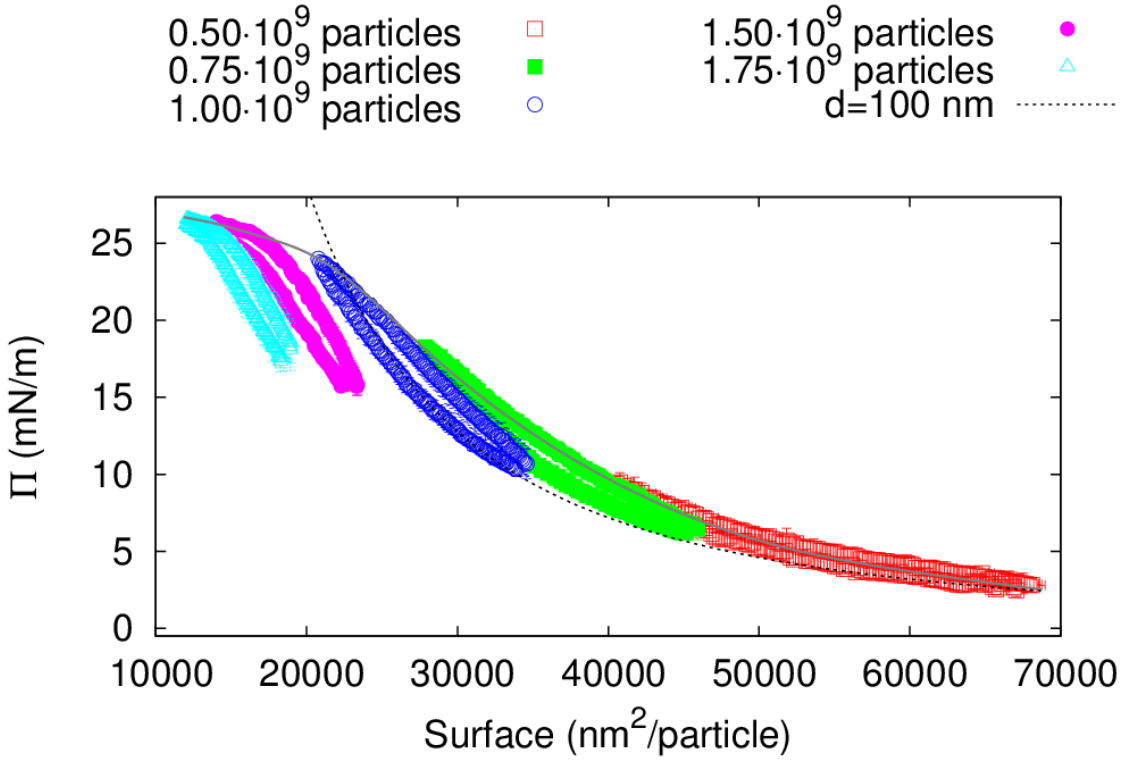

Figure 1.17: Surface pressure as a function of surface area per particle for different silver Janus-like particle concentrations using methanol as spreading agent. The gray line is an eye guide and the dashed line the fitting with the Frumkin model [90]. Reproduced by permission of The Royal Society of Chemistry.

For each shrinking and growing experiment, the surface pressure Π against the drop area divided by the number of JPs was plotted in Fig. 1.17. The effective surface tension γ of a JP-laden interface was lower than the surface tension of the bare interface due to the bidimensional osmotic pressure Π generated by the colloidal monolayer.

The hysteresis displayed by the isotherms in Fig. 1.17 is much smaller than that shown by the isotherms obtained by the conventional Langmuir balance [43]. This indicates that the pendant drop tensiometry enables to measure surface pressure values under experimental conditions very close to the thermodynamic equilibrium and that the migration of JPs deposited at the interface into the aqueous phase was almost negligible. The interface compression produced changes in the surface pressure (around $5\,mN/m$) at high values of area ($5 \cdot 10^4\,nm^2$/particle), which reveals the sensitivity of this technique. Below this point a gas-liquid transition can be identified from the steep rise in the surface pressure. It is noticeable that the complete compression isotherm throughout the range of interfacial area is not single-valued, i.e. the curves obtained with different particle concentration do not overlap perfectly. This can be explained because each part of the compression isotherm corresponds to a different shrinking and growing experiment with different JP amounts in

which different self-assembly dynamics could take place. The isotherm collapse is found in Fig. 1.17 between 10^4 and $2 \cdot 10^4\, nm^2$/particle. This collapse corresponds with the close packing of $100\, nm$ particles at the interface, which takes place when the area per particle is $4R^2$ being R the particle radius (a hexagonally close-packed monolayer). Moreover, the surface tension at the collapse state (around $25\, mN/m$) is in agreement with the reported values for similar JPs [43].

The contact angles of both hemispheres of the JPs are expected to be around $80°$ and $92°$, which does not represent a large wettability contrast in both faces of the JPs used in this study [43]. This reveals that the colloidal stability of the JPs in the bulk solution and at the interface plays a more important role in their interfacial activity rather than the contact angle difference between their faces. Finally, they fitted the Frumkin model [92] (Eq. 1.14), which relates the surface pressure (Π) with the area per particle at the interface (A_p).

$$\Pi(A_p) = -\frac{k_B T}{A_0} \ln\left(1 - \frac{A_0}{A_p}\right) - \frac{\beta}{A_p^2} \tag{1.14}$$

where A_0 is the particle geometrical area and β is the interaction constant. The first term was negligible and the second term was fitted with a positive value of $\beta = (1.15 \pm 0.08) \cdot 10^{-26}\, mJ \cdot m^2$. The negligible geometrical term in comparison with the high interaction term pointed out to the dominant effect of the lateral attractive interactions between JPs at the water/air interface.

As above mentioned, the shape and wettability of particles have a strong effect on the configuration and interactions between particles placed at fluid-fluid interfaces. In this sense, Park et al [93] performed a very interesting experimental study on the behavior of double hydrophilic Janus cylinders at air-water and decane-water interfaces. The assemblies of multiple double hydrophilic Janus cylinders at the air-water interface showed structures of nondeterministic assembly behaviors, which are noticeably different from those observed in geometrically anisotropic but chemically homogeneous particles, such as ellipsoids and cylinders [66].

1.4 Interfacial rheology of Janus particles adsorbed onto liquid interfaces

The viscosity increase of a solution containing JPs of SiO_2 and Fe_3O_4 when it is applied with an external AC electric and magnetic fields due to the formation of chains was studied by Ren and Kretzschmar [94]. However these measurements referred to particles in the bulk of a solution. In order to study the viscosity and elasticity of the JPs at a fluid-fluid interface it is necessary to study the interfacial rheology of the interface [95]. The dilatational rheology of the colloidal layers formed at the pendant drop interface can be measured with the oscillating pendant drop tensiometry. An oscillatory perturbation is applied to the interface by injecting and extracting volume to the drop. The system records the response of the surface tension to the area deformation. The average dilatational modulus (E), the mean surface tension (γ) and the surface dilatational viscosity (η_d) are

obtained from this response [95]. To obtain the dilatational modulus it is required a quasi-equilibrium drop shape for the calculation of the surface tension to avoid excessive perturbation of the colloidal monolayer and the departure from the viscoelastic linear region as discussed by Hilles et al. [96]. However, above this viscoelastic linear region it is still possible to obtain an average dilatational modulus in which the main contribution comes from the dilatational modulus in the viscoelastic linear region. Fernandez et al. [90] studied the interfacial rheology of silver Janus-like particles in water/air interface. The initial pendant drop volume was $20\,\mu L$ or $10\,muL$, which depended on the surface particle concentration. In all rheology experiments, they applied a sinusoidal oscillation in the pendant drop volume with $1\mu L$ amplitude and a frequency of $0.1\,Hz$, which was above the viscoelastic linear region. They distinguished two different behaviors depending on the spreading agents used in the deposition of the JPs. The average dilatational modulus changed dramatically when the colloidal monolayer collapsed (from $E = (62 \pm 2)\,mN/m$ to $(620{\pm}50)\,mN/m$) when 2-propanol and methanol mixture was used as spreading agent. On the other hand, when methanol only was used as spreading agent, the average dilatational modulus was low in comparison and did not change significantly after the collapse (always below $E < 28\,mN/m$). In all cases the average dilatational viscosity was very low ($\eta_d < 14\,mN/(m \cdot s)$). The values of E and η_d obtained upon these states agree, which indicates that the collective behavior of the JPs is practically independent of the geometrical arrangement of particles in the colloidal monolayer. This illustrates again the decisive role played by the spreading agent. The elastic network formed by the JPs at the interface at high surface pressure is strongly influenced by the presence of solvent molecular clusters established with water [91].

1.5 Conclusions

Since de Gennes published in 1992 his inspiring work coining the term Janus particle (JP), there has been a strong effort to develop different routes to synthesize JPs. These particles with two spatial domains of different wettability are able to stabilize Pickering emulsions rather than homogeneous particles (HPs) due to the desorption energy of JPs, three times greater than for HPs. Different methods are being used to characterize the interfacial activity of JPs-laden interfaces as the Langmuir balance, but often the synthesis produces small amount of JPs, not enough to perform an experiment of Langmuir balance. Otherwise, pendant drop tensiometry allows exploring the interfacial activity of JPs in different fluid-fluid interfaces with much less number of JPs. Furthermore, if the particles are deposited onto the interface dispersed in a spreading solvent, the necessary quantity of JPs is even lower and the evaporation of the spreading solvent provides enough energy to place the JPs at the interface faster than the diffusion-driven adsorption of JPs from the bulk of the pendant drop. Also, the pendant drop tensiometry enables to easily perform dilatational surface rheology to characterize the collective behavior of the JPs at the interface of the pendant drop. In all the theoretical and experimental works there are several parameters that condition the interfacial activity of the JPs: shape, morphology and distribution of the spatial domains which confers the Janus character to the particle, spreading solvent, colloidal stability, charge and composition of the JP. Finally, regardless of the synthesis

and characterization methods, the JPs show an enhanced interfacial activity compared to the corresponding HPs.

Acknowledgements

This work was supported by the Spanish MINECO (projects MAT2011-23339 and MAT2013-44429-R), by "Junta de Andalucía" and FEDER (projects P10-FQM-5977 and P12-FQM-1443).

References

[1] De Gennes, P. G. Soft Matter. *Science* **1992**, *256*, 495–497, DOI: 10.1126/science.256.5056.495.

[2] Yan, J.; Bae, S. C.; Granick, S. Rotating crystals of magnetic Janus colloids. *Soft Matter* **2015**, *11*, 147–153, DOI: 10.1039/C4SM01962H.

[3] Bradley, M.; Rowe, J. Cluster formation of Janus polymer microgels. *Soft Matter* **2009**, *5*, 3114–3119, DOI: 10.1039/B904316K.

[4] Onishi, S.; Tokuda, M.; Suzuki, T.; Minami, H. Preparation of Janus Particles with Different Stabilizers and Formation of One-Dimensional Particle Arrays. *Langmuir* **2015**, *31*, 674–678, DOI: 10.1021/la504535k.

[5] Kaewsaneha, C.; Tangboriboonrat, P.; Polpanich, D.; Eissa, M.; Elaissari, A. Janus Colloidal Particles: Preparation, Properties, and Biomedical Applications. *ACS Appl. Mater. Interfaces* **2013**, *5*, 1857–1869, DOI: 10.1021/am302528g.

[6] Gao, Y.; Yu, Y. Macrophage Uptake of Janus Particles Depends upon Janus Balance. *Langmuir* **2015**, *31*, 2833–2838, DOI: 10.1021/la504668c.

[7] Tu, F.; Lee, D. Shape-Changing and Amphiphilicity-Reversing Janus Particles with pH-Responsive Surfactant Properties. *J. Am. Chem. Soc.* **2014**, *136*, 9999–10006, DOI: 10.1021/ja503189r.

[8] Cui, F.; Lin, J.; Li, Y.; Li, Y.; Wu, H.; Yu, F.; Jia, M.; Yang, X.; Wu, S.; Xie, L.; Ye, S.; Luo, F.; Hou, Z. Bacillus-Shape Design of Polymer Based Drug Delivery Systems with Janus-Faced Function for Synergistic Targeted Drug Delivery and More Effective Cancer Therapy. *Mol. Pharm.* **2015**, *12*, 1318–1327, DOI: 10.1021/mp500464b.

[9] Garbuzenko, O. B.; Winkler, J.; Tomassone, M. S.; Minko, T. Biodegradable Janus Nanoparticles for Local Pulmonary Delivery of Hydrophilic and Hydrophobic Molecules to the Lungs. *Langmuir* **2014**, *30*, 12941–12949, DOI: 10.1021/la502144z.

[10] Mammen, L.; Bley, K.; Papadopoulos, P.; Schellenberger, F.; Encinas, N.; Butt, H.-J.; Weiss, C. K.; Vollmer, D. Functional superhydrophobic surfaces made of Janus micropillars. *Soft Matter* **2015**, *11*, 506–515, DOI: 10.1039/C4SM02216E.

[11] Nedev, S.; Carretero-Palacios, S.; Kühler, P.; Lohmüller, T.; Urban, A. S.; Anderson, L. J. E.; Feldmann, J. An Optically Controlled Microscale Elevator Using Plasmonic Janus Particles. *ACS Photonics* **2015**, *2*, 491–496, DOI: 10.1021/ph500371z.

[12] Bormashenko, E.; Bormashenko, Y.; Pogreb, R.; Gendelman, O. Janus Droplets: Liquid Marbles Coated with Dielectric/Semiconductor Particles. *Langmuir* **2011**, *27*, 7–10, DOI: 10.1021/la103653p.

[13] Teo, B. M.; Suh, S. K.; Hatton, T. A.; Ashokkumar, M.; Grieser, F. Sonochemical Synthesis of Magnetic Janus Nanoparticles. *Langmuir* **2011**, *27*, 30–33, DOI: 10.1021/la104284v.

[14] Yuet, K. P.; Hwang, D. K.; Haghgooie, R.; Doyle, P. S. Multifunctional Superparamagnetic Janus Particles. *Langmuir* **2010**, *26*, 4281–4287, DOI: 10.1021/la903348s.

[15] Ren, B.; Ruditskiy, A.; Song, J. H. (; Kretzschmar, I. Assembly Behavior of Iron Oxide-Capped Janus Particles in a Magnetic Field. *Langmuir* **2012**, *28*, 1149–1156, DOI: 10.1021/la203969f.

[16] Bharti, B.; Velev, O. D. Assembly of Reconfigurable Colloidal Structures by Multidirectional Field-Induced Interactions. *Langmuir* **2015**, *31*, 7897–7908, DOI: 10.1021/la504793y.

[17] Smoukov, S. K.; Gangwal, S.; Marquez, M.; Velev, O. D. Reconfigurable responsive structures assembled from magnetic Janus particles. *Soft Matter* **2009**, *5*, 1285–1292, DOI: 10.1039/B814304H.

[18] Gangwal, S.; Cayre, O. J.; Velev, O. D. Dielectrophoretic Assembly of Metallodielectric Janus Particles in AC Electric Fields. *Langmuir* **2008**, *24*, 13312–13320, DOI: 10.1021/la8015222.

[19] Komazaki, Y.; Hirama, H.; Torii, T. Electrically and magnetically dual-driven Janus particles for handwriting-enabled electronic paper. *J. Appl. Phys.* **2015**, *117*, 154506, DOI: 10.1063/1.4917379.

[20] Hu, J.; Zhou, S.; Sun, Y.; Fang, X.; Wu, L. Fabrication, properties and applications of Janus particles. *Chem. Soc. Rev.* **2012**, *41*, 4356–4378, DOI: 10.1039/C2CS35032G.

[21] Perro, A.; Reculusa, S.; Ravaine, S.; Bourgeat-Lami, E.; Duguet, E. Design and synthesis of Janus micro- and nanoparticles. *J. Mater. Chem.* **2005**, *15*, 3745–3760, DOI: 10.1039/B505099E.

[22] Suzuki, D.; Tsuji, S.; Kawaguchi, H. Janus Microgels Prepared by Surfactant-Free Pickering Emulsion-Based Modification and Their Self-Assembly. *J. Am. Chem. Soc.* **2007**, *129*, 8088–8089, DOI: 10.1021/ja072258w.

[23] Binks, B. P. Particles as surfactants-similarities and differences. *Curr. Opin. Colloid Interface Sci.* **2002**, *7*, 21–41, DOI: 10.1016/S1359-0294(02)00008-0.

[24] Lattuada, M.; Hatton, T. A. Synthesis, properties and applications of Janus nanoparticles. *Nano Today* **2011**, *6*, 286–308, DOI: 10.1016/j.nantod.2011.04.008.

[25] Casagrande, C.; Fabre, P.; Raphaël, E.; Veyssié, M. "Janus Beads": Realization and Behaviour at Water/Oil Interfaces. *EPL (Europhys. Lett.)* **1989**, *9*, 251, DOI: 10.1209/0295-5075/9/3/011.

[26] Kumar, A.; Park, B. J.; Tu, F.; Lee, D. Amphiphilic Janus particles at fluid interfaces. *Soft Matter* **2013**, *9*, 6604–6617, DOI: 10.1039/C3SM50239B.

[27] Pradhan, S.; Xu, L.; Chen, S. Janus Nanoparticles by Interfacial Engineering. *Adv. Funct. Mater.* **2007**, *17*, 2385–2392, DOI: 10.1002/adfm.200601034.

[28] Glaser, N.; Adams, D. J.; Böker, A.; Krausch, G. Janus Particles at Liquid-Liquid Interfaces. *Langmuir* **2006**, *22*, 5227–5229, DOI: 10.1021/la060693i.

[29] Walther, A.; Müller, A. H. E. Janus Particles: Synthesis, Self-Assembly, Physical Properties, and Applications. *Chem. Rev.* **2013**, *113*, 5194–5261, DOI: 10.1021/cr300089t.

[30] Chen, B.; Jia, Y.; Gao, Y.; Sanchez, L.; Anthony, S. M.; Yu, Y. Janus Particles as Artificial Antigen-Presenting Cells for T Cell Activation. *ACS Appl. Mater. Interfaces* **2014**, *6*, 18435–18439, DOI: 10.1021/am505510m.

[31] Binks, B. P.; Fletcher, P. D. I. Particles Adsorbed at the Oil-Water Interface: A Theoretical Comparison between Spheres of Uniform Wettability and "Janus" Particles. *Langmuir* **2001**, *17*, 4708–4710, DOI: 10.1021/la0103315.

[32] Hirose, Y.; Komura, S.; Nonomura, Y. Adsorption of Janus particles to curved interfaces. *J. Chem. Phys.* **2007**, *127* 054707, pages, DOI: 10.1063/1.2756828.

[33] Jiang, S.; Granick, S. Janus balance of amphiphilic colloidal particles. *J. Chem. Phys.* **2007**, *127* 161102, pages, DOI: 10.1063/1.2803420.

[34] Ruhland, T. M.; Gröschel, A. H.; Walther, A.; Müller, A. H. E. Janus Cylinders at Liquid-Liquid Interfaces. *Langmuir* **2011**, *27*, 9807–9814, DOI: 10.1021/la201863x.

[35] Ruhland, T. M.; Gröschel, A. H.; Ballard, N.; Skelhon, T. S.; Walther, A.; Müller, A. H. E.; Bon, S. A. F. Influence of Janus Particle Shape on Their Interfacial Behavior at Liquid-Liquid Interfaces. *Langmuir* **2013**, *29*, 1388–1394, DOI: 10.1021/la3048642.

[36] Larson-Smith, K.; Pozzo, D. C. Pickering Emulsions Stabilized by Nanoparticle Surfactants. *Langmuir* **2012**, *28*, 11725–11732, DOI: 10.1021/la301896c.

[37] Reguera, J.; Ponomarev, E.; Geue, T.; Stellacci, F.; Bresme, F.; Moglianetti, M. Contact angle and adsorption energies of nanoparticles at the air-liquid interface determined by neutron reflectivity and molecular dynamics. *Nanoscale* **2015**, *7*, 5665–5673, DOI: 10.1039/C5NR00620A.

[38] Xu, H.; Liu, X.; Su, G.; Zhang, B.; Wang, D. Electrostatic Repulsion-Controlled Formation of Polydopamine-Gold Janus Particles. *Langmuir* **2012**, *28*, 13060–13065, DOI: 10.1021/la302394e.

[39] Fujii, S.; Yokoyama, Y.; Miyanari, Y.; Shiono, T.; Ito, M.; Yusa, S.-i.; Nakamura, Y. Micrometer-Sized Gold-Silica Janus Particles as Particulate Emulsifiers. *Langmuir* **2013**, *29*, 5457–5465, DOI: 10.1021/la400697a.

[40] Meng, X.; Guan, Y.; Zhang, Z.; Qiu, D. Fabrication of a Composite Colloidal Particle with Unusual Janus Structure as a High-Performance Solid Emulsifier. *Langmuir* **2012**, *28*, 12472–12478, DOI: 10.1021/la302392s.

[41] Zhang, J.; Jin, J.; Zhao, H. Surface-Initiated Free Radical Polymerization at the Liquid-Liquid Interface: A One-Step Approach for the Synthesis of Amphiphilic Janus Silica Particles. *Langmuir* **2009**, *25*, 6431–6437, DOI: 10.1021/la9000279.

[42] Liu, L.; Ren, M.; Yang, W. Preparation of Polymeric Janus Particles by Directional UV-Induced Reactions. *Langmuir* **2009**, *25*, 11048–11053, DOI: 10.1021/la901364a.

[43] Sashuk, V.; Hołyst, R.; Wojciechowski, T.; Fiałkowski, M. Close-packed monolayers of charged Janus-type nanoparticles at the air-water interface. *J. Colloid Interface Sci.* **2012**, *375*, 180–186, DOI: 10.1016/j.jcis.2012.02.057.

[44] Garbin, V.; Crocker, J. C.; Stebe, K. J. Nanoparticles at fluid interfaces: Exploiting capping ligands to control adsorption, stability and dynamics. *J. Colloid Interface Sci.* **2012**, *387*, 1–11, DOI: 10.1016/j.jcis.2012.07.047.

[45] Park, B. J.; Brugarolas, T.; Lee, D. Janus particles at an oil-water interface. *Soft Matter* **2011**, *7*, 6413–6417, DOI: 10.1039/C1SM05460K.

[46] Nie, L.; Liu, S.; Shen, W.; Chen, D.; Jiang, M. One-Pot Synthesis of Amphiphilic Polymeric Janus Particles and Their Self-Assembly into Supermicelles with a Narrow Size Distribution. *Angew. Chem. Int. Ed. Engl.* **2007**, *46*, 6321–6324, DOI: 10.1002/anie.200700209.

[47] Chen, Q.; Whitmer, J. K.; Jiang, S.; Bae, S. C.; Luijten, E.; Granick, S. Supracolloidal Reaction Kinetics of Janus Spheres. *Science* **2011**, *331*, 199–202, DOI: 10.1126/science.1197451.

[48] Yu, C.; Zhang, J.; Granick, S. Selective Janus Particle Assembly at Tipping Points of Thermally-Switched Wetting. *Angew. Chem. Int. Ed. Engl.* **2014**, *53*, 4364–4367, DOI: 10.1002/anie.201310465.

[49] Shah, A. A.; Schultz, B.; Zhang, W.; Glotzer, S. C.; Solomon, M. J. Actuation of shape-memory colloidal fibres of Janus ellipsoids. *Nat. Mater.* **2015**, *14*, 117–124, DOI: 10.1038/nmat4111.

[50] Beltran-Villegas, D. J.; Schultz, B. A.; Nguyen, N. H. P.; Glotzer, S. C.; Larson, R. G. Phase behavior of Janus colloids determined by sedimentation equilibrium. *Soft Matter* **2014**, *10*, 4593–4602, DOI: 10.1039/C3SM53136H.

[51] Luo, M.; Olivier, G. K.; Frechette, J. Electrostatic interactions to modulate the reflective assembly of nanoparticles at the oil-water interface. *Soft Matter* **2012**, *8*, 11923–11932, DOI: 10.1039/C2SM26890F.

[52] Hong, L.; Cacciuto, A.; Luijten, E.; Granick, S. Clusters of Charged Janus Spheres. *Nano Lett.* **2006**, *6*, 2510–2514, DOI: 10.1021/nl061857i.

[53] Santos, A.; López de Haro, M.; Yuste, S. An accurate and simple equation of state for hard disks. *J. Chem. Phys.* **1995**, *103*, 4622–4625, DOI: 10.1063/1.470649.

[54] Isa, L.; Amstad, E.; Schwenke, K.; Del Gado, E.; Ilg, P.; Kroger, M.; Reimhult, E. Adsorption of core-shell nanoparticles at liquid-liquid interfaces. *Soft Matter* **2011**, *7*, 7663–7675, DOI: 10.1039/C1SM05407D.

[55] Liu, Z.; Guo, R.; Xu, G.; Huang, Z.; Yan, L.-T. Entropy-Mediated Mechanical Response of the Interfacial Nanoparticle Patterning. *Nano Lett.* **2014**, *14*, 6910–6916, DOI: 10.1021/nl5029396.

[56] Lee, K. J.; Yoon, J.; Lahann, J. Recent advances with anisotropic particles. *Curr. Opin. Colloid Interface Sci.* **2011**, *16*, 195–202, DOI: http://dx.doi.org/10.1016/j.cocis.2010.11.004.

[57] Cheung, D. L.; Bon, S. A. F. Stability of Janus nanoparticles at fluid interfaces. *Soft Matter* **2009**, *5*, 3969–3976, DOI: 10.1039/B908462B.

[58] Aveyard, R. Can Janus particles give thermodynamically stable Pickering emulsions? *Soft Matter* **2012**, *8*, 5233–5240, DOI: 10.1039/C2SM07230K.

[59] Tu, F.; Park, B. J.; Lee, D. Thermodynamically Stable Emulsions Using Janus Dumbbells as Colloid Surfactants. *Langmuir* **2013**, *29*, 12679–12687, DOI: 10.1021/la402897d.

[60] Park, B. J.; Lee, D. Equilibrium Orientation of Nonspherical Janus Particles at Fluid-Fluid Interfaces. *ACS Nano* **2012**, *6*, 782–790, DOI: 10.1021/nn204261w.

[61] Luu, X.-C.; Yu, J.; Striolo, A. Ellipsoidal Janus Nanoparticles Adsorbed at the Water-Oil Interface: Some Evidence of Emergent Behavior. *J. Phys. Chem. B* **2013**, *117*, 13922–13929, DOI: 10.1021/jp407495z.

[62] Rezvantalab, H.; Shojaei-Zadeh, S. Role of Geometry and Amphiphilicity on Capillary-Induced Interactions between Anisotropic Janus Particles. *Langmuir* **2013**, *29*, 14962–14970, DOI: 10.1021/la4039446.

[63] Luu, X.-C.; Striolo, A. Ellipsoidal Janus Nanoparticles Assembled at Spherical Oil/Water Interfaces. *J. Phys. Chem. B* **2014**, *118*, 13737–13743, DOI: 10.1021/jp5085422.

[64] Güell, O.; Sagués, F.; Tierno, P. Magnetically driven Janus micro-ellipsoids realized via asymmetric gathering of the magnetic charge. *Adv. Mater.* **2011**, *23*, 3674–3679, DOI: 10.1002/adma.201100902.

[65] Basavara, M. G.; Fuller, G. G.; Fransaer, J.; Vermant, J. Packing, Flipping, and Buckling Transitions in Compressed Monolayers of Ellipsoidal Latex Particles. *Langmuir* **2006**, *22*, 6605–6612, DOI: 10.1021/la060465o.

[66] Madivala, B.; Fransaer, J.; Vermant, J. Self-Assembly and Rheology of Ellipsoidal Particles at Interfaces. *Langmuir* **2009**, *25*, 2718–2728, DOI: 10.1021/la803554u.

[67] Madivala, B.; Vandebril, S.; Fransaer, J.; Vermant, J. Exploiting particle shape in solid stabilized emulsions. *Soft Matter* **2009**, *5*, 1717–1727, DOI: 10.1039/B816680C.

[68] Gao, H.-M.; Lu, Z.-Y.; Liu, H.; Sun, Z.-Y.; An, L.-J. Orientation and surface activity of Janus particles at fluid-fluid interfaces. *J. Chem. Phys.* **2014**, *141*, 134907, DOI: 10.1063/1.4897185.

[69] Detrich, Á.; Deák, A.; Hild, E.; Kovács, A. L.; Hórvölgyi, Z. Langmuir and Langmuir-Blodgett Films of Bidisperse Silica Nanoparticles. *Langmuir* **2010**, *26*, 2694–2699, DOI: 10.1021/la9027207.

[70] Kim, J.; Raja, S.; Stellacci, F. Evolution of Langmuir film of nanoparticles through successive compression cycles. *Small* **2011**, *7*, 2526–2532, DOI: 10.1002/smll.201100290.

[71] Pradhan, S.; Brown, L.; Konopelski, J.; Chen, S. Janus nanoparticles: reaction dynamics and NOESY characterization. *J. Nanopart. Res.* **2009**, *11*, 1895–1903, DOI: 10.1007/s11051-008-9543-4.

[72] Centrone, A.; Hu, Y.; Jackson, A.; Zerbi, G.; Stellacci, F. Phase separation on mixed-monolayer-protected metal nanoparticles: A study by infrared spectroscopy and scanning tunneling microscopy. *Small* **2007**, *3*, 814–817, DOI: 10.1002/smll.200600736.

[73] Jackson, A.; Myerson, J.; Stellacci, F. Spontaneous assembly of subnanometre-ordered domains in the ligand shell of monolayer-protected nanoparticles. *Nat. Mater.* **2004**, *3*, 330–336, DOI: 10.1038/nmat1116.

[74] Rotenberg, Y.; Boruvka, L.; Neumann, A. Determination of surface tension and contact angle from the shapes of axisymmetric fluid interfaces. *J. Colloid Interface Sci.* **1983**, *93*, 169–183, DOI: 10.1016/0021-9797(83)90396-X.

[75] Cabrerizo-Vílchez, M. A.; Wege, H. A.; Holgado-Terriza, J. A.; Neumann, A. W. Axisymmetric drop shape analysis as penetration Langmuir balance. *Rev. Sci. Instrum.* **1999**, *70*, 2438–2444, DOI: 10.1063/1.1149773.

[76] Kwok, D.; Vollhardt, D.; Miller, R.; Li, D.; Neumann, A. A collection of papers presented at the 67th Colloid and Surface Science Symposium of the Colloid and Surface Science Division of the American Chemical Society Axisymmetric drop shape analysis as a film balance. *Colloids Surf. A* **1994**, *88*, 51–58, DOI: http://dx.doi.org/10.1016/0927-7757(94)80085-5.

[77] Ferdous, S.; Ioannidis, M.; Henneke, D. Adsorption kinetics of alkanethiol-capped gold nanoparticles at the hexane-water interface., English *J. Nanopart. Res.* **2011**, *13*, 6579–6589, DOI: 10.1007/s11051-011-0565-y.

[78] Yu, H.; Chen, M.; Rice, P. M.; Wang, S. X.; White, R. L.; Sun, S. Dumbbell-like Bifunctional Au-Fe3O4 Nanoparticles. *Nano Lett.* **2005**, *5*, 379–382, DOI: 10.1021/nl047955q.

[79] Pieranski, P. Two-Dimensional Interfacial Colloidal Crystals. *Phys. Rev. Lett.* **Aug. 1980**, *45*, 569–572, DOI: 10.1103/PhysRevLett.45.569.

[80] Morgan, A. R.; Ballard, N.; Rochford, L. A.; Nurumbetov, G.; Skelhon, T. S.; Bon, S. A. F. Understanding the multiple orientations of isolated superellipsoidal hematite particles at the oil-water interface. *Soft Matter* **2013**, *9*, 487–491, DOI: 10.1039/C2SM26556G.

[81] Maestro, A.; Bonales, L. J.; Ritacco, H.; Rubio, R. G.; Ortega, F. Effect of the spreading solvent on the three-phase contact angle of microparticles attached at fluid interfaces. *Phys. Chem. Chem. Phys.* **2010**, *12*, 14115–14120, DOI: 10.1039/C0CP00570C.

[82] Stamou, D.; Duschl, C.; Johannsmann, D. Long-range attraction between colloidal spheres at the air-water interface: The consequence of an irregular meniscus. *Phys. Rev. E* **Oct. 2000**, *62*, 5263–5272, DOI: 10.1103/PhysRevE.62.5263.

[83] Martínez-López, F.; Cabrerizo-Vílchez, M.; Hidalgo-Álvarez, R. Colloidal interaction at the air-liquid interface. *J. Colloid Interface Sci.* **2000**, *232*, 303–310, DOI: 10.1006/jcis.2000.7172.

[84] Frost, D. S.; Nofen, E. M.; Dai, L. L. Particle self-assembly at ionic liquid-based interfaces. *Adv. Colloid Interface Sci.* **2014**, *206*, 92–105, DOI: 10.1016/j.cis.2013.09.004.

[85] Poulichet, V.; Garbin, V. Ultrafast desorption of colloidal particles from fluid interfaces. *Proc. Natl. Acad. Sci. USA* **2015**, *112*, 5932–5937, DOI: 10.1073/pnas.1504776112.

[86] Tran, N.; Mulet, X.; Hawley, A. M.; Conn, C. E.; Zhai, J.; Waddington, L. J.; Drummond, C. J. First Direct Observation of Stable Internally Ordered Janus Nanoparticles Created by Lipid Self-Assembly. *Nano Lett.* **2015**, *15*, 4229–4233, DOI: 10.1021/acs.nanolett.5b01751.

[87] Fernandez-Rodriguez, M. A.; Song, Y.; Rodríguez-Valverde, M. Á.; Chen, S.; Cabrerizo-Vilchez, M. A.; Hidalgo-Alvarez, R. Comparison of the Interfacial Activity between Homogeneous and Janus Gold Nanoparticles by Pendant Drop Tensiometry. *Langmuir* **2014**, *30*, 1799–1804, DOI: 10.1021/la404194e.

[88] Brust, M.; Walker, M.; Bethell, D.; Schiffrin, D. J.; Whyman, R. Synthesis of thiol-derivatised gold nanoparticles in a two-phase Liquid-Liquid system. *J. Chem. Soc., Chem. Commun.* **1994**, 801–802, DOI: 10.1039/C39940000801.

[89] Xu, L.-P.; Pradhan, S.; Chen, S. Adhesion Force Studies of Janus Nanoparticles. *Langmuir* **2007**, *23*, 8544–8548, DOI: 10.1021/la700774g.

[90] Fernandez-Rodriguez, M. A.; Rodriguez-Valverde, M. A.; Cabrerizo-Vilchez, M.; Hidalgo-Alvarez, R. Surface activity and collective behaviour of colloidally stable Janus-like particles at the air-water interface. *Soft Matter* **2014**, *10*, 3471–3476, DOI: 10.1039/C3SM52624K.

[91] Großmann, G. H.; Ebert, K. H. Formation of Clusters in 1-Propanol/Water-Mixtures. *Ber. Bunsenges. Phys. Chem.* **1981**, *85*, 1026–1029, DOI: 10.1002/bbpc.19810851118.

[92] Rusanov, A. I. New theory of equation of state for surface monolayer. *J. Chem. Phys.* **2004**, *120*, 10736–10747, DOI: 10.1063/1.1737301.

[93] Park, B. J.; Choi, C.-H.; Kang, S.-M.; Tettey, K. E.; Lee, C.-S.; Lee, D. Double Hydrophilic Janus Cylinders at an Air-Water Interface. *Langmuir* **2013**, *29*, 1841–1849, DOI: 10.1021/la304829s.

[94] Ren, B.; Kretzschmar, I. Viscosity-dependent janus particle chain dynamics. *Langmuir* **2013**, *29*, 14779–14786, DOI: 10.1021/la402597s.

[95] Maldonado-Valderrama, J.; Wege, H. A.; Rodríguez-Valverde, M. A.; Gálvez-Ruiz, M. J.; Cabrerizo-Vílchez, M. A. Comparative Study of Adsorbed and Spread β-Casein Monolayers at the Water-Air Interface with the Pendant Drop Technique. *Langmuir* **2003**, *19*, 8436–8442, DOI: 10.1021/la034242z.

[96] Hilles, H.; Monroy, F.; Bonales, L.; Ortega, F.; Rubio, R. Fourier-transform rheology of polymer Langmuir monolayers: Analysis of the non-linear and plastic behaviors. *Adv. Colloid Interface Sci.* **2006**, *122*, 67–77, DOI: 10.1016/j.cis.2006.06.013.

Science is a way of thinking much more than it is a body of knowledge.

Carl Sagan

2 Expanding our knowledge on Janus nanoparticles with interfacial activity

In this chapter we will describe the different approaches and strategies that we have followed to improve our knowledge on the interfacial activity of Janus nanoparticles. One important issue is that we have focused on the physicochemical characterization of Janus nanoparticles rather than in their synthesis. At the beginning of this thesis, we performed a careful survey in literature after the year 2010 about Janus nanoparticles and next, we wrote several emails to stablish collaborations. The deal was simple: they would provide us with Janus nanoparticles and we would explore their interfacial activity. It was a successful strategy since a lot of colleagues answered positively. However, we realized soon two things: i) we needed nanoparticles with no surfactants, that hinders the interfacial activity of the nanoparticles (we had to discard some nanoparticles synthesized by using a high amount of surfactants) and ii) the usual quantities of synthesized Janus nanoparticles were really small, typically in the range of 1 mg, to perform experiments with the Langmuir balance or even to prepare oil/water emulsions (e.g. there are no enough Janus nanoparticles to mix them with water and oil and examine the final emulsion in a small flask). Thus, we decided that the pendant drop tensiometry was the most suitable technique because it needed small amounts of nanoparticles to measure their interfacial activity. In fact, because in most cases we did not have enough nanoparticles for the bulk of the pendant drop, we had to deposit the nanoparticles from outside as it is described in Chapter 3. Nonetheless, we achieved to study such scarce nanoparticles and designed several strategies to cover the different aspects of Janus nanoparticles.

In the previous Chapter 1, we collect the models, methodologies, strategies and results obtained with Janus nanoparticles at fluid-fluid interfaces as a description of the state-of-the-art. Regarding the *Methodology* used in this thesis, we describe in Chapter 3 the pendant drop tensiometry through the interfacial characterization of 3.5 nm-diameter homogeneous gold nanoparticles functionalized with hexanethiol, synthesized by Dr. Yang Song and Prof. Shaowei Chen (Department of Chemistry and Biochemistry, University of California), at the water/air

and water/decane interfaces. In this chapter, we explain how it is conducted the deposition of nanoparticles at the pendant drop interface with a spreading solvent and how a piecewise-like compression isotherm can be built from different pendant drop experiments.

In Chapter 4, we adapt the pendant drop tensiometry to cover the characterization of highly surface-active nanoparticles by using a bigger capillary and further the interfacial dilatational rheology that enables to characterize the interfacial dilatational elasticity and viscosity of the water/air and water/decane particle-laden interfaces. Also, in this Chapter 4, we explain the importance of cleaning in all their aspects because the interfacial tension is very sensitive to any pollutants. Also, we describe the Dynamic Light Scattering-based techniques that we used to characterize the size and electrophoretic mobility of the nanoparticles in water. Finally, we describe in this chapter the new technique developed by Prof. Lucio Isa in which the microscopic contact angle of nanoparticles can be obtained by Freeze Fracture Shadow-Casting cryo-SEM. This technique was used during the short-term research stay in the Laboratory for Interfaces, Soft matter and Assembly at ETH-Zurich under the supervision of Prof. Lucio Isa.

Next, in the *Results and Discussion* part we compile several published and unpublished works as a result of the aforementioned international collaborations. In Chapter 5, we compare the interfacial activity of homogeneous gold nanoparticles as in Chapter 3 with true Janus gold nanoparticles half functionalized by hexanethiol and half by 2-(2-mercapto-ethoxy)ethanol (MEE), where the former capping ligand acts as the hydrophobic one and the later one as the hydrophilic one. Both nanoparticles were also synthesized by Dr. Yang Song and Prof. Shaowei Chen. Thus, we can answer to the question: *Are Janus nanoparticles more interfacially active than homogeneous nanoparticles?*

In Chapter 6, we study in more depth silver Janus nanoparticles, including their interfacial dilatational rheology characterization. The nanoparticles studied in this chapter are composed of a larger 100-nm diameter silver core and 1-undecanthiol and 11-mercaptoundecanoic acid as hydrophobic and hydrophilic capping ligands, respectively, synthesized by our partner enterprise Icon Nanotech (Spain). In this case, we cannot ensure that they are true Janus nanoparticles since they are synthesized in a *one pot*-method that assumes that spontaneous separation of capping ligands occurs in bulk. For this reason, we refer to them as Janus-like nanoparticles.

The next step is to study the microstructure of the Janus nanoparticles at the interface. With this aim, in Chapter 7 we study systematically the interfacial activity and intend to relate it to the arrangement and orientation of the nanoparticles at the interface. This is performed by the direct measurement of contact angle at the water/decane interface of homogeneous 119 nm-diameter PMMA nanoparticles (purchased to Microparticles in Germany), 181 nm-diameter silica nanoparticles functionalized with methacryloxypropyltrimethoxysilane (synthesized by Dr. Jose

Ramos, from POLYMAT, Bionanoparticles Group, Applied Chemistry Department, Faculty of Chemical Sciences, University of País Vasco) and the 100 nm-diameter silver Janus-like nanoparticles studied in Chapter 6. We used the Freeze Fracture Shadow-Casting cryo-SEM technique, described in Chapter 4, during my 3 month research stay at the ETH-Zurich.

In order to study how the interfacial activity of the Janus nanoparticles is affected by their capping ligand constituents, in Chapter 8 we compare the interfacial activity, including the interfacial dilatational rheology, of the 3.5 nm-diameter gold Janus nanoparticles previously studied in Chapter 5 and similar gold Janus nanoparticles but with a shorter and more hydrophilic capping ligand (1,2-mercaptopropanediol). These nanoparticles were synthesized by Dr. Limei Chen, Dr. Christopher P. Deming and Prof. Shaowei Chen (Department of Chemistry and Biochemistry, University of California).

Next, in Chapter 9 we explored the role of the capping ligands of Janus gold nanoparticles of 13 nm and 23 nm-diameter half covered by polystyrene and half by polyethylene glycol. The role of the polymers is studied by comparing between homogeneous and Janus nanoparticles. Different spreading solvents used during deposition of the homogeneous and Janus nanoparticles at the pendant drop interface were explored: water, a mixture of water and chloroform and pure chloroform. All the nanoparticles were synthesized by Dr. Ana Maria Percebom, Dr. Juan Jose Giner Casares and Prof. Luis Liz-Marzan (CIC biomaGUNE in Donostia-San Sebastián), during the postdoctoral research stay of Dr. Percebom.

All the Janus nanoparticles mentioned before were composed of an inorganic core plus two different capping ligands. In Chapter 10, we study true Janus nanoparticles made of two hemispheres of different organic polymers with a wettability contrast: poly-tert-butylmethacrylate as the hydrophobic part and polymethylmethacrylate as the hydrophilic part. The homogeneous and Janus nanoparticles were synthesized by Electrohydrodynamic Co-Jetting conducted by Dr. Sahar Rahmani, Dr. Chris K. J. Yu, Dr. Charnelle A. Michel and Prof. Joerg Lahann at the Biointerfaces Institute in the University of Michigan. The problem with these nanoparticles was that they were synthesized using CTAB, a cationic surfactant, that made the nanoparticles cationic. The cationic nanoparticles are known to be polluted easily even with the negatively charged silicates of clean glass flasks.

Finally, in Chapter 11 we present the difficulties that we found when we tried to use a known theoretical model to fit our compression isotherms developed by Prof. Aveyard et al. (University of Hull, UK). We tried to publish this as a comment to his work but since it was first published in 2000, it was rejected. Nevertheless, we prefer to explain here the difficulties that we found to try to apply this model.

II Methodology

The universe is not required to be in perfect harmony with human ambition.

Carl Sagan

3 Interfacial activity of AuC6 nanoparticles using the pendant drop technique

Published in Journal of Colloid Science and Biotechnology, Volume 3, Number 2, 2014, Pages 184-187, ISSN 2164-9634, DOI: 10.1166/jcsb.2014.1084

M.A. Fernandez-Rodriguez[†], Y. Song[‡], M.A. Rodriguez-Valverde[†], S. Chen[‡], M.A. Cabrerizo-Vilchez[†] and R. Hidalgo-Alvarez[†,*]

[†] *Biocolloid and Fluid Physics Group, Applied Physics Department, Faculty of Sciences, University of Granada, 18071 Granada (Spain)*

[‡] *Department of Chemistry and Biochemistry, University of California, 1156 High Street, Santa Cruz, CA 95064 (USA)*

[*] *rhidalgo@ugr.es*

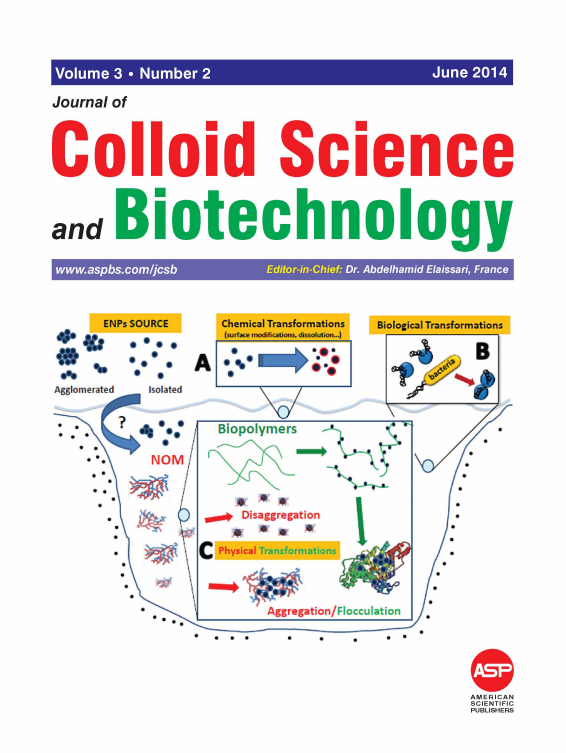

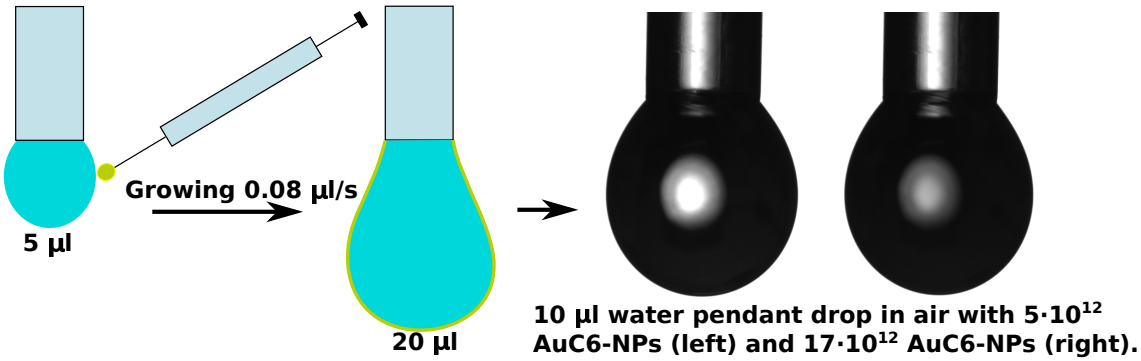

Figure 3.1: Graphical abstract.

Abstract

The structure and orientation of nanoparticles at the liquid-liquid interface may be useful for the preparation of robust, self-assembled structures, devices, and membranes. The pendant drop technique enables to study the interfacial activity of nanoparticles with smaller amounts and upon more controlled conditions than with the traditional Langmuir film balance technique. The pendant drop technique was applied to characterize the interfacial activity of $2\,nm$-diameter AuC6 nanoparticles. The AuC6 nanoparticles in tetrahydrofuran solution deposited at the water/air interface described a violent adsorption process as the tetrahydrofuran was evaporated. Growing and shrinking experiments for the water/air and water/decane interfaces enabled to explore the arrangement of the AuC6 nanoparticles at each interface. A simply scaled particle theory of hard disks model was in agreement with the experimental data.

Keywords: Pendant drop; Interfacial activity; Nanoparticles; Water/air interface; Water/oil interface.

3.1 Introduction

The Langmuir film balance is a technique widely used to study the arrangement and interfacial activity of nanoparticles at water/air and water/oil interfaces [1–3]. It is further used to synthesize nanoparticles with interfacial activity [4, 5]. On the other hand, the pendant drop tensiometer is usually used to characterize the diffusion of nanoparticles from bulk toward the interface [6, 7]. Due to the interface geometry and sample size in both techniques, the pendant drop technique enables to study the interfacial activity of nanoparticles with smaller amounts and upon more controlled conditions than with the traditional Langmuir film balance technique. Also, the pendant drop technique enables the study of interfacial dilatational rheology and subphase exchange when a coaxial double capillary is used [8].

Diffusion of alkanethiol-capped gold nanoparticles from the oil phase to the interface is studied by pendant drop technique due to the colloidal stability of these nanoparticles [6]. When the nanoparticle diameter is in the range of a few nanometers, the adsorption energy of the nanoparticles at the interface is of the order of k_BT, thus the nanoparticles are expected to leave the interface due to thermal fluctuations [6]. The pendant drop technique has been proven to study complex systems as Janus cylinders which exhibit strong interfacial activity with different adsorption regimes [7].

Direct deposition of nanoparticles at the interface of a pendant drop from a volatile solvent produces a violent process in which solvent evaporation helps the nanoparticles to be adsorbed at the interface faster than the slower process of diffusion from the bulk toward the interface [9]. Also, this procedure allows to precisely control the amount of nanoparticles that are deposited at the interface.

There are several models that intend to explain the behavior of the nanoparticles at liquid/liquid interfaces. The simplest attempt is the hard disk model in which the nanoparticles are modeled like hard entities placed at the interface. The nanoparticles behave as hard disks without interaction when there is room enough for every nanoparticle but become a close-packed arrangement when the area per nanoparticle is decreased [10]. Nevertheless, if the particles were charged, it should be considered the repulsion between like-charged particles [11]. On the other hand, Montecarlo simulations and experimental data of nanoparticles functionalized with large polymers exhibit a complex behavior compared to hard objects at liquid/liquid interfaces [12].

In this study, we characterized the interfacial activity of $2\,nm$-diameter gold nanoparticles capped with hexanethiol at the water/air and water/decane interfaces by the growing and shrinking pendant drop technique. The nanoparticles dispersed in a volatile solvent were directly deposited at the water/air interface using a microsyringe. The different arrangements of the nanoparticles at the interface were explored by changing the drop volume, thus the interface area available was changed for a fixed amount of nanoparticles.

3.2 Materials and Methods

3.2.1 Sample preparation

The Brust protocol [13] was used for the synthesis of gold homogeneous nanoparticles capped with hexanethiol (AuC6-NPs). Next, the fraction of $2\,nm$-diameter nanoparticles was selected by fractionation [4, 5]. The nanoparticles were redispersed in tetrahydrofuran (THF, Sigma Aldrich) and the final concentration was $1.7 \cdot 10^{12}$ AuC6-NPs per $1\,\mu l$ of THF solution.

3.2.2 Electrophoretic mobility

The electrophoretic mobility of the AuC6-NPs was measured with a Malvern Zetasizer Nano (Malvern) device. It was measured at $25\,^{\circ}C$ in MilliQ water $(-1.4 \pm 1.2) \cdot 10^{-8}\,m^2/(V \cdot$

s) and in sodium citrate (Sigma Aldrich) at $10^{-2}\,M$ concentration $(-1.1\pm0.7)\cdot10^{-8}\,m^2/(V\cdot s)$.

3.2.3 Growing and shrinking pendant drop

The pendant drop technique consists in increasing and decreasing the volume of a MilliQ water pendant drop with the AuC6-NPs deposited at the interface. Real time drop images are processed at each step of volume variation and the drop area and surface tension are calculated by Axysymmetric Drop Shape Analysis Profile (ADSA-P) [14]. The pendant drop technique can explore the interfacial activity of nanoparticles at the water/air and water/oil interfaces. In this study, the oil phase studied was decane (Sigma Aldrich). THF was used as spreading solvent and $5\,\mu l$ of THF deposited at a water pendant drop were fully evaporated (i.e. recovered the initial surface tension) after 350 s. For that reason, we waited twice this time to ensure that there was no presence of THF in all depositions.

Each pendant drop experiment involves two stages:

- First stage: deposition of the desired amount of AuC6-NPs in THF solution onto the surface of a $5\,\mu l$ MilliQ water pendant drop in air with a $5\,\mu l$ microsyringe (Hamilton) and a micropositioner (Fig. 3.2a). While the THF was evaporating, the volume of the pendant drop was slowly increased at $0.08\,\mu l/s$ up to the final $20\,\mu l$ volume and maintained until the surface tension was stable.
- Second stage: growing and shrinking the water/air or water/decane interface.
    * Water/air interface: the shrinking and growing volume rate was $0.08\,\mu l/s$ and the volume range was $20\mu l \leftrightarrow 10\mu l$, the shrinking was repeated 3 times and the growing twice (Fig.3.2b).
    * Water/decane interface: first the pendant drop was placed inside the oil phase but with a volume of $5\,\mu l$ to avoid the fall of the drop when it was immersed in the decane phase. Next the pendant drop was grown up to $30\mu l$ and the process was repeated like for water/air case but with drop volumes between $30\mu l \leftrightarrow 10\mu l$ (Fig.3.2c).

The surface pressure $\Pi = \gamma_0 - \gamma$, where γ_0 is the surface tension of the phase without nanoparticles and γ is the measured surface tension, is plotted against the area of the pendant drop divided by the deposited AuC6-NPs number. Due to the low hysteresis of the growing/shrinking cycles, within the order of resolution of the technique, the cycles were averaged for each AuC6-NPs concentration.

3.3 Results and Discussion

Growing and shrinking pendant drop experiments were performed for water/air and water/decane interfaces and for different AuC6-NPs concentrations directly deposited at the

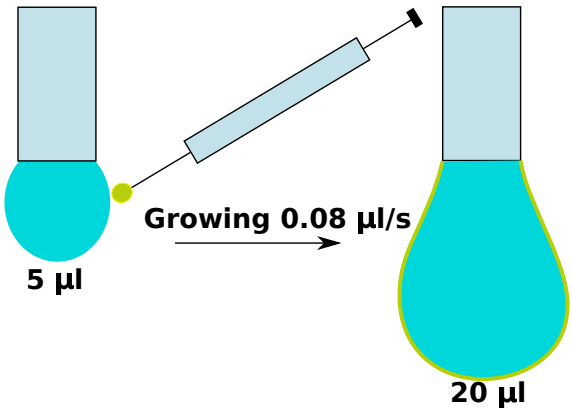

(a) Diagram of AuC6-NPs deposition at the surface of a initial $5\,\mu l$ MilliQ water pendant drop and subsequent growing at a $0.08\,\mu l/s$ rate and up to $20\,\mu l$.

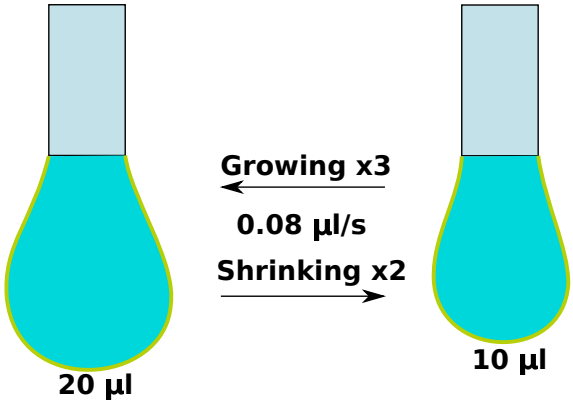

(b) Growing and shrinking pendant drop experiment in water/air interface between $20\mu l \leftrightarrow 10\mu l$ at a $0.08\,\mu l/s$ rate.

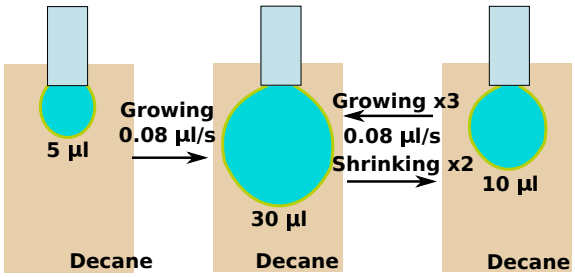

(c) Immersion of $5\,\mu l$ water pendant drop with AuC6-NPs deposited at the interface and growing and shrinking pendant drop experiment in water/decane interface between $30\mu l \leftrightarrow 10\mu l$ at a $0.08\,\mu l/s$ rate.

Figure 3.2: Diagram of deposition of AuC6-NPs at a water/air interface and subsequent growing and shrinking pendant drop experiments with water/air and water/decane interfaces.

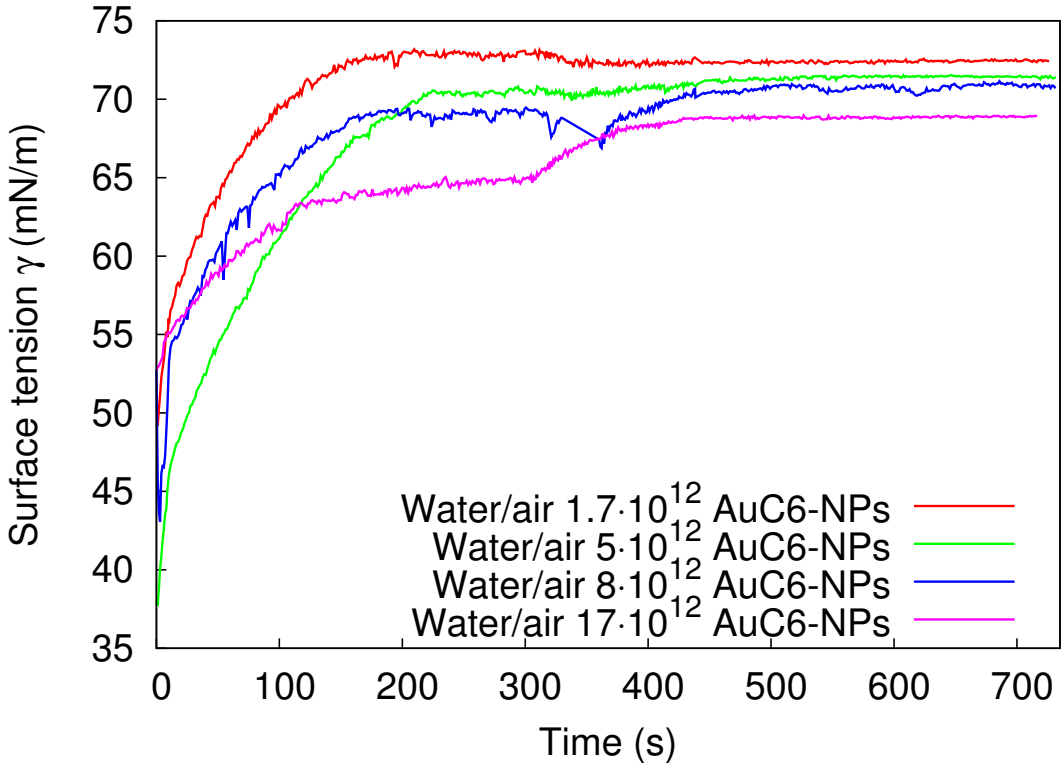

Figure 3.3: Surface tension against time when different number of AuC6-NPs in THF were deposited onto the MilliQ water pendant drop. The initial drop volume was $5\,\mu l$ and it grew at $0.08\,\mu l/s$ rate up to $20\,\mu l$. After the THF evaporation, the surface tension remained stable. The error due to the calculation of the surface tension from each pendant drop profile was in the range of $1\,mN/m$ and the room temperature was $25\,^{\circ}C$.

interface as described in the Section 3.2.3. For the first stage of the pendant drop experiments the surface tension was plotted against time for different AuC6-NPs concentrations in Fig. 3.3. After the deposition of the AuC6-NPs onto the initial $5\,\mu l$ water drop, the surface tension strongly decreased because of the surfactant effect of THF at the interface. After the THF evaporation the surface tension remained constant over time. A decrease in the final surface tension was observed as the AuC6-NPs concentration was increased for the same drop area (the area corresponding to a final $20\,\mu l$ pendant drop, as described in Section 3.2.3). It can also be noticed a change in the pendant drop opacity as the AuC6-NPs concentration was increased (see Fig. 3.4).

Although the $2\,nm$-diameter AuC6-NPs were expected to desorb from the interfaces due to thermal fluctuations [6], in our experiments the AuC6-NPs exhibited a significant and stable effect on the surface tension after the THF evaporation. Moreover, the surface tension was lower as the AuC6-NPs number was increased (see Fig. 3.3). These evidences are pointing out that the AuC6-NPs interface coverage is stable and that the thermal fluc-

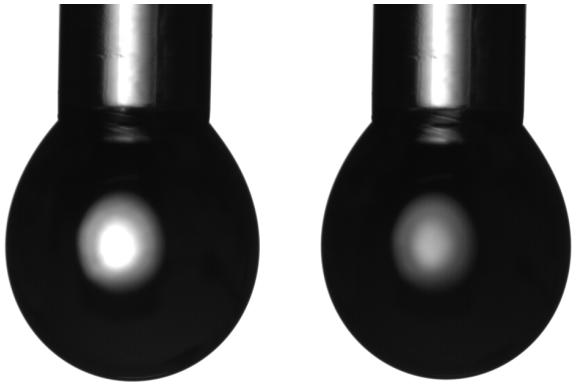

Figure 3.4: $10\,\mu l$ MilliQ water pendant drop in air with $\sim 5 \cdot 10^{12}$ AuC6-NPs (left) and $\sim 17 \cdot 10^{12}$ AuC6-NPs (right).

tuations are not forcing the AuC6-NPs to leave the water/air or water/decane interfaces.

Due to limitations in the area range coverage in a single growing and shrinking experiment, several growing and shrinking experiments were performed with different AuC6-NPs number at the interface in order to cover a wide range of AuC6-NPs per area of pendant drop. The surface pressure against the area per nanoparticle from the growing and shrinking pendant drop experiments are plotted in Fig. 3.5, for water/air and water/decane interfaces and for different AuC6-NPs concentrations.

The particles exhibited a near zero electrophoretic mobility (see Section 3.2.2). This affects to the models based in the repulsion between charged particles [11] which predict negligible surface pressures due to the low effective electric charge of the AuC6-NPs. Moreover, the relative short chains of the hexanethiol coverage of the AuC6-NPs are readily oriented rather than large polymers [12]. In fact, the simply scaled particle theory of hard disks model [10] (see Eq. 3.1) is in agreement with the experimental data for hard disks with $1\,nm$ diameter (see Fig. 3.5).

$$\Pi(A_{particle}) = \frac{k_B \cdot T}{A_{particle} \cdot \left(1 - \frac{\pi \cdot d^2}{4 \cdot A_{particle}}\right)^2} \tag{3.1}$$

Equation 3.1 is written in terms of surface pressure Π against the area per particle at the interface $A_{particle}$, where k_B is the Boltzmann constant, T is the temperature and d is the hard disk diameter. The agreement between experimental results and the simply scaled particle theory of hard disks model (Fig. 3.5) was good with $1\,nm$ diameter rather than $2\,nm$ diameter of the AuC6-NPs. This result may point out that not all the AuC6-NPs deposited at the interface were really adsorbed at it. If the actual amount of AuC6-NPs was lower, then there was necessary less available area to get a close-packed arrangement and thus the hard disk model provide a lower effective diameter.

The hard disk behavior can be explained because at low concentrations there is not significant effect on the surface tension and at high concentrations (i.e. lower area per particle) the particles are near close-packed. Although the final amount of AuC6-NPs at the interface might not be equal to the nominal value, the low hysteresis of growing and

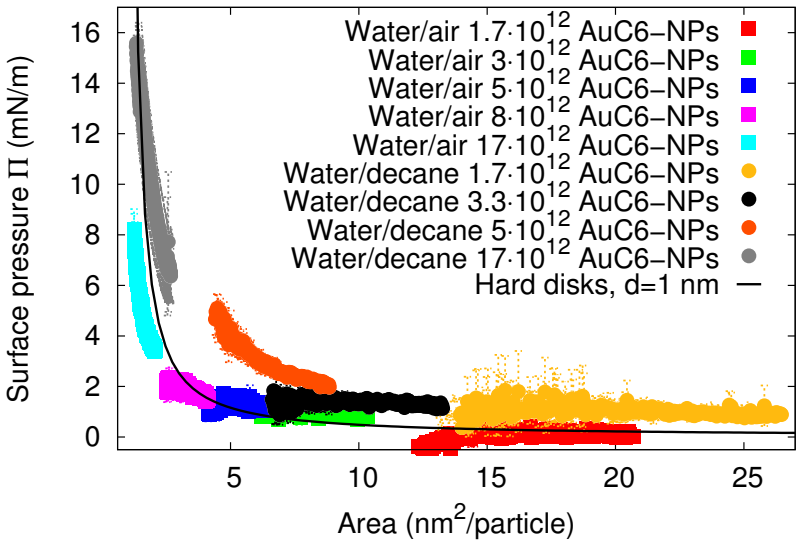

Figure 3.5: Surface pressure against the interface area of the pendant drop divided by the deposited AuC6-NPs number for water/air and water/decane interfaces and for different AuC6-NPs concentrations. The solid line is the hard disks model (Eq. 3.1) for disks of $1\,nm$ diameter.

shrinking experiments (see Section 3.2.3) might point out that the remaining AuC6-NPs at the water/air or water/decane interfaces are effectively anchored to the interface. At the water/air interface, the hydrophobic character of the hexanethiol coverage of the AuC6-NPs can explain that the AuC6-NPs were successfully adsorbed at the interface. Instead, at the water/decane interface, the gold core may act as the hydrophilic part of an amphiphilic nanoparticle that is placed at the interface.

3.4 Conclusions

The pendant drop technique was successfully used to characterize the interfacial activity of nanoparticles available in small amounts. The pendant drop technique was applied to $2\,nm$-diameter AuC6 nanoparticles at water/air and water/decane interfaces. The external deposition of the nanoparticles dispersed in tetrahydrofuran onto the water/air interface and the subsequent growing and shrinking experiments enabled to characterize the arrangement of the AuC6 nanoparticles at the interface, as the area per nanoparticle available on the pendant drop was changed. Finally, the results of surface pressure against area per AuC6 nanoparticle were in agreement with the simply scaled particle theory of hard disks model.

Acknowledgements

This study was supported by the by the "Junta de Andalucía" (projects P09-FQM-4698, P10-FQM-5977, P12-FQM-1443), the "Ministerio de Economía y Competitividad" (project MAT2011-23339) and by US National Science Foundation (DMR-0804049). Authors thank to Dr. J.A. Holgado-Terriza for the software Contacto© used for surface tension measurements.

References

[1] Detrich, Á.; Deák, A.; Hild, E.; Kovács, A. L.; Hórvölgyi, Z. Langmuir and Langmuir-Blodgett Films of Bidisperse Silica Nanoparticles. *Langmuir* **2010**, *26*, 2694–2699, DOI: 10.1021/la9027207.

[2] Kim, J. Y.; Raja, S.; Stellacci, F. Evolution of Langmuir Film of Nanoparticles Through Successive Compression Cycles. *Small* **2011**, *7*, 2526–2532, DOI: 10.1002/smll.201100290.

[3] Sashuk, V.; Hołyst, R.; Wojciechowski, T.; Fiałkowski, M. Close-packed monolayers of charged Janus-type nanoparticles at the air-water interface. *J. Colloid Interface Sci.* **2012**, *375*, 180–186, DOI: 10.1016/j.jcis.2012.02.057.

[4] Pradhan, S.; Brown, L.; Konopelski, J.; Chen, S. Janus nanoparticles: reaction dynamics and NOESY characterization. *J. Nanopart. Res.* **2009**, *11*, 1895–1903, DOI: 10.1007/s11051-008-9543-4.

[5] Pradhan, S.; Xu, L.; Chen, S. Janus Nanoparticles by Interfacial Engineering. *Adv. Funct. Mater.* **2007**, *17*, 2385–2392, DOI: 10.1002/adfm.200601034.

[6] Ferdous, S.; Ioannidis, M.; Henneke, D. Adsorption kinetics of alkanethiol-capped gold nanoparticles at the hexane-water interface. *J. Nanopart. Res.* **2011**, *13*, 6579–6589, DOI: 10.1007/s11051-011-0565-y.

[7] Ruhland, T. M.; Gröschel, A. H.; Walther, A.; Müller, A. H. E. Janus Cylinders at Liquid-Liquid Interfaces. *Langmuir* **2011**, *27*, 9807–9814, DOI: 10.1021/la201863x.

[8] Torcello-Gómez, A.; Jódar-Reyes, A.; Maldonado-Valderrama, J.; Martín-Rodríguez, A. Effect of emulsifier type against the action of bile salts at oil-water interfaces. *Food Res. Int.* **2012**, *48*, 140–147, DOI: 10.1016/j.foodres.2012.03.007.

[9] Garbin, V.; Crocker, J. C.; Stebe, K. J. Nanoparticles at fluid interfaces: Exploiting capping ligands to control adsorption, stability and dynamics. *J. Colloid Interface Sci.* **2012**, *387*, 1–11, DOI: 10.1016/j.jcis.2012.07.047.

[10] Santos, A.; López de Haro, M.; Yuste, S. An accurate and simple equation of state for hard disks. *J. Chem. Phys.* **1995**, *103*, 4622–4625, DOI: 10.1063/1.470649.

[11] Aveyard, R.; Clint, J.; Nees, D.; Paunov, V. Compression and Structure of Monolayers of Charged Latex Particles at Air/Water and Octane/Water Interfaces. *Langmuir* **2000**, *16*, 1969–1979, DOI: 10.1021/la990887g.

[12] Isa, L.; Amstad, E.; Schwenke, K.; Del Gado, E.; Ilg, P.; Kroger, M.; Reimhult, E. Adsorption of core-shell nanoparticles at liquid-liquid interfaces. *Soft Matter* **2011**, *7*, 7663–7675, DOI: 10.1039/C1SM05407D.

[13] Brust, M.; Walker, M.; Bethell, D.; Schiffrin, D. J.; Whyman, R. Synthesis of thiol-derivatised gold nanoparticles in a two-phase Liquid-Liquid system. *J. Chem. Soc., Chem. Commun.* **1994**, *7*, 801–802, DOI: 10.1039/C39940000801.

[14] Montes Ruiz-Cabello, F.; Rodriguez-Valverde, M.; Cabrerizo-Vilchez, M. Contact angle hysteresis on polymer surfaces: an experimental study. *J. Adhes. Sci. Technol.* **2011**, *25*, 2039–2049, DOI: 10.1163/016942410X544848.

To succeed, planning alone is insufficient. One must improvise as well.

Isaac Asimov, Foundation

4 Physicochemical characterization techniques and models

In this chapter we will describe the different techniques, procedures and models that we have used to characterize physicochemically homogeneous and Janus nanoparticles. In particular, the pendant drop tensiometry was an effective way to measure the interfacial activity of nanoparticles from very low amounts as usually the synthesis at the laboratory scale produces. The interfacial dilatational rheology enabled to study the interfacial properties under stress conditions. The Dynamic Light Scattering techniques were used to characterize the size and the electrostatic charge of the nanoparticles in bulk. The Freeze Fracture Shadow Casting Cryo-Scanning Electron Microscopy offered a microscopic view of the arrangement of the nanoparticles at the water/oil interfaces.

4.1 Pendant drop tensiometry and interfacial dilatational rheology

Part of the pendant drop tensiometry experiments were described in the previous Chapter 3. The experimental setup was completely designed and assembled by Prof. Miguel Angel Cabrerizo-Vilchez in the Biocolloid and Fluid Physics group at the University of Granada. The setup is formed by a Hamilton microinjector pump with a syringe of $250\,\mu L$ that inject and extract water to/from the capillary from a water reservoir, a capillary micropositioner, a light source, a camera and a micropositioner for the microsyringe used for deposition of the nanoparticle dispersion at the water/air interface (see Fig 4.1 and 4.2).

Previous to any measurement, optics has to be properly calibrated. First, the $pixel/cm$ ratio is extracted from a calibration mesh image taken with the camera (see Fig. 4.3a) where the mesh interspacing is $0.025\,cm$. Next, we take a picture of a plumb-line to correct any possible tilting of the camera and a picture of a bar immersed in decane to correct any refraction effect. With these calibrations and taking into account the differences between the densities of the water/air and

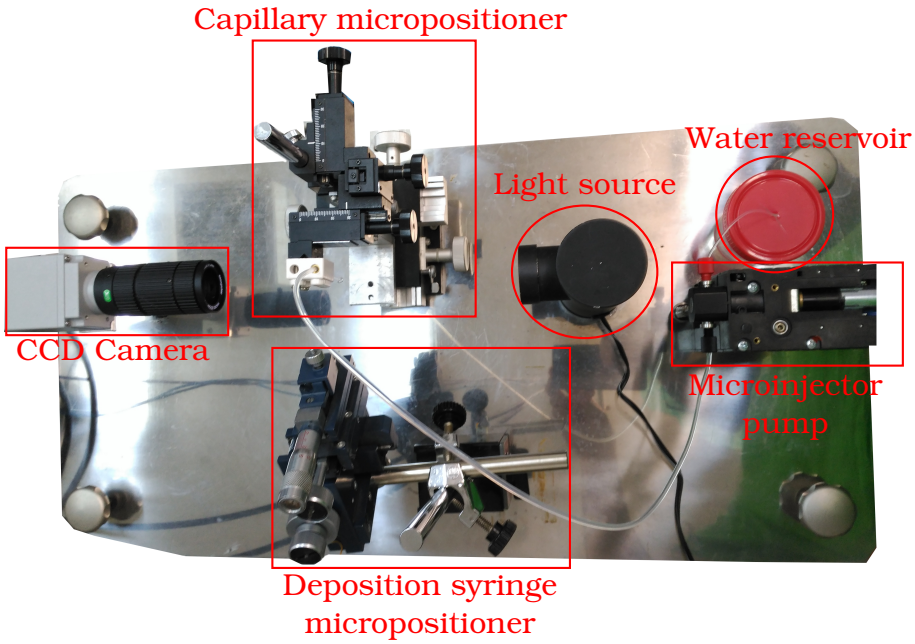

(a) Top view

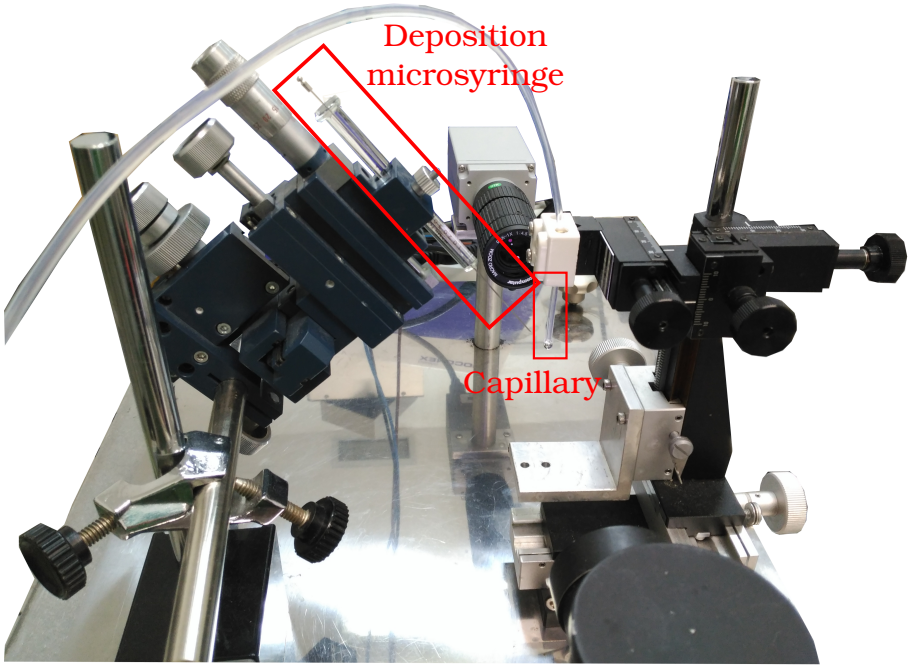

(b) Side view

Figure 4.1: (a) Top view and (b) side view of the pendant drop tensiometer. The setup was completely designed and assembled by Prof. Miguel Angel Cabrerizo-Vilchez in the Biocolloid and Fluid Physics group.

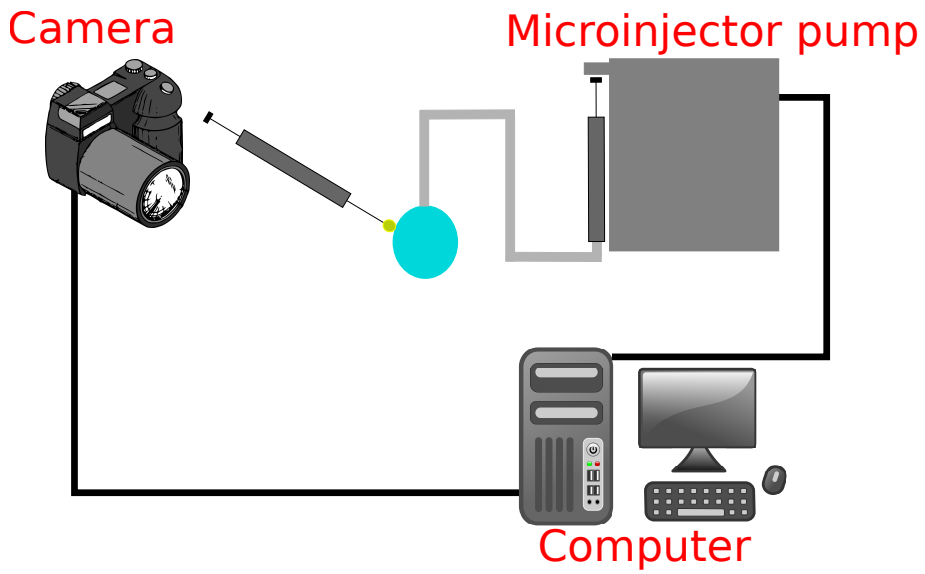

Figure 4.2: Pendant drop setup layout. The camera and the microinjector pump are controlled automatically by the computer. The camera and computer pictograms were downloaded from openclipart.org.

water/decane phases, we can start to measure surface (water/air) and interfacial (water/decane) tension. As explained in the previous Chapter 3, all experiments begin with the deposition of nanoparticle dispersion at the water/air pendant drop interface. If a spreading solvent is used, then we must monitor the evaporation of the solvent. Next, to measure the water/decane interface, the pendant drop is immersed in a decane filled cuvette as in Fig. 4.3b.

The software Dinaten© created by Dr. Juan Antonio Holgado-Terriza and Prof. Miguel Angel Cabrerizo-Vilchez in the Biocolloid and Fluid Physics group is used to manage the microinjector pump and to perform processes in which the pendant drop volume is maintained constant during solvent evaporation, the growing and shrinking cycles and the dilatational rheology experiments. Also this software controls the image acquisition and computes in real time the interfacial tension, volume and area of the pendant drop and other control parameters as can be seen in Fig. 4.4a. Once that the pictures are stored, we can perform different analysis with the software Contacto© made by Dr. Juan Antonio Holgado-Terriza and Prof. Miguel Angel Cabrerizo-Vilchez in the Biocolloid and Fluid Physics group, such as the fitting of the Laplacian curve to the pendant drop interface and rheology calculations, as can be seen in Fig. 4.4b. Both softwares are based on the algorithm Axisymmetric Drop Shape Analysis-Profile (ADSA-P). This method assumes that the pendant drop is axisymmetric and solves the Young-Laplace equation using the profile of the pendant drop [1]:

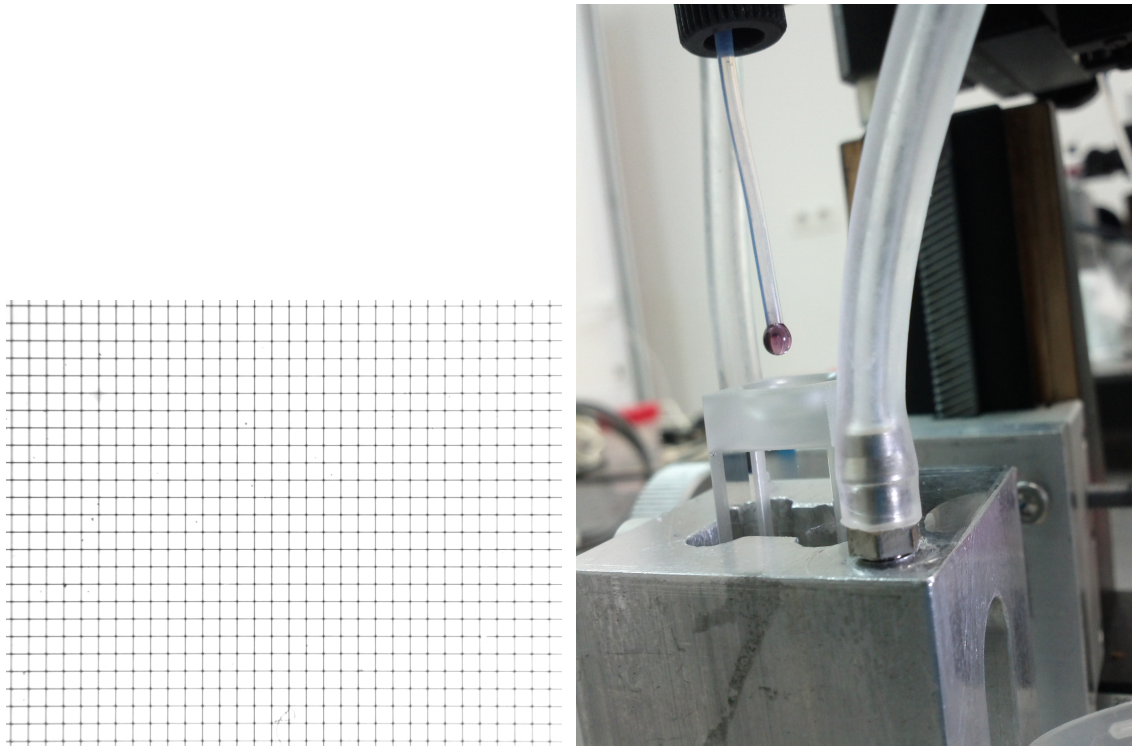

(a) (b)

Figure 4.3: (a) Image (1280x1024 pixels) of the calibration mesh of $0.025\,cm$ and (b) water pendant drop of $10\,\mu L$ with deposited gold Janus nanoparticles just before the immersion in the decane filled cuvette.

$$\Delta P = \gamma \left(\frac{1}{R_1} + \frac{1}{R_2} \right) \tag{4.1}$$

where ΔP is the pressure difference along the interface, γ is the unknown surface/interfacial tension and R_1 and R_2 are the principal curvature radii.

4.1.1 Low interfacial tension pendant drop tensiometry

The ADSA-P method works fine when there is an effective counterbalance of the gravity force and the surface or interfacial tension. Thus, there are two extreme cases in which the pendant drop tensiometry fails, when the pendant drop is small, the gravity is not so significant and the drop shape is nearly a hemisphere. On the other hand, there is a maximum pendant drop weight that a given capillary can support, where the gravity effect exceeds the surface or interfacial tension and the drop falls. In Fig. 4.5 it can be seen that for the first "small" capillary that we used, the range in which ADSA-P works is between 10 and $20\,\mu L$ for water/air and up to $30\,\mu L$ for water/decane interfaces. Comparing the surface or interfacial tension γ to the drop volume and the expected values for pure water/air ($\sim 72.5\,mN/m$) and water/decane interfaces ($\sim 52.3\,mN/m$). This volume range changes as the surface or interface tension is lower, displacing to lower volumes because the maximum pendant drop volume decreases.

This setup was useful for the first nanoparticles that we explored, but the nanoparticles studied in Chapter 7 and the following Chapters were very interfacially active and the pendant drop fell off even for very low volumes such as $10\,\mu L$. For this reason, we changed the initial "small" capillary by a "bigger" capillary with a "hat" or pedestal (see Fig. 4.6) that enabled to extend the pendant drop volume range to 15 and $45\,\mu L$ for both water/air and water/decane interfaces.

4.1.2 Interfacial dilatational rheology

The growing and shrinking cycles mentioned in Chapter 3 are performed at the lowest microinjection speed possible of $0.08\,\mu L/s$. This experiment at fixed low injection/extraction speed does not cover the possible dependence with the injection speed. In fact, if we perform growing and shrinking experiments by using a sinusoidal oscillating volume at different speeds, we end up with an attenuation and a phase shift between the volume input of microinjector and the surface or interfacial tension output. These attenuation and phase shift account for a relaxation process where a dilatational elastic E modulus can be defined as [2]:

$$E = E_d + \omega \eta_d \tag{4.2}$$

where E_d is the interfacial dilatational elasticity as storage part, $\omega = 2\pi\nu$ is the angular speed of the sinusoidal oscillation of frequency ν and η_d is the interfacial

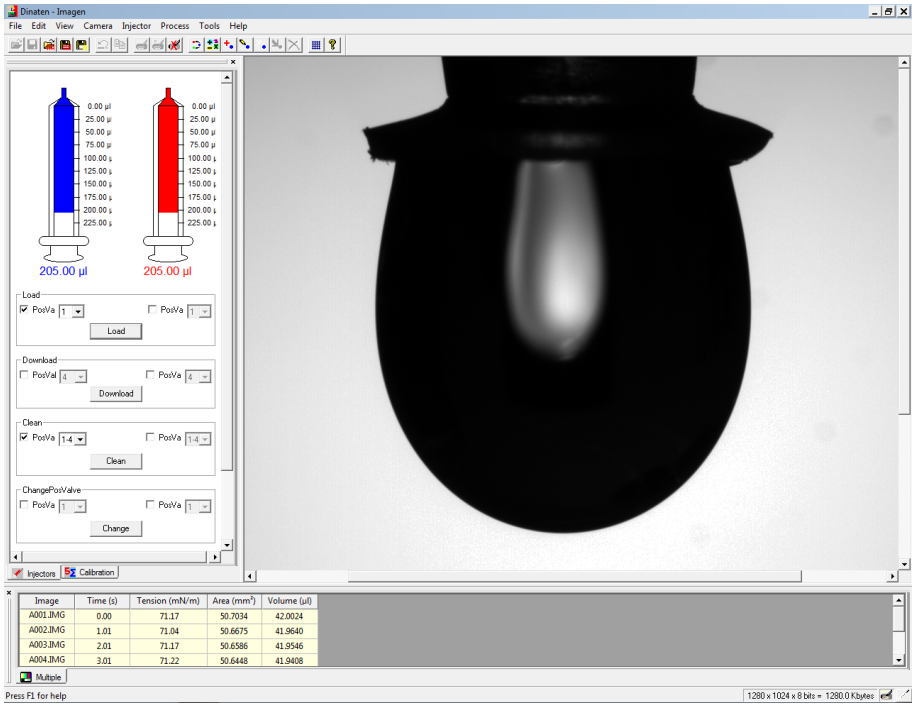

(a) Dinaten software

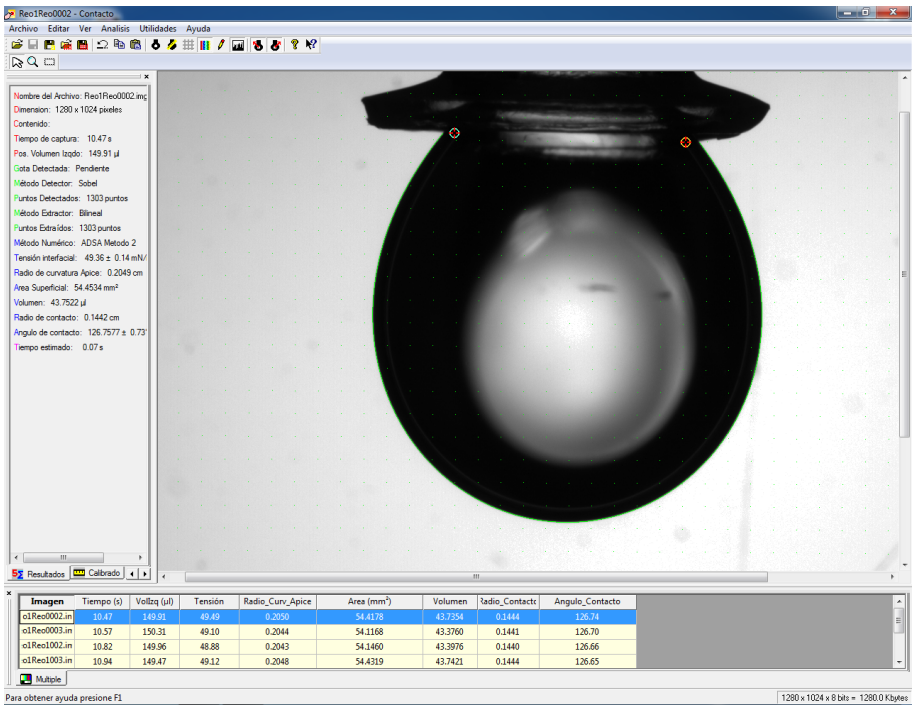

(b) Contacto software

Figure 4.4: (a) Water/air pendant drop in Dinaten©, the software to control the microinjector and the picture acquisition and with ADSA-P real time calculation and (b) water/decane pendant drop in Contacto©, the software to finely control the ADSA-P fitting and more complex calculations as the dilatational rheology parameters.

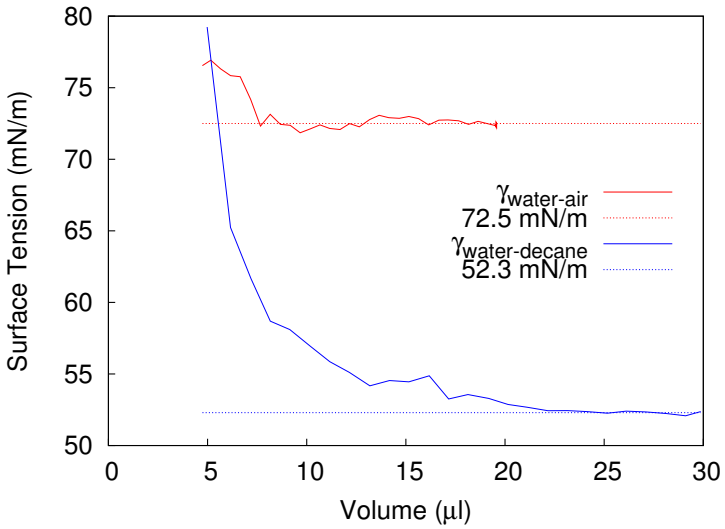

Figure 4.5: Surface and interfacial tension of a growing water pendant drop in air (red) and decane (blue) against the volume of the pendant drop. The horizontal lines correspond to the expected values of pure water/air and water/decane interfaces, respectively.

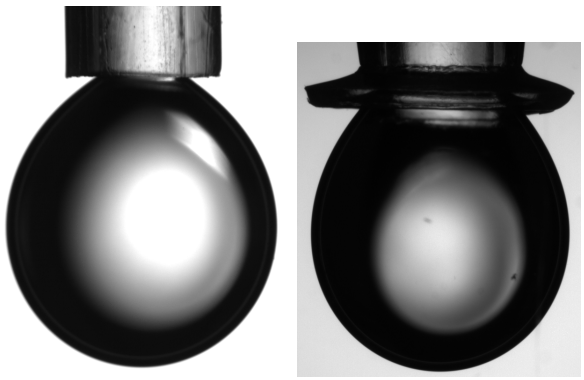

(a) "Small" capillary (b) "Big" capillary

Figure 4.6: (a) "Small" capillary with a $20\,\mu L$ water pendant drop (1.55 mm external diameter) and (b) "big" capillary with a $45\,\mu L$ water pendant drop, both immersed in decane (2.8 mm and 4.2 mm external diameters for the capillary and the cap, respectively). Both capillaries are made of polytetrafluoroethylene. Note that the magnification of both pictures is different.

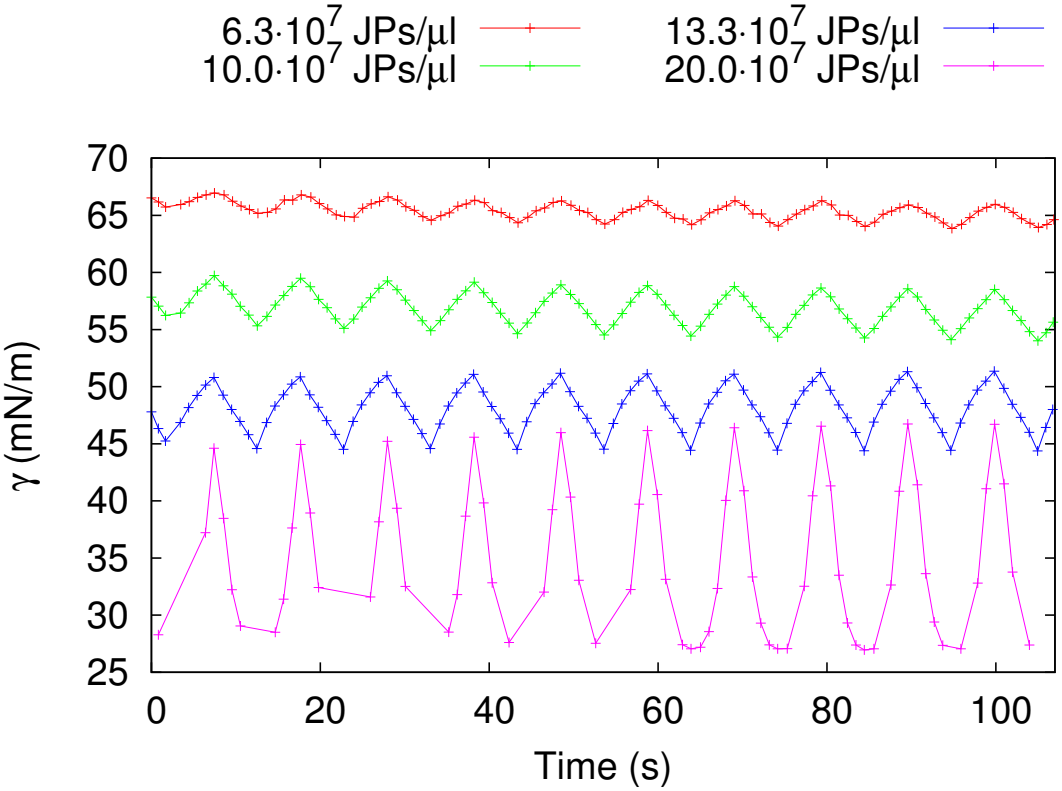

Figure 4.7: Interfacial tension response to the sinusoidal volume oscillation. The mean value decreases and the amplitude increases as the number of interfacially active nanoparticles per volume of drop increases.

dilatational viscosity accounting for the loss part. In Fig. 4.7, we plot the sinusoidal form of increasing concentrations of interfacially active nanoparticles, as the number of particles increases, the mean interfacial tension decreases and the amplitude increases as the interfacial tension changes much more for the same volume oscillation.

For example, an usual behavior when the E_d modulus is very high is that the pendant drop is shaped as a "pacifier" when the volume extracted is high enough. In Fig. 4.8 we illustrate this behavior. This corresponds to a really high E_d modulus and we refer to it in the following Chapters as an "elastic shell" behavior.

4.2 Cleaning procedure

Given that the presence of any agent with interfacial activity would hinder the effect of the homogeneous and Janus nanoparticles at interfaces, we need to be sure that no surfactant nor unknown pollutant are present in our experiments. This is assured by following several actions:

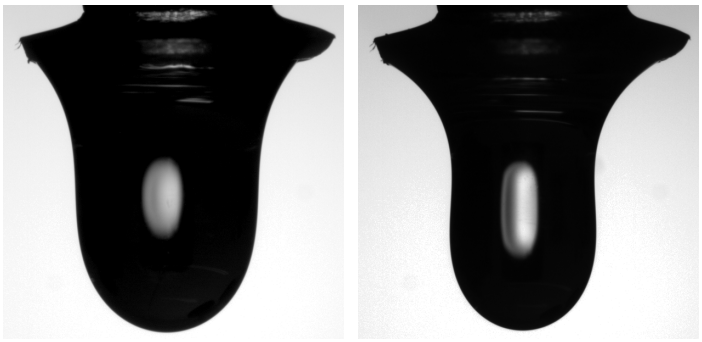

(a) $20\,\mu L$ (b) $15\,\mu L$

Figure 4.8: Water/air pendant drops with nanoparticles with high interfacial activity of (a) $20\,\mu L$ and (b) after extraction of $5\,\mu L$.

- The dispersion to characterize must be surfactant-free. This is specially critical because certain Janus nanoparticles are synthesized by emulsion processes in which surfactants are needed. We discarded those nanoparticles.

- The chemicals and specially the spreading agents must be of HPLC grade. To detect any impurity, we measured the surface tension of the pure solvent (see Fig. 4.9). We have used chloroform ($CHCl_3$), tetrahydrofurane (THF), methanol, methanol+propanol and MilliQ water as spreading solvents.

- When an organic solvent is used, the flasks must be of glass and with $CHCl_3$ and THF even the caps and the microsyringes must be made of glass as in Fig. 4.10. This was specially critical with centrifugation, because we had to restrict to glass tubes. However, the use of glass flasks was a bad choice for cationic nanoparticles as explained in Chapter 10.

- All glassware was cleaned as the following protocol: washing with Micron 90, rinsing with tap water, distilled water, 2-propanol, distilled water and finally MilliQ water. The glassware was left to dry in an oven or at room temperature because drying with N_2 actually increased pollution.

- All pendant drop tensiometry measurements were performed in an isolated room with controlled temperature. We used Kimtech paper towels that do not release fibers when used on the capillary of the pendant drop tensiometer.

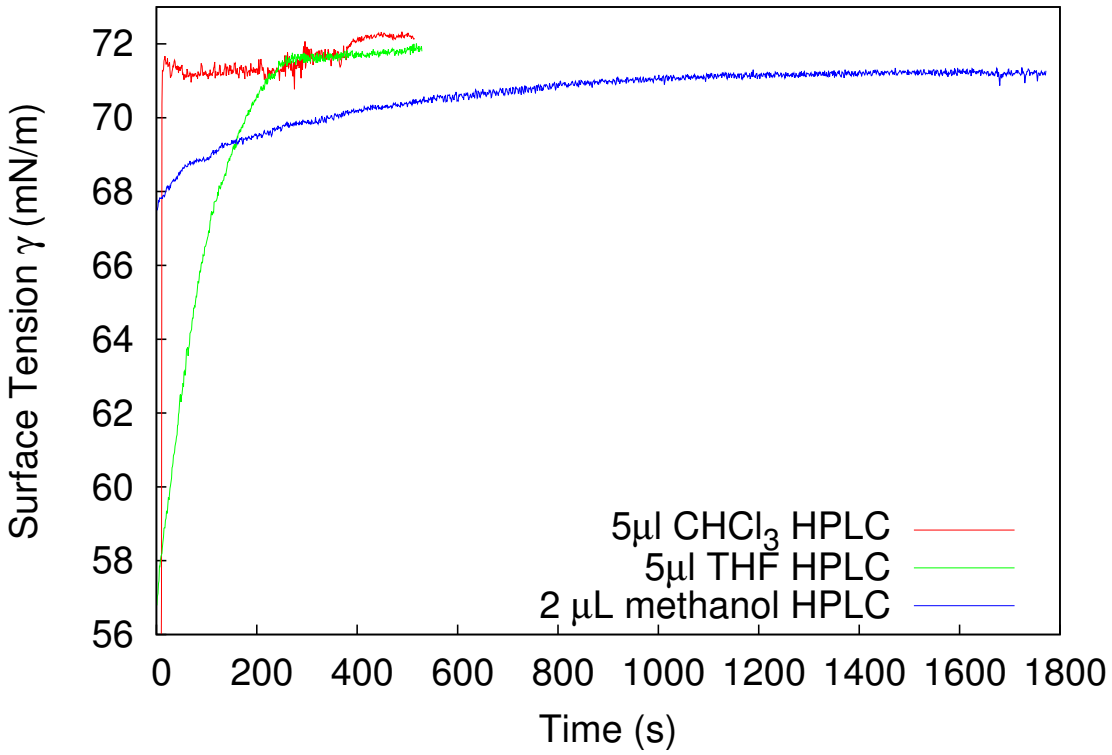

Figure 4.9: Interfacial tension evolution over time when different HPLC-grade solvents are deposited at the interface. The $CHCl_3$ fully evaporates for the first seconds, the THF needs less than $300\,s$ to be fully evaporated and the methanol up to $30\,min$ but the interfacial tension is slightly lower than the pure water/air interface, probably due to the azeotropes formed between methanol and water.

(a) Glass flask (b) Glass microsyringes

Figure 4.10: (a) Glass flasks and (b) glass microsyringes used with the organic spreading solvents, such as $CHCl_3$ and THF.

4.3 Dynamic Light Scattering

The Malvern Zeta Sizer Nano Z is a device based on Dynamic Light Scattering enables to measure the size and electrophoretic mobility of a nanoparticle water dispersion. The basic principle is a light source that produces light scattering when passes through a colloidal dispersion. The mean value of the intensity $I(q,t)$ collected upon a given wave number q respect to the incident light beam and time t is given by:

$$\langle I(q)\rangle = \lim_{T\to\infty}\frac{1}{T}\int_0^T I(q,t')dt' \tag{4.3}$$

and the autocorrelation function $G_I(q,\tau)$ at a time τ is given by:

$$G_I(q,\tau) \equiv \langle I(q,t)I(q,t+\tau)\rangle = \lim_{T\to\infty}\frac{1}{T}\int_t^{t+T} I(q,t')I(q,t'+\tau)dt' \tag{4.4}$$

where $G_I(q,\tau) \approx \langle I(q,t)^2\rangle$ when $\tau \to 0$ and $G_I(q,\tau) \approx \langle I(q,t)\rangle^2$ when $\tau \to \infty$. If we normalize $g_I(q,\tau) = \dfrac{G_I(q,\tau)}{\langle I(q,t)\rangle^2}$, we can write the Siegert relation [3] as:

$$g_I(q,\tau) \equiv 1 + \beta\left|g_E(q,t)\right|^2 \tag{4.5}$$

where β is a constant depending on the device optics and $g_E(q,t)$ is the normalized correlation function of the electric field, rather than the intensity of the light. For monodisperse, independent and identical particles, the expression becomes:

$$g_E(q,t) = e^{-\frac{q^2}{6}\langle\Delta R^2(t)\rangle} \tag{4.6}$$

where the mean squared displacement for Brownian motion is $\langle\Delta R^2(t)\rangle = 6D_0t$, and the Stokes-Einstein diffusion constant is $D_0 = \dfrac{k_BT}{6\pi\eta r_h}$, where η is the viscosity of the solvent and r_h is the hydrodynamic radius of the particles.
The Malvern NanoSight device is based on the same principle than Nano Z but it measures the particles one by one, from the diffraction of individual nanoparticles and measuring their individual tracks. From these measurements the mean squared displacement is obtained and the size is calculated similarly to the aforementioned (see Fig. 4.11). It is worth to mention that the hydrodynamic radius is always higher than the radius extracted from HRTEM and SEM pictures because it accounts for the effective radius of the moving particle immersed in the water dispersion bulk.

The electrophoretic mobility is also measured with the Malvern Zeta Sizer Nano Z from the gold plates that are available in the sample cuvette. An external electric

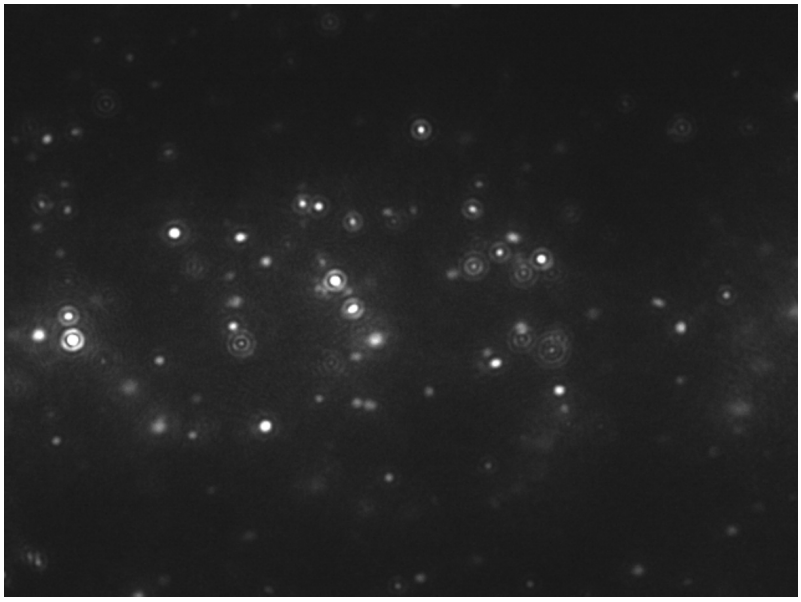

(a) Diffraction of nanoparticles

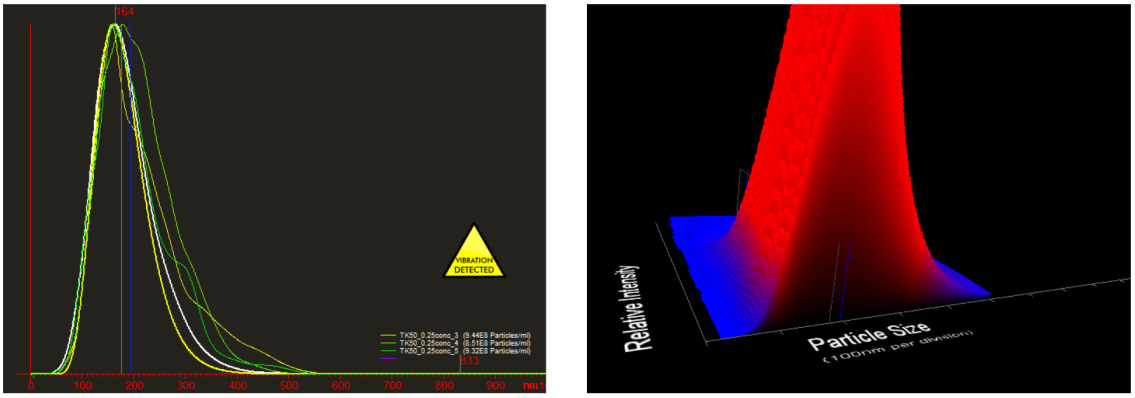

(b) Particle size distribution

Figure 4.11: (a) Frame of a movie in which the nanoparticles are tracked in the Malvern NanoSight and (b) size distribution of the nanoparticles in (a).

field $\overrightarrow{E}$ is applied to the cuvette through the gold plates and the charged nanoparticles move according to:

$$\overrightarrow{v}_e = \mu_e \overrightarrow{E} \tag{4.7}$$

where μ_e is the electrophoretic mobility and $\overrightarrow{v}_e$ can be extracted from the mean squared displacement as mentioned above subtracting the Brownian motion.

4.4 Freeze Fracture Shadow Casting Cryo-Scanning Electron Microscopy

One problem when we perform an interfacial activity characterization from macroscopic techniques like the pendant drop tensiometry is that there is no information on the orientation/microstructure of the nanoparticles placed at the interface. During my visit at the Interfaces, Soft Matter and Assembly Laboratory at the ETH-Zurich under the supervision of Prof. Lucio Isa, we were able to measure directly the contact angle of the nanoparticles at the water/decane interface as discussed in Chapter 7. We used a novel technique developed by Prof. Lucio Isa [4] which consisted in the following steps summarized in Fig. 4.12:

- Filling $1\,mm$ square copper wells and copper caps with the water particle dispersion and decane (see Fig 4.13a).
- Jet freezing the wells with propane to vitrify the sample (see Fig 4.13b).
- The vitrified sample is inserted in a vacuum device which splits the well into two and the sample fractures by the interface, keeping the nanoparticles at the interface and the hollows in the other phase (see Fig 4.13c).
- In this same step, inside the device, a tungsten filament is turned on and a thin tungsten layer is deposited over the interface at $30°$.
- The sample is then examined under cryo-SEM (see Fig 4.13c).

At all steps the sample must be placed in a special arm filled with liquid nitrogen. When the tungsten layer is deposited at $30°$, the nanoparticles act as masks and produce a shadow of tungsten behind them. From the size of this shadow and the nominal size of the nanoparticle, it can been obtained the direct contact angle as explained in Fig. 4.12.

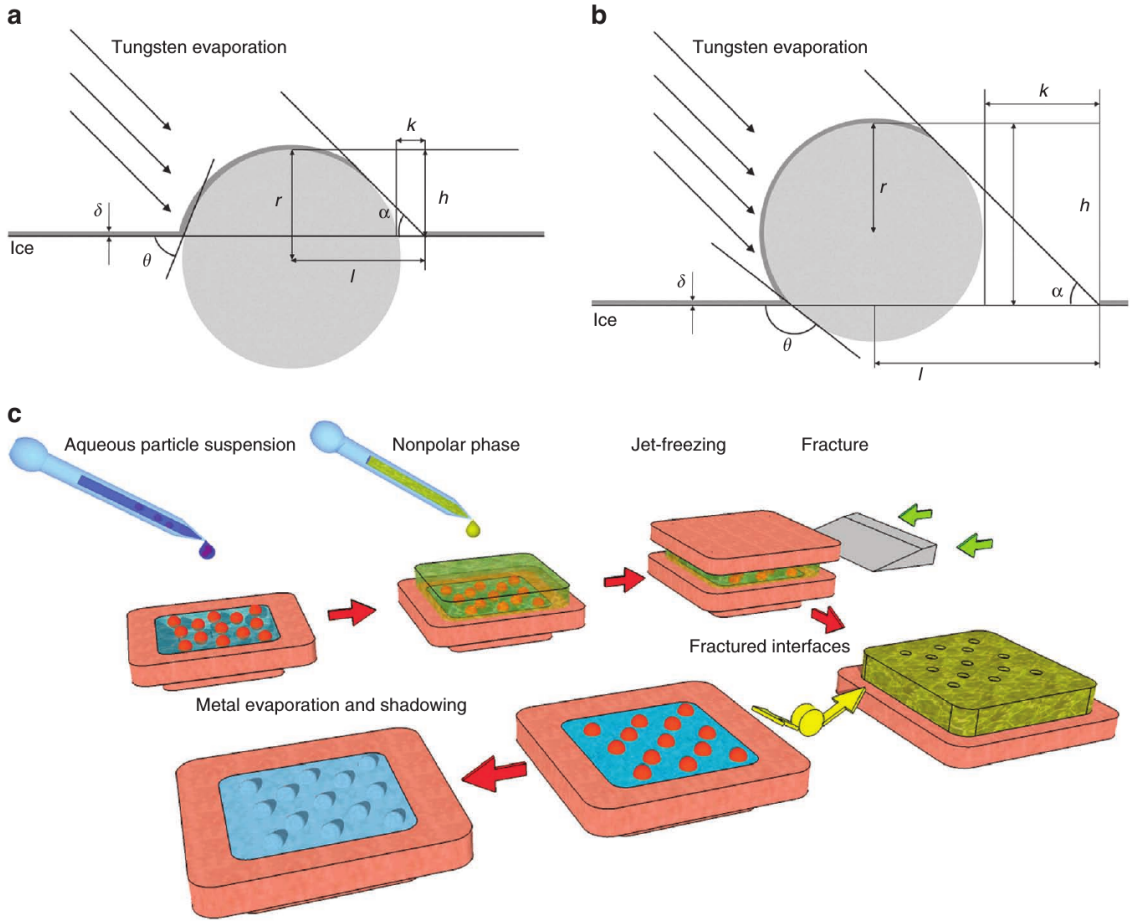

Figure 4.12: Representation of (a) a hydrophilic and (b) a hydrophobic nanoparticle of radius r at the ice interface after metal evaporation. The three-phase contact angle θ, the metal deposition angle α and thickness δ, the height h of the particle relative to the interface, its projection l along the metal deposition direction and the length of the shadow k are highlighted. (c) Scheme of the sample preparation for FreSCa cryo-SEM imaging. Reprinted from [4] with permission of Nature Publishing Group.

(a) $1\,mm$ copper wells

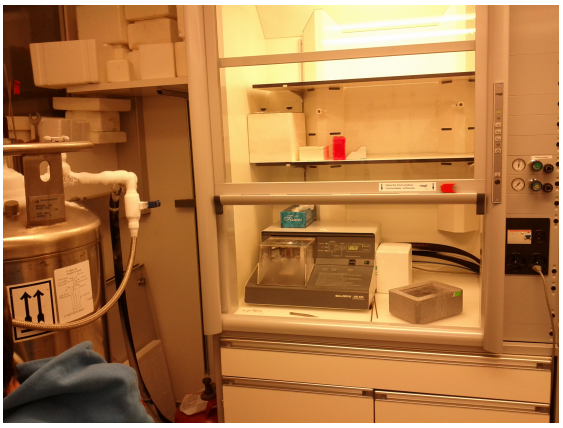

(b) Propane jet freezer

(c) Freeze-fracture device

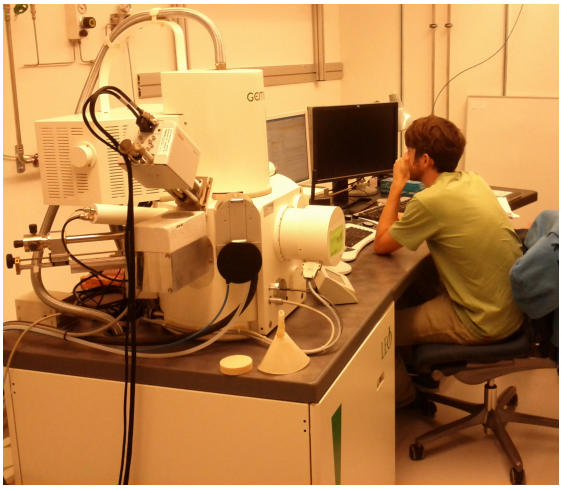

(d) Cryo-SEM

Figure 4.13: (a) Prof. Lucio Isa preparing the $1\,mm$ copper wells with the nanoparticle water dispersion and decane. (b) Propane jet freezer to vitrify the sample. In (c) the pre-cooled freeze-fracture device at $-140°C$ (Bal-Tec/Leica BAF060) where the tungsten coating occurs. In (d) Prof. Lucio Isa examines the samples with cryo-SEM.

4.5 Theoretical models for compression isotherms

One of the main results of our pendant drop tensiometry experiments is a piecewise-like compression isotherm in which interfacial pressure Π is plotted against the area per particle (area of the pendant drop divided by the number of deposited nanoparticles) or the normalized area (area of the pendant drop divided by the area of all nanoparticles as if they were forming an hexagonal compact monolayer). One characteristic of these experiments is that typically the range of volume and area that can be sweeped is not enough to cover the whole compression isotherm as in typical Langmuir balance experiments [5]. Thus, in order to extract any information about the compression isotherm it is needed to find the envelope curve. We first used the Aveyard's model [6] which resulted in nanoparticle charges too high (several orders of magnitude of the expected charge). For this reason we tried to use the data in his paper: "Compression and Structure of Monolayers of Charged Latex Particles at Air/Water and Octane/Water Interfaces" [6] to test his model on his own data. We obtained meaningless particle charge values as described in Chapter 11. We tried to contact Prof. Aveyard unsuccessfully and as a result we wrote a comment to his work submitted to Langmuir journal that was rejected because this work was published in year 2000.

After no reply from Prof. Aveyard, finally we got a reply from Prof. Kralchevsky who expanded the work of Aveyard in "Surface Pressure Isotherm for a Monolayer of Charged Colloidal Particles at a Water/Nonpolar-Fluid Interface: Experiment and Theoretical Model Interface: Experiment and Theoretical Model" in 2014 [7]. Even though he warned us: "q is the charge in CGSE units, as in the Aveyard's formulas", using CGSE units was also unsuccessful.

On the other hand, we applied successfully the hard disk model of Santos et al. [8] to our piecewise-like compression isotherm of homogeneous gold nanoparticles as described in Chapter 3. Moreover, the Frumkin model which adds a second term to the hard disk equation describing the interaction between the particles at the interface [9] succeeded for our piecewise-like compression isotherm of silver Janus-like nanoparticles in Chapter 6.

References

[1] Rodríguez-Valverde, M.; Cabrerizo-Vílchez, M.; Rosales-López, P.; Páez-Dueñas, A.; Hidalgo-Álvarez, R. Contact angle measurements on two (wood and stone) non-ideal surfaces. *Colloid. Surface. A* **2002**, *206*, 485–495, DOI: 10.1016/S0927-7757(02)00054-7.

[2] Powell, K. C.; Chauhan, A. Interfacial Tension and Surface Elasticity of Carbon Black (CB) Covered Oil-Water Interface. *Langmuir* **2014**, *30*, 12287–12296, DOI: 10.1021/la503049m.

[3] Callejas Fernández, J.; Tirado Miranda, M.; Quesada Perez, M.; Odriozola, G.; Schmitt, A. In *Encyclopedia of surface and colloid science*, Somasundaran, P., Ed.; CRC Press: 2006, pp 4072–4089.

[4] Isa, L.; Lucas, F.; Wepf, R.; Reimhult, E. Measuring single-nanoparticle wetting properties by freeze-fracture shadow-casting cryo-scanning electron microscopy. *Nat. Commun.* **2011**, *2*, DOI: 10.1038/ncomms1441.

[5] Sashuk, V.; Holyst, R.; Wojciechowski, T.; Fialkowski, M. Close-packed monolayers of charged Janus-type nanoparticles at the air-water interface. *J. Colloid Interface Sci.* **2012**, *375*, 180–186, DOI: 10.1016/j.jcis.2012.02.057.

[6] Aveyard, R.; Clint, J.; Nees, D.; Paunov, V. Compression and Structure of Monolayers of Charged Latex Particles at Air/Water and Octane/Water Interfaces. *Langmuir* **2000**, *16*, 1969–1979, DOI: 10.1021/la990887g.

[7] Petkov, P. V.; Danov, K. D.; Kralchevsky, P. A. Surface Pressure Isotherm for a Monolayer of Charged Colloidal Particles at a Water/Nonpolar-Fluid Interface: Experiment and Theoretical Model. *Langmuir* **2014**, *30*, 2768–2778, DOI: 10.1021/la500126d.

[8] Santos, A.; López de Haro, M.; Yuste, S. An accurate and simple equation of state for hard disks. *J. Chem. Phys.* **1995**, *103*, 4622–4625, DOI: 10.1063/1.470649.

[9] Rusanov, A. I. New theory of equation of state for surface monolayer. *J. Chem. Phys.* **2004**, *120*, 10736–10747, DOI: 10.1063/1.1737301.

III Results and Discussion

If you wish to make an apple pie from scratch, you must first invent the universe.

Carl Sagan

5 Comparison of the Interfacial Activity between Homogeneous and Janus Gold Nanoparticles by Pendant Drop Tensiometry

Published in Langmuir, Volume 30, Issue 7, 2014, Pages 1799-1804, ISSN 0743-7463, DOI: 10.1021/la404194e

M.A. Fernandez-Rodriguez[†], Y. Song[‡], M.A. Rodriguez-Valverde[†], S. Chen[‡], M.A. Cabrerizo-Vilchez[†] and R. Hidalgo-Alvarez[†,*]

[†] *Biocolloid and Fluid Physics Group, Applied Physics Department, Faculty of Sciences, University of Granada, 18071 Granada (Spain)*

[‡] *Department of Chemistry and Biochemistry, University of California, 1156 High Street, Santa Cruz, CA 95064 (USA)*

[*] *rhidalgo@ugr.es*

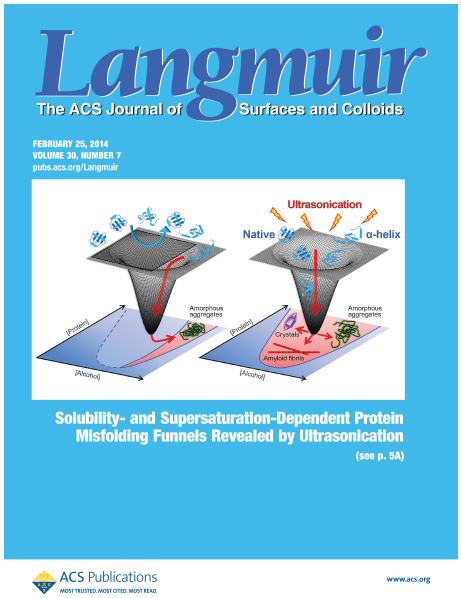

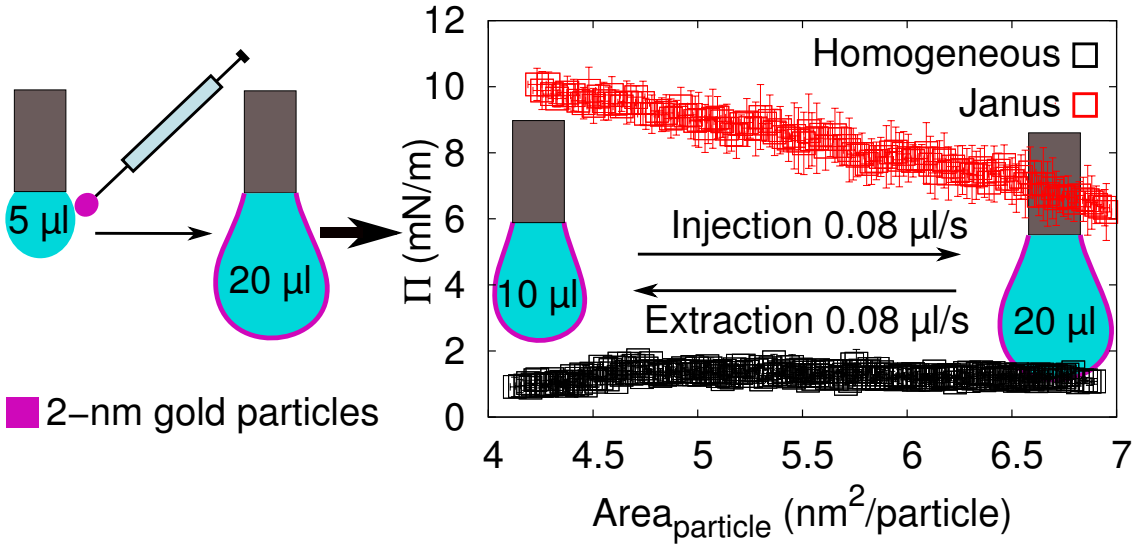

Figure 5.1: Graphical abstract.

Abstract

The interfacial activity of 3.5 nm homogeneous (HPs) and amphiphilic Janus gold nanoparticles (JPs) was characterized by pendant drop tensiometry for water/air and water/decane interfaces. This technique requires a smaller quantity of nanoparticles than the traditional Langmuir balance technique. The direct deposition at the interface of the nanoparticles dispersed in a spreading solvent also requires smaller quantities of sample than does adsorption from the bulk. From the growing and shrinking of the pendant drops, the interfacial activity of the nanoparticles can be evaluated and compared within a wide range of area per particle. In this work, the JPs exhibited a higher interfacial activity than did the HPs in all cases. A hard disk model fits the piecewise compression isotherm of the HPs, yet this model underestimates the interactions between the JPs adsorbed at the interface.

Keywords: Janus gold nanoparticle; Interfacial activity; Water/air interface; Water/oil interface; Pendant drop tensiometry.

5.1 Introduction

Janus nanoparticles are anisotropic colloidal entities with two regions of different physicochemical properties. This anisotropy can lead to the spontaneous self-assembly of nanoparticles or can be responsive to an external stimulus such as a magnetic or electric field, pH or temperature gradients, and so forth [1, 2]. Depending on the particular

anisotropy of the nanoparticles, they cover a wide range of applications such as biosensors [2], drug delivery and immunotherapy [3], water-repellent textiles [4] and nanoparticles that become aligned in an external electric or magnetic field [5–7].

Janus nanoparticles with a wettability anisotropy can be used to stabilize Pickering emulsions. Unlike homogeneous nanoparticles, amphiphilic Janus nanoparticles can exhibit a high interfacial activity regardless of the degree of amphiphilicity because of the spatial separation of the different wettability regions [8]. Thus, amphiphilic Janus-like gold nanoparticles functionalized with thiol-terminated poly(ethylene glycol) chains and short alkane thiols have been used as water/oil emulsion stabilizers because they rearrange when placed at the interface [9]. Moreover, Janus gold nanoparticles half functionalized with polydopamine show that the electrostatic repulsion between nanoparticles determines the resulting particle self-assembly at water/oil interfaces as a result of the hydrophilic polydopamine and hydrophobic gold faces of each particle [10]. In addition, micrometer-sized Janus gold-silica nanoparticles have been found to stabilize water/oil emulsions for longer than 1 year, compared to 2 h of demulsification when homogeneous silica nanoparticles were used [11]. Importantly, not only does the wettability contrast of the Janus nanoparticles condition the interfacial activity but also their morphology controls the interfacial activity at a given water/oil interface, which determines the packing behavior of the Janus nanoparticles [12]. Therefore, nonspherical emulsion droplets have been obtained by using Janus nanoparticles with asymmetrical morphology [13]. There are different synthesis strategies involving bulk methods in which the Janus nanoparticles are synthesized in a solvent, usually one pot methods [6, 9, 14]. However, other strategies involve the particles being placed at a given liquid interface to be functionalized [15, 16], usually resulting in noticeably smaller quantities of Janus nanoparticles than in bulk methods. The Langmuir film balance technique is widely used to characterize the interfacial activity and arrangement of nanoparticles at water/air and water/oil interfaces [16–20]. Another experimental approach is to use growing/shrinking drop tensiometry [21, 22] because the quantity of nanoparticles required is much smaller than for a standard Langmuir film balance experiment. Nevertheless, a certain number of nanoparticles are still necessary for the experiments that involve the adsorption of Janus nanoparticles at the interface of a pendant drop from the bulk [2, 12, 23, 24]. When the amount of sample available is insufficient for studying the adsorption from the bulk to the interface of the pendant drop, the direct deposition of nanoparticles at the pendant drop interface from a volatile solvent allows the study of the interfacial activity. Moreover, solvent evaporation is a violent and rapid process that helps the nanoparticles to be adsorbed at the interface of the pendant drop, faster than diffusion from the bulk toward the pendant drop interface [25]. This technique enables us to control the number of nanoparticles deposited at the pendant drop interface. The simplest model used to describe the interfacial arrangement of the nanoparticles at the interface is the hard disk model in which the nanoparticles are represented by hard entities placed at the interface. The nanoparticles do not interact when there is enough room for every nanoparticle, but they become close packed when the area per particle is sufficiently low [26]. However, when the nanoparticles are functionalized with large polymers, Monte Carlo simulations and experimental data show complex behavior compared to that of hard objects at liquid/liquid interfaces [27].

In this study, we characterized the interfacial activity of 3.5-nm-diameter homogeneous

gold nanoparticles capped with hexanethiol and Janus gold nanoparticles with hydrophobic hexanethiolates on one hemisphere and hydrophilic 2-(2-mercapto-ethoxy)ethanol on the other. The pendant drop technique enabled the study of the interfacial activity of those particles at the water/air and water/decane interfaces. Moreover, because of the small number of nanoparticles available, the nanoparticles dispersed in a volatile solvent were directly deposited at the pendant drop water/air interface using a microsyringe. By the controlled deposition of a desired number of nanoparticles at the pendant drop interface and subsequent shrinkage-growth cycles of the pendant drop, we studied the different interfacial arrangements of nanoparticles for different values of the drop area available per nanoparticle.

5.2 Materials and Methods

5.2.1 Sample preparation

Homogeneous gold nanoparticles capped with hexanethiol (HPs) were synthesized following Brust's protocol [28]. Janus gold nanoparticles (JPs) were synthesized by functionalizing a hemisphere of the HPs with 2-(2-mercapto-ethoxy)ethanol (MEE) using Chen's protocol [16, 20]. The terminal groups were $-CH_3$ and $-OH$ for the hexanethiol- and MEE-functionalized hemispheres, respectively. The Janus morphology of JPs was thoroughly evaluated by Chen and co-workers [16, 20, 29]. They reported contact angle measurements of nanoparticle ensembles [16], AFM adhesion force measurements of individual nanoparticles [29], and NOESY NMR measurements of the polarization interactions between neighboring spins of the nanoparticle surface capping ligands [16]. The wettability differences between hexanethiol and MEE terminal groups suggest interfacial activity of the JPs. Both nanoparticles were redispersed separately in tetrahydrofuran (THF) as the spreading agent. The JP diameter quantified from high-resolution TEM micrographs of the isolated nanoparticles was $(3.5 \pm 0.9)\, nm$ (see Figure 5.2a and 5.2b).

5.2.2 Electrophoretic mobility

The electrophoretic mobility of both HPs and JPs was measured with a Zetasizer Nano device (Malvern) in a $10^{-2}\, M$ sodium citrate MilliQ water solution, and these were the values found: $\mu_{e,HP} = (-1.1 \pm 0.7) \cdot 10^{-8}\, m^2/(V \cdot s)$ and $\mu_{e,JP} = (-3.2 \pm 0.6) \cdot 10^{-8}\, m^2/(V \cdot s)$. The 1:1 electrolyte added to the nanoparticle solutions enabled the measurement of stable mobility values because the electrical double layer of both nanoparticles was fairly stabilized.

5.2.3 Growing and shrinking pendant drop

We used a homemade pendant drop tensiometer [30] that enables a change in the drop volume and area using a microinjector (Hamilton). The volume of a water pendant drop, usually in the range of 10 to 30 μL, allows us to work with smaller quantities of nanoparticle rather than the higher working volumes of the traditional Langmuir balance

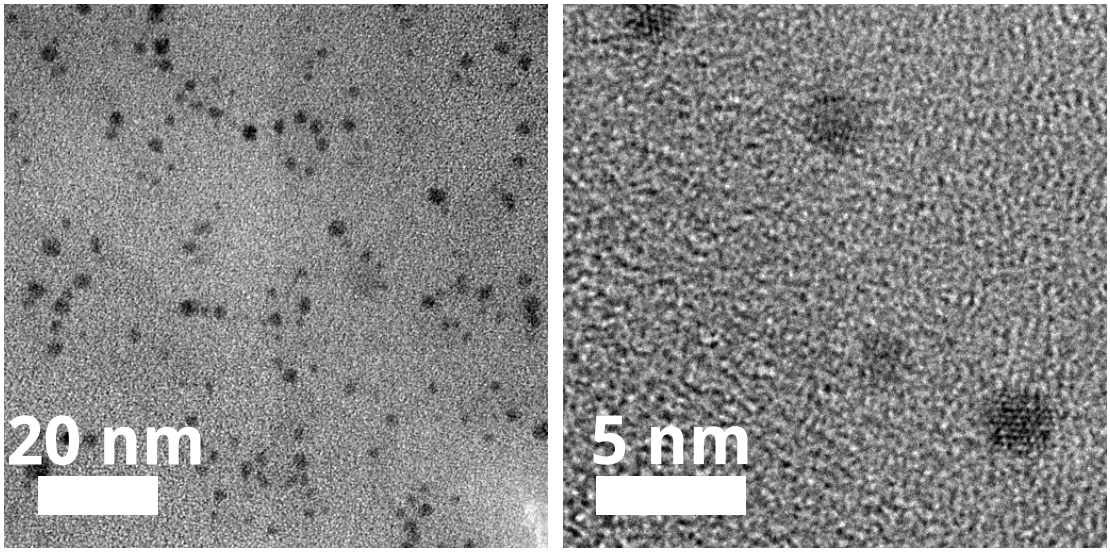

(a) (b)

Figure 5.2: (a) High-resolution TEM micrograph of the JPs studied. (b) High-resolution TEM micrograph of the JPs at higher magnification.

tensiometer [16–20]. The growth and shrinkage of the pendant drop volume enables different nanoparticle arrangements at the interface once a fixed number of nanoparticles is adsorbed. Real time drop images are processed by the axisymmetric drop shape analysis profile (ADSA-P) [31] providing the pendant drop area and surface tension. Water/oil interfaces can be explored with the pendant drop tensiometer readily by submerging the pendant drop in oil. In this study, as-received decane (Sigma-Aldrich) was used as the oil phase.

To perform a growing and shrinking pendant drop experiment, first it is necessary to adsorb the nanoparticles at the drop interface. Usually, the experiments are performed with adsorption of nanoparticles from the bulk to the pendant drop interface [2, 12, 23, 24]. but when the quantity of nanoparticles available is insufficient for this kind of study, the direct deposition of the desired number of nanoparticles in a spreading solvent at the interface with a microsyringe is an alternative. In this study, the spreading solvent used was THF and the deposition was performed on the surface of a 5 μL Milli-Q water pendant drop in air with a 5 μL microsyringe (Hamilton) and a micropositioner. Immediately after the deposition of the nanoparticles, the surface tension decreased markedly because of the spreading solvent. While the THF was evaporating, the volume of the pendant drop was slowly increased at 0.08 $\mu L/s$ up to the final 20 μL volume and maintained until the surface tension was stable. Thereby, this process avoided the fall of the pendant drop due to the abrupt decrease in the surface tension because of the spreading solvent effect on the interface. For higher volumes of spreading solvent, to avoid the drop fall it was necessary to perform a 10 μL stabilization step before the final growth up to 20 μL. In all cases, the

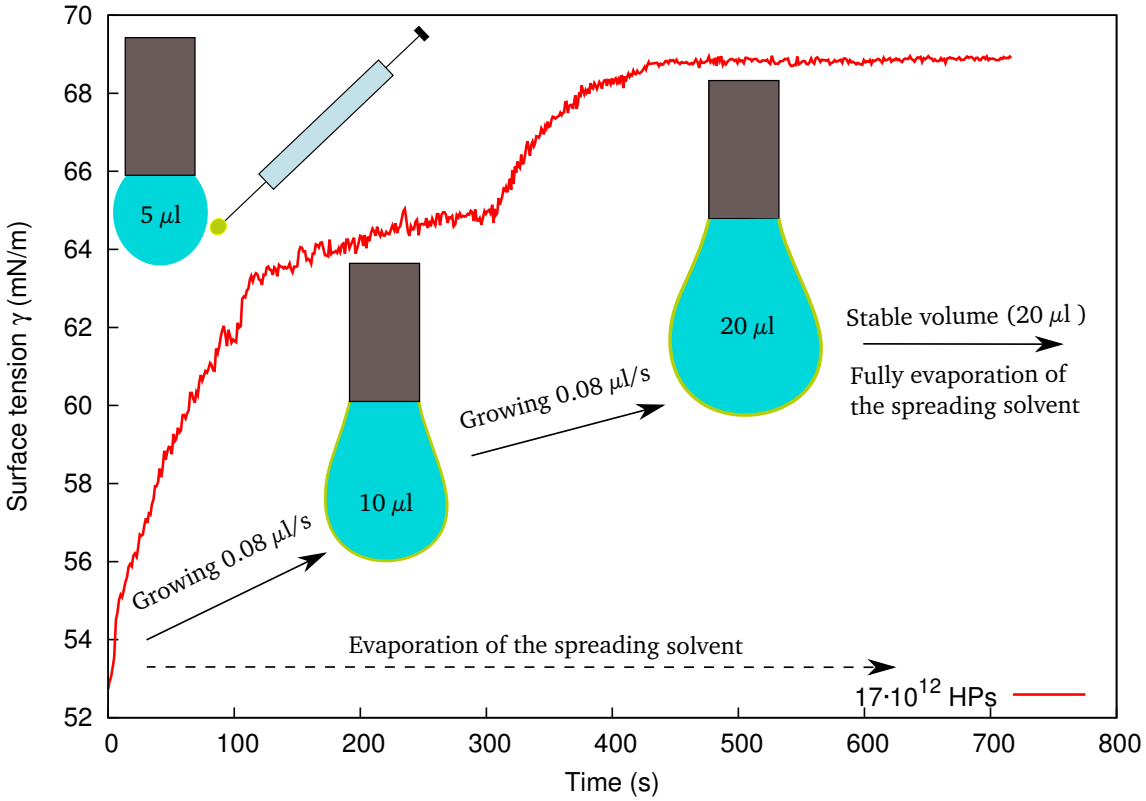

Figure 5.3: Surface tension evolution over time of JP deposition at the surface of a initial 5 μL MilliQ water pendant drop and subsequent growth to 20 μL at a 0.08 $\mu L/s$ rate. After the solvent evaporation, the surface tension remained stable.

evaporation of the spreading solvent ensured that the nanoparticles had enough energy to adsorb at the interface, compared to the slow process of adsorption from the bulk [25]. In Figure 5.3, we can observe the surface tension evolution over time after the JP deposition at the water/air interface. The procedure followed is illustrated with a visual scheme.

The growing and shrinking pendant drop experiment was performed with slightly different protocols for water/air or water/decane interfaces. For both water/air and water/decane interfaces, the shrinking and growing volume rate was 0.08 $\mu L/s$ but the volume range was 20 $\mu l \leftrightarrow$10 μl for water/air and 30 $\mu l \leftrightarrow 10\mu l$ for water/decane interfaces because the pendant drop was larger when immersed in decane before the drop fall. Additionally, the volume was decreased up to 5 μL prior to the immersion of the water pendant drop in decane to avoid the drop fall. For each particle concentration, the shrinkage was repeated three times and the growth was repeated twice. The surface pressure $\Pi = \gamma_0 - \gamma$, where γ_0 is the surface tension of the phase without nanoparticles and γ is the measured surface tension, is plotted against the area of the pendant drop divided by the number of deposited nanoparticles. A growing and shrinking pendant drop experiment is illustrated in Figure 5.4.

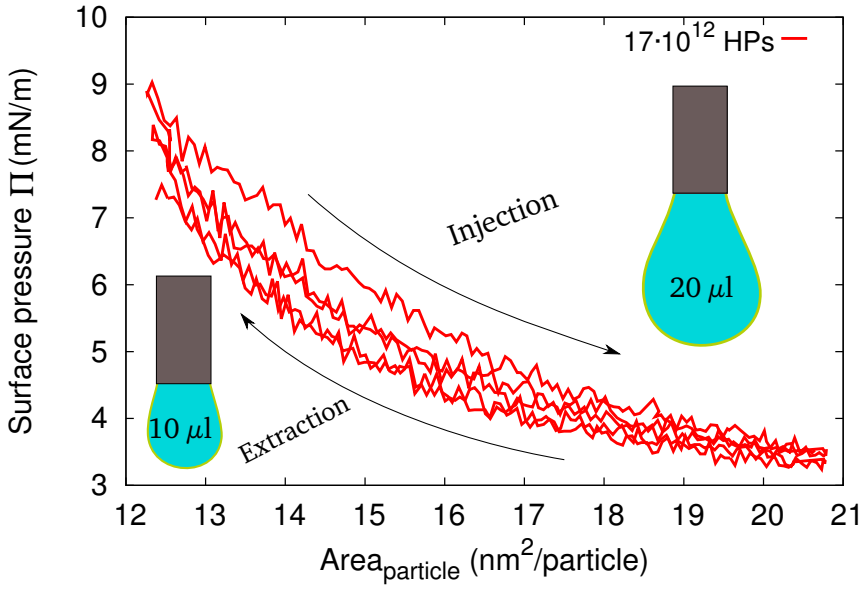

Figure 5.4: Surface pressure against area per particle for a growing and shrinking pendant drop experiment at the water/decane interface. The pendant drop volume was changed to between 30 and 10 μL at a 0.08 $\mu L/s$ rate. The growth was repeated three times and the shrinkage twice. The reproducibility between growth and shrinkage repetitions and the low hysteresis of the cycle are remarkable.

5.3 Results and Discussion

The direct deposition of the JPs and HPs at the water/air interface produced a decrease in the surface tension once the spreading solvent was fully evaporated. The surface tension evolution over time for different amounts of HPs and JPs deposited at the drop surface is plotted in Figure 5.5. The stable values of surface tension after the spreading solvent evaporation are compiled in Table 5.1. The surface tension decreased as the nanoparticle concentration increased. This decrease is greater for JPs than for HPs, suggesting an enhanced interfacial activity of the JPs as compared to the HPs [32].

The Pickering emulsions become increasingly stabilized with increasing particle size. In this context, small nanoparticles (∼100 nm) need to be tightly anchored at the inter-

Table 5.1: Stable Surface Tension after the Spreading Solvent Evaporation for Different Numbers of Deposited HPs and JPs

Deposited particles	γ_{HP} (mN/m)	γ_{JP} (mN/m)
1.7·10^{12}	72.40 ± 0.07	71.5 ± 0.3
5·10^{12}	71.38 ± 0.11	66.7 ± 0.3
8·10^{12}	70.78 ± 0.10	63.7 ± 0.3
17·10^{12}	68.84 ± 0.06	59.50 ± 0.20

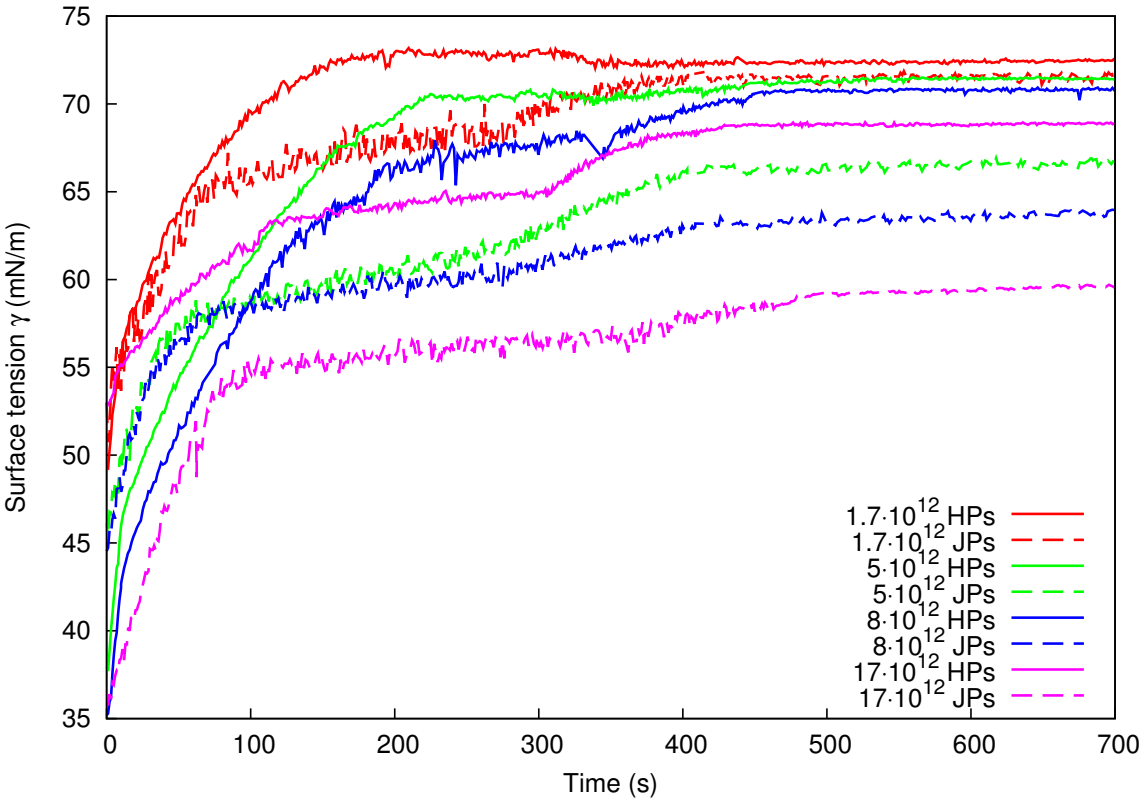

Figure 5.5: Surface tension evolution over time after the deposition of HPs and JPs at the surface of a initial 5 μL Milli-Q water pendant drop and subsequent growth up to 20 μL at a 0.08 $\mu L/s$ rate. Each line corresponds to different depositions with different amounts of HPs and JPs, respectively. After solvent evaporation, the surface tension remained stable.

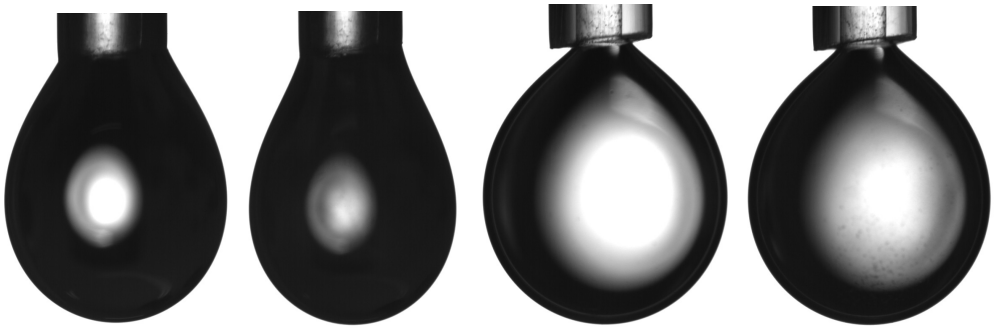

(a) $1.7{\cdot}10^{12}$ JPs in water/air (b) $17{\cdot}10^{12}$ JPs in water/air (c) $1.7{\cdot}10^{12}$ JPs in water/decane (d) $17{\cdot}10^{12}$ JPs in water/decane

Figure 5.6: Images of pendant drops with different concentrations of JPs and at different interfaces. The pendant drop volumes were 20 and 30 μL for the water/air and water/decane interfaces, respectively.

face to avoid desorption [2]. The adsorption energy at the interface is on the order of k_BT when the nanoparticle diameter is in the range of a few nanometers [23]. Thus, the 3.5-nm-diameter HPs and JPs were expected to be expelled from the pendant drop interface because of thermal fluctuations or even by the drop shrinkage [33]. Although the drop surface revealed visible aggregates and noticeable opacity as the nanoparticle concentration increased (Figure 5.6), both HPs and JPs exhibited a significant and stable effect on the surface tension after THF evaporation. This suggests that a significant number of nanoparticles did not desorb from the drop interface over time. From molecular dynamics, Udayana-Ranatunga et al. [34] suggest that ligand rearrangement contributes significantly to the energetics of nanoparticles at interfaces.

Because of the experimental limitations in the drop area range reproduced with a single growth and shrinkage experiment, several growth and shrinkage experiments were performed for different numbers of deposited nanoparticles to probe a wider range of area per particle. Results for the growing and shrinking pendant drop experiments at the water/air and water/decane interfaces are plotted in Figure 5.7 for different concentrations of HPs and JPs. We averaged the different growth and shrinkage cycles for each nanoparticle concentration because of the low hysteresis. It can be seen that the surface pressure increased as the area per particle decreased for both JPs and HPs. The interfacial activity reached similar values with both types of nanoparticles for the most expanded interfacial states (i.e., highest values of area per particle, >18 nm^2/particle). However, the interfacial activity was higher with the JPs than with the HPs for the most compressed states (<2 nm^2/particle) where the surface pressure was 2.5 times higher for the JPs than for the HPs at the water/air interface and 1.2 times higher at the water/decane interface. At both interfaces, the JPs reached the same surface pressure: 19.3 $\pm$ 0.4 mN/m for the most compressed interfacial state. The higher interfacial activity of HPs at the water/decane interface for the most compressed state may reveal that the HPs move more freely in the presence of the decane phase because of its affinity for hydrophobic particles. This nanoparticle mobility allowed us to realize arrangements with greater interfacial coverage and higher surface pressure.

Different models were explored to fit the experimental data with a hypothetical piecewise compression isotherm. A model based on the repulsion between charged particles [35] results in negligible surface pressure resulting from the low effective electric charge of HPs and JPs, with its small size and effective charge. Moreover, the short chains of the hexanethiol and MEE capping ligands did not require a large polymer correction [27]. The simply scaled particle theory of the hard disks model [26] is in reasonable agreement with the HP results for both water/air and water/decane interfaces for hard disks with 1 nm diameter (Figure 5.7). In the hard disk model, the surface pressure Π for a given area per particle at the interface $A_{particle}$ is written as follows

$$\Pi(A_{particle}) = \frac{k_B \cdot T}{A_{particle} \cdot \left(1 - \frac{\pi \cdot d^2}{4 \cdot A_{particle}}\right)^2} \tag{5.1}$$

where k_B is the Boltzmann constant, T is the temperature, and d is the hard disk diameter. The hard disk model predicts no interactions when there is enough room for all

nanoparticles at the interface and a significant effect on the surface tension at high concentrations when the nanoparticles are near close-packed. The fitted diameter of 1 nm points out that not all of the nanoparticles were really adsorbed at the interface or that they were aggregated. In such a situation, the number of particles at the interface was smaller than expected, and it is necessary to shrink the pendant drop further to reach the close-packed regime, resulting in a lower effective diameter of the hard disk model. This simple model underestimates the results of surface pressure against area per particle for the JPs. Further models taking into account the interaction between the Janus nanoparticles are needed to explain the results. Such models should incorporate the role of the wettability contrast between the two hemispheres of the JPs, with the low effective charge and steric interactions between these nanoparticles.

Although there is evidence that not all nanoparticles are uniformly distributed at the pendant drop interface (visible aggregates in Figure 5.6 and underestimated effective diameter for the HPs as discussed before), the nanoparticles placed at the interface seem to be well anchored at both the water/air and water/decane interfaces because the different growth and shrinkage cycles for a given nanoparticle concentration show a very low hysteresis value, pointing out that the nanoparticles did not desorb from the interface as the drop area was changed. From these results, the JPs exhibited enhanced interfacial activity as compared to the HPs.

5.4 Conclusions

The interfacial activity of homogeneous 3.5 nm gold nanoparticles capped with hexanethiol and Janus 3.5 nm gold nanoparticles capped half with hexanethiol and half with MEE was explored using pendant drop tensiometry. The direct deposition of the nanoparticles in a spreading solvent at the interface of the pendant drop with a microsyringe rendered it possible to explore the surface tension evolution over time as the spreading solvent was evaporating at different nanoparticle concentrations. The direct deposition needed only a small quantity of nanoparticles in contrast to the conventional adsorption of nanoparticles from the pendant drop bulk or a conventional Langmuir balance experiment. The growing and shrinking pendant drop technique allowed us to study the surface pressure for a wide range of area per nanoparticle at the water/air and water/decane interfaces by varying the drop area and the number of nanoparticles deposited on the drop surface. For both interfaces studied, the homogeneous nanoparticles showed lower interfacial activity than the Janus nanoparticles. A hard disk model could fit the experimental results for the homogeneous particles, but it underestimated the interaction between the Janus nanoparticles at the interface.

Acknowledgements

This study was supported by the Junta de Andalucía (projects P09-FQM-4698 and P10-FQM-5977), the Ministerio de Economía y Competitividad (project MAT2011-23339) and

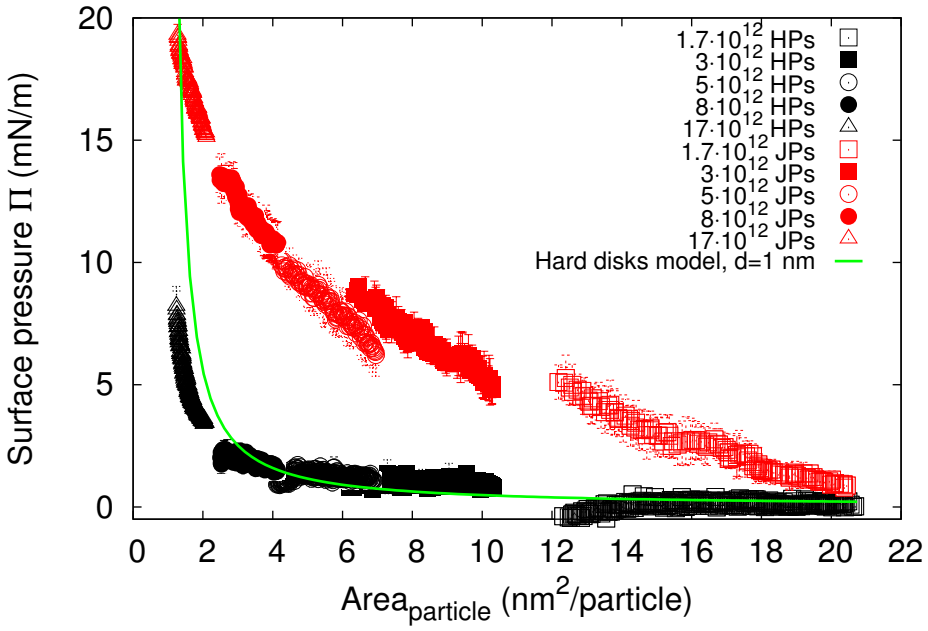

(a) Water/air interface

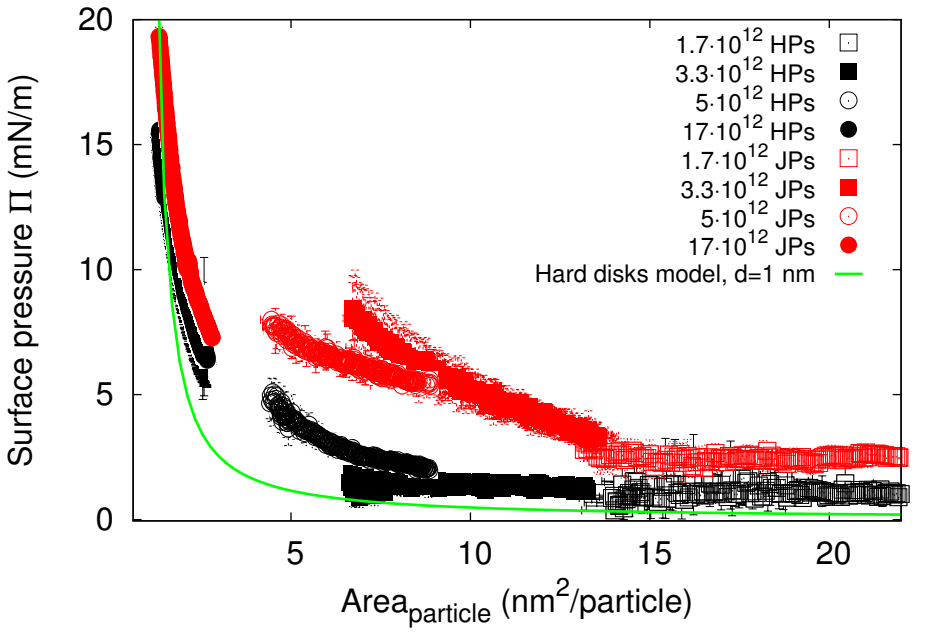

(b) Water/decane interface

Figure 5.7: Surface pressure against area per particle for different numbers of HPs (black symbols) and JPs (red symbols) deposited at the interface. Each black or red symbol corresponds to a single HP or JP deposition at the interface of the pendant drop, respectively. The solid line is the hard disk model (eq 5.1) for disks of 1 nm diameter.

the U.S. National Science Foundation (DMR-0804049). We thank Dr. J. A. Holgado-Terriza for the Contacto software used for surface tension measurements.

References

[1] Yoshida, M.; Lahann, J. Smart Nanomaterials. *ACS Nano* **2008**, *2*, 1101–1107, DOI: 10.1021/nn800332g.

[2] Walther, A.; Müller, A. H. E. Janus Particles: Synthesis, Self-Assembly, Physical Properties, and Applications. *Chem. Rev.* **2013**, *113*, 5194–5261, DOI: 10.1021/cr300089t.

[3] Kaewsaneha, C.; Tangboriboonrat, P.; Polpanich, D.; Eissa, M.; Elaissari, A. Janus Colloidal Particles: Preparation, Properties, and Biomedical Applications. *ACS Appl. Mater. Interfaces* **2013**, *5*, 1857–1869, DOI: 10.1021/am302528g.

[4] Synytska, A.; Khanum, R.; Ionov, L.; Cherif, C.; Bellmann, C. Water-Repellent Textile via Decorating Fibers with Amphiphilic Janus Particles. *ACS Appl. Mater. Interfaces* **2011**, *3*, 1216–1220, DOI: 10.1021/am200033u.

[5] Bormashenko, E.; Bormashenko, Y.; Pogreb, R.; Gendelman, O. Janus Droplets: Liquid Marbles Coated with Dielectric/Semiconductor Particles. *Langmuir* **2011**, *27*, 7–10, DOI: 10.1021/la103653p.

[6] Teo, B. M.; Suh, S. K.; Hatton, T. A.; Ashokkumar, M.; Grieser, F. Sonochemical Synthesis of Magnetic Janus Nanoparticles. *Langmuir* **2011**, *27*, 30–33, DOI: 10.1021/la104284v.

[7] Yuet, K. P.; Hwang, D. K.; Haghgooie, R.; Doyle, P. S. Multifunctional Superparamagnetic Janus Particles. *Langmuir* **2010**, *26*, 4281–4287, DOI: 10.1021/la903348s.

[8] Binks, B. P.; Fletcher, P. D. I. Particles Adsorbed at the Oil-Water Interface: A Theoretical Comparison between Spheres of Uniform Wettability and Janus Particles. *Langmuir* **2001**, *17*, 4708–4710, DOI: 10.1021/la0103315.

[9] Larson-Smith, K.; Pozzo, D. C. Pickering Emulsions Stabilized by Nanoparticle Surfactants. *Langmuir* **2012**, *28*, 11725–11732, DOI: 10.1021/la301896c.

[10] Xu, H.; Liu, X.; Su, G.; Zhang, B.; Wang, D. Electrostatic Repulsion-Controlled Formation of Polydopamine-Gold Janus Particles. *Langmuir* **2012**, *28*, 13060–13065, DOI: 10.1021/la302394e.

[11] Fujii, S.; Yokoyama, Y.; Miyanari, Y.; Shiono, T.; Ito, M.; Yusa, S.-i.; Nakamura, Y. Micrometer-Sized Gold-Silica Janus Particles as Particulate Emulsifiers. *Langmuir* **2013**, *29*, 5457–5465, DOI: 10.1021/la400697a.

[12] Ruhland, T. M.; Gröschel, A. H.; Ballard, N.; Skelhon, T. S.; Walther, A.; Müller, A. H. E.; Bon, S. A. F. Influence of Janus Particle Shape on Their Interfacial Behavior at Liquid-Liquid Interfaces. *Langmuir* **2013**, *29*, 1388–1394, DOI: 10.1021/la3048642.

[13] Meng, X.; Guan, Y.; Zhang, Z.; Qiu, D. Fabrication of a Composite Colloidal Particle with Unusual Janus Structure as a High-Performance Solid Emulsifier. *Langmuir* **2012**, *28*, 12472–12478, DOI: 10.1021/la302392s.

[14] Zhang, J.; Jin, J.; Zhao, H. Surface-Initiated Free Radical Polymerization at the Liquid-Liquid Interface: A One-Step Approach for the Synthesis of Amphiphilic Janus Silica Particles. *Langmuir* **2009**, *25*, 6431–6437, DOI: 10.1021/la9000279.

[15] Liu, L.; Ren, M.; Yang, W. Preparation of Polymeric Janus Particles by Directional UV-Induced Reactions. *Langmuir* **2009**, *25*, 11048–11053, DOI: 10.1021/la901364a.

[16] Pradhan, S.; Xu, L.; Chen, S. Janus Nanoparticles by Interfacial Engineering. *Adv. Funct. Mater.* **2007**, *17*, 2385–2392, DOI: 10.1002/adfm.200601034.

[17] Detrich, Á.; Deák, A.; Hild, E.; Kovács, A. L.; Hórvölgyi, Z. Langmuir and Langmuir-Blodgett Films of Bidisperse Silica Nanoparticles. *Langmuir* **2010**, *26*, 2694–2699, DOI: 10.1021/la9027207.

[18] Kim, J. Y.; Raja, S.; Stellacci, F. Evolution of Langmuir Film of Nanoparticles Through Successive Compression Cycles. *Small* **2011**, *7*, 2526–2532, DOI: 10.1002/smll.201100290.

[19] Sashuk, V.; Hołyst, R.; Wojciechowski, T.; Fiałkowski, M. Close-packed monolayers of charged Janus-type nanoparticles at the air-water interface. *J. Colloid Interface Sci.* **2012**, *375*, 180–186, DOI: 10.1016/j.jcis.2012.02.057.

[20] Pradhan, S.; Brown, L.; Konopelski, J.; Chen, S. Janus nanoparticles: reaction dynamics and NOESY characterization. *J. Nanopart. Res.* **2009**, *11*, 1895–1903, DOI: 10.1007/s11051-008-9543-4.

[21] Xu, H.; Melle, S.; Golemanov, K.; Fuller, G. Shape and Buckling Transitions in Solid-Stabilized Drops. *Langmuir* **2005**, *21*, 10016–10020, DOI: 10.1021/la0507378.

[22] Monteux, C.; Kirkwood, J.; Xu, H.; Jung, E.; Fuller, G. G. Determining the mechanical response of particle-laden fluid interfaces using surface pressure isotherms and bulk pressure measurements of droplets. *Phys. Chem. Chem. Phys.* **2007**, *9*, 6344–6350, DOI: 10.1039/B708962G.

[23] Ferdous, S.; Ioannidis, M.; Henneke, D. Adsorption kinetics of alkanethiol-capped gold nanoparticles at the hexane-water interface. *J. Nanopart. Res.* **2011**, *13*, 6579–6589, DOI: 10.1007/s11051-011-0565-y.

[24] Ruhland, T. M.; Gröschel, A. H.; Walther, A.; Müller, A. H. E. Janus Cylinders at Liquid-Liquid Interfaces. *Langmuir* **2011**, *27*, 9807–9814, DOI: 10.1021/la201863x.

[25] Garbin, V.; Crocker, J. C.; Stebe, K. J. Nanoparticles at fluid interfaces: Exploiting capping ligands to control adsorption, stability and dynamics. *J. Colloid Interface Sci.* **2012**, *387*, 1–11, DOI: 10.1016/j.jcis.2012.07.047.

[26] Santos, A.; López de Haro, M.; Yuste, S. An accurate and simple equation of state for hard disks. *J. Chem. Phys.* **1995**, *103*, 4622–4625, DOI: 10.1063/1.470649.

[27] Isa, L.; Amstad, E.; Schwenke, K.; Del Gado, E.; Ilg, P.; Kroger, M.; Reimhult, E. Adsorption of core-shell nanoparticles at liquid-liquid interfaces. *Soft Matter* **2011**, *7*, 7663–7675, DOI: 10.1039/C1SM05407D.

[28] Brust, M.; Walker, M.; Bethell, D.; Schiffrin, D. J.; Whyman, R. Synthesis of thiol-derivatised gold nanoparticles in a two-phase Liquid-Liquid system. *J. Chem. Soc., Chem. Commun.* **1994**, *7*, 801–802, DOI: 10.1039/C39940000801.

[29] Xu, L.-P.; Pradhan, S.; Chen, S. Adhesion Force Studies of Janus Nanoparticles. *Langmuir* **2007**, *23*, 8544–8548, DOI: 10.1021/la700774g.

[30] Wege, H.; Holgado-Terriza, J.; Gálvez-Ruiz, M.; Cabrerizo-Vílchez, M. Development of a new Langmuir-type pendant-drop film balance. *Colloid. Surface. B* **1999**, *12*, 339–349, DOI: 10.1016/S0927-7765(98)00088-5.

[31] Montes Ruiz-Cabello, F.; Rodriguez-Valverde, M.; Cabrerizo-Vilchez, M. Contact angle hysteresis on polymer surfaces: an experimental study. *J. Adhes. Sci. Technol.* **2011**, *25*, 2039–2049, DOI: 10.1163/016942410X544848.

[32] Glaser, N.; Adams, D. J.; Böker, A.; Krausch, G. Janus Particles at Liquid-Liquid Interfaces. *Langmuir* **2006**, *22*, 5227–5229, DOI: 10.1021/la060693i.

[33] Garbin, V.; Crocker, J. C.; Stebe, K. J. Forced Desorption of Nanoparticles from an Oil-Water Interface. *Langmuir* **2012**, *28*, 1663–1667, DOI: 10.1021/la202954c.

[34] Ranatunga, R. J. K. U.; Kalescky, R. J. B.; Chiu, C.-c.; Nielsen, S. O. Molecular Dynamics Simulations of Surfactant Functionalized Nanoparticles in the Vicinity of an Oil/Water Interface. *J. Phys. Chem. C* **2010**, *114*, 12151–12157, DOI: 10.1021/jp105355y.

[35] Aveyard, R.; Clint, J.; Nees, D.; Paunov, V. Compression and Structure of Monolayers of Charged Latex Particles at Air/Water and Octane/Water Interfaces. *Langmuir* **2000**, *16*, 1969–1979, DOI: 10.1021/la990887g.

The true delight is in the finding out rather than in the knowing.

Isaac Asimov

6 Surface activity and collective behaviour of colloidally stable Janus-like particles at the air-water interface

Published in Soft Matter, Issue 10, 2014, Pages 3471-3476, ISSN 1744-683X,
DOI: 10.1039/C3SM52624K

M.A. Fernandez-Rodriguez[†], M.A. Rodriguez-Valverde[†], M.A. Cabrerizo-Vilchez[†] and R. Hidalgo-Alvarez[†,*]

[†] *Biocolloid and Fluid Physics Group, Applied Physics Department, Faculty of Sciences, University of Granada, 18071 Granada (Spain)*

[*] *rhidalgo@ugr.es*

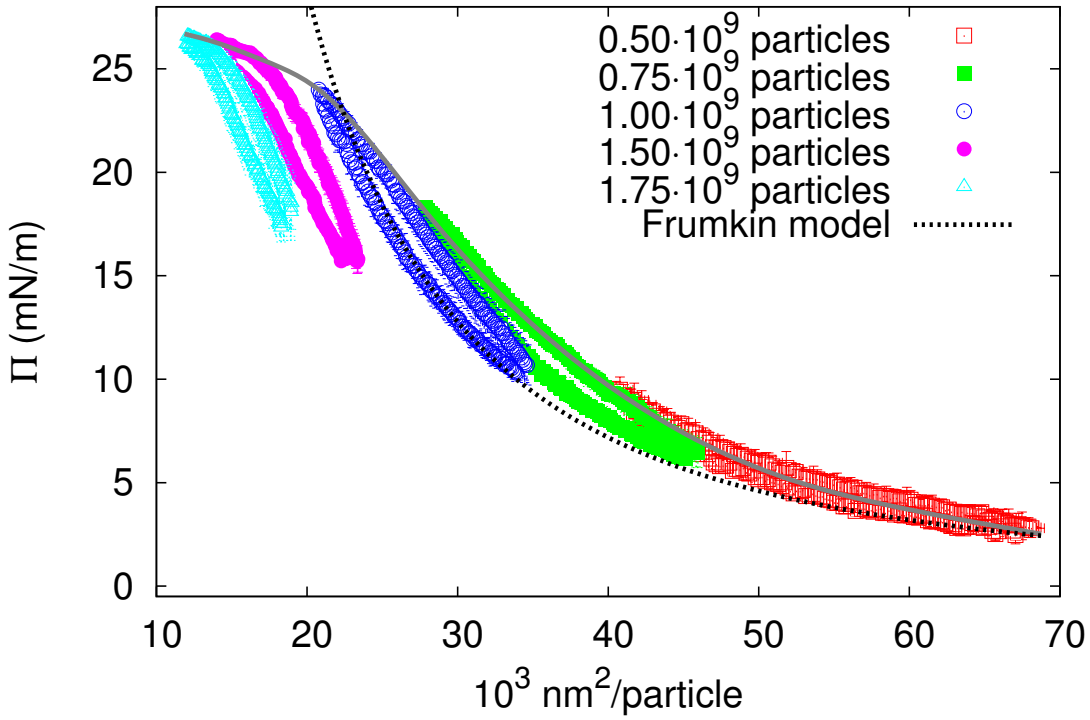

Figure 6.1: Graphical abstract.

Abstract

In this work we report an experimental study on the surface activity and the collective behaviour of colloidally stable Janus-like silver particles at the air-water interface. The colloidal stability of silver nanoparticles has been enhanced using different capping ligands. Two polymers coated the silver particles: 11-mercaptoundecanoic acid and 1-undecanthiol. These capping ligands adsorbed onto the particle surface are spontaneously rearranged at the air-water interface. This feature leads to Janus behaviour in the silver particles with amphiphilic character. The surface activity of the silver particles at the air-water interface has been measured using pendant drop tensiometry. The Janus-like silver particles revealed a surface activity similar to that shown by conventional amphiphilic molecules but with much larger area per particle. The variation of the surface pressure with the area per particle was described properly using the Frumkin isotherm up to the collapse state. Furthermore, oscillating pendant drop tensiometry provided very useful data on the rheological properties of Janus particle monolayers; these properties depended on the lateral interactions between particles and were closely related to the monolayer microstructure. We revealed the close relationship be-

tween the collective behavior and the surface activity of Janus-like silver particles.

6.1 Introduction

Janus Particles (JPs) are special types of particles whose hemispheres have two or more distinct physical or chemical properties [1]. In recent years, there is an increasing interest in the design and synthesis of JPs and their self-assembly and physical properties are being further addressed [2–8]. There are many reasons to think that JPs are a very interesting colloidal system for electronic paper, asymmetrical carriers for catalysis, sensing and drug delivery, nanoscale machinery in the conversion of solar energy into electrical current and colloidal surfactants [9]. To develop these applications it is mandatory to evaluate properly the colloidal stability in bulk and the interfacial activity of JPs and their connection. However, there are a few works devoted to study these properties. The first experiments on the interfacial activity of JPs (gold and an iron oxide moiety) at liquid-liquid interfaces (water-hexane) were reported by Glaser et al., using pendant drop tensiometry [10]. Most recently, Ruhland et al. [11] have performed the first study on the self-assembly behaviour of Janus cylinders at liquid-liquid interfaces using pendant drop technique and microscopic imaging. Kumar et al. [8] have published a review on amphiphilic JPs at fluid interfaces where they survey the recent development in the use of these particles as colloidal surfactants to stabilize multiphasic mixtures such as emulsions. They also discuss on the importance of controlling the shape of JPs, which has a significant impact on their behaviour at fluid interfaces. Obviously, the area of JPs occupied at the interface changes drastically as they aggregate because they lose their original size and shape.
The surface characterization of colloidal monolayers formed by JPs becomes a difficult task [12, 13]. To explore the surface activity of spherical JPs at fluid interfaces, the following factors are crucial: the colloidal stability of the particles in bulk, the presence of traces of the surface-active reagents used in the particle synthesis and of the spreading agent employed to prepare the colloidal monolayer. These factors hinder the effect of the interface area on the surface pressure due exclusively to the presence of amphiphilic particles. Park et al. [14] have studied the self-assembly behaviour of JPs at fluid interfaces in detail. These authors found that JPs form a fractal-like aggregate structure spontaneously, which means that their interactions are predominantly attractive. The formation of aggregates at fluid interfaces makes unrealizable the study of colloidal monolayers, because these aggregates lead to multilayers or unresolved monolayers. Instead, as reported by Luo et al. [15] a stable colloidal monolayer can be formed with electrically charged JPs. Simulations performed by Hong et al. [16] on the assembly of charged Janus spheres showed that the charge asymmetry of individual JPs is preserved in the cluster acting as a larger charged JP.

The extremely low colloidal stability of JPs is a serious limitation in their utilization as colloidal surfactants. From theoretical calculations, an amphiphilic particle, half hydrophobic and half hydrophilic, can be up to three times more surface active than the corresponding homogeneous particle [17]. In these energetic calculations, the JPs are not coagulated, which is rather difficult to achieve experimentally if the particles exhibit a strong wettability contrast between both hemispheres. To avoid the coagulation of the JPs we have prepared silver particles coated by a mixture of hydrophobic and hydrophilic ligands in appropriate proportions, which go through a phase separation when the particles are located at the air-water interface. Very recently, Sashuk et al. [12] have experimentally confirmed the Janus behaviour of this type of particles. The electrical charges of the hydrophilic ligand play a decisive role in the stabilization of silver particles and the long alkyl chain of the hydrophobic ligand also introduce a steric effect between particles. A combination of both effects is expected to stabilize silver particles through an electrosteric mechanism. As reported by Garbin et al., capping ligands play a prominent role in determining both interparticle interactions and the particle-fluid interactions [13].
In this work, we examined the surface activity and the collective behaviour of colloidally stable silver Janus-like particles (AgJPs) deposited at the air-water interface. First, using pendant drop tensiometry, we measured the surface tension of JP monolayers as a function of time at different particle surface concentrations and the corresponding adsorption isotherms (surface pressure as a function of area per particle). Next, the rheological response of these colloidal monolayers was evaluated using oscillating pendant drop tensiometry. An attempt has been made to relate the rheological properties of JP monolayers to the lateral interactions between particles and the monolayer microstructure.

6.2 Experimental

6.2.1 Preparation of negative Janus-like Ag particles (AgJPs)

Silver nanoparticles (AgNPs) were prepared using the procedure described by Jana and Peng. [18] Firstly, $344\,mg$ of decanoic acid (DA) were dissolved into $20\,mL$ of toluene. Next, $6.4\,\mu L$ of anhydrous N2H4 were dissolved into DA solution by sonication. This solution was then mixed with $0.2\,mL$ of dilute tert-buthyl ammonium bromide (TBAB) solution ($5.0\,mg$ of TBAB in $20\,mL$ of toluene). Finally, $34\,mg$ of silver acetate dissolved in $0.4\,mL$ of dodecyl amine solution (1 M) in toluene were injected during stirring. Dark red colour appears within 5 minutes of mixing indicating particle formation. Stirring continued for 10-15 minutes till the reaction was completed. Next, Janus-like silver particles (AgJPs) were prepared using the procedure described by Sashuket al. [12], with cer-

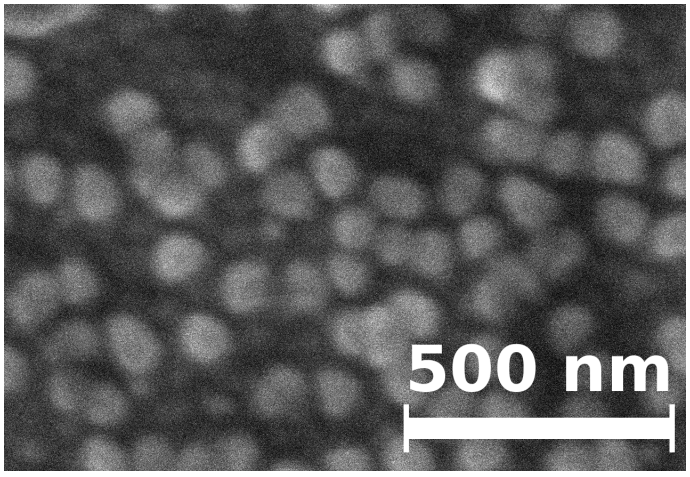

Figure 6.2: SEM micrograph of the AgJPs studied.

tain modifications. Firstly, $20\,mL$ of methanol were added to a solution of DA-capped AgNPs ($0.02\,mmol$-Ag, $2\,mL$). After precipitation of nanoparticles, the supernatant solution was decanted. The resulting nanoparticles were dissolved in $5\,mL$ of chloroform. Nanoparticle solution was injected into a solution of 11-mercaptoundecanoic acid and 1-undecanthiol ligands ($0.04\,mmol$) of a given ratio ($1:1$) in dichloromethane ($5\,mL$) upon stirring. The reaction mixture left stirring overnight. Then the nanoparticles were centrifuged and purified by dissolution-precipitation. The nanoparticles precipitate was dissolved in methanol ($1.5\,mL$) followed with addition of $1.5\,mL$ of 2-propanol and precipitated with n-cyclohexane ($40-50\,mL$). Precipitated AgJPs were centrifuged ($5000\,rpm$) and the dissolution-precipitation cycle was repeated twice. Finally, $2\,mmol$ of AgJPs were dissolved in $3\,mL$ solvent ($1.5\,mL$ 2-propanol and $1.5\,mL$ methanol). From Scanning Electron Microscopy (SEM), an average particle diameter of (100 ± 40) nm was obtained by particle size distribution (see Fig. 6.2).
Using Photon Correlation Spectroscopy (Malvern 4700c Dynamic Light Scattering) we monitored the time dependence of the average diameter at a $10^{-2}\,M$ KBr solution and it remained practically constant during almost one and a half hour. Longer times were not possible to be measured due to particle sedimentation. This proved that the AgJPs were stable in the colloidal sense. Sashuket al. [12] demonstrated the Janus behaviour of this type of silver particles at the air-water interface, although they indeed do not behave as JPs in bulk solution. The average size of our AgJPs is much larger than the nanoparticles prepared by Sashuk et al, ($\sim 5\,nm$) [12]. Fresh Milli-Q water was used for the preparation of aqueous solutions. All glassware was washed with 10% Micro-90 cleaning solution and exhaustively rinsed with water, isopropanol, deionized water, and Milli-Q water in this sequence. All chemicals (Aldrich and Panreac) were of analytical grade and used as received.

6.2.2 Experimental Methods

The electrophoretic mobility of the AgJPs was measured with a Nano Zeta-Sizer (Malvern) at room temperature. Pendant drop tensiometry is an extensively employed method for measuring surface and interfacial tension of liquids [19]. The surface tension of AgJPs was measured using pendant drop tensiometry. This technique enables to measure the surface or interfacial tension of colloidal monolayers using a much smaller amount of particles than that conventional technique of Langmuir balance, where the particles are spread on a fluid subphase from a volatile solvent to form the monolayer [13]. Instead, the colloidal monolayer is formed onto the surface of a $20\,\mu L$ pendant drop depositing a given amount of solution with nanoparticles (see Fig. 6.3).
This is very important because simple strategies are still being developed for the preparation of large amounts of JPs. 4Our set-up is composed of a CMOS camera interfaced with a computer-based data acquisition system, which is used to capture the image of an equilibrium drop [20]. Then edge-detecting software is used to fit the drop shape to the Young-Laplace equation using the Axisymmetric Drop Shape Analysis Profile (ADSA-P) [19]. In our case, increasing and decreasing the volume of a Milli-Q water pendant drop with AgJPs deposited carefully at the air-water interface allowed to explore the dynamic surface response of the monolayer. Real time drop images were processed at each step of volume variation and the drop area and surface tension were calculated (see Fig. 6.4) [20].
The dilatational rheology of the colloidal monolayers formed at the air-water interface from different surface particle concentrations was measured with the oscillating pendant drop tensiometry. An oscillatory perturbation was applied to the interface by injecting and extracting volume to the drop. The system monitors the response of the surface tension to the drop area deformation. The dilatational modulus (E), the mean surface tension (γ) and the surface dilatational viscosity (η_d) were obtained from this response. This experimental procedure requires a quasi-equilibrium drop shape for the calculation of surface tension. Hence, the oscillations applied to the drop area were maintained below 1% of amplitude to avoid excessive perturbations of the colloidal monolayer and the departure from the viscoelastic linear region. The initial pendant drop volume was $20\,\mu L$ or $10\,\mu L$, which depended on the surface particle concentration. In all rheology experiments, we applied a sinusoidal oscillation in the pendant drop volume with $1\,\mu L$ amplitude and a frequency of $0.1\,Hz$.

6.3 Results and discussion

The electric state of the AgJPs in aqueous media was analysed by measuring the electrophoretic mobility as a function of pH at constant ionic strength of $10^{-2}\,M$ of KBr. As can be seen in Fig. 6.5, the electrophoretic mobility of AgJPs is negative

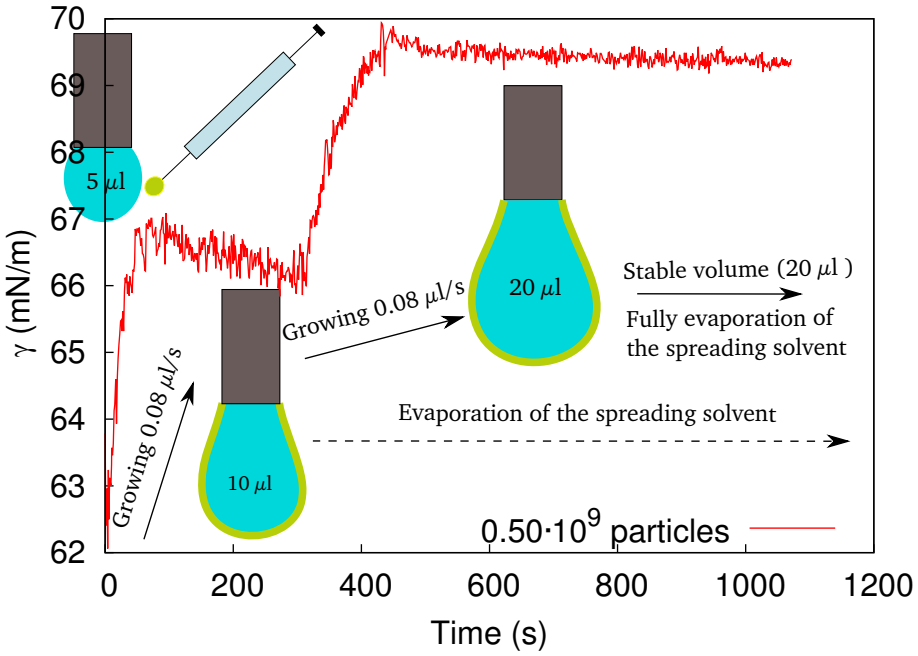

Figure 6.3: Temporal evolution of surface tension at the air-water interface with $0.50 \cdot 10^9$ particles deposited over a droplet of $5\,\mu L$.

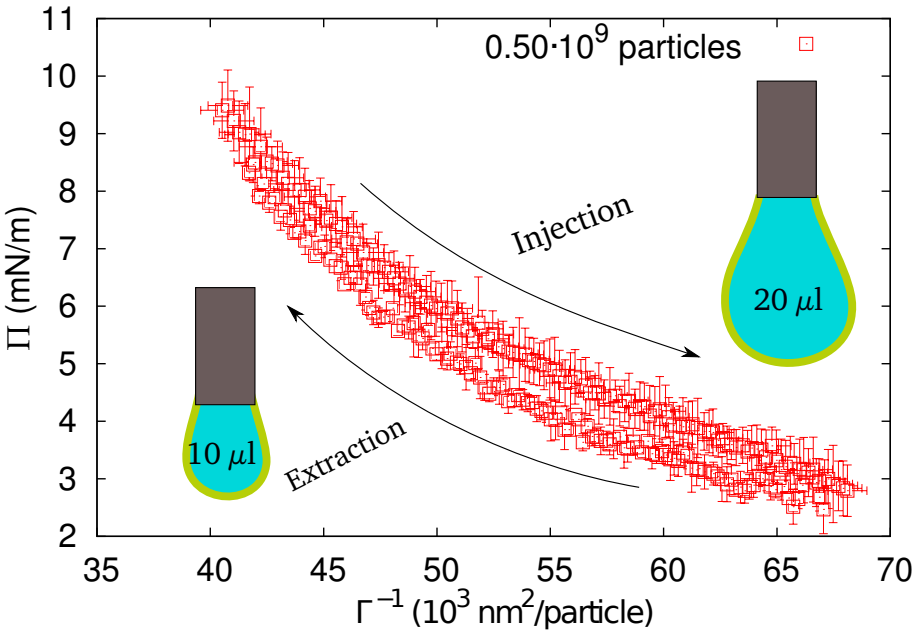

Figure 6.4: Hysteresis cycle of the growing and shrinking of the pendant droplet with $0.50 \cdot 10^9$ particles.

and pH-dependent. The ξ-potential of AgJPs obtained using the Smoluchowski equation varies from $-(8 \pm 6)\, mV$ $(3.3\, pH)$ to $-(46 \pm 11)\, mV$ $(10.8\, pH)$. According to these ξ-potential values, the AgJPs were colloidally stable at pH values above 5. All experiments of surface activity and collective behaviour were performed at $pH \sim 6$.
To explore different interfacial coverage degrees of AgJPs, the surface activity experiments were performed with different amounts of particles deposited at the surface of a MilliQ water pendant drop. Each experiment involved two stages:

1. Deposition of a certain amount of AgJPs suspended in a spreading agent onto the surface of a $5\,\mu L$ drop in air using a $5\,\mu L$ microsyringe (Hamilton) and a micropositioner. As can be seen in Fig. 6.3, while the spreading solvent was evaporating, the drop volume was slowly increased at $0.08\,\mu L/s$ up to $10\,\mu L$ (first increase of surface tension observed in Fig. 6.6). Next, the drop volume was maintained constant during 3 minutes. Then, the drop volume was increased up to $20\,\mu L$ (second increase of surface tension) and maintained until the surface tension stabilized. This stage of the pendant drop experiment finished once the spreading solvent was fully evaporated.

2. Shrinking and growing of the air/water interface at $0.08\,\mu L/s$ within a volume range from $20\,\mu L$ to $10\,\mu L$. The shrinking of the pendant drop was repeated three times and the growing twice. The shrinking and growing stages were accordingly averaged for each particle concentration.

After the first stage of the pendant drop experiments, the final surface tension decreased as increasing amounts of AgJPs were deposited at the interface. As can be seen in Fig. 6.6, the final surface tension decreased $15\, mN/m$ when the amount of AgJPs deposited was increased 3.5 times. Furthermore, it is observed a decreasing trend in the surface tension with time particularly as particle concentration increases. As it is well known, get completely stationary values of surface tension when particles are adsorbed at fluid interfaces is a very difficult task to accomplish. In our case the maximum rate of variation of the surface tension with time is around $10^{-3}\, mN/(m \cdot s)$. In any case this variation of the surface tension is within the experimental fluctuations of our measurements.
To examine the effect of the spreading agent on the surface tension of the AgJPs monolayers, we used two different volatile liquids (methanol and $1:1$ methanol-propanol). Two pendant drops were formed with the supernatants obtained from the solutions with 10^9 particles dispersed in methanol and the methanol-propanol mixture (centrifugation at 14000 rpm for 15 minutes). The methanol-propanol as spreading agent was not fully evaporated compared to methanol for 2-3 minutes because the surface tension reached values lower with methanol-propanol than with methanol (see Fig. 6.7) [21].
For each shrinking and growing experiment, the surface pressure $\Pi = \gamma_0 - \gamma$,

where γ_0 is the surface tension of water and γ is the measured surface tension of the colloidal monolayer, against the drop area divided by the number of AgJPs was plotted. The effective surface tension γ of a JP-laden interface is lower than the surface tension γ_0 of the bare interface due to the bidimensional osmotic pressure Π generated by the colloidal monolayer, $\gamma = \gamma_0 - \Pi$. In thermodynamic equilibrium, Π is a function of the surface density of JPs, Γ. To the best of our knowledge, there are no experimental data of $\Pi(\Gamma)$ for JPs monolayers formed at the air-water interface.

In Fig. 6.8, the compression isotherm of the AgJPs dispersed in methanol-propanol is plotted. Near the collapse zone, the highest surface pressure measured is $\sim 45\, mN/m$. This value of surface pressure is higher than that obtained in previous works using similar AgJPs, which is attributable to the spreading solvent effect, not fully evaporated because of the stable molecular aggregates formed between propanol and water [21]. However, the hysteresis displayed by the isotherm in Fig. 6.8 is much smaller than that shown by the isotherms obtained by the conventional Langmuir balance [12]. This indicates that the pendant drop tensiometry enables to measure surface pressure values under experimental conditions very close to the thermodynamic equilibrium and that the migration of AgJPs deposited at the interface into the aqueous phase is almost negligible. In the case of high surface pressure (i.e. low surface tension), the pendant drop was highly deformed (see inset in Fig. 6.8). Under these conditions, the pendant drop also exhibited higher surface elasticity as the rheology results (see Table 6.1).

We performed shrinking and growing experiments for different amounts of AgJPs deposited at the air-water interface. Since the values of drop volume and area were fixed in all experiments, the drop area divided by the number of AgJPs deposited at the interface enabled to reproduce a piecewise compression isotherm rather than a traditional compression isotherm, such as obtained with the Langmuir balance [12]. This is noticeable in Fig. 6.9 using methanol as spreading agent. The number of particles was enough to form a monolayer for all concentrations and compression states above $1.0 \cdot 10^9$ particles. We observe in Fig. 6.9 how the low hysteresis found in the isotherms is further lower due to the surface tension error. The interface compression produced changes in the surface pressure ($\sim 5\, mN/m$) at high values of area ($5\dot{1}0^4\, nm^2$/particle), which reveals the sensitivity of this technique. Below this point a gas-liquid transition can be identified from the steep rise in the surface pressure. It is noticeable that the complete compression isotherm throughout the range of interfacial area is not single-valued, i.e. the curves obtained with different particle concentration do not overlap perfectly. This can be explained because each part of the compression isotherm corresponds to a different shrinking and growing experiment with different AgJP amounts in which different self-assembly dynamics could take place. The isotherm collapse is found in Fig. 6.9 between 10^4 and $2 \cdot 10^4\, nm^2$/particle.

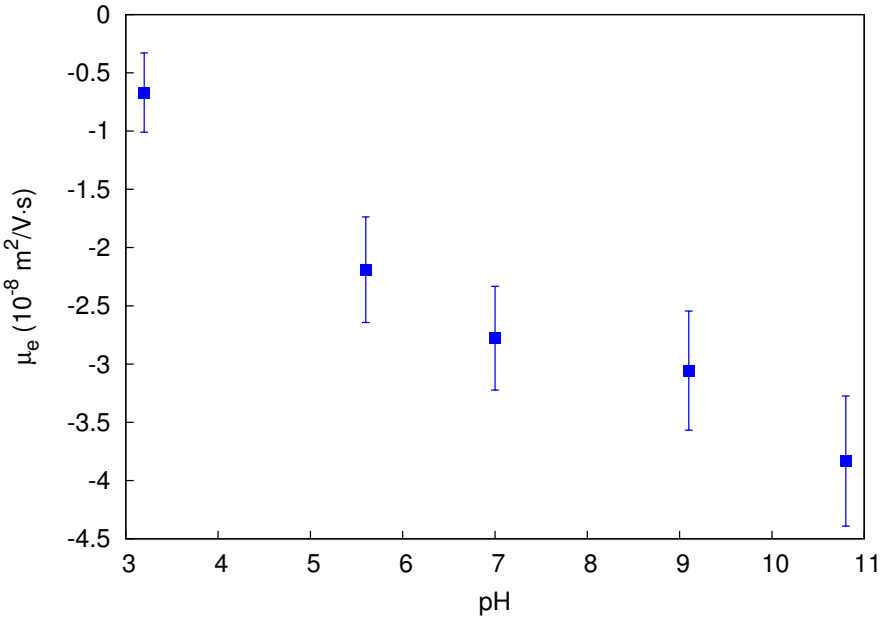

Figure 6.5: Electrophoretic mobility of the AgJPs as a function of pH at $2 \cdot 10^{11}$ particles/ mL and $10^{-2}\,M$ KBr.

This collapse might correspond with the close packing of $100\,nm$ particles at the interface, which takes place when the area per particle is $4R^2$ being R the particle radius (a hexagonally close-packed monolayer). Moreover, the surface tension at the collapse state ($\sim 25\,mN/m$) is in agreement with the reported values for similar AgJPs [12]. The contact angles of both hemispheres of the AgJPs are expected to be around $80°$ and $92°$, which do not represent a large wettability contrast in both faces of the AgJPs used in this study [12]. This reveals that the colloidal stability of the AgJPs in the bulk solution and at the interface plays a more important role in their interfacial activity ratherthan the contact angle difference between their faces.

The Frumkin equation for a monolayer relates the surface pressure (Π) with the area per particle at the interface (Γ^{-1}) as follows [22]:

$$\Pi\left(\Gamma\right) = -\frac{k_B T}{a} \ln 1 - a\Gamma - \beta\Gamma^2$$

where k_B is the Boltzmann constant, T is the temperature, a is the particle geometrical area and β is the interaction constant. The Frumkin equation was fitted to the experimental data in Fig. 6.9 before the collapse, resulting in the dashed black line.
The first term of the equation is referred to the geometry of the system (i.e. how the particles are arranged at the interface) and the second term describes the

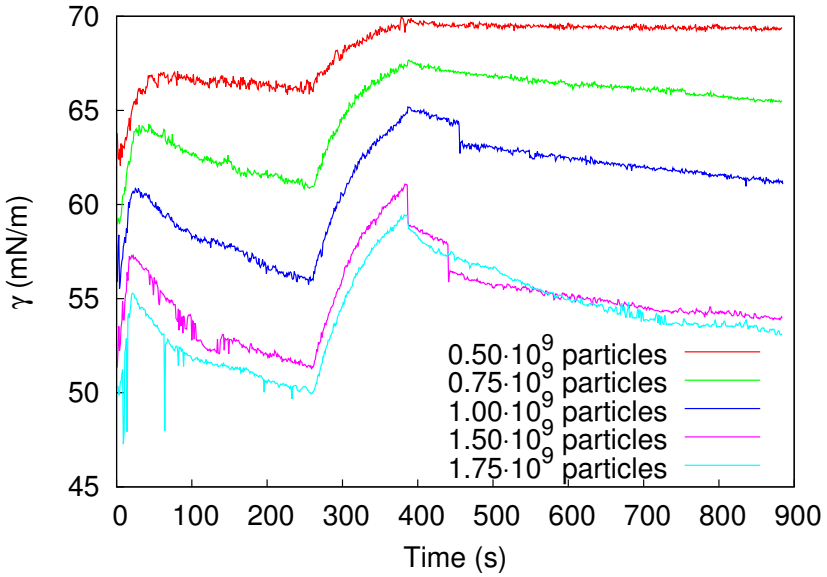

Figure 6.6: Surface tension as a function of time during the formation of pendant drop just after the deposition of the AgJPs, at different particle concentrations. The first increase observed in the surface tension was produced by the spreading agent evaporation and the second increase at $250\,s$ was produced by the drop growing.

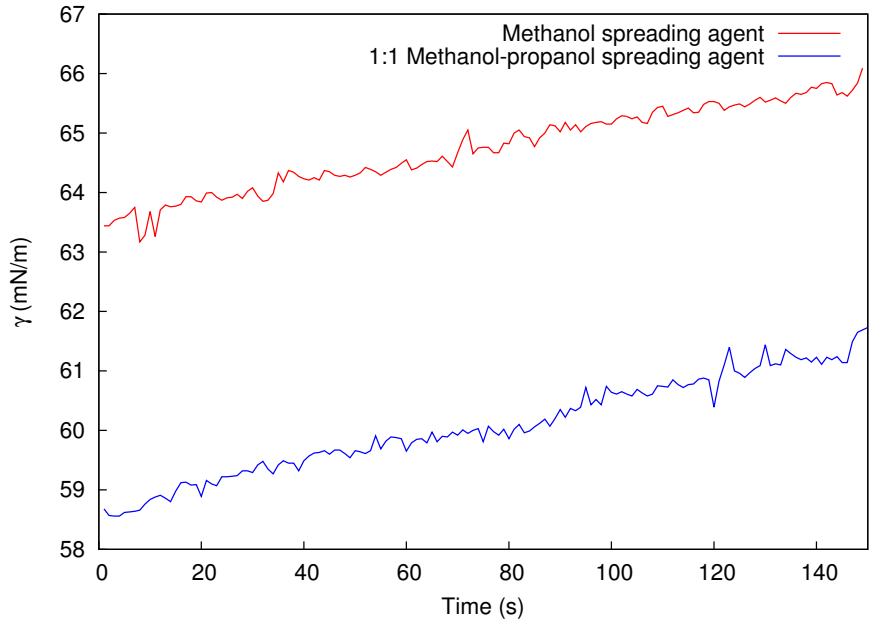

Figure 6.7: Surface tension as a function of time for the supernatants extracted from methanol and $1:1$ methanol-propanol solutions of AgJPs. The increase observed is due to the drop evaporation.

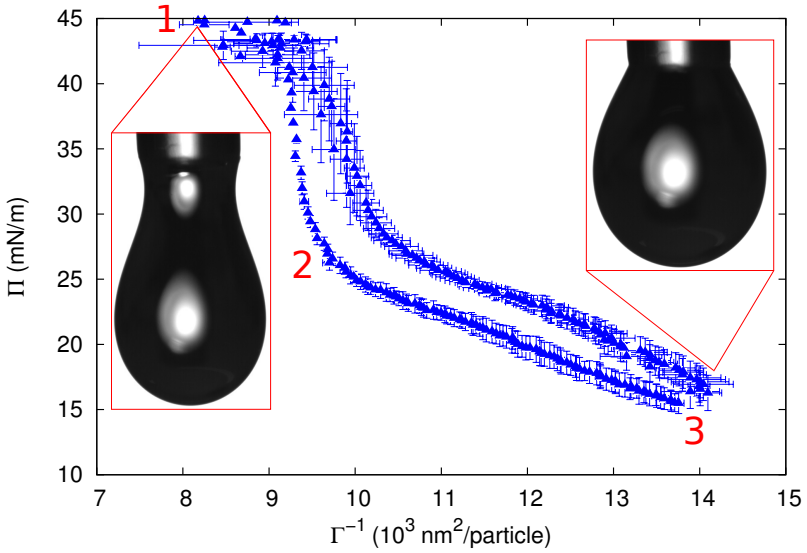

Figure 6.8: Surface pressure as a function of surface area per particle for $2.5 \cdot 10^9$ AgJPs using $1:1$ methanol-propanol solution as spreading agent. This experiment was conducted with several growing/shrinking cycles but at a fixed amount of AgJPs. Inset: drop pictures under the most compressed and expanded states. Inset numbers indicate the compression states of the colloidal monolayer used in the rheology experiments (see Table 6.1).

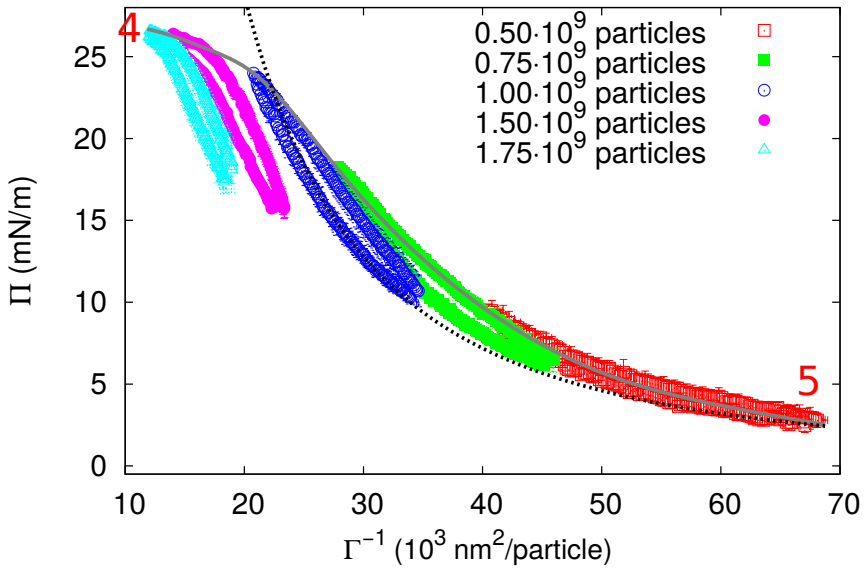

Figure 6.9: Surface pressure as a function of surface area per particle for different particle concentrations using methanol as spreading agent. The dashed line corresponds to the Frumkin model fitting and the solid line serves as a guide to the eye. Inset numbers indicate the compression states of the colloidal monolayer used in the rheology experiments (see Table 6.1).

Table 6.1: Dilatational rheology response of the AgJP monolayer under different compression states. States 1, 2 and 3 correspond to the values obtained with three different compression states on the isotherm shown in Fig. 6.8; whereas states 4 and 5 refer to two compression states of the isotherm shown in Fig. 6.9.

Compression state of AgJP monolayer	$E\,(mN/m)$	$\eta_d\,(mN/ms)$	$\gamma\,(mN/m)$
1	620 ± 50	14.0 ± 0.1	34 ± 1
2	69 ± 2	3.3 ± 0.2	48 ± 1
3	62 ± 2	2.2 ± 0.2	57 ± 1
4	23 ± 1	1.71 ± 0.05	47 ± 1
5	28 ± 2	1.0 ± 0.1	65 ± 1

interaction between the particles at the interface. The first term is negligible for our experimental data but the second term is fitted with a positive value of $\beta = (1.15 \pm 0.08) \cdot 10^{-26} mJ \cdot m^2$. The negligible geometrical term in comparison with the high interaction term points out to the dominant effect of the lateral attractive interactions between AgJPs at the air-water interface.

The dilatational rheology of the colloidal monolayers at the air-water interface has been studied using the procedure described in the experimental methods with different AgJP concentrations and under different values of surface pressure and compression states. This has allowed us to explore the collective behaviour of the AgJPs particles at the interface. Table 6.1 shows the values obtained for the dilatational modulus (E) of the colloidal monolayer, the mean surface tension (γ) and the surface dilatational viscosity (η_d) [23]. We can distinguish two different behaviours depending on the spreading agents used for the deposition of the AgJPs. The results, corresponding to the states 1, 2 and 3 obtained from the compression isotherm performed with the methanol-propanol mixture (Fig. 6.8), indicate that the dilatational modulus changed dramatically when the colloidal monolayer collapsed (state 1), whereas the dilatational modulus remains practically constant when the AgJPs adopted a close-packed hexagonal structure (states 2 and 3). A similar behaviour was observed for the values of surface dilatational viscosity obtained with the three compression states. The states 4 and 5, reproduced from the isotherm performed with methanol as spreading agent (Fig. 6.9), corresponded to the collapsed and extended colloidal monolayer, respectively. The values of both E and η_d obtained upon these compression states agree, which indicates that the collective behaviour of the AgJPs is practically independent of the arrangement of particles in the colloidal monolayer. This illustrates again the decisive role played by the spreading agent. The collapsed monolayer was reproduced to lower values of surface pressure using methanol ($\sim 25\,mN/m$) instead of the mixture of methanol-propanol ($\sim 45\,mN/m$). The elastic network formed by the AgJPs at the interface at high surface pressure is strongly influenced by the presence of solvent molecular clusters established with water [21].

6.4 Conclusions

The surface activity of colloidally stable Janus-like silver particles at the air-water interface was experimentally determined using the pendant drop tensiometry. These particles revealed a surface activity similar to that shown by amphiphilic molecules but with much larger area per particle. We have demonstrated the interplay between bulk colloidal stability and surface activity of Janus-like particles. Oscillating pendant drop tensiometry provided very useful data on the rheological properties of the Janus-like silver particle monolayers; these properties depended on the lateral interactions between particles and were closely related to the monolayer microstructure.

Acknowledgements

This work was supported by MINECO, MAT2010-15101 and MAT2011-23339 projects (Spain) and by "Junta de Andalucía" and FEDER under project P10-FQM-5977. We thank to Dr. J.A. Holgado-Terriza by Dinaten software used for the pendant drop tensiometry. Also, we thank to the company Icon Nanotech by the synthesis of the Janus-like silver particles. Finally, we thank Prof. Lucio Isa for fruitful discussion and for kindly offering facilities and equipment.

References

[1] De Gennes, P. G. Soft matter. *Rev. Mod. Phys.* **July 1992**, *64*, 645–648, DOI: 10.1103/RevModPhys.64.645.

[2] Binks, B. P. Particles as surfactants-similarities and differences. *Curr. Opin. Colloid Interface Sci.* **2002**, *7*, 21–41, DOI: 10.1016/S1359-0294(02)00008-0.

[3] Perro, A.; Reculusa, S.; Ravaine, S.; Bourgeat-Lami, E.; Duguet, E. Design and synthesis of Janus micro- and nanoparticles. *J. Mater. Chem.* **2005**, *15*, 3745–3760, DOI: 10.1039/B505099E.

[4] Lattuada, M.; Hatton, T. A. Synthesis, properties and applications of Janus nanoparticles. *Nano Today* **2011**, *6*, 286–308, DOI: 10.1016/j.nantod.2011.04.008.

[5] Hu, J.; Zhou, S.; Sun, Y.; Fang, X.; Wu, L. Fabrication, properties and applications of Janus particles. *Chem. Soc. Rev.* **2012**, *41*, 4356–4378, DOI: 10.1039/C2CS35032G.

[6] Walther, A.; Müller, A. H. E. Janus Particles: Synthesis, Self-Assembly, Physical Properties, and Applications. *Chem. Rev.* **2013**, *113*, 5194–5261, DOI: 10.1021/cr300089t.

[7] Kaewsaneha, C.; Tangboriboonrat, P.; Polpanich, D.; Eissa, M.; Elaissari, A. Janus Colloidal Particles: Preparation, Properties, and Biomedical Applications. *ACS Appl. Mater. Interfaces* **2013**, *5*, 1857–1869, DOI: 10.1021/am302528g.

[8] Kumar, A.; Park, B. J.; Tu, F.; Lee, D. Amphiphilic Janus particles at fluid interfaces. *Soft Matter* **2013**, *9*, 6604–6617, DOI: 10.1039/C3SM50239B.

[9] Pradhan, S.; Xu, L.; Chen, S. Janus Nanoparticles by Interfacial Engineering. *Adv. Funct. Mater.* **2007**, *17*, 2385–2392, DOI: 10.1002/adfm.200601034.

[10] Glaser, N.; Adams, D. J.; Böker, A.; Krausch, G. Janus Particles at Liquid-Liquid Interfaces. *Langmuir* **2006**, *22*, 5227–5229, DOI: 10.1021/la060693i.

[11] Ruhland, T. M.; Gröschel, A. H.; Walther, A.; Müller, A. H. E. Janus Cylinders at Liquid-Liquid Interfaces. *Langmuir* **2011**, *27*, 9807–9814, DOI: 10.1021/la201863x.

[12] Sashuk, V.; Holyst, R.; Wojciechowski, T.; Fialkowski, M. Close-packed monolayers of charged Janus-type nanoparticles at the air-water interface. *J. Colloid Interface Sci.* **2012**, *375*, 180–186, DOI: 10.1016/j.jcis.2012.02.057.

[13] Garbin, V.; Crocker, J. C.; Stebe, K. J. Nanoparticles at fluid interfaces: Exploiting capping ligands to control adsorption, stability and dynamics. *J. Colloid Interface Sci.* **2012**, *387*, 1–11, DOI: 10.1016/j.jcis.2012.07.047.

[14] Park, B. J.; Brugarolas, T.; Lee, D. Janus particles at an oil-water interface. *Soft Matter* **2011**, *7*, 6413–6417, DOI: 10.1039/C1SM05460K.

[15] Luo, M.; Olivier, G. K.; Frechette, J. Electrostatic interactions to modulate the reflective assembly of nanoparticles at the oil-water interface. *Soft Matter* **2012**, *8*, 11923–11932, DOI: 10.1039/C2SM26890F.

[16] Hong, L.; Cacciuto, A.; Luijten, E.; Granick, S. Clusters of Charged Janus Spheres. *Nano Lett.* **2006**, *6*, 2510–2514, DOI: 10.1021/nl061857i.

[17] Binks, B. P.; Fletcher, P. D. I. Particles Adsorbed at the Oil-Water Interface: A Theoretical Comparison between Spheres of Uniform Wettability and "Janus" Particles. *Langmuir* **2001**, *17*, 4708–4710, DOI: 10.1021/la0103315.

[18] Jana, N. R.; Peng, X. Single-Phase and Gram-Scale Routes toward Nearly Monodisperse Au and Other Noble Metal Nanocrystals. *J. Am. Chem. Soc.* **2003**, *125*, 14280–14281, DOI: 10.1021/ja038219b.

[19] Rotenberg, Y.; Boruvka, L.; Neumann, A. Determination of surface tension and contact angle from the shapes of axisymmetric fluid interfaces. *J. Colloid Interface Sci.* **1983**, *93*, 169–183, DOI: 10.1016/0021-9797(83)90396-X.

[20] Cabrerizo-Vílchez, M. A.; Wege, H. A.; Holgado-Terriza, J. A.; Neumann, A. W. Axisymmetric drop shape analysis as penetration Langmuir balance. *Rev. Sci. Instrum.* **1999**, *70*, 2438–2444, DOI: 10.1063/1.1149773.

[21] Großmann, G. H.; Ebert, K. H. Formation of Clusters in 1-Propanol/Water-Mixtures. *Ber. Bunsenges. Phys. Chem.* **1981**, *85*, 1026–1029, DOI: 10.1002/bbpc.19810851118.

[22] Rusanov, A. I. New theory of equation of state for surface monolayer. *J. Chem. Phys.* **2004**, *120*, 10736–10747, DOI: 10.1063/1.1737301.

[23] Maldonado-Valderrama, J.; Wege, H. A.; Rodríguez-Valverde, M. A.; Gálvez-Ruiz, M. J.; Cabrerizo-Vílchez, M. A. Comparative Study of Adsorbed and Spread β-Casein Monolayers at the Water-Air Interface with the Pendant Drop Technique. *Langmuir* **2003**, *19*, 8436–8442, DOI: 10.1021/la034242z.

I'll believe anything, no matter how wild and ridiculous, if there is evidence for it. The wilder and more ridiculous something is, the firmer and solid the evidence will have to be.

Isaac Asimov

7 Interfacial activity and contact angle of homogeneous, functionalized and Janus nanoparticles at the water/decane interface

Published in Langmuir, Volume 31, Issue 32, 2015, Pages 8818-8823, ISSN 0743-7463, DOI: 10.1021/acs.langmuir.5b02137

M.A. Fernandez-Rodriguez[†], J. Ramos[‡,§], L. Isa[∥], M.A. Rodriguez-Valverde[†], M.A. Cabrerizo-Vilchez[†] and R. Hidalgo-Alvarez[†,*]

[†] *Biocolloid and Fluid Physics Group, Applied Physics Department, Faculty of Sciences, University of Granada, Granada, Spain*

[‡] *POLYMAT, Bionanoparticles Group, Applied Chemistry Department, UFI 11/56, Faculty of Chemical Sciences, University of País Vasco UPV/EHU Donostia-San Sebastián, Spain*

[∥] *Laboratory for Interfaces, Soft matter and Assembly, ETH Zürich, Vladimir-Prelog-Weg 5, 8093 Zürich, Switzerland*

[§] *Department of Materials, Department of Bioengineering, and the Institute for Biomedical Engineering, Imperial College London, London SW7 2AZ, United Kingdom*

[*] *rhidalgo@ugr.es*

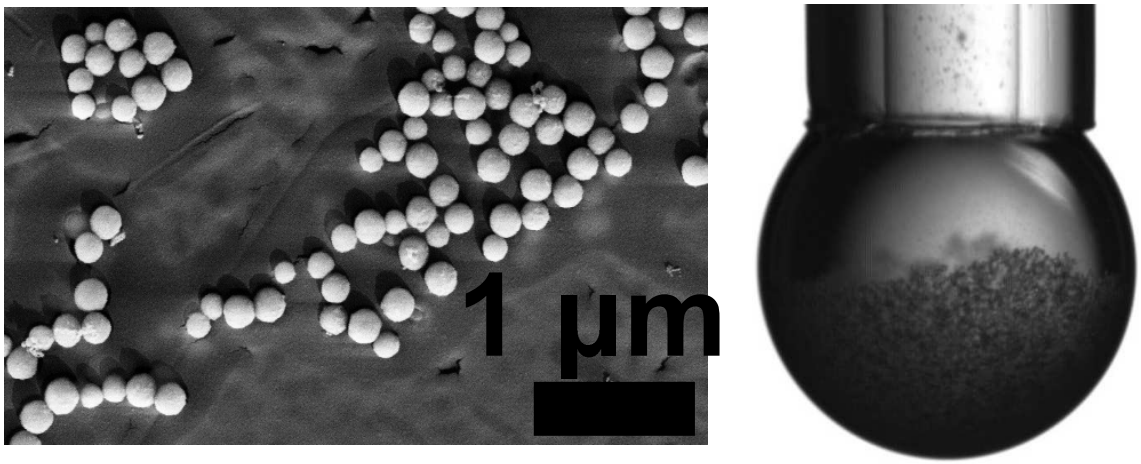

Figure 7.1: Graphical abstract.

Abstract

Surface heterogeneity affects the behavior of nanoparticles at liquid interfaces. To gain a deeper understanding on the details of these phenomena, we have measured the interfacial activity and contact angle at water/decane interfaces for three different types of nanoparticles: homogeneous poly(methyl methacrylate) (PMMA), silica functionalized with a capping ligand containing a methacrylate terminal group, and Ag-based Janus colloids with two capping ligands of different hydrophobicity. The interfacial activity was analyzed by pendant drop tensiometry, and the contact angle was measured directly by freeze-fracture shadow-casting cryo-scanning electron microscopy. The silver Janus nanoparticles presented the highest interfacial activity, compared to the silica nanoparticles and the homogeneous PMMA nanoparticles. Additionally, increasing the bulk concentration of the PMMA and silica nanoparticles up to 100-fold compared to the Janus nanoparticles led to silica particles forming fractal-like structures at the interface, contrary to the PMMA particles that did not show any spontaneous adsorption.

Keywords: Interfacial activity; FreSCA cryo-SEM; Pendant drop tensiometry; Janus nanoparticles; Water/decane interface.

7.1 Introduction

Janus particles with two spatially separated domains displaying different physicochemical properties are suitable to develop responsive nanomaterials [1, 2]. The physicochemical differences between the domains of such nanoparticles enable their self-assembly or reorientation as a response to a given stimulus (e.g., changes in the pH, temperature, ionic

strength, etc.) [2].

In particular, Janus particles obtained from the partial surface modification of silica particles via silane functionalization have been successfully validated for different applications, such as catalysis [3], ultrahydrophobic films [4], water-repellent fabrics [5] and as emulsion [6–8] and foam [9] stabilizers.

The usual way to synthesize Janus nanoparticles involves the selective functionalization of each hemisphere with different capping ligands [1]. A different approach has been reported for heterogeneous silver nanoparticles functionalized with two capping ligands with different hydrophobicity [10]. The capping ligands on such silver nanoparticles reorient toward the preferred liquid phase when placed at a water/oil interface, becoming Janus nanoparticles in situ [10, 11].

Although they are used as interfacial stabilizers, the behavior of Janus particles at liquid interfaces is still controversial [9, 12]. The measured contact angle (CA) of nanoparticles at interfaces depends upon the technique used [12]. In particular, the hydrophobicity of silica nanoparticles is affected by the addition of surface-active molecules, such as surfactants or alcohols [13]. Thus, the effect of the spreading agent in Langmuir isotherm experiments must be taken into account because it can affect the final surface tension and the CA of the deposited particles [11, 12].

The problem of measuring CAs of Janus particles is even more complex. Whether Janus particles actually behave as amphiphiles at the interface or not depends upon the Janus ratio (i.e., the ratio between the areas of the two different domains) and the wettability contrast between both patches. Strictly, real Janus behavior, namely, the correspondence of the three-phase contact line with the boundary between domains, can only be observed for Janus ratios close to unity and large wettability contrasts. How this scenario demonstrated for microparticles is applicable to nanoparticles is still a matter of debate [14].

Regardless of all of the controversy, Janus nanoparticles act as better emulsion stabilizers than homogeneous nanoparticles. It is known that Janus nanoparticles obtained by surface modification of bare silica particles successfully allow for the stabilization of oil droplets in water with higher long-term stability than emulsions stabilized with homogeneous silica nanoparticles [15]. This fact agrees with the theoretical prediction that a Janus particle with equal hydrophilic and hydrophobic areas is 3 times more surface-active than the corresponding homogeneous particle at a water/oil interface [16]. Moreover, in the case of nanoparticles, the thickness of the capping ligands is usually comparable to the core size. Therefore, ligand reconfiguration can affect the adsorption of the nanoparticles at liquid interfaces, as shown by molecular dynamic simulations and experiments [9], and complicated energies and interactions within the polymer-capped nanoparticles govern the formation of nanostructures [17].

In this work, we focused on the comparison between CA and interfacial activity of three different nanoparticles at the water/decane interface: poly(methyl methacrylate) (PMMA) homogeneous nanoparticles, silica nanoparticles functionalized with methacryloxypropyltrimethoxysilane (MPS), and silver Janus nanoparticles. We measured the CA of these nanoparticles with freeze-fracture shadow-casting cryo-scanning electron microscopy (FreSCa Cryo-SEM) [14, 18] and the interfacial tension with a pendant drop tensiometer.

7.2 Materials and Methods

7.2.1 Homogeneous, Functionalized and Janus Nanoparticles

PMMA research particles with a radius of 105 nm, standard deviation (SD) of 4 nm, and 5% (w/v) aqueous suspension (values supplied by Microparticles GmbH, Germany) were used as homogeneous nanoparticles (labeled as PMMA-HPs).

Tetraethyl orthosilicate (TEOS, Acros Organics, 98%), ethanol (Scharlau, absolute, reagent grade), ammonia (Scharlau, 32% solution), MPS (Sigma-Aldrich), and ultrapure distilled water (Milli-Q Academic, Millipore) were used for the synthesis of silica nanoparticles according to the Stöber procedure [19]. For each reaction, absolute ethanol, ammonia, and water were mixed in a 500 mL reaction vessel. Then, TEOS was added quickly, and the reaction mixture was stirred at 350 rpm and room temperature for 24 h. The molar concentration of the mixed solution was 2.49:1.06 water/ammonia for the synthesis of silica nanoparticles of 208 nm in diameter. The volume of absolute ethanol was adjusted up to 500 mL, and the concentration of TEOS was fixed to 0.2 M. Silica nanoparticles were collected by centrifugation (15000 rpm for 15 min) and washed by repeated redispersion in absolute ethanol 3 times. The final product was dried in a vacuum oven at 80°C for 24 h. The method of partial functionalization of silica nanoparticles was reported in previous works [20–22]. First, 1.6 g of silica nanoparticles was introduced into a beaker. Next, 0.8 mL of deionized water was added to the silica nanoparticles. Then, 52 mL of toluene containing 1.0 mL of MPS and 2.0 mL of triethylamine was added. The mixture was stirred for 3 days at room temperature. Subsequently, the solid was collected by centrifugation (12000 rpm for 5 min) and dried under vacuum for 24 h after being washed 3 times in ethanol. These silica nanoparticles are partially modified with MPS because a fraction of the particle surface remains covered with hydroxyl groups with high affinity to water and the other fraction of the particle surface is modified with MPS groups, less polar and with higher affinity to oil. From thermogravimetric analysis, assuming that the amount of MPS is homogeneously distributed over all of the surface, the MPS surface coverage is $2.27 \cdot 10^{-4}\, mol_{MPS}/g_{SiO_2}$. The final functionalized silica nanoparticles are labeled as silica-FPs and are dispersed in Milli-Q water.

Silver Janus nanoparticles (labeled as Ag-JPs) were synthesized as described in previous work [11], with a size of 175 nm measured by FreSCa Cryo-SEM. The synthesis is based in the exchange of 11-mercaptoundecanoic acid and 1-undecanthiol ligands with silver nanoparticles functionalized with decanoic acid. The Ag-JPs are dispersed in methanol.

All nanoparticle dispersions are surfactant-free. The size and electrophoretic mobility of the nanoparticles were measured by dynamic light scattering (DLS) with a Malvern Zetasizer Nano Z device in a solution of BrK at an ionic strength of 10^{-4} M and a pH of 5.5.

7.2.2 Pendant drop tensiometry

Pendant drop tensiometry was performed with a homemade setup as described in previous works [11, 23]. First, a water pendant drop was formed in a capillary with a Hamilton microinjector pump. Different amounts of Ag-JPs dispersed in methanol were deposited with a Hamilton microsyringe on the surface of the initial water pendant drop. In the case of PMMA-HPs and silica-FPs, the microsyringe was loaded with a 1:1 particle dispersion/methanol mixture. Once the pendant drop was formed, side-view images of the droplet were captured by a CMOS camera and processed with the Dinaten software to obtain the corresponding surface tension by axisymmetric drop shape analysis of the pendant drop profile (ADSA-P) [24]. The surface tension was monitored until full evaporation of methanol (i.e., Langmuir layer formation [9]). Next, we immersed the pendant drop in decane [high-performance liquid chromatography (HPLC) grade, Sigma] and performed growing and shrinking cycles at 0.08 μL/s, varying the drop volume within 40 and 15 μL as described in previous works [11, 23], and the corresponding interfacial tension was measured. In addition, drops of the suspensions containing the nanoparticles at different concentrations were formed in the case of aqueous suspensions (PMMA-HPs and silica-FPs). In this process, the particles adsorb at the interface from the pendant drop bulk (i.e., Gibbs layer formation, significantly slower than the Langmuir layer formation [9]).

7.2.3 Freeze-fracture Shadow-Casting

The FreSCa cryo-SEM technique, described in previous works [14, 18], consists of the immobilization and imaging of nanoparticles at a water/oil interface in a cryo-SEM. The immobilization is provided by vitrification of the interface with a propane jet freezer, and the imaging is performed after fracturing the sample in cryo and ultrahigh vacuum conditions and after directional coating by a thin tungsten layer, deposited at a 30° angle relative to the interface. The shadow projected by the nanoparticles trapped in the water/decane interface upon tungsten casting is measured by cryo-SEM and used to calculate the CAs of individual nanoparticles. The silica-FPs and PMMA-HPs are measured after adsorption directly from the water phase, and the Ag-JPs are deposited from methanol in a water phase, waiting until full evaporation of the methanol. Thus, the methanol evaporation process is absent for silica-FPs and PMMA-HPs, and we expect a lower number of nanoparticles reaching the interface because of the absence of the energy provided by the methanol evaporation.

7.3 Results and Discussion

The results of electrophoretic mobility, size, and CA measured for the different nanoparticles are collected in Table 7.1. First, we discuss the similarities and differences between nanoparticles to establish possible comparisons. The capping ligands of the silica-FPs consist of a silane group anchored to the silica core, a propyl hydrocarbon chain, and a terminal methacrylate group. The silica-FPs are comparable in size and mobility with the PMMA-HPs, both dispersed in water. The PMMA-HPs serve as an example of a homoge-

neous organic nanoparticle, and the silica-FPs serve as an example of a heterogeneous nanoparticle made of a silica inorganic core (hydrophilic) and less hydrophilic organic capping ligands. On the other hand, the Ag-JPs are also comparable in size to the other nanoparticles; however, their mobility is lower (half), and they are dispersed in methanol. Moreover, the capping ligands of the Ag-JPs are reoriented at the water/oil interface into different spatial domains, with the more hydrophilic one toward the water phase and the more hydrophobic one toward the oil phase [10, 11]. When the capping ligands do not present a difference in hydrophobicity, simulations have shown that the Janus particles place randomly at the interface, although there is some ordering when the interface is stretched [25].

From Table 7.1, the nanoparticle size is systematically overestimated by DLS compared to the direct measurement obtained from the FreSCa cryo-SEM images (see Figure 7.3). This is expected because DLS gives an effective hydrodynamic radius that is greater than the real radius of the dehydrated nanoparticles.

The CA distribution was measured counting 176 PMMA-HPs, 229 silica-FPs, and 53 Ag-JPs. The lower number of Ag-JPs is due to the lower concentration that we could obtain with these nanoparticles. The values of CA in Table 7.1 were calculated as the mean and standard deviation of the measured CAs for each kind of nanoparticle. The CAs obtained with the FreSCa cryo-SEM technique for the silica-FPs, PMMA-HPs, and Ag-JPs deposited at water/decane interfaces present a wide distribution (see Figure 7.2). Nevertheless, the distribution is narrower for the PMMA-HPs than for the silica-FPs and Ag-JPs. The silica-FPs presented the highest CA (over 90°), followed by the Ag-JPs (close to 90°), and finally the PMMA-HPs (76°). The values of CA enable prediction of the behavior of the nanoparticles as emulsifiers: CAs smaller than 90° tend to stabilize oil-in-water emulsions, and values greater than 90° tend to stabilize water-in-oil emulsions [26]. Nonetheless, this emulsion stabilization mechanism has to be taken carefully into consideration because it is affected by coalescence effects. Stancik et al. [27] studied the coalescence of particle-laden drops with homogeneous particles and found that the precise nature of the particle dynamics and microstructures during coalescence are not straightforward to anticipate.

The wide distribution of measured CAs agrees with the results obtained with other techniques for direct CA measurement of nanoparticles placed at liquid interfaces such as the gel trapping technique [28] or Bessel beam microscopy [29]. We assume that this scattering is due to the dependence of the CA upon the details of the different nanoparticles and their kinetics as they reach the interface. Furthermore, the narrower distribution of CAs for the PMMA-HPs might point to less CA variation of the homogeneous nanoparticles rather than the heterogeneous nanoparticles. The high CA of the silica-FPs compared to PMMA-HPs is in agreement with previous molecular dynamics simulations of silica nanoparticles (3 nm diameter) with tunable surface activity at a water/decane interface [26]. In this work, the surface activity was modulated through the ratio between methyl and hydroxyl groups at the interface and the homogeneous nanoparticles presented CAs typically lower than 90°, whereas the Janus nanoparticles revealed CAs usually greater than 90°. Even though our silica-FPs are not strictly Janus nanoparticles, they are less hydrophilic than the homogeneous PMMA nanoparticles. The macroscopic CA of a water drop deposited on a smooth PMMA film was reported to be 67.8° $\pm$ 1.4° (water/air interface); although with a later treatment that provided more roughness and functional group

Table 7.1: Electrophoretic Mobility and Size Measured by DLS and Size and CA Measured by FreSCa cryo-SEM of the Nanoparticles Studied

	Mobility $(10^{-8}\, m^2/(V \cdot s))$	DLS size (nm)	FreSCa size (nm)	FreSCa CA (deg)
PMMA-HPs	-2.7 ± 0.6	156.9 ± 0.5	119 ± 27	76 ± 9
Silica-FPs	-3.0 ± 0.4	216 ± 16	181 ± 23	94 ± 14
Ag-JPs	-1.5 ± 0.6	210 ± 18	175 ± 43	86 ± 19

Table 7.2: Interfacial Tension of a 20 μL Water Pendant Drop in Air and a 30 μL Water Pendant Drop in Decane, for Different Concentrations of Each Nanoparticle upon Spreading.

	$\gamma_{\text{Water/Air}}\,(mN/m)$	$\gamma_{\text{Water/Decane}}\,(mN/m)$
$2.43 \cdot 10^8$ PMMA-HPs	72.7 ± 0.1	50.2 ± 0.2
$4.86 \cdot 10^8$ PMMA-HPs	70.5 ± 0.1	52.2 ± 0.1
$9.72 \cdot 10^8$ PMMA-HPs	72.4 ± 0.1	52.3 ± 0.1
$1.05 \cdot 10^8$ silica-FPs	70.3 ± 0.1	52.2 ± 0.1
$2.10 \cdot 10^8$ silica-FPs	71.4 ± 0.1	50.3 ± 0.1
$4.20 \cdot 10^8$ silica-FPs	70.0 ± 0.1	51.1 ± 0.1
$0.96 \cdot 10^8$ Ag-JPs	71.8 ± 0.2	48.3 ± 0.5
$1.92 \cdot 10^8$ Ag-JPs	71.0 ± 0.4	48.5 ± 0.5
$3.84 \cdot 10^8$ Ag-JPs	64.1 ± 0.4	42.9 ± 0.4

reorientation to the PMMA film, the CA increased up to 154.3° ± 3.9° [30]. The CA of PMMA-HPs of the same manufacturer but with a larger size (1–2 μm) measured by the gel trapping technique in a water/n-octane interface was 56° ± 2° [31], which is significantly lower than the value obtained for our PMMA-HPs at a water/decane interface measured by FreSCa cryo-SEM. This reveals a strong dependence of the observed CA and specific PMMA surface, i.e., in terms of the particle size and roughness and in relation to the type of oil phase. This invalidates any comparison between the CA of a sessile water drop on a PMMA substrate and the CA of PMMA-HPs deposited at a water/oil interface. Finally, the Ag-JPs CA seems lower than the CA of the silica-FPs, but actually, they overlap within their standard deviations. From this, we cannot state differences between these nanoparticles.

To investigate further the effects of surface chemistry on the behavior at the interface, the interfacial activity of the nanoparticles was explored by pendant drop tensiometry. Stable interfacial tension values were obtained after forming water pendant drops with different numbers of particles deposited in air and, subsequently, immersed in decane. The numbers of particles were chosen to obtain the same coverage between different nanoparticles, starting from the assumption that all of them were placed at the interface, assuming close-packing. The stable values of interfacial tension are collected in Table 7.2, measured after 30 min.

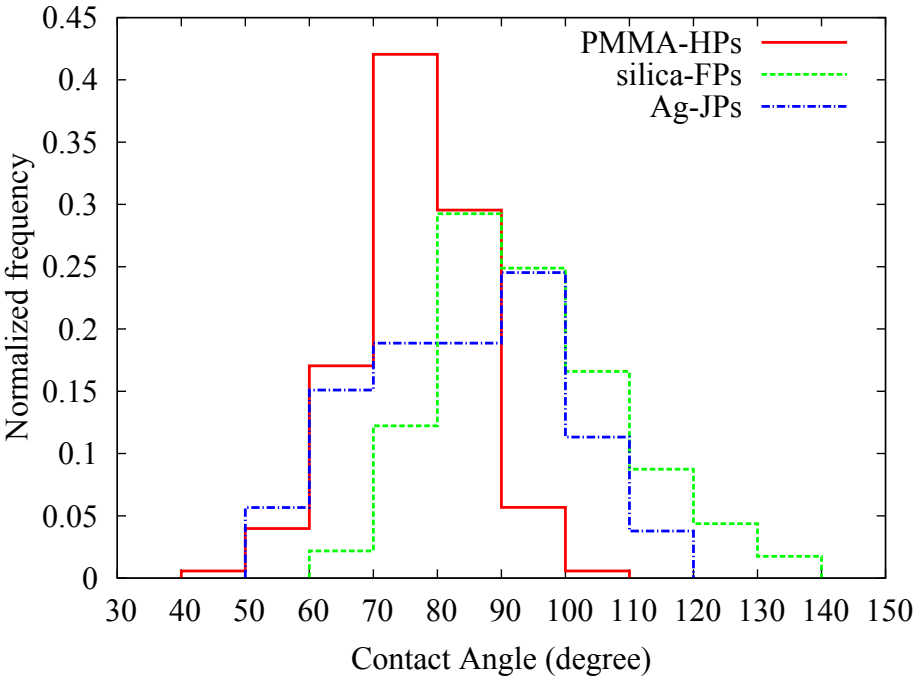

Figure 7.2: CAs of PMMA-HPs, silica-FPs, and Ag-JPs at water/decane interfaces measured by FreSCa cryo-SEM.

At room temperature, the water surface tension is around 72 mN/m and the water/decane interfacial tension is around 52 mN/m. The values in Table 7.2 confirm that the surface tension of the PMMA-HPs and silica-FPs suspensions do not depend upon the particle concentration. Although the errors are low because the values are constant over time, within a 2 mN/m margin, it is not possible to say that they differ significantly because of the limits of the pendant drop tensiometry. Only for the Ag-JPs at the highest concentration, the surface tension was significantly decreased. This might point out that the PMMA-HPs and silica-FPs are scarcely adsorbed at the water/air interface or that they are very poorly interfacially active. However, all nanoparticles certainly adsorbed at the water/decane interface as shown in Table 7.2 and Figure 7.3. Provided the extensive use of silica nanoparticles as emulsion stabilizers, these results point out that they stabilize through a steric effect rather than by their amphiphile character [16].

The results of compression/expansion cycles of each water pendant drop immersed in decane are plotted in Figure 7.4, where the interfacial pressure Π is defined as $\Pi = \gamma_0 - \gamma$, with γ_0 being the interfacial tension in the absence of nanoparticles. The interfacial pressure is plotted against the normalized area. The normalized area is calculated as the pendant drop area divided by the total area that the nanoparticles would occupy if they were all placed at the interface, assuming close packing. The piecewise-like compression isotherms are similar to the observed ones for other Janus systems studied previously, and they are piecewise-like as a result of the limitations to vary the interfacial area over a large range in a single pendant drop experiment [11, 23].

When a film is compressed beyond a certain pressure (i.e., the pendant drop is shrunk),

a particle-laden drop may undergo buckling [32]. When buckling occurs, it is expected to observe a change in the slope of the compression isotherm [33]. However, this behavior is not observed in our measurements, and this suggests the absence of such buckling processes within the range of volumes and interfacial tensions studied. Also, the compression/expansion cycles in Figure 7.4 were closed for each concentration and nanoparticle, pointing out that there was no significant adsorption or desorption during the experiments. The Ag-JPs showed discontinuities in the surface pressure for similar compression states. This might indicate that they are very sensitive to the initial compression state upon adsorption of different particle numbers. In fact, the monolayers may evolve differently when the surface is compressed, and the internal stress may relax in different ways. Finally, it can be concluded that Ag-JPs presented significantly higher interfacial activity compared to the negligible interfacial activity of silica-FPs and PMMA-HPs, as previously demonstrated. To try to obtain a similar surface pressure as the Ag-JPs for the other two nanoparticle types, we performed different experiments in which the pendant drop was made of the aqueous silica-FPs and PMMA-HPs dispersions. In this case, we did not spread the particles aided by methanol, but we monitored the spontaneous adsorption from the bulk. Under these conditions, the available number of particles that can adsorb at the interface could be increased 100 times. The results of compression/expansion cycles of such water pendant drops immersed in decane are plotted in Figure 7.6 of the Supporting Information.

The PMMA-HPs and silica-FPs, similar in size and with the same particle number in the water bulk phase, behave differently at the water/decane pendant drop interface. In comparison to the homogeneous aspect of the pendant drop of PMMA-HPs (Figure 7.5a), the silica-FPs are visibly accumulated with fractal-like structures at the bottom of the drop (Figure 7.5b). The number of particles that reach the interface will be different as a result of electrostatic repulsions and dipolar interactions through the oil phase and the different and slow relaxation processes of such particles reaching the interface [34]. The fractal-like structure of silica-FPs is in agreement with a study in which silica nanoparticles form dense, connected patches surrounding uncovered areas [7]. Some authors report that the homogeneous nanoparticles are arranged in a hexagonal pattern as a result of long-range electrostatic repulsion, contrary to Janus nanoparticles that show a fractal-like arrangement as a result of attractive interactions [35, 36]. Furthermore, Xu et al. [37] observed attraction and repulsion of homogeneous particles in a water/oil pendant drop. This effect was observed when a water drop (immersed in an oil phase) was brought close to a flat oil-water interface as a result of electrostatic interactions between the two interfaces. The attractive interactions for silica-FPs might be due to capillary interactions, where different roughness or chemical heterogeneity may deform the three-phase contact line around the particle, leading to nanoparticle aggregation [38]. Finally, the FreSCa images in Figure 2 also indicate that the silica-FPs have stronger tendency to aggregate at the interface compared to the PMMA-HPs.

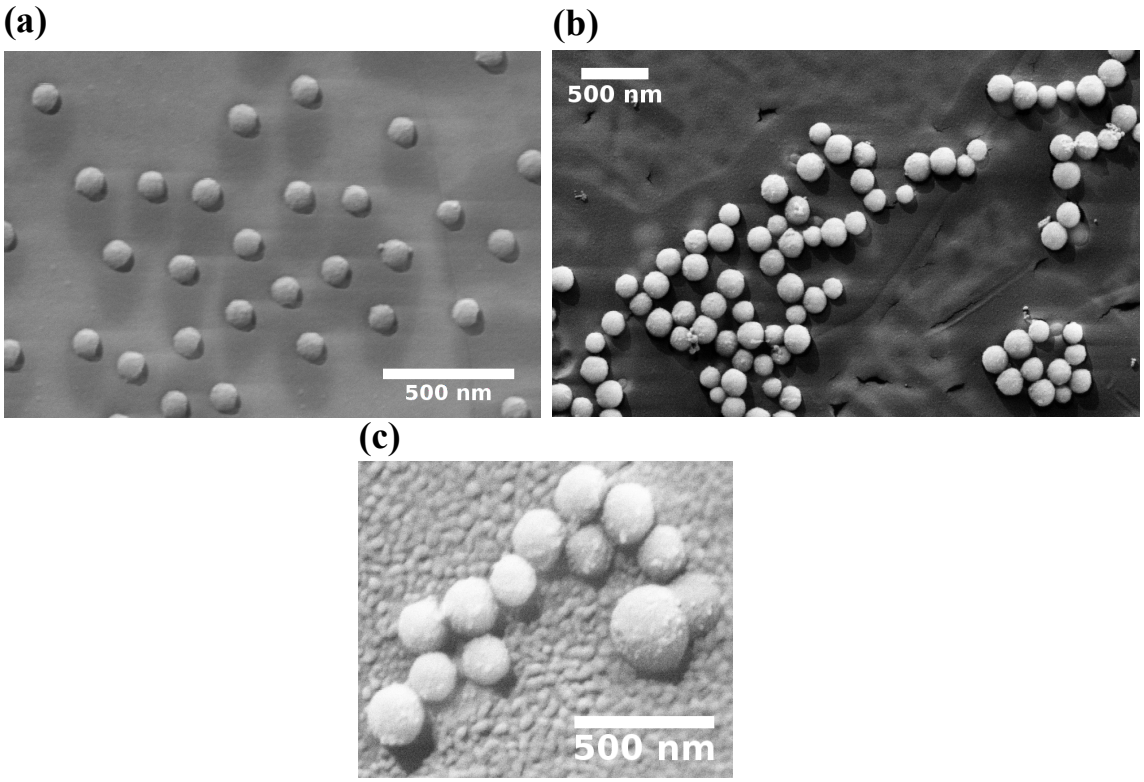

Figure 7.3: FreSCa cryo-SEM pictures of (a) PMMA-HPs, (b) silica-FPs, and (c) Ag-JPs. The tungsten shadow projected by the nanoparticles enables estimating the CA of the nanoparticles. All of the scale bars are 500 nm.

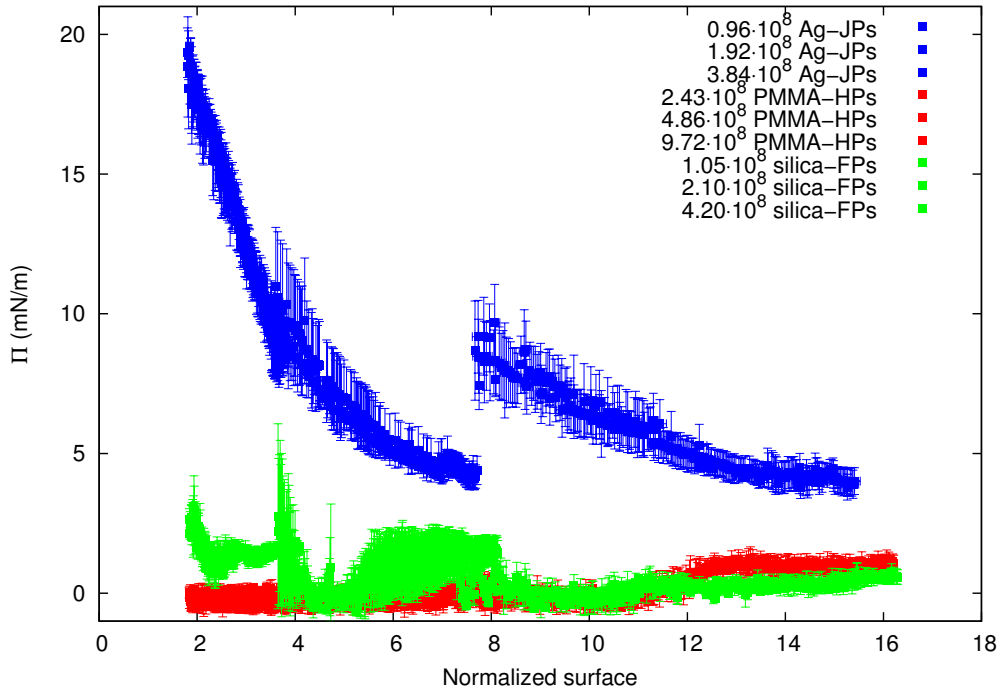

Figure 7.4: Interfacial pressure for compression/expansion cycles of water/decane pendant drops against the normalized area for different concentrations of deposited PMMA-HPs, silica-FPs, and Ag-JPs. The normalized area is calculated as the pendant drop area divided by the area that would be occupied by the nanoparticles if they were all placed at the interface, assuming close packing.

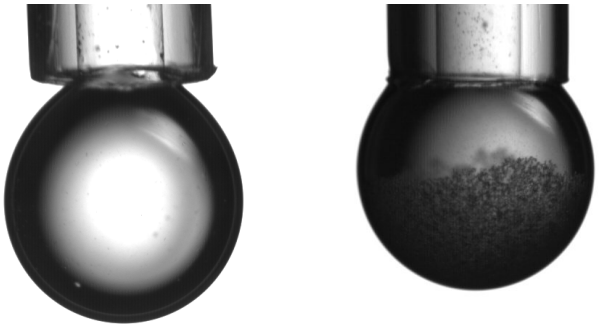

(a) Homogeneous PMMA nanoparticles (b) Functionalized silica nanoparticles

Figure 7.5: Pendant drops (5 μL) with a suspension of $21.7 \cdot 10^{11}$ nanoparticles/mL of (a) PMMA-HPs and (b) silica-FPs, both immersed in decane. The presence of fractal-like clusters of the silica-FPs is clearly noticeable in the images.

7.4 Conclusions

The interfacial activity of PMMA-HPs, silica-FPs, and Ag-JPs with similar sizes (∼200 nm) was studied at the water/decane interface via interfacial tension and direct CA measurements. The highest CA was obtained for the silica-FPs and Ag-JPs, and the lowest CA was obtained for the PMMA-HPs. The wide CA distribution for all nanoparticles might be due to the heterogeneity in the surface properties and adsorption of the nanoparticles that reach the interface. The interfacial activity of Ag-JPs was significantly higher compared to silica-FPs and PMMA-HPs at equivalent particle concentrations. Although the silica-FPs and PMMA-HPs did not show a strong effect in reducing the water/decane interfacial tension, they were certainly adsorbed as reflected by FreSCA cryo-SEM images. A 100-fold higher concentration of silica-FPs and PMMA-HPs was necessary to obtain a similar reduction of the interfacial tension at the water/decane interface as for the case of the Ag-JPs. Thus, the silica nanoparticles are expected to stabilize emulsions by steric effect rather than by its amphiphile character. At higher concentrations, the silica-FPs exhibited fractal-like structures as a result of attractive interactions, unlike PMMA-HPs. Despite the fact that the CAs of silica-FPs and Ag-JPs were similar within errors, only the latter led to a significant reduction of the interfacial tension at the same surface coverage, probably as a result of its surface chemistry and Janus character. From our findings, in the absence of surfactants, Janus silver nanoparticles may act as better emulsifiers as a result of their remarkable interfacial activity at the water/decane interface compared to homogeneous PMMA or heterogeneously functionalized silica nanoparticles.

Acknowledgements

This work was supported by the Spanish MINECO (Projects MAT2011-23339 and MAT2013-44429-R), "Junta de Andalucía" and FEDER (Projects P10-FQM-5977 and P12-FQM-1443), and the COST Action "Smart and green interfaces" (STSM MP1106-14761). Lucio Isa acknowledges financial support from the Swiss National Science Foundation (Grant PP00P2-144646/1). The authors thank Prof. Nicholas Spencer at ETH Zurich for access to equipment and facilities and J. A. Holgado-Terriza and J. L. Muros-Cobos for the software Dinaten used for the interfacial tension measurements. The authors acknowledge support of ScopeM at the ETH Zürich for the FreSCa cryo-SEM measurements.

7.5 Supporting Information

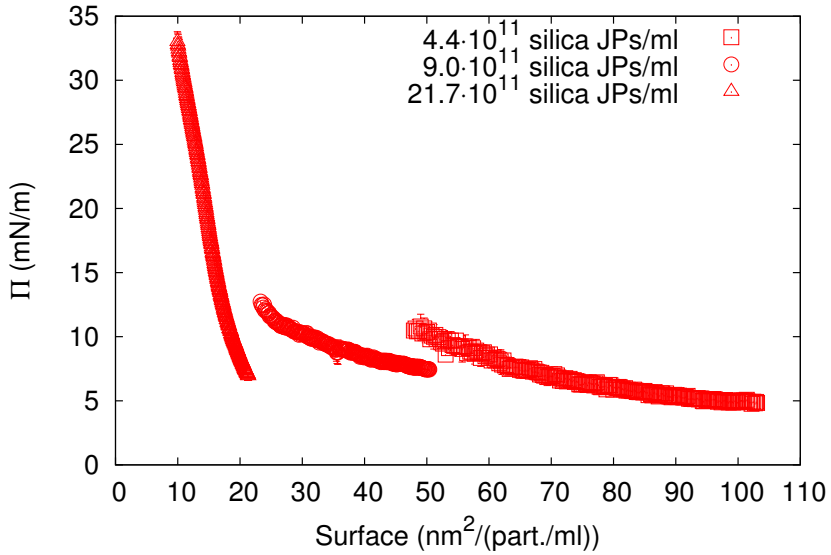

(a) PMMA homogeneous nanoparticles (PMMA-HPs)

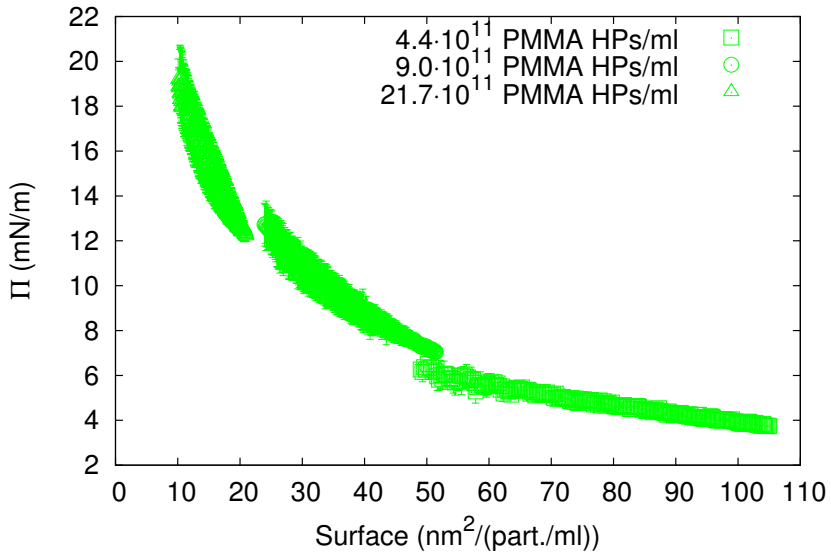

(b) Silica functionalized nanoparticles (silica-FPs)

Figure 7.6: Interfacial pressure for compression/expansion cycles of water/decane pendant drops against area per concentration for different concentrations of (a) PMMA-HPs, (b) silica-FPs in the water phase.

References

[1] Walther, A.; Müller, A. H. E. Janus Particles: Synthesis, Self-Assembly, Physical Properties, and Applications. *Chem. Rev.* **2013**, *113*, 5194–5261, DOI: 10.1021/cr300089t.

[2] Yoshida, M.; Lahann, J. Smart Nanomaterials. *ACS Nano* **2008**, *2*, 1101–1107, DOI: 10.1021/nn800332g.

[3] Faria, J.; Ruiz, M. P.; Resasco, D. E. Phase-Selective Catalysis in Emulsions Stabilized by Janus Silica-Nanoparticles. *Adv. Synth. Catal.* **2010**, *352*, 2359–2364, DOI: 10.1002/adsc.201000479.

[4] Berger, S.; Ionov, L.; Synytska, A. Engineering of Ultra-Hydrophobic Functional Coatings Using Controlled Aggregation of Bicomponent Core/Shell Janus Particles. *Adv. Funct. Mater.* **2011**, *21*, 2338–2344, DOI: 10.1002/adfm.201100155.

[5] Synytska, A.; Khanum, R.; Ionov, L.; Cherif, C.; Bellmann, C. Water-Repellent Textile via Decorating Fibers with Amphiphilic Janus Particles. *ACS Appl. Mater. Interfaces* **2011**, *3*, 1216–1220, DOI: 10.1021/am200033u.

[6] Binks, B. P.; Tyowua, A. T. Influence of the degree of fluorination on the behaviour of silica particles at air-oil surfaces. *Soft Matter* **2013**, *9*, 834–845, DOI: 10.1039/C2SM27395K.

[7] Destribats, M.; Gineste, S.; Laurichesse, E.; Tanner, H.; Leal-Calderon, F.; Héroguez, V.; Schmitt, V. Pickering Emulsions: What Are the Main Parameters Determining the Emulsion Type and Interfacial Properties? *Langmuir* **2014**, *30*, 9313–9326, DOI: 10.1021/la501299u.

[8] Liang, F.; Shen, K.; Qu, X.; Zhang, C.; Wang, Q.; Li, J.; Liu, J.; Yang, Z. Inorganic Janus Nanosheets. *Angew. Chem. Int. Ed. Engl.* **2011**, *50*, 2379–2382, DOI: 10.1002/anie.201007519.

[9] Garbin, V.; Crocker, J. C.; Stebe, K. J. Nanoparticles at fluid interfaces: Exploiting capping ligands to control adsorption, stability and dynamics. *J. Colloid Interf. Sci.* **2012**, *387*, 1–11, DOI: 10.1016/j.jcis.2012.07.047.

[10] Sashuk, V.; Hołyst, R.; Wojciechowski, T.; Fiałkowski, M. Close-packed monolayers of charged Janus-type nanoparticles at the air-water interface. *J. Colloid Interface Sci.* **2012**, *375*, 180–186, DOI: 10.1016/j.jcis.2012.02.057.

[11] Fernandez-Rodriguez, M. A.; Rodriguez-Valverde, M. A.; Cabrerizo-Vilchez, M.; Hidalgo-Alvarez, R. Surface activity and collective behaviour of colloidally stable Janus-like particles at the air-water interface. *Soft Matter* **2014**, 3471–3476, DOI: 10.1039/C3SM52624K.

[12] Maestro, A.; Guzmán, E.; Ortega, F.; Rubio, R. G. Contact angle of micro- and nanoparticles at fluid interfaces. *Curr. Opin. Colloid Interface Sci.* **2014**, *19*, 355–367, DOI: 10.1016/j.cocis.2014.04.008.

[13] Maestro, A.; Guzman, E.; Santini, E.; Ravera, F.; Liggieri, L.; Ortega, F.; Rubio, R. G. Wettability of silica nanoparticle-surfactant nanocomposite interfacial layers. *Soft Matter* **2012**, *8*, 837–843, DOI: 10.1039/C1SM06421E.

[14] Synytska, A.; Kirillova, M. S.; Isa, L. Synthesis and Contact Angle Measurements of Janus Particles. *ChemPlusChem* **2014**, *79*, 656–661, DOI: 10.1002/cplu.201400020.

[15] Jiang, S.; Chen, Q.; Tripathy, M.; Luijten, E.; Schweizer, K. S.; Granick, S. Janus Particle Synthesis and Assembly. *Adv. Mater.* **2010**, *22*, 1060–1071, DOI: 10.1002/adma.200904094.

[16] Binks, B. P.; Fletcher, P. D. I. Particles Adsorbed at the Oil-Water Interface: A Theoretical Comparison between Spheres of Uniform Wettability and "Janus" Particles. *Langmuir* **2001**, *17*, 4708–4710, DOI: 10.1021/la0103315.

[17] Yan, L.-T.; Xie, X.-M. Computational modeling and simulation of nanoparticle self-assembly in polymeric systems: Structures, properties and external field effects. *Prog. Polym. Sci.* **2013**, *38*, 369–405, DOI: 10.1016/j.progpolymsci.2012.05.001.

[18] Isa, L.; Lucas, F.; Wepf, R.; Reimhult, E. Measuring single-nanoparticle wetting properties by freeze-fracture shadow-casting cryo-scanning electron microscopy. *Nat. Commun.* **2011**, *2*, DOI: 10.1038/ncomms1441.

[19] Stöber, W.; Fink, A.; Bohn, E. Controlled growth of monodisperse silica spheres in the micron size range. *J. Colloid Interface Sci.* **1968**, *26*, 62–69, DOI: 10.1016/0021-9797(68)90272-5.

[20] Qiang, W.; Wang, Y.; He, P.; Xu, H.; Gu, H.; Shi, D. Synthesis of Asymmetric Inorganic/Polymer Nanocomposite Particles via Localized Substrate Surface Modification and Miniemulsion Polymerization. *Langmuir* **2008**, *24*, 606–608, DOI: 10.1021/la703607s.

[21] Takahara, Y. K.; Ikeda, S.; Ishino, S.; Tachi, K.; Ikeue, K.; Sakata, T.; Hasegawa, T.; Mori, H.; Matsumura, M.; Ohtani, B. Asymmetrically Modified Silica Particles: A Simple Particulate Surfactant for Stabilization of Oil Droplets in Water. *J. Am. Chem. Soc.* **2005**, *127*, 6271–6275, DOI: 10.1021/ja043581r.

[22] Ge, X.; Wang, M.; Yuan, Q.; Wang, H.; Ge, X. The morphological control of anisotropic polystyrene/silica hybrid particles prepared by radiation miniemulsion polymerization. *Chem. Commun.* **2009**, 2765–2767, DOI: 10.1039/B901094G.

[23] Fernandez-Rodriguez, M. A.; Song, Y.; Rodriguez-Valverde, M. A.; Chen, S.; Cabrerizo-Vilchez, M. A.; Hidalgo-Alvarez, R. Comparison of the Interfacial Activity between Homogeneous and Janus Gold Nanoparticles by Pendant Drop Tensiometry. *Langmuir* **2014**, *30*, 1799–1804, DOI: 10.1021/la404194e.

[24] Montes Ruiz-Cabello, F.; Rodriguez-Valverde, M.; Cabrerizo-Vilchez, M. Contact angle hysteresis on polymer surfaces: an experimental study. *J. Adhes. Sci. Technol.* **2011**, *25*, 2039–2049, DOI: 10.1163/016942410X544848.

[25] Liu, Z.; Guo, R.; Xu, G.; Huang, Z.; Yan, L.-T. Entropy-Mediated Mechanical Response of the Interfacial Nanoparticle Patterning. *Nano Lett.* **2014**, *14*, 6910–6916, DOI: 10.1021/nl5029396.

[26] Fan, H.; Resasco, D. E.; Striolo, A. Amphiphilic Silica Nanoparticles at the Decane-Water Interface: Insights from Atomistic Simulations. *Langmuir* **2011**, *27*, 5264–5274, DOI: 10.1021/la200428r.

[27] Stancik, E. J.; Kouhkan, M.; Fuller, G. G. Coalescence of Particle-Laden Fluid Interfaces. *Langmuir* **2004**, *20*, 90–94, DOI: 10.1021/la0356093.

[28] Vogel, N.; Ally, J.; Bley, K.; Kappl, M.; Landfester, K.; Weiss, C. K. Direct visualization of the interfacial position of colloidal particles and their assemblies. *Nanoscale* **2014**, *6*, 6879–6885, DOI: 10.1039/C4NR00401A.

[29] Snoeyink, C.; Barman, S.; Christopher, G. F. Contact Angle Distribution of Particles at Fluid Interfaces. *Langmuir* **2015**, *31*, 891–897, DOI: 10.1021/la5040195.

[30] Ma, Y.; Cao, X.; Feng, X.; Ma, Y.; Zou, H. Fabrication of super-hydrophobic film from PMMA with intrinsic water contact angle below 90°. *Polymer* **2007**, *48*, 7455–7460, DOI: 10.1016/j.polymer.2007.10.038.

[31] Maestro, A.; Bonales, L. J.; Ritacco, H.; Rubio, R. G.; Ortega, F. Effect of the spreading solvent on the three-phase contact angle of microparticles attached at fluid interfaces. *Phys. Chem. Chem. Phys.* **2010**, *12*, 14115–14120, DOI: 10.1039/C0CP00570C.

[32] Xu, H.; Melle, S.; Golemanov, K.; Fuller, G. Shape and Buckling Transitions in Solid-Stabilized Drops. *Langmuir* **2005**, *21*, 10016–10020, DOI: 10.1021/la0507378.

[33] Zang, D.; Stocco, A.; Langevin, D.; Wei, B.; Binks, B. P. An ellipsometry study of silica nanoparticle layers at the water surface. *Phys. Chem. Chem. Phys.* **2009**, *11*, 9522–9529, DOI: 10.1039/b907903c.

[34] Kaz, D. M.; McGorty, R.; Mani, M.; Brenner, M. P.; Manoharan, V. N. Physical ageing of the contact line on colloidal particles at liquid interfaces. *Nat. Mater.* **2012**, *11*, 138–142, DOI: 10.1038/nmat3190.

[35] Walther, A.; Müller, A. H. E. Janus Particles: Synthesis, Self-Assembly, Physical Properties, and Applications. *Chem. Rev.* **2013**, *113*, 5194–5261, DOI: 10.1021/cr300089t.

[36] Iwashita, Y.; Kimura, Y. Orientational order of one-patch colloidal particles in two dimensions. *Soft Matter* **2014**, *10*, 7170–7181, DOI: 10.1039/C4SM00932K.

[37] Xu, H.; Kirkwood, J.; Lask, M.; Fuller, G. Charge Interaction between Particle-Laden Fluid Interfaces. *Langmuir* **2010**, *26*, 3160–3164, DOI: 10.1021/la903099a.

[38] Kumar, A.; Park, B. J.; Tu, F.; Lee, D. Amphiphilic Janus particles at fluid interfaces. *Soft Matter* **2013**, *9*, 6604–6617, DOI: 10.1039/C3SM50239B.

The good thing about science is that it's true whether or not you believe in it.

Neil deGrasse Tyson

8 A simple strategy to improve the interfacial activity of true Janus gold nanoparticles: a shorter hydrophilic capping ligand

Published in Soft Matter, Accepted Manuscript, 2015, ISSN 1744-683X, DOI: 10.1039/C5SM01908G

Miguel Angel Fernandez-Rodriguez[a], Limei Chen[b], Christopher P. Deming[b], Miguel Angel Rodriguez-Valverde[a], Shaowei Chen[b], Miguel Angel Cabrerizo-Vilchez[a], and Roque Hidalgo-Alvarez[a,*]

[a] *Biocolloid and Fluid Physics Group, Applied Physics Department, Faculty of Sciences, University of Granada, Granada, Spain.*
[b] *Department of Chemistry and Biochemistry, University of California, 1156 High Street, Santa Cruz, CA 95064, USA.*
* *rhidalgo@ugr.es*

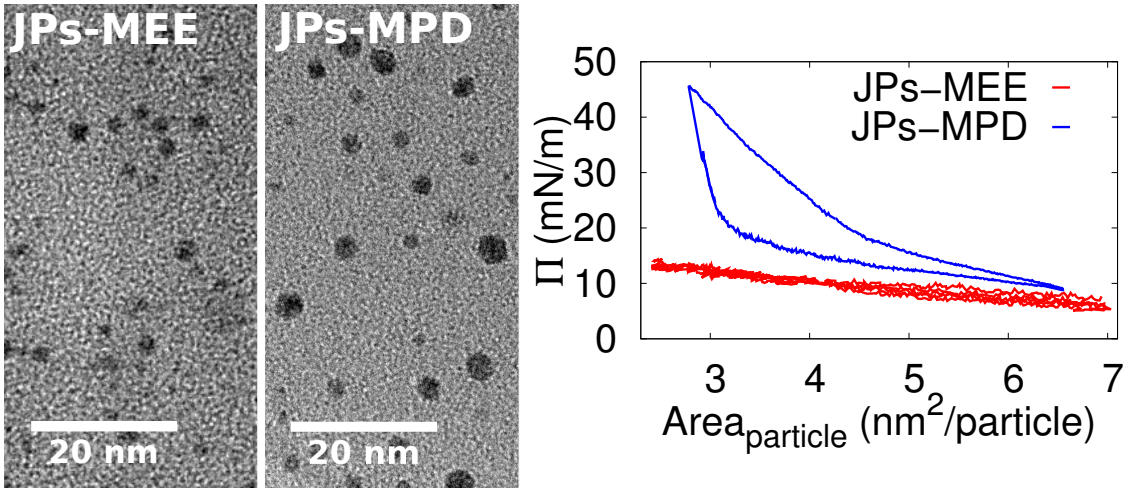

Figure 8.1: Graphical abstract.

Abstract

Janus gold nanoparticles (JPs) of $\sim$ 4 nm-diameter half functionalized with 1-hexanethiol as hydrophobic capping ligand exhibit significantly higher interfacial activity, reproducibility and rheological response when the other half is functionalized with 1,2-mercaptopropanediol (JPs-MPD) than with 2-(2-mercaptoethoxy)ethanol (JPs-MEE), both acting as the hydrophilic capping ligand. The interfacial pressure measured by pendant drop tensiometry reaches 50 mN/m and 35 mN/m for the JPs-MPD at the water/air and water/decane interface, respectively. At the same area per particle, the JPs-MEE reveal significantly lower interfacial pressure: 15 mN/m and 5 mN/m at the water/air and water/decane interface, respectively. Interfacial dilatational rheology measurements also show an elastic shell behaviour at higher compression states for JPs-MPD while the JPs-MEE present near-zero elasticity. The enhanced interfacial activity of JPs-MPD is explained in terms of chemical and hydration differences between the MPD and MEE ligands, where MPD has a shorter hydrocarbon chain and twice more hydroxyl terminal groups than MEE.

8.1 Communication

Pickering emulsions can be thermodynamically stabilized by amphiphilic Janus nanoparticles (JPs) with a wettability anisotropy [1–3].It is known that JPs show three times more adsorption energy than homogeneous nanoparticles [2, 4]. Strong efforts have been made to synthesize and simulate JPs with different morphologies and surface chemistry to control the way in which these particles self-

assemble at fluid interfaces [5–9].

Gold nanoparticles randmonly functionalized with 1-undecanethiol and N,N,N-trimethyl (11-mercaptoundecyl) ammonium chloride are reported to become Janus-like when the capping ligands rearrange at the water/air interface [10]. Nevertheless, recently Reguera et al. [11] demonstrated by neutron reflectivity that such rearrangement does not happen with gold nanoparticles functionalized with 1-octanethiol and 6-mercapto-1-hexanol at the water/air interface. A way to obtain gold JPs with true separate domains is to selectively functionalize each hemisphere of the core with the desired capping ligands immobilizing the nanoparticles in a Langmuir balance [12, 13].

It is fundamental to select the appropiate capping ligands that will confer the Janus character to the nanoparticles because of the significant dependence between these capping ligands and the interfacial activity of the final JPs. We propose a simple strategy to enhance the interfacial activity, rheological response and reproducibility through colloidal stability of true gold Janus nanoparticles. We synthesized Janus gold nanoparticles half capped by 1-hexanethiol and the other half by 2-(2-mercapto-ethoxy)ethanol (JPs-MEE) or 1,2-mercaptopropanediol (JPs-MPD) in surfactant-free conditions as described in previous works (see Fig. 8.2) [12–14]. The sizes obtained by high resolution TEM measurements (see Fig. S1†) are $3.5 \pm 0.9\,nm$ and $3.7 \pm 1.9\,nm$ for the JPs-MEE and JPs-MPD, respectively. The electrophoretic mobility of both JPs was measured with a ZetaSizer Nano (Malvern) in a $10^{-2}\,M$ sodium citrate MilliQ water solution to stabilize the electrical double layer obtaining $\mu_{e,JPs-MEE} = (-2.2 \pm 1.5) \cdot 10^{-8}\,m^2/(V \cdot s)$ and $\mu_{e,JPs-MPD} = (-2.9 \pm 0.4) \cdot 10^{-8}\,m^2/(V \cdot s)$. From previous works, the JPs-MEE showed an average macroscopic contact angle of $(56.1 \pm 1.8)^\circ$ and $(49.0 \pm 1.3)^\circ$ in each hemisphere, whereas the JPs-MPD showed $(63.3 \pm 2.7)^\circ$ and $(53.4 \pm 2.9)^\circ$ in their respective hydrophobic and hydrophilic hemispheres [12, 13]. The contact angles are slightly lower for the JPs-MEE likely due to the fabrication process: for MEE adsorption, the close-packed monolayer of 1-hexanethiol covered gold nanoparticles was immersed in a water solution containing MEE [13] and this might produce greater hydrophilic capping ligand exchange and thus lower contact angle than for the JPs-MPD in which the functionalization with MPD was performed directly in the Langmuir balance, exchanging the MPD ligands from the water subphase [12]. The contact angle values in the hydrophilic hemispheres are similar within errors, which reflects that the differences between MPD and MEE are not reflected macroscopically in the contact angle and the wettability contrast (i.e. contact angle differences between hemispheres) is simila.r in both JPs-MEE and JPs-MPD within errors. The pendant drop tensiometry was conducted as follows: different amounts of Janus nanoparticles (JPs-MEE and JPs-MPD) dispersed in tetrahydrofuran (THF, HPLC grade) were deposited on a water pendant drop with a handheld microsyringe and a micropositioner. The surface tension was obtained by axisymmetric drop shape analysis upon THF evaporation, while the

Figure 8.2: MEE (left) and MPD (right) capping ligands. The SH group is the anchor group at the gold nanoparticle surface.

pendant drop volume was kept constant. The results in Fig. 8.3 show a decrease in the final surface tension after evaporation of THF which is higher as the concentration of JPS-MPD is increased (refer to previous work for the JPs-MEE similar characterization [15]). The experiments are highly reproducible as can be seen in the different runs for a fixed concentration of JPs (different curves with same color in Fig. 8.3).

After the THF evaporation, growing and shrinking experiments were performed at $0.08\,\mu L/s$ for each JP concentration. Next, the pendant drop was immersed in decane and the growing and shrinking experiments were performed again. We plot the interfacial pressure ($\Pi = \gamma_0 - \gamma$, where γ_0 is $72.5 mN/m$ for the water/air (W/A) and $52.3\,mN/m$ for the water/decane (W/O) interfaces and γ is the measured interfacial tension) against the drop area per particle (A_p, the area of the pendant drop divided by the number of deposited JPs). A piecewise compression isotherm can be seen in Fig. 8.4a and Fig. 8.4b for W/A and W/O interfaces, respectively. The first remarkable fact is the lower interfacial activity of JPs-MEE compared to JPs-MPD at the same A_p values. At the lowest A_p reached for JPs-MPD, Π is $50\,mN/m$ and $35\,mN/m$ and $15\,mN/m$ and $5\,mN/m$ for the JPs-MEE at the W/A and W/O interfaces, respectively. The highest Π values obtained for JPs-MEE, after further compression, are $30\,mN/m$ and $20\,mN/m$ at the W/A and W/O interfaces, respectively. Contrary to JPs-MEE, the compression isotherms for JPs-MPD at the W/A interface exhibit open cycles at the beginning of the experiments pointing out that the colloidal monolayer rearranges into a final state that is preserved in further compression cycles. This behaviour is attenuated at the W/O interface as the hysteresis cycles are much smaller (i.e. the upper compression and lower expansion curves are closer) which might be due to the fact that enough energy is provided to reach a more relaxed state when it is immersed in decane. Moreover, the low hysteresis of the JPs-MEE compression cycles compared to the JPs-MPD might be due to the lower interfacial activity of these particles. Since the fabrication process, hydrophobic capping ligand, wettability contrast, size and charge were similar for both JPs-MEE and JPs-MPD, the differences between interfacial activity must come from the interfacial activity of the MEE and MPD hydrophilic capping ligands. Whereas MEE has a longer hydrocarbon chain (four CH_2 and one oxygen) and one hydroxyl terminal group, the MPD has a shorter

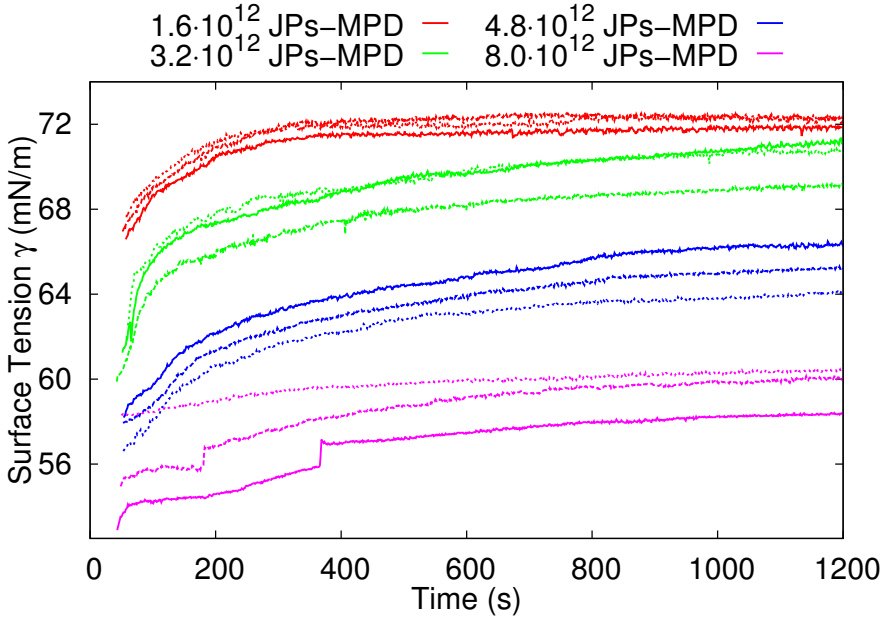

Figure 8.3: Surface tension evolution over the time after the deposition of different number of JPs-MPD in THF on the surface of an initial $5\,\mu L$ MilliQ water pendant drop and growth up to $45\,\mu L$. Same color curves correspond to different experiments with the same number of deposited JPs-MPD. After the solvent evaporation, the surface tension remained stable.

hydrocarbon chain (three CH_2) and two hydroxyl terminal groups (see Fig. 8.2). The lower number of hydrocarbon groups and higher number of hydroxyl groups of MPD might result in higher hydration of the hydrophilic hemisphere of the JPs (i.e. establishing hydrogen bonds between water and the hydrophilic capping ligands). These chemical differences might play a decisive role in the final interfacial activity of these JPs.

The interfacial dilatational rheology of the JPs was evaluated by ten periodic volume variations of $1\,\mu L$ for different periods. When a periodic injection/extraction of volume is performed to the pendant drop, the interface tries to re-establish the equilibrium. This counteraction is represented by a complex quantity composed by a storage part and a loss part:

$$E = E_d + i\omega\eta_d \tag{8.1}$$

where E is the surface dilatational modulus that accounts for the change in surface tension produced by a small change in a surface area, E_d is the interfacial dilatational elasticity, ω is the oscillation frequency and η_d is the interfacial dilatational viscosity [16]. If the viscosity is negligible during the relaxation process after perturbation of the interface, the interface present an essentially elastic behavior. The extraordinary interfacial activity of JPs-MPD is reflected in the rheology results in Fig. 8.5a and 8.5b (see Fig. S2 and S3†). For both W/A and W/O interfaces, E decreases slightly and η increases for increasing periods. For the W/A interface, E_d and η_d increases clearly with the compression state of the colloidal monolayer. This trend is also observed for the W/O interface but with lower values of both E_d and η_d. The high E_d value is a signal that the colloidal monolayer creates an elastic shell on the pendant drop at higher compression states. This elastic behaviour again suggests the ability of the JPs-MPD as emulsifiers. Further rheology experiments were performed for a fixed period of $10\,s$ comparing the response of JPs-MEE and JPs-MPD. The results in Fig. 8.6a and 8.6b point out that the JPs-MPD reach significantly higher E_d and η_d values upon compression (i.e. lower A_p) than the JPs-MEE (~ 10 times higher E_d and η_d for JPs-MPD than JPs-MEE at the W/A interface and 2 times at the W/O interface), suggesting that the elastic shell behaviour is not present for the JPs-MEE. A final consideration must be taken into account for gold nanoparticles in the range of a few nanometers (i.e. less than $10\,nm$), the adsorption energy at the interface is of the order of K_BT [17] and they are expected to easily leave the interface. Nevertheless, the stable interfacial tension over time after the THF evaporation, the closed growing/shrinking cycles and the dilatational rheology seem to point out that the JPs-MEE and JPs-MPD are irreversibly anchored at the W/A and W/O interfaces, probably due to its Janus character.

In conclusion, the JPs-MEE and JPs-MPD are similar in fabrication process, hydrophobic capping ligand, wettability contrast, size and charge, but are functionalized with different hydrophilic capping ligand. The JPs-MPD exhibit a significantly

(a) Water/air interface

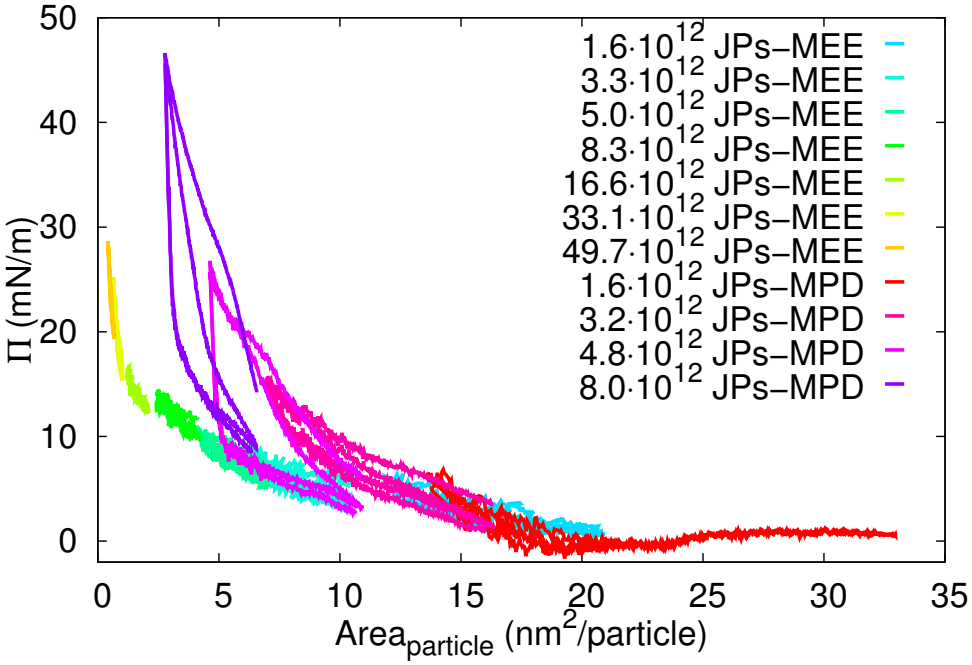

(b) Water/decane interface

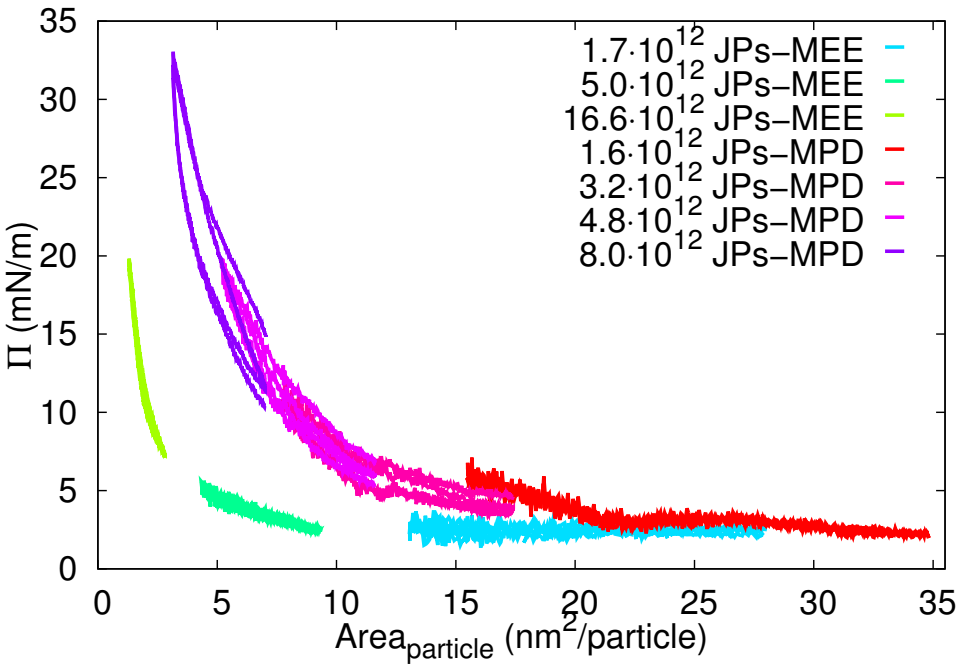

Figure 8.4: Surface pressure against the area per particle for different number of JPs-MEE and JPs-MPD deposited at the **(a)** W/A and **(b)** W/O interfaces. For a more detailed characterization of the JPs-MEE, please refer to Fernandez et al.[15]

higher interfacial activity at W/A and W/O interfaces. Moreover, the dilatational rheology suggests an elastic shell-like behaviour of the pendant drop when the JPs-MPD are deposited at W/A and W/O interfaces. This elastic shell behaviour seems to be absent with the JPs-MEE. This points out the importance of the chemical structure of the capping ligands in JPs to predict the interfacial activity and therefore their ability as emulsifiers. Shorter hydrocarbon chain and more hydroxyl terminal groups in the hydrophilic capping ligands seems to be a route to obtain enhanced interfacial activity of this kind of JPs via enhanced hydration of the hydrophilic hemisphere of the JPs. To the best of our knowledge, it is the first time that such high interfacial activity is obtained with $\sim 4\,nm$-diameter gold nanoparticles in surfactant-free conditions.

Acknowledgements

This work was supported by the Spanish MINECO (projects MAT2013-44429-R and MAT2014-60615R), by "Junta de Andalucía" and FEDER (projects P10-FQM-5977 and P12-FQM-1443) and by US National Science Foundation (DMR-1409396). Authors thank to Dr. J.A. Holgado-Terriza for the software Contacto© used for surface tension measurements.

(a) Interfacial dilatational elasticity E_d

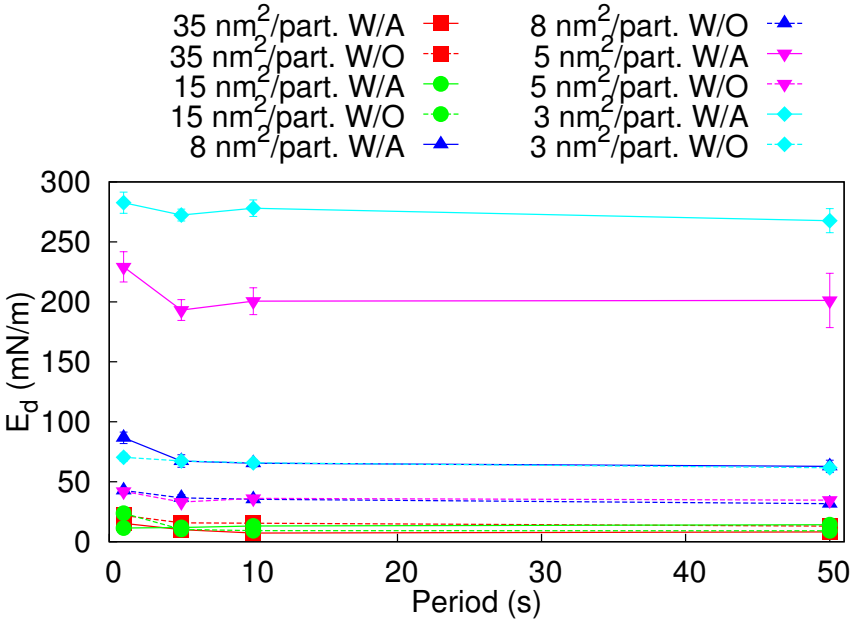

(b) Interfacial dilatational viscosity η_d

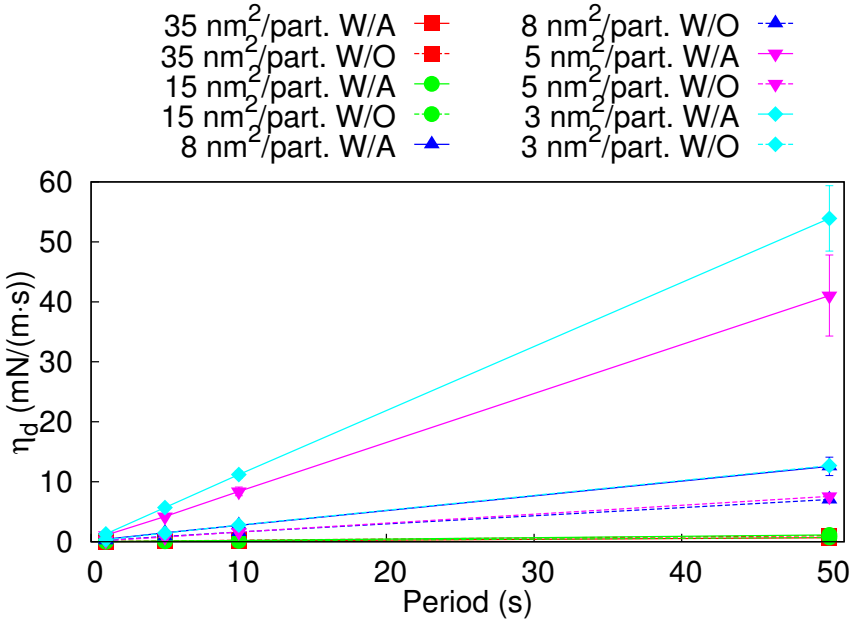

Figure 8.5: **(a)** Interfacial dilatational elastic modulus (E_d) and **(b)** viscosity (η_d) of JPs-MPD against different periods for different A_p compression states at the W/A and W/O interfaces.

(a) Interfacial dilatational elasticity E_d for $10\,s$ period

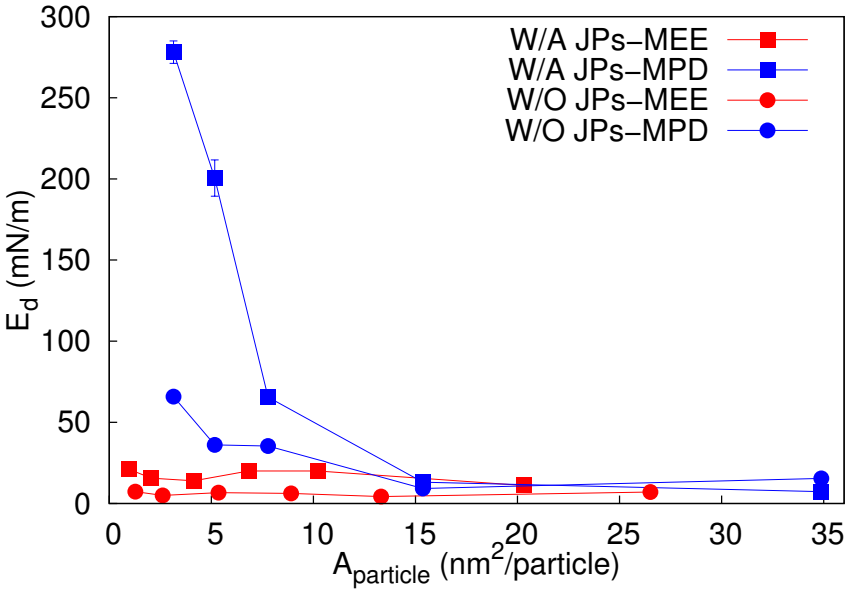

(b) Interfacial dilatational viscosity η_d for $10\,s$ period

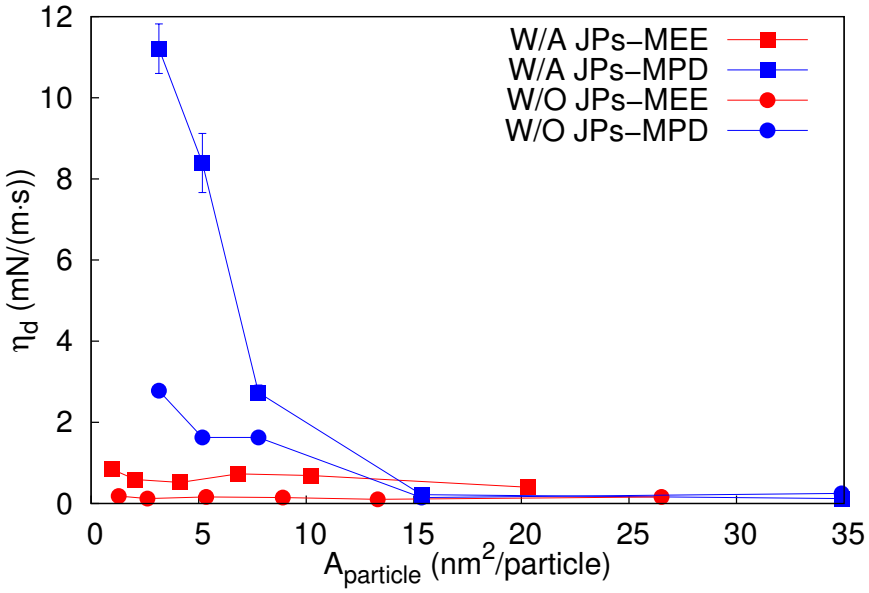

Figure 8.6: **(a)** Interfacial dilatational elastic modulus E_d and **(b)** viscosity η_d of JPs-MEE and JPs-MPD against the A_p at the W/A and W/O interfaces, for $10\,s$ period.

8.2 Supporting Information

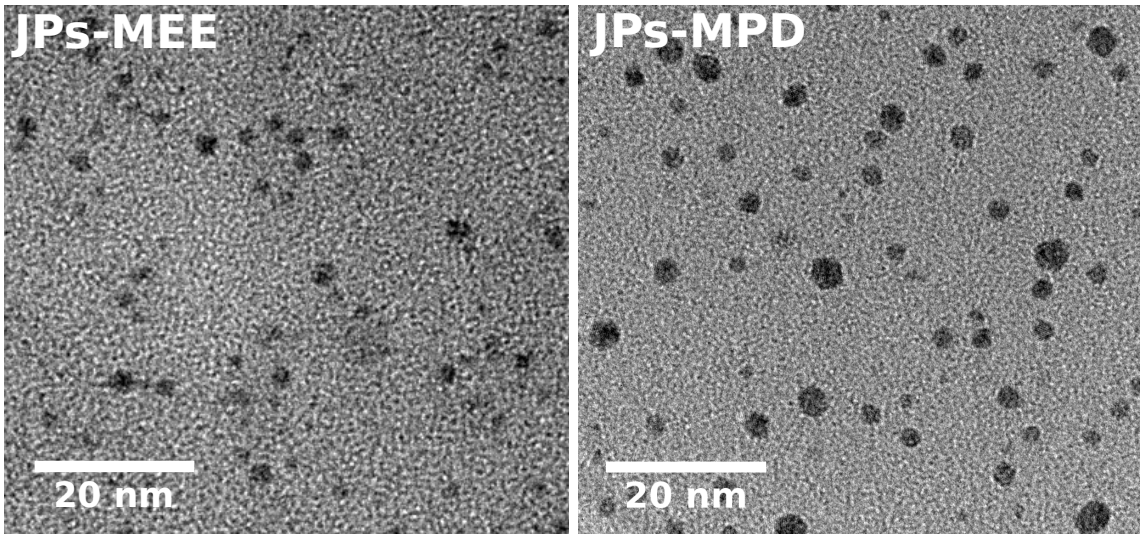

Figure 8.7: High Resolution TEM micrographies of the JPs-MEE (left) and JPs-MPD (right). The sizes are $3.5 \pm 0.9\,nm$ and $3.7 \pm 1.9\,nm$ for the JPs-MEE and JPs-MPD, respectively.

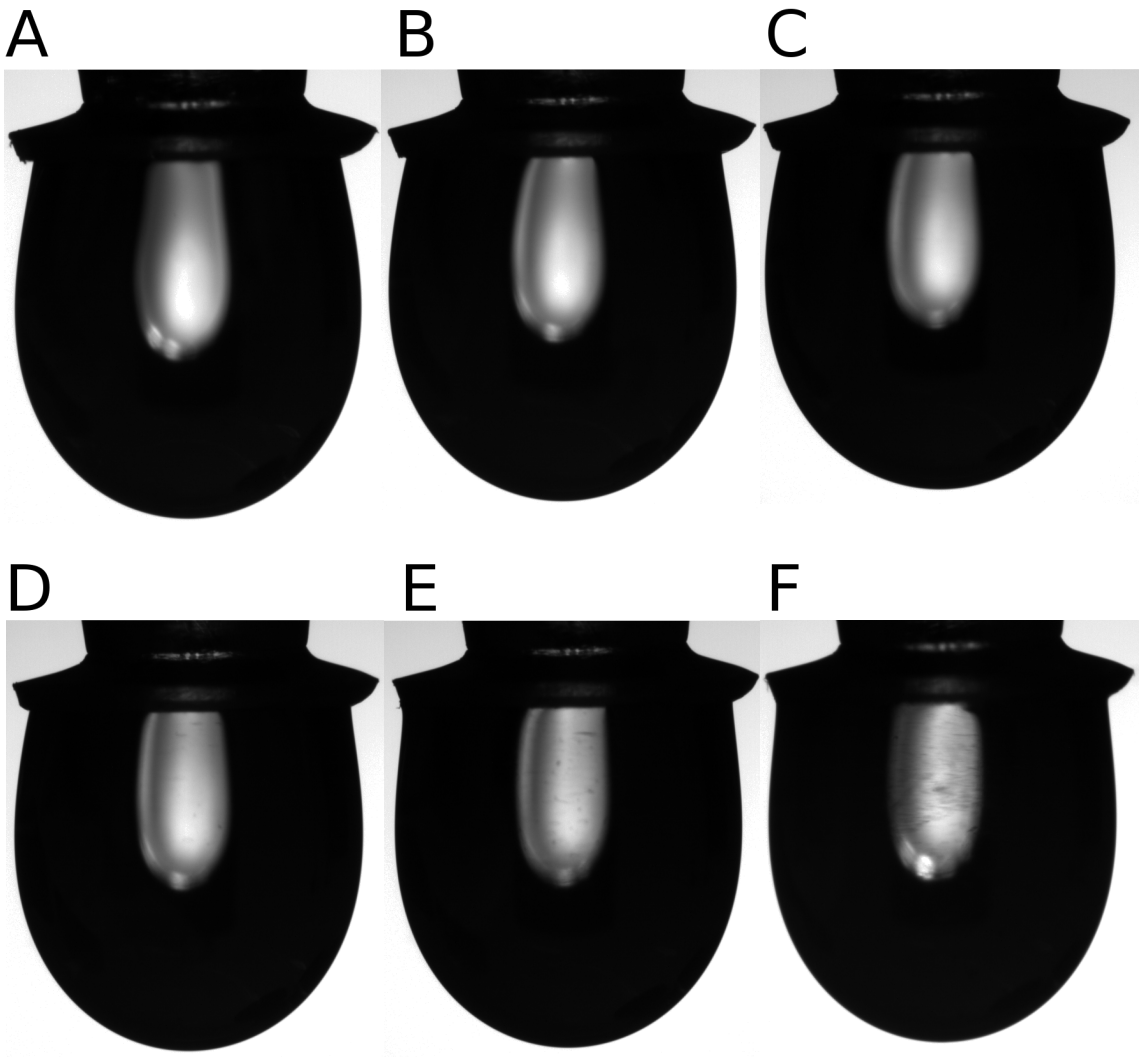

Figure 8.8: $45\,\mu l$ water pendant drops in air with different number of JPs-MPD deposited at the interface, after THF evaportion: **(A)** Bare water/air interface, (B) $1.6 \cdot 10^{12}$ JPs-MPD, **(C)** $3.2 \cdot 10^{12}$ JPs-MPD, **(D)** $4.8 \cdot 10^{12}$ JPs-MPD, **(E)** $8.0 \cdot 10^{12}$ JPs-MPD and **(F)** $16.0 \cdot 10^{12}$ JPs-MPD, this last pendant drop fell off due to the low surface tension and it wasn't possible to perform the rheology experiments. It is noticeable the increasing opacity and shape change of the pendant drop with increasing number of JPs-MPD deposited at the interface.

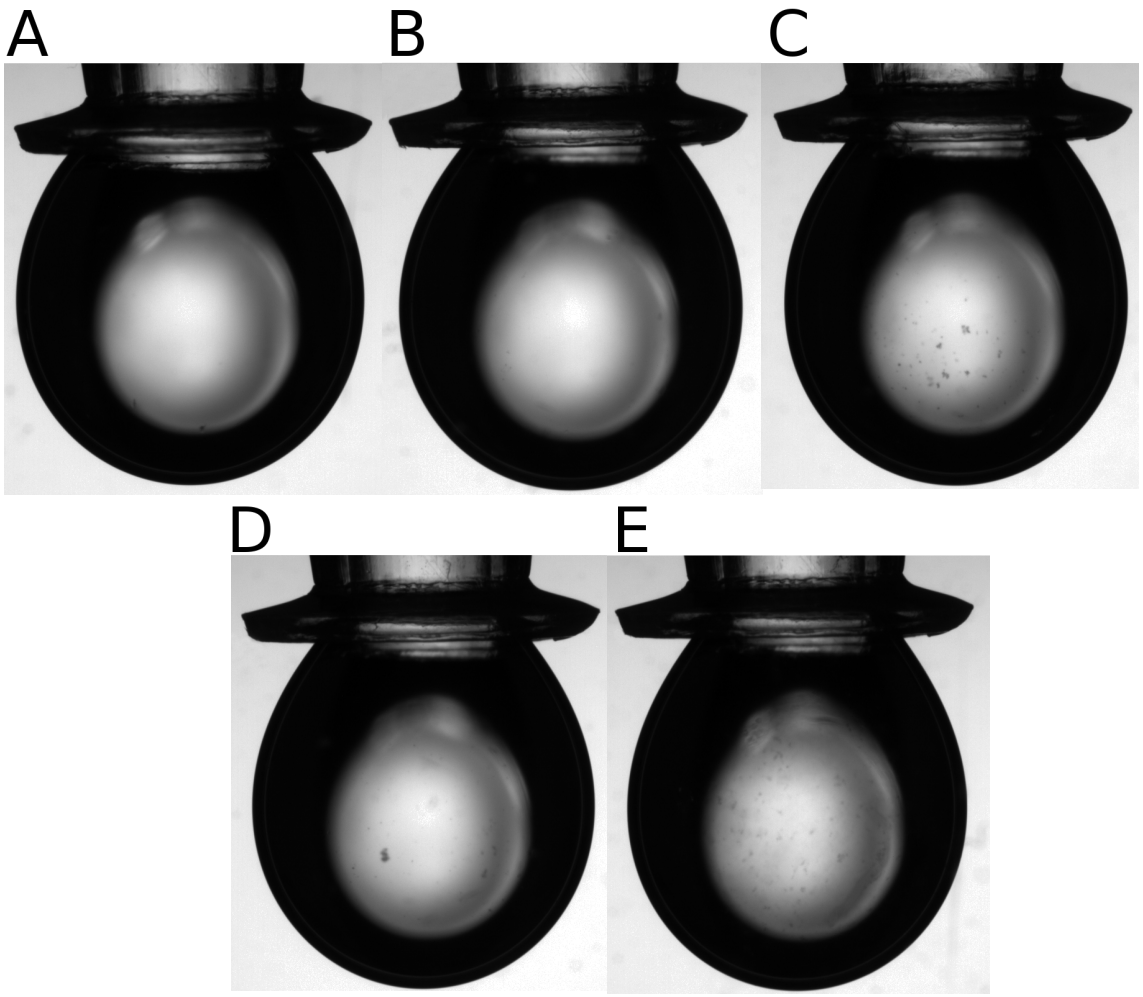

Figure 8.9: $45\,\mu l$ water pendant drops immersed in decane with different number of JPs-MPD deposited at the interface, corresponding to the drops in Fig. 8.8: **(A)** Bare water/decane interface, (B) $1.6 \cdot 10^{12}$ JPs-MPD, **(C)** $3.2 \cdot 10^{12}$ JPs-MPD, **(D)** $4.8 \cdot 10^{12}$ JPs-MPD and **(E)** $8.0 \cdot 10^{12}$ JPs-MPD. It is noticeable the increasing opacity and shape change of the pendant drop with increasing number of JPs-MPD deposited at the interface.

References

[1] Hu, J.; Zhou, S.; Sun, Y.; Fang, X.; Wu, L. Fabrication, properties and applications of Janus particles. *Chem. Soc. Rev.* **2012**, *41*, 4356–4378, DOI: 10.1039/C2CS35032G.

[2] Kumar, A.; Park, B. J.; Tu, F.; Lee, D. Amphiphilic Janus particles at fluid interfaces. *Soft Matter* **2013**, *9*, 6604–6617, DOI: 10.1039/C3SM50239B.

[3] Pham, B. T. T.; Such, C. H.; Hawkett, B. S. Synthesis of polymeric janus nanoparticles and their application in surfactant-free emulsion polymerizations. *Polym. Chem.* **2015**, *6*, 426–435, DOI: 10.1039/C4PY01125B.

[4] Aveyard, R. Can Janus particles give thermodynamically stable Pickering emulsions? *Soft Matter* **2012**, *8*, 5233–5240.

[5] Walther, A.; Muller, A. H. E. In *Janus Particle Synthesis, Self-Assembly and Applications*; The Royal Society of Chemistry: 2012, pp 1–28, DOI: 10.1039/9781849735100-00001.

[6] Du, J.; O'Reilly, R. K. Anisotropic particles with patchy, multicompartment and Janus architectures: preparation and application. *Chem. Soc. Rev.* **2011**, *40*, 2402–2416, DOI: 10.1039/C0CS00216J.

[7] Park, B. J.; Brugarolas, T.; Lee, D. Janus particles at an oil-water interface. *Soft Matter* **2011**, *7*, 6413–6417, DOI: 10.1039/C1SM05460K.

[8] Rezvantalab, H.; Shojaei-Zadeh, S. Capillary interactions between spherical Janus particles at liquid-fluid interfaces. *Soft Matter* **2013**, *9*, 3640–3650, DOI: 10.1039/C3SM27380F.

[9] Li, Z.-W.; Lu, Z.-Y.; Sun, Z.-Y.; An, L.-J. Model, self-assembly structures, and phase diagram of soft Janus particles. *Soft Matter* **2012**, *8*, 6693–6697, DOI: 10.1039/C2SM25397F.

[10] Song, Y.; Liu, X.; Chen, S. In *Functional Nanometer-Sized Clusters of Transition Metals: Synthesis, Properties and Applications*; The Royal Society of Chemistry: 2014, pp 407–433, DOI: 10.1039/9781782628514-00407.

[11] Reguera, J.; Ponomarev, E.; Geue, T.; Stellacci, F.; Bresme, F.; Moglianetti, M. Contact angle and adsorption energies of nanoparticles at the air-liquid interface determined by neutron reflectivity and molecular dynamics. *Nanoscale* **2015**, *7*, 5665–5673.

[12] Pradhan, S.; Xu, L.; Chen, S. Janus Nanoparticles by Interfacial Engineering. *Adv. Funct. Mater.* **2007**, *17*, 2385–2392.

[13] Pradhan, S.; Brown, L.; Konopelski, J.; Chen, S. Janus nanoparticles: reaction dynamics and NOESY characterization. *J. Nanopart. Res.* **2009**, *11*, 1895–1903.

[14] Song, Y.; Chen, S. Janus Nanoparticles: Preparation, Characterization, and Applications. *Chem. Asian J.* **2014**, *9*, 418–430, DOI: 10.1002/asia.201301398.

[15] Fernandez-Rodriguez, M. A.; Song, Y.; Rodriguez-Valverde, M. A.; Chen, S.; Cabrerizo-Vilchez, M. A.; Hidalgo-Alvarez, R. Comparison of the Interfacial Activity between Homogeneous and Janus Gold Nanoparticles by Pendant Drop Tensiometry. *Langmuir* **2014**, *30*, 1799–1804.

[16] Powell, K. C.; Chauhan, A. Interfacial Tension and Surface Elasticity of Carbon Black (CB) Covered Oil-Water Interface. *Langmuir* **2014**, *30*, 12287–12296, DOI: 10.1021/la503049m.

[17] Jiang, S.; Granick, S. In *Janus Particle Synthesis, Self-Assembly and Applications*; The Royal Society of Chemistry: 2012, pp 244–256, DOI: 10.1039/9781849735100-00244.

Most human beings have an almost infinite capacity for taking things for granted.

Aldous Huxley, Brave New World

9 Interfacial activity of gold nanoparticles coated by a polymeric Janus shell and the role of spreading agents

Miguel Angel Fernandez-Rodriguez[1], Ana Maria Percebom[2,3,4], Juan Jose Giner-Casares[3], Miguel Angel Rodriguez-Valverde[1], Miguel Angel Cabrerizo-Vilchez[1], Luis M. Liz-Marzan[3] and Roque Hidalgo-Alvarez[1,*]

[1] *Biocolloid and Fluid Physics Group, Applied Physics Department, Faculty of Sciences, University of Granada, Granada, Spain.*
[2] *Department of Physical Chemistry, Institute of Chemistry, University of Campinas - UNICAMP, P.O. Box 6154, 13083-970 Campinas, SP, Brazil.*
[3] *CIC biomaGUNE, Paseo de Miramón 182, 20009 Donostia-San Sebastián, Spain.*
[4] *Department of Chemistry, Pontifical Catholic University of Rio de Janeiro (PUC-Rio), Rua Marquês de São Vicente 225, Gávea, 22451-900, Rio de Janeiro, RJ, Brazil.*
[*] *rhidalgo@ugr.es*

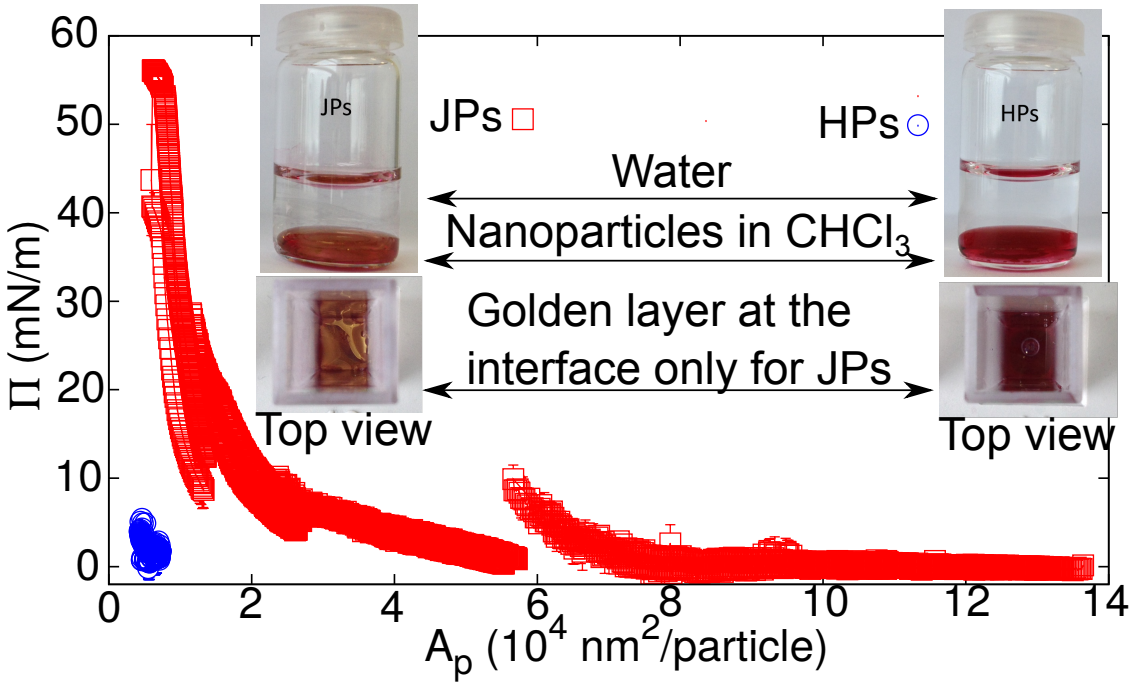

Figure 9.1: Graphical abstract.

Abstract

Gold Janus nanoparticles (JPs) of 13 nm and 23 nm were synthesized in surfactant free conditions, half functionalized with polystyrene and half with polyethylene glycol as hydrophobic and hydrophilic ligands, respectively. The interfacial activity of the JPs was compared to homogeneous hydrophilic nanoparticles (HPs) fully functionalized with PEG by pendant drop tensiometry. The nanoparticles were placed at the water/air and water/decane interfaces. We compared three different spreading agents: water, water/chloroform and pure chloroform to evaluate their effect on the final interfacial activity exhibited by both JPs and HPs. The JPs interfacial activity was close to zero ($\sim 2\,mN/m$) when the spreading agent was water and increased to ($\sim 14\,mN/m$) when the spreading agent was water/chloroform. When the nanoparticles were deposited with pure chloroform the interfacial activity reached $\sim 60\,mN/m$ when the maximum surface pressure was achieved by compression. In all cases, JPs exhibited higher interfacial activity than HPs which were not interfacial active, regardless of the spreading agent. The interfacial activity at the water/decane interface was significantly lower than at the water/air interface because of aggregation in decane. Interfacial dilatational rheology showed that the JPs formed a strong elastic shell at the pendant drop interface, compared to HPs. The significantly high interfacial activity obtained with JPs in this study reflects the importance of the polymeric Janus shell and the

spreading agent.

Keywords: Janus nanoparticles; Interfacial activity; Polymer shell; Water/air interfaces; Water/decane interfaces; Dilatational interfacial rheology.

9.1 Introduction

Janus nanoparticles (JPs) with a wettability contrast are extensively studied as emulsion stabilizers due to their interfacial activity [1, 2]. These JPs combine the benefits of wettability contrast of surfactants, the benefits of Pickering emulsions [3], and the plasmonic features of the Au core [4]. The capabilities of Janus nanoparticles to stabilize emulsions come from the spatial separation of the different wettability domains. This spatial separation lead to an enhanced interfacial activity regardless of the amphiphilicity of the nanoparticles, compared to homogeneous nanoparticles [5]. In fact, JPs show up to three times more adsorption energy than the corresponding homogeneous nanoparticles with randomly placed capping ligands [5]. Thus, it is necessary to understand the role of the capping ligands that form the two separate wettability domains of such JPs on the final interfacial activity [6].

Amphiphilic gold nanoparticles with thiol-terminated polyethylene glycol chains and short alkane-thiols as capping ligands are proper water/oil emulsion stabilizers [3]. The authors claim that these nanoparticles only become Janus-like when the capping ligands rearrange at the interface of the emulsion. Nevertheless, this capping ligand rearrangement did not occur with gold nanoparticles functionalized with 1-octanethiol and 6-mercapto-1-hexanol at the water/air interface when it was studied by neutron reflectivity [7]. Thus, different approaches are needed to ensure that the nanoparticles are true JPs [8]. For example, controlling the adsorption of the capping ligands to ensure spatial separation in different domains while the capping ligands are exchanged from bulk [9]. Previous attempts to obtain amphiphilic gold nanoparticles functionalized by PEG and PS were made by Zubarev et al. [10], where 2 nm-diameter gold and silver cores were functionalized by V-shaped PS-b-PEG diblock polymers. The V-shaped polymers are expected to reorient at the interface in a Janus-like way thanks to the small size of the gold core compared to the polymers. In fact, they found that if the molecular weight of PS block was adjusted to be two times higher than the PEG block, the nanoparticles aggregated in water forming cylindrical micelles due to this capping ligand reorientation.

Janus gold nanoparticles can also be obtained through the spontaneous segregation of two dissimilar polymers on the surface of the nanoparticle. The Janus character is well-defined by characterization by Nuclear Overhauser Effect Spectroscopy (NOESY NMR), by the growth of a silica half shell only over the hemisphere coated by one of the polymers and by Transmission Electron Microscopy (TEM) Tomography images of the Janus gold nanoparticles selectively stained. Since one hemisphere is coated by a hydrophilic polymer (polyethylene glycol) and the other by a hydrophobic one (polystyrene), the nanoparticles can assemble in definite clusters, whose sizes can be tuned by alterations in different factors as: polymer length, polymer proportion, core size and polarity of the medium [11].

The spreading agent also plays a decisive role when the particles are deposited at fluid interfaces. This is because the evaporation of volatile spreading agents provide energy to the nanoparticles to reach and anchor to the interface. This process forms the so-called Langmuir monolayer, in contrast with a Gibbs monolayer in which the nanoparticles have to reach the interface from the bulk. The latter process is very slow compared with the usual laboratory timescales and are impractical in industrial processes [6].

In this study, we examine the importance of the polymeric Janus shell in gold nanoparticles and the spreading agent used during the deposition at water/air and water/decane interfaces. We compare the interfacial activity by pendant drop tensiometry of true gold JPs of 13 nm and 23 nm half functionalized with polystyrene (PS) and half with polyethylene glycol (PEG) and homogeneous nanoparticles functionalized only with PEG. Moreover, the spreading agent role is studied by comparing pure water, water/$CHCl_3$ and pure $CHCl_3$. Finally, the particle-laden interfaces are studied by interfacial dilatational rheology.

9.2 Methods

Preparation of Janus nanoparticles

The nanoparticles investigated in the present study were prepared by using the methodology proposed in reference [11]. In summary, gold nanoparticles were synthesized by reduction of $HAuCl_4$ in presence of citrate and added to a solution of thiol-terminated polymers for coating. For the HPs, an aqueous equimolar mixture solution of PEG-SH was used. For the JPs, a mixture of PEG-SH and PS-SH in THF was used. The main difference between the preparation of the nanoparticles in this study and the previous one in reference [11] is the purification process. To guarantee that there were no traces of citrate, free polymer or THF in the sample, the step of centrifugation with supernatant exchange was repeated 5 times in the present study. The last supernatant was also analyzed to verify the purity, and the absence of substances that could interfere in the surface tension measurements.

Characterization of Nanoparticles

As described in reference [11], the nanoparticles were characterized by TEM and DLS to obtain information regarding the sizes of the individual nanoparticles and their assembles. Table 7.1 summarizes the obtained results.

Pendant drop tensiometry

We used a homemade setup described in previous work [12]. We started depositing a given amount of nanoparticle dispersion with a microsyringe on a $20\,\mu l$ MilliQ water pendant drop in air. Next, the pendant drop was grown up to $45\,\mu l$ and we monitored the surface tension keeping constant the pendant drop volume. We used a bigger polytetrafluoroethylene capillary with a cap (with an external diameter of 2.8 mm and 4.2 mm of the

Sample	Polymer coating	Core size (TEM) / nm	Solvent	Electrophoretic mobility ($10^{-8}\, m^2/(V \cdot s)$)
13 nm-JPs	PEG 1 kDa + PS 2 kDa	13 ± 1	H_2O	-2.0 ± 0.9
13 nm-HPs	PEG 1 kDa	13 ± 1	H_2O	-1.3 ± 1.1
23 nm-JPs	PEG 1 kDa + PS 2 kDa	23 ± 2	$CHCl_3$	-0.5 ± 0.3
23 nm-HPs	PEG 1 kDa	23 ± 2	H_2O	-1.5 ± 0.9

*All results, except the electrophoretic mobility, from reference [11].

Table 9.1: Results from characterization of each system of nanoparticles.*

capillary and the cap, respectively, see Fig. 9.2) to avoid the fall of the pendant drop due to the low tension values reached. We monitor the surface tension (γ) evolution over time for these experiments.

After 20 min, the surface tension was stable over time in most cases. Next, we performed growing and shrinking cycles in air varying the total volume of the drop between $45 \leftrightarrow 15\,\mu l$. When pure $CHCl_3$ was used as spreading solvent, the evaporation process was violent and in few seconds was completed (see Fig. 9.2). In the case of using water/$CHCl_3$ as spreading agent, half of the microsyringe was loaded with the water nanoparticle dispersion and half with $CHCl_3$. We also performed growing and shrinking experiments at the water/decane interface. This was done by shrinking the pendant drop to $10\,\mu l$, next immersing in decane and growing again up to $45\,\mu l$. Finally the same growing and shrinking cycles were performed in contact with the decane phase. For these experiments the surface pressure is plotted, defined as $\Pi = \gamma_0 - \gamma$, were γ_0 is $72.5\,mN/m$ and $52.3\,mN/m$ for water/air and water/decane interfaces and γ is the surface tension measured with nanoparticles. The surface pressure is plotted against the pendant drop area or the area per particle A_p (the area of the pendant drop divided by the number of deposited nanoparticles).

The dilatational interfacial rheology was performed as described in previous work [13] by growing and shrinking the pendant drop at different periods with a fixed $1\,\mu l$ amplitude. From the differences in amplitude and phase of the input volume oscillation and the output surface tension it is possible to obtain the interfacial elastic modulus E_d and viscosity η_d, analogous to the storage and loss modulus in 3D rheology.

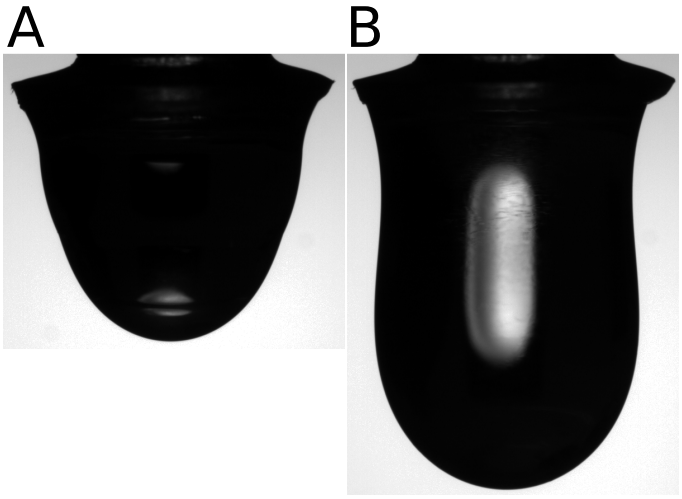

Figure 9.2: (A) $20\,\mu l$ water pendant drop in air with $5.9 \cdot 10^9$ of 23 nm-JPs in $CHCl_3$ deposited. Note the $CHCl_3$ on the bottom of the pendant drop. (B) $45\,\mu l$ water pendant drop after evaporation of $CHCl_3$ in (A), this pendant drop fell off because of the low surface tension.

9.3 Results and Discussion

Effect of Spreading Agent

The role of the spreading agent is studied by depositing a given amount of 13 nm-JPs at the water/air interface. First, it is deposited using only water and next it is deposited with the microsyringe half loaded with the water nanoparticle dispersion and half with $CHCl_3$, the result is that the interfacial activity is close to zero ($\sim 2\,mN/m$ for the highest compression state) when it is deposited using water (see Fig. 9.3a and 9.3b). The interfacial activity increases up to $\sim 14\,mN/m$ when the water/$CHCl_3$ is used. In Fig. 9.3a, the purity of the $CHCl_3$ used as spreading agent is confirmed in the black curve, corresponding to the deposition of $5\,\mu l$ of $CHCl_3$. Chloroform was chosen as the spreading agent due to an effect observed when the JPs were dispersed in $CHCl_3$ and water was added to this dispersion. Since chloroform and water are immiscible and the first is denser, addition of water generates a top phase. Interestingly, the interface between the two phases became golden when we had JPs in the bottom phase (see Fig.9.4). It indicates that the nanoparticles coated by PEG+PS tend to assemble at the $CHCl_3$/water interface. On the other hand, the homogeneous nanoparticles do not present this assembly. From this observation, we expected that chloroform would be an efficient spreading agent for this system. The interfacial activity difference between using pure water or water/$CHCl_3$ as spreading agent can be explained in terms of the Langmuir monolayer vs Gibbs monolayer formation [6]. When the JPs are deposited from water, they join the water subphase and a Gibbs monolayer process occur in which they have to reach the pendant drop interface very slowly [6]. This is specially unfavorable for few nanometers sized nanoparticles

in which the adsorption energy is in the range of k_BT [14]. On the other hand, when water/$CHCl_3$ is used as spreading agent, the abrupt evaporation of the $CHCl_3$ promotes a Langmuir monolayer process in which the nanoparticles are able to reach the interface much faster, which it is evidenced by the stable surface tension reached in Fig. 9.3a.

Concerning the homogeneous vs Janus interfacial activity, the 13 nm-HPs show no interfacial activity compared to the 13 nm-JPs (see Fig. 9.3a and 9.3b), even for higher concentrations of 13 nm-HPs and using the water/$CHCl_3$ as spreading agent. The PS ligands are hydrophobic and the PEG hydrophilic. Thus, the 13 nm-HPs only functionalized with PEG are expected to be more hydrophilic, preferring to stay in the water subphase. On the other hand, the interfacial activity of the 13 nm-JPs must come from the Janus character of these nanoparticles.

Nanoparticles Dispersed in an Organic Solvent

We redisperse the JPs in pure $CHCl_3$ to study if the interfacial activity could be increased this way. For this purpose, we redispersed 23 nm-JPs in $CHCl_3$. First, we characterized the water/air interface as it can be seen in Fig. 9.5. In Fig. 9.5a, the black curve corresponds to the supernatant of the 23 nm-JPs, after centrifugation at 5500 g and 30 min in a glass tube (to avoid the $CHCl_3$ from dissolving the centrifugation tube plastic). It can be seen that the supernatant was clean, recovering the interfacial activity of pure water/air interface ($\sim 72.5\, mN/m$) which points out that the redispersion in $CHCl_3$ did not desorbed the polymers nor contaminated the nanoparticle dispersion. Moreover, Fig. 9.5a shows that the final stable surface tension after $CHCl_3$ evaporation increased with the concentration of 23 nm-JPs used and was moderately reproducible for two separate runs (solid and dashed lines of each color in Fig. 9.5a) whereas the 23 nm-HPs, dispersed in water, exhibited no interfacial activity for even higher concentrations as expected. Thus, the 23 nm-HPs serves as the control case of nanoparticles with no interfacial activity. In Fig. 9.5b, the growing and shrinking cycles performed for the different initial concentrations enabled to build a piecewise-like compression isotherm. At high values of surface area between $8 \cdot 10^4\, nm^2$/particle and $14 \cdot 10^4\, nm^2$/particle, the surface pressure Π starts in zero and increases upon decreasing A_p (i.e. increasing the compression state) up to $\sim\ 60\, mN/m$ (see Fig. S1 in Supplementary Information) which is the highest surface pressure reached with these few nanometers gold Janus nanoparticles to the best of our knowledge. This value is significantly higher than the maximum value $Pi \sim 20\, mN/m$ reported with gold JPs of $\sim\ 4\, nm$ half functionalized with hexanethiol and half with 2-(2-mercapto-ethoxy)ethanol and dispersed in tetrahydrofuran [12]. Also, a change in the slope is visible in Fig. 9.5b around $A_p = 10^4\, nm^2/particle$ which was also observed for silver Janus-like nanoparticles measured by Fernandez et al. [15]. In this case, as we don't have enough particles to obtain a close-packed monolayer, it is possible that the change in the slope is due to the nanoparticles becoming in contact with each other by percolating domains in a fractal-like way, as observed by several authors for JPs [16, 17]. Also, other main factor might be the role of the nanoparticle size in the interfacial adhesion energy E_ads at interfaces that follows Equation 9.1 [5], where R is the radius of the particle, γ_{12} is the surface tension of the bare fluid-fluid interface and θ_{12} is the three-phase contact angle. The $E_{ads} \propto R^2$ is more than three times bigger for the 23 nm-nanoparticles than

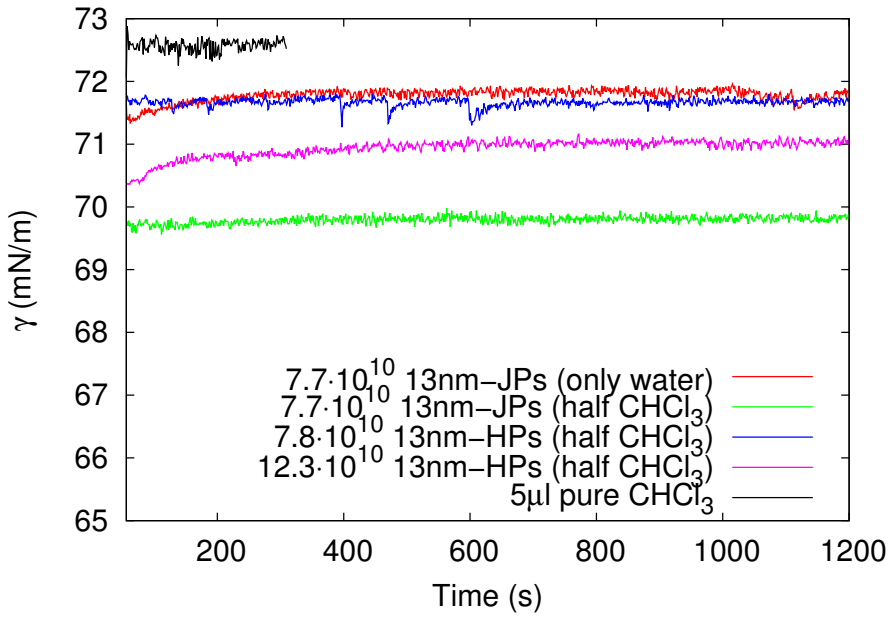

(a) γ evolution over time

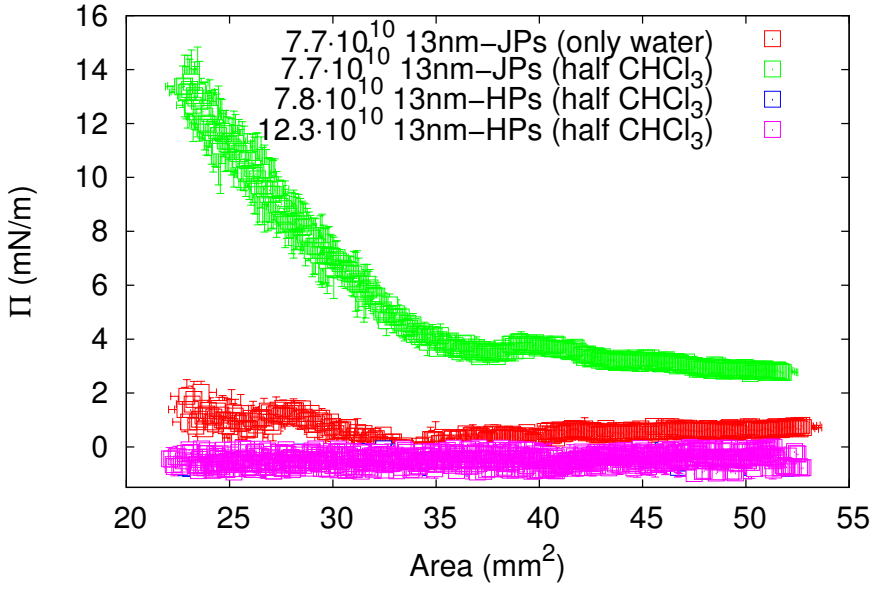

(b) Growing/shrinking cycles

Figure 9.3: γ evolution over time after deposition of **(a)** 13 nm-JPs (squares) and -HPs (circles) at water/air interfaces with different spreading agents (pure water or a mixture of water/$CHCl_3$). The Π against A_p of the growing and shrinking cycles for **(a)** curves is plotted in **(b)**. The black curve in **(a)** corresponds to the evaporation of pure $CHCl_3$ deposited at the interface to test the purity of the spreading solvent.

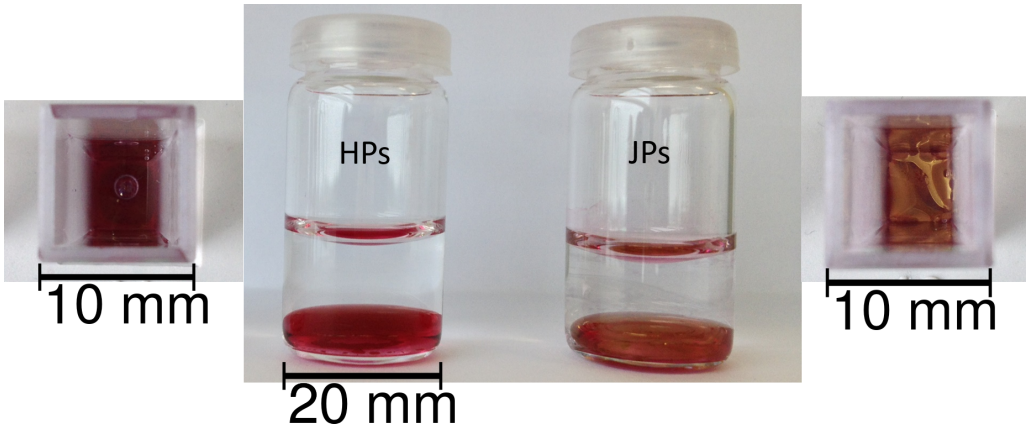

Figure 9.4: Pictures of samples of nanoparticles dispersed in chloroform in the presence of an extra top phase of water. The interface between the two phases does not change in color for homogeneous nanoparticles (left), but it is golden for nanoparticles coated by two polymers (right). The insets show top views.

for the 13 nm-nanoparticles. Thereby, the bigger nanoparticles are expected to be better anchored at the interface.

$$E_{ads} = \pi R^2 \gamma_{12} \left(1 \pm \cos\theta_{12}\right)^2 \tag{9.1}$$

Finally, the interfacial activity of the 23 nm-JPs is compared to the 23 nm-HPs for the higher concentrations and in Fig. 9.5b can be seen that the 23 nm-HPs show no interfacial activity, compared to the $\Pi \sim 60\, mN/m$ that reach the 23 nm-JPs. This is a clear proof that the combination of size and polymers used to synthesize the 23 nm-JPs lead to high interfacial activity than homogeneous nanoparticles. The foamability of these nanoparticles was previously reported by Hunter and Jameson, who studied the adsorption of 120 nm and 300 nm polystyrene nanoparticles functionalized by PEG-Monomethacrylate (PEGMA) at the water/air interface [18]. The PEGMA functionalization stabilized sterically the nanoparticles. The highest surface pressure obtained for the 300 nm particles greatly depended on the water subphase pH: 27 mN/m for pH 2 and 7 mN/m for pH 6, because these nanoparticles are strongly positively charged at pH 2, and discharged at pH 6 (namely producing aggregation of the nanoparticles). Similar behavior was found for the 120 nm nanoparticles (22-25 mN/m at pH 2). These nanoparticles showed a good ability to produce foams, with good agreement between the Langmuir balance experiments at the water/air interface and the foaming behavior: lower pH leads to stronger adsorption and the formation of a more robust steric barrier. Nevertheless, these nanoparticles were randomly functionalized and this is probably why the interfacial activity was much lower than that obtained for our 23 nm-JPs.

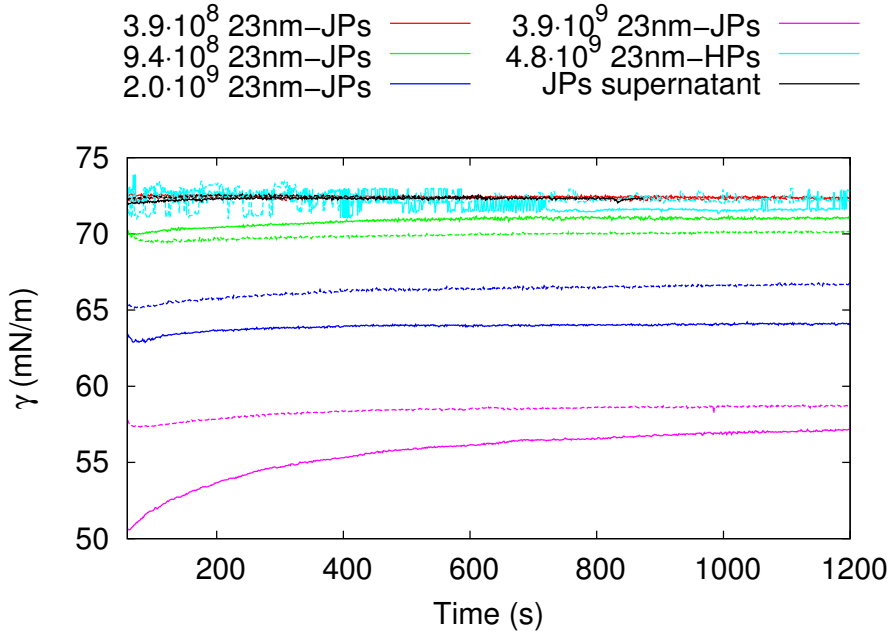

(a) γ evolution over time

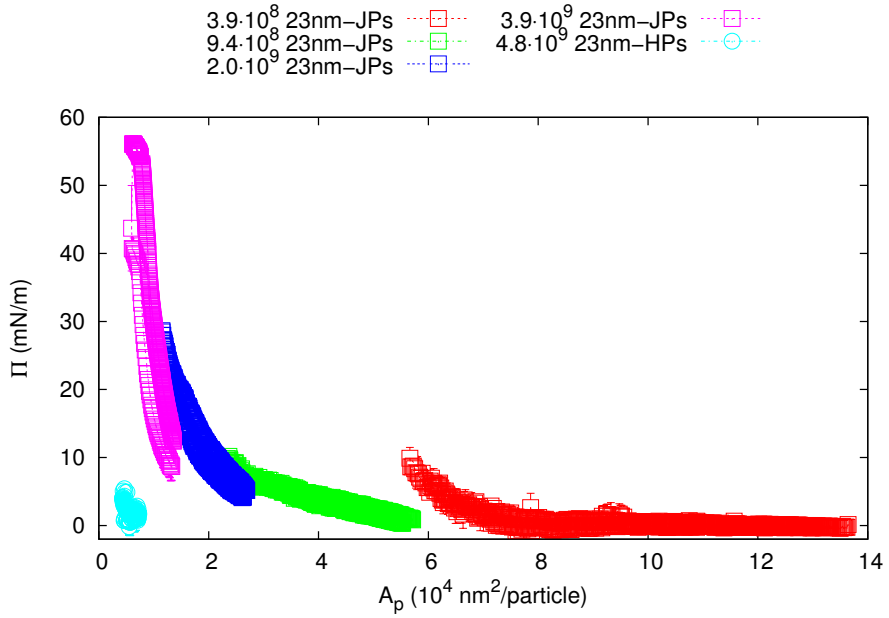

(b) Growing/shrinking cycles

Figure 9.5: **(a)** γ evolution over time after deposition of 23 nm-JPs (squares) and -HPs (circles) at water/air interfaces dispersed in $CHCl_3$ (which is used as spreading agent) and **(b)** the Π against A_p of the growing and shrinking cycles corresponding to the curves in **(a)**. The black curve in **(a)** corresponds to the evaporation of $1\,\mu l$ of the supernatant of 23 nm-JPs dispersed in $CHCl_3$ after centrifugation, to test that the $CHCl_3$ is not desorbing the polymers of the 23 nm-JPs.

Interfacial Dilatational Rheology

Moreover, the interfacial dilatational rheology in Fig. 9.6 show that E_d is of one order of magnitude bigger than η_d for each A_p studied, pointing out a solid elastic-shell behavior. E_d decreases and η_d increases with the period because for higher periods the perturbation is lower and the surface show less elastic behavior. There is a clear trend of increasing E_d and η_d for decreasing A_p for the 23 nm-JPs, showing the elastic shell behavior that becomes more important as there are more particles per unit of area. On the other hand, the 23 nm-HPs at higher concentrations show once more no interfacial activity through no elasticity nor viscosity, similar to the bare water/air interface. This elastic shell behavior in which the elastic modulus increases from $25\,mN/m$ to $450\,mN/m$ point out the interfacial activity of such JPs and their capability as foam stabilizers (see Fig. S2 in Supplementary Information).

Tension at Interface of Two Liquids

Next, the pendant drop was immersed in decane for the highest concentrations measured with 23 nm-JPs, see the results plotted in Fig. 9.7. The interfacial activity of the pendant drop immersed in decane is near zero. No interfacial activity is observed for the 23 nm-HPs both in water/air and in water/decane interfaces. The immersion of the pendant drop in decane might produce aggregation of the nanoparticles, leading to a low interfacial activity in water/decane compared to water/air interfaces. However, from previous works with similar methodology and also true Janus gold nanoparticles but of $4\,nm$-diameter and functionalized by hexanethiol and mercaptoethoxyethanol [12], the surface tension measured at water/air and water/decane interfaces was similar for similar A_p. Thus, the difference of interfacial activity of the 23 nm-JPs at water/air and water/decane interfaces must come from either the size or the polymers. From Equation 9.1, the $E_a ds$ is 33 times higher for the 23-nm gold nanoparticles than for the 4-nm nanoparticles of our previous work [12] and then the bigger particles are expected to withstand better the immersion in decane. This points out to the polymers as responsible of the interfacial activity differences at water/air and water/decane interfaces. When we tried to transfer the JPs to decane it was not possible because they irreversibly aggregated and precipitated. Thus, the aggregation hypothesis is the most probable. In any case, this is an evidence that not all nanoparticles that show a high interfacial activity in water/air interfaces show also a high interfacial activity in water/oil interfaces (see Fig. S3 in Supporting Information).

This behavior is reproduced with interfacial dilatational rheology in Fig. 9.8, where it can be seen that the elasticity and viscosity is always greater for water/air than for water/decane interfaces. Also, for water/air interfaces, when the pendant drop is shrunk, the elasticity and viscosity increases significantly as explained before.

9.4 Conclusions

The interfacial activity of gold Janus nanoparticles (JPs) in the range 13-23 nm, synthesized in surfactant free conditions is studied by pendant drop tensiometry. The particles

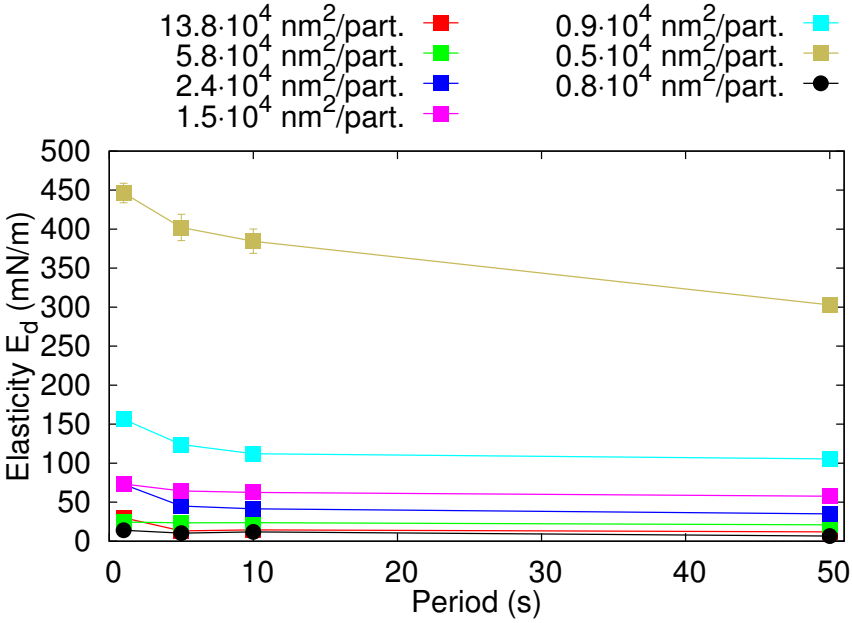

(a) Elastic interfacial dilatational modulus E_d

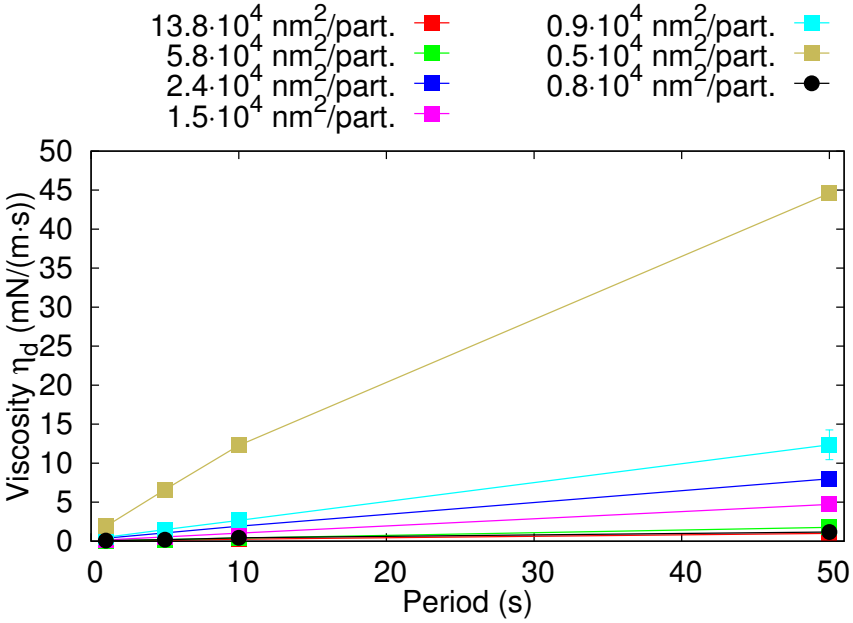

(b) Interfacial dilatational viscosity η_d

Figure 9.6: **(a)** Interfacial dilatational elastic modulus (E) and **(b)** viscosity (η_d) of 23 nm-JPs (squares) and -HPs (circles) dispersed in $CHCl_3$ against different periods for different A_p compression states at the water/air interface.

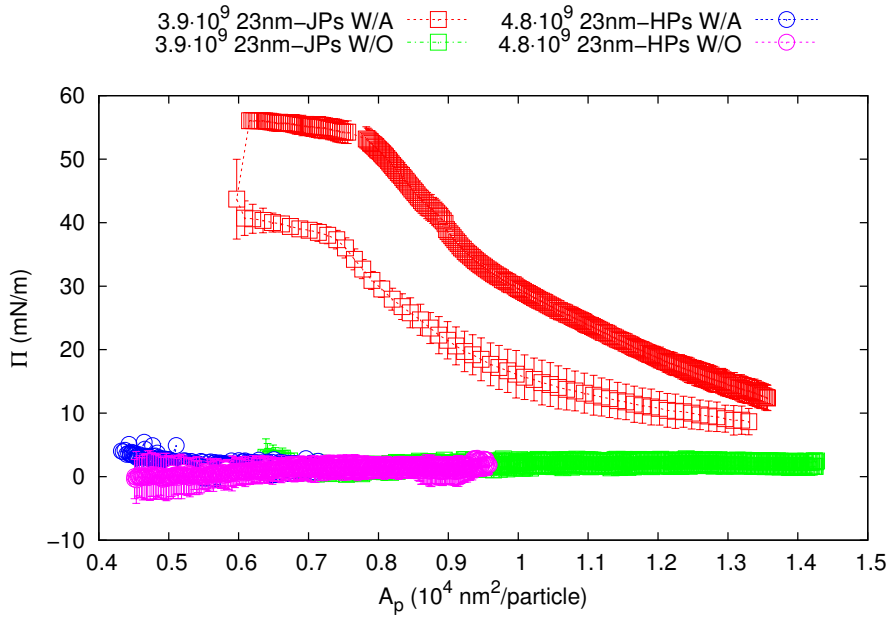

Figure 9.7: Π against A_p of the growing and shrinking cycles of 23 nm-JPs (squares) and -HPs (circles) dispersed in $CHCl_3$ at water/air (solid lines) and water/decane (dashed lines) interfaces.

are half functionalized with polystyrene (PS of 2 kDa) and half with polyethylene glycol (PEG of 1 kDa) as hydrophobic and hydrophilic polymers, respectively. Homogeneous hydrophilic nanoparticles (HPs) fully functionalized with PEG are synthesized to compare the interfacial activity with the corresponding JPs. The HPs exhibited no interfacial activity compared to the JPs, pointing out the ability of the laters as better foam stabilizers. Moreover, we tested the ability of water and a water/$CHCl_3$ as spreading agents, and the better spreading agent was pure $CHCl_3$ reaching surface pressures of $60\,mN/m$ at water/air interface. In these conditions, the water/air interface behaved as an elastic shell which pointed out also the ability of these JPs as foam stabilizers. Finally, the interfacial activity was near zero when the pendant drops were immersed in decane, which might be due to an irreversibly aggregation of the nanoparticles during immersion in decane. Thus, the role of the polymers and spreading agent is revealed as very important when designing JPs with high interfacial activity in a specific interface.

Acknowledgements

This work was supported by the Spanish MINECO (projects MAT2013-44429-R and MAT2014-60615R), by "Junta de Andalucía" and FEDER (projects P10-FQM-5977 and P12-FQM-1443), by the European Research Council (ERC Advanced Grant #267867 Plasmaquo) and by Brazilian Funding Agency FAPESP (2012/21930-3 and 2014/01807-8). J.J.G.-C. acknowledges the Ministry of Economy and Competitiveness for a Juan de la

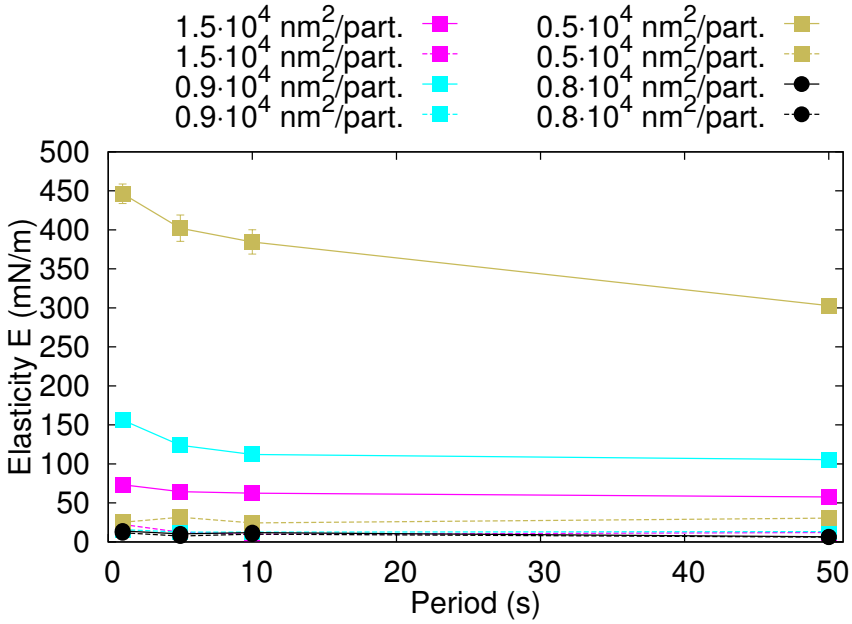

(a) Elastic interfacial dilatational modulus E_d

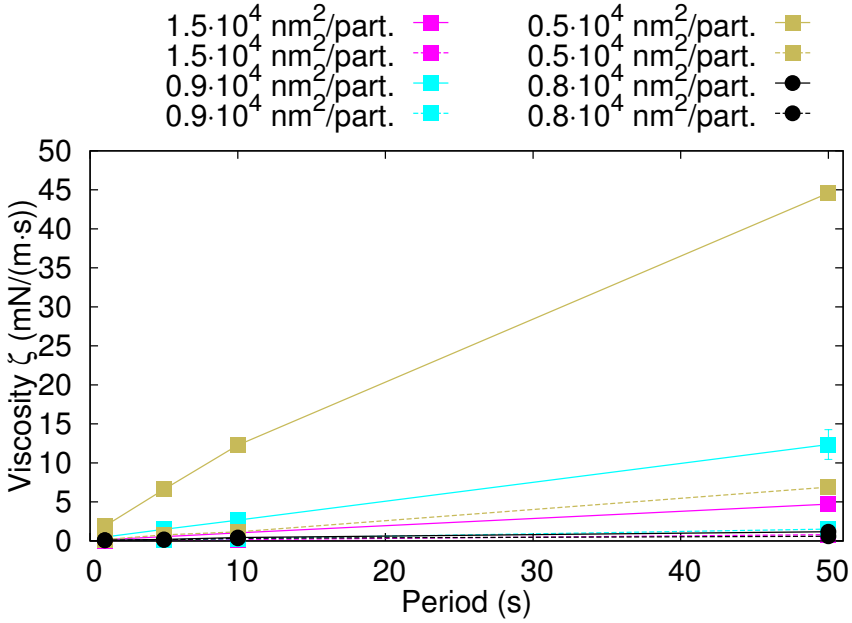

(b) Interfacial dilatational viscosity η_d

Figure 9.8: **(a)** Interfacial dilatational elastic modulus (E) and **(b)** viscosity (η_d) of 23 nm-JPs (squares) and -HPs (circles) dispersed in $CHCl_3$ against different periods for different A_p compression states at the water/air (solid lines) and water/decane (dashed lines) interfaces.

Cierva fellowship (#JCI-2012-12517). Authors thank to Dr. J.A. Holgado-Terriza and Dr. J.L. Muros-Cobos for the software Contacto© used for surface tension measurements.

9.5 Supporting Information

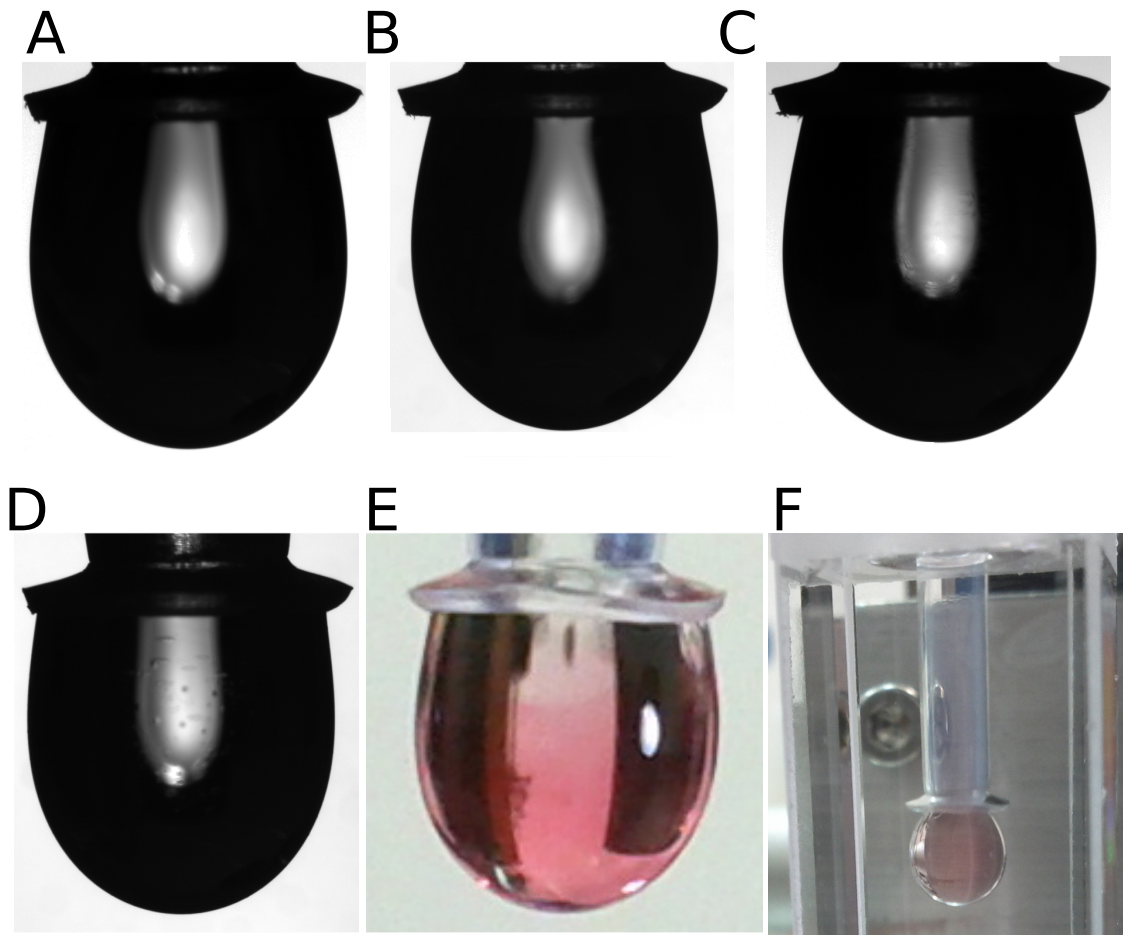

Figure 9.9: $45\,\mu l$ water pendant drop with (A) no particles, (B) $3.9{\cdot}10^8$, (C) $9.4{\cdot}10^8$ and (D) $3.9 \cdot 10^9$ 23nm-JPs, after $CHCl_3$ evaporation. It can be seen the changes in opacity and shape for increasing number of particles deposited at the interface. (E) correspond to the picture in color of (D) in which it can be seen the red color of the interface and (D) is after immersion in decane.

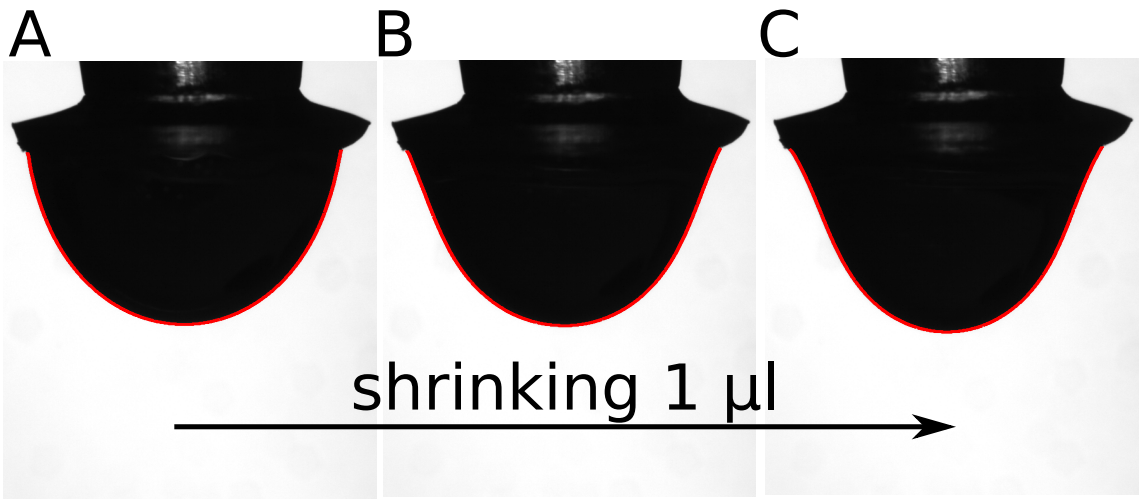

Figure 9.10: $15\,\mu l$ water pendant drop with $3.9 \cdot 10^9$ 23nm-JPs, after $CHCl_3$ evaporation. The (A), (B) and (C) correspond to the initial, medium and final states of the interfacial rheology (extracting $1\,\mu l$). It can be seen the change in the shape which reflects an elastic shell behavior.

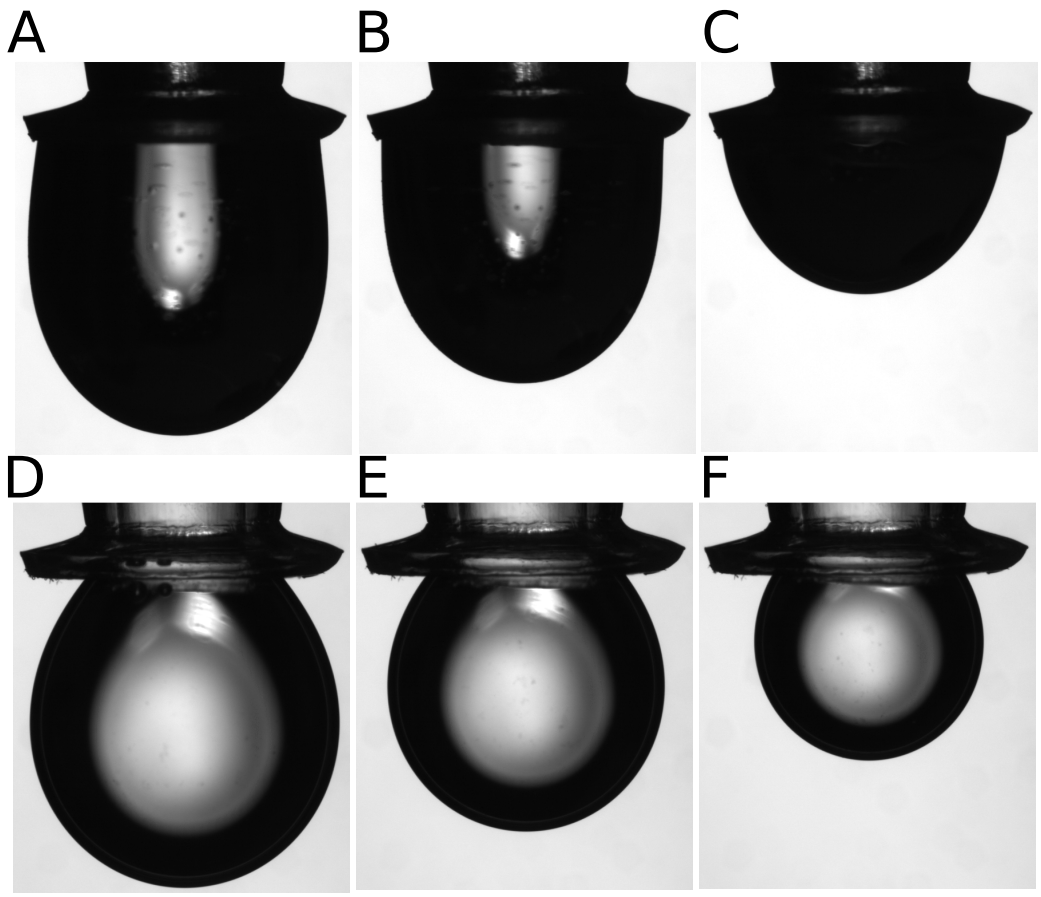

Figure 9.11: Water/air (A-C) and water/decane (D-F) interfaces with $3.9 \cdot 10^9$ 23nm-JPs particles deposited at the pendant drop, after $CHCl_3$ evaporation. Pendant drop volumes: $45\,\mu l$ (A,D), $30\,\mu l$ (B,E) and $15\,\mu l$ (C,F).

References

[1] Xu, H.; Liu, X.; Su, G.; Zhang, B.; Wang, D. Electrostatic Repulsion-Controlled Formation of Polydopamine-Gold Janus Particles. *Langmuir* **2012**, *28*, 13060–13065, DOI: 10.1021/la302394e.

[2] Fujii, S.; Yokoyama, Y.; Miyanari, Y.; Shiono, T.; Ito, M.; Yusa, S.-i.; Nakamura, Y. Micrometer-Sized Gold-Silica Janus Particles as Particulate Emulsifiers. *Langmuir* **2013**, *29*, 5457–5465, DOI: 10.1021/la400697a.

[3] Larson-Smith, K.; Pozzo, D. C. Pickering Emulsions Stabilized by Nanoparticle Surfactants. *Langmuir* **2012**, *28*, 11725–11732, DOI: 10.1021/la301896c.

[4] Gorgoll, R. M.; Tsubota, T.; Harano, K.; Nakamura, E. Cooperative Self-Assembly of Gold Nanoparticles on the Hydrophobic Surface of Vesicles in Water. *J. Am. Chem. Soc.* **2015**, *137*, 7568–7571, DOI: 10.1021/jacs.5b03632.

[5] Binks, B. P.; Fletcher, P. D. I. Particles Adsorbed at the Oil-Water Interface: A Theoretical Comparison between Spheres of Uniform Wettability and Janus Particles. *Langmuir* **2001**, *17*, 4708–4710, DOI: 10.1021/la0103315.

[6] Garbin, V.; Crocker, J. C.; Stebe, K. J. Nanoparticles at fluid interfaces: Exploiting capping ligands to control adsorption, stability and dynamics. *J. Colloid Interface Sci.* **2012**, *387*, 1–11, DOI: 10.1016/j.jcis.2012.07.047.

[7] Reguera, J.; Ponomarev, E.; Geue, T.; Stellacci, F.; Bresme, F.; Moglianetti, M. Contact angle and adsorption energies of nanoparticles at the air-liquid interface determined by neutron reflectivity and molecular dynamics. *Nanoscale* **2015**, *7*, 5665–5673.

[8] Reguera, J.; Kim, H.; Stellacci, F. Advances in Janus Nanoparticles. *Chimia* **2013**, *67*, 811–818, DOI: doi:10.2533/chimia.2013.811.

[9] Iida, R.; Kawamura, H.; Niikura, K.; Kimura, T.; Sekiguchi, S.; Joti, Y.; Bessho, Y.; Mitomo, H.; Nishino, Y.; Ijiro, K. Synthesis of Janus-Like Gold Nanoparticles with Hydrophilic/Hydrophobic Faces by Surface Ligand Exchange and Their Self-Assemblies in Water. *Langmuir* **2015**, *31*, 4054–4062, DOI: 10.1021/la504647z.

[10] Zubarev, E. R.; Xu, J.; Sayyad, A.; Gibson, J. D. Amphiphilicity-Driven Organization of Nanoparticles into Discrete Assemblies. *J. Am. Chem. Soc.* **2006**, *128*, PMID: 17117855, 15098–15099, DOI: 10.1021/ja066708g.

[11] Percebom, A. M.; Giner-Casares, J. J.; Bals, S.; Loh, W.; Liz-Marzán, L. M. Janus Gold Nanoparticles Obtained via Spontaneous Polymer Shell Segregation. *Manuscript in preparation* **2015**.

[12] Fernandez-Rodriguez, M. A.; Song, Y.; Rodriguez-Valverde, M. A.; Chen, S.; Cabrerizo-Vilchez, M. A.; Hidalgo-Alvarez, R. Comparison of the Interfacial Activity between Homogeneous and Janus Gold Nanoparticles by Pendant Drop Tensiometry. *Langmuir* **2014**, *30*, 1799–1804, DOI: 10.1021/la404194e.

[13] Fernandez-Rodriguez, M. A.; Chen, L.; Deming, C. P.; Rodriguez-Valverde, M. A.; Chen, S.; Cabrerizo-Vilchez, M.; Hidalgo-Alvarez, R. A simple strategy to improve the interfacial activity of true Janus gold nanoparticles: a shorter hydrophilic capping ligand. *Soft Matter* **2015**, DOI: 10.1039/C5SM01908G.

[14] Ferdous, S.; Ioannidis, M.; Henneke, D. Adsorption kinetics of alkanethiol-capped gold nanoparticles at the hexane-water interface. *J. Nanopart. Res.* **2011**, *13*, 6579–6589, DOI: 10.1007/s11051-011-0565-y.

[15] Fernandez-Rodriguez, M. A.; Rodriguez-Valverde, M. A.; Cabrerizo-Vilchez, M.; Hidalgo-Alvarez, R. Surface activity and collective behaviour of colloidally stable Janus-like particles at the air-water interface. *Soft Matter* **2014**, 3471–3476, DOI: 10.1039/C3SM52624K.

[16] Walther, A.; Müller, A. H. E. Janus Particles: Synthesis, Self-Assembly, Physical Properties, and Applications. *Chem. Rev.* **2013**, *113*, 5194–5261, DOI: 10.1021/cr300089t.

[17] Fernandez-Rodriguez, M. A.; Ramos, J.; Isa, L.; Rodriguez-Valverde, M. A.; Cabrerizo-Vilchez, M. A.; Hidalgo-Alvarez, R. Interfacial Activity and Contact Angle of Homogeneous, Functionalized, and Janus Nanoparticles at the Water/Decane Interface. *Langmuir* **2015**, *31*, 8818–8823, DOI: 10.1021/acs.langmuir.5b02137.

[18] Hunter, T. N.; Jameson, G. J.; Wanless, E. J.; Dupin, D.; Armes, S. P. Adsorption of Submicrometer-Sized Cationic Sterically Stabilized Polystyrene Latex at the Air-Water Interface: Contact Angle Determination by Ellipsometry. *Langmuir* **2009**, *25*, 3440–3449, DOI: 10.1021/la803879p.

A subtle thought that is in error may yet give rise to fruitful inquiry that can establish truths of great value.

Isaac Asimov

10 Synthesis and interfacial activity of PMMA/PtBMA Janus and homogeneous nanoparticles: the difficulties of using cationic nanoparticles

M.A. Fernandez-Rodriguez[1], Sahar Rahmani[2,3,6], Chris K. J. Yu[2,5], M.A. Rodriguez-Valverde[1], M.A. Cabrerizo-Vilchez[1], Charnelle A. Michel[2,4], Joerg Lahann[2−6] and R. Hidalgo-Alvarez[1,*]

[1] *Biocolloid and Fluid Physics Group, Applied Physics Department, Faculty of Sciences, University of Granada, 18071 Granada, Spain.*
[2] *Biointerfaces Institute, University of Michigan, Ann Arbor, MI 48109, USA.*
[3] *Biomedical Engineering, University of Michigan, Ann Arbor, MI 48109, USA.*
[4] *Chemical Engineering, University of Michigan, Ann Arbor, MI 48109, USA.*
[5] *Material Science & Engineering, University of Michigan, Ann Arbor, MI 48109, USA.*
[6] *Institute of Functional Interfaces (IFG), Karlsruhe Institute of Technology (KIT), 76131 Karlsruhe, Germany.*
[*] *rhidalgo@ugr.es*

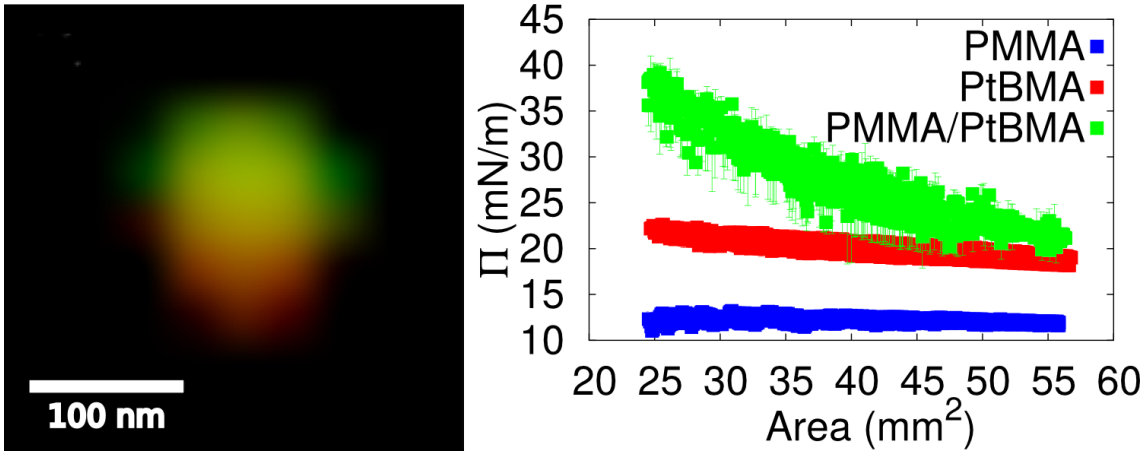

Figure 10.1: Graphical abstract.

Abstract

Polymethylmethacrylate/Poly-tert-butylmethacrylate Janus nanoparticles were synthesized by Electrohydrodynamic Co-Jetting. The Janus character was demonstrated by super-resolution imaging with Structured Illumination Microscopy. The Janus nanoparticles and the corresponding homogeneous ones were morphologically characterized. All nanoparticles presented interfacial activity which was measured by pendant drop tensiometry at water/decane interfaces. At high concentrations and compression states, the Janus nanoparticles exhibited higher interfacial activity than the homogeneous nanoparticles. This is in agreement with theoretical and experimental works in which Janus nanoparticles present higher interfacial activity than homogeneous nanoparticles. The Janus nanoparticles also produced an elastic shell behaviour from measurements of interfacial dilatational rheology and this points out to their ability as emulsifiers.

Keywords: Electrohydrodynamic co-jetting; PMMA/PtBMA; Janus nanoparticles; Interfacial activity; Pendant drop tensiometry.

10.1 Introduction

Polymeric Janus nanoparticles are able to self-assemble spontaneously at interfaces due to the contrast between their spatial domains and further to be responsive to external magnetic or electric fields, pH or temperature gradients and light [1–4]. Janus particles have a theoretical stability at liquid-liquid interfaces higher than their homogenous counterparts and can act as surfactants to stabilize such systems [5]. There are three main strategies to synthesize Janus nanoparticles with polymeric capping ligands concerning the core and molecules used. The first one involves the selective functionalization of an inorganic or

polymeric core with different polymers in each hemisphere as capping ligands [6, 7]. The second approach consists of selective polymerization over an inorganic core [8–10]. The last strategy involves the selective polymerization of entirely Janus polymeric nanoparticles [2–4, 11]. Another possible technique is the template-assisted synthesis in which a bulk film of block terpolymers is cross-linked [12]. Depending on the affinity of the polymer constituents toward water or oil, it is possible to produce amphiphilic polymeric Janus particles with enhanced interfacial activity [11]. One particular technique used to synthesize polymeric Janus nanoparticles is the Electrohydrodynamic Co-Jetting [6, 13]. This technique can be used to fabricate nanoparticles and fibers with multiple compartments, each of which can contain a different polymer or perhaps encapsulate a different molecule [13]. With respect to self-assembly applications, this technique is advantageous due to its ability to incorporate a wide range of polymers into each hemisphere of the particles regardless of the polymers' amphiphilic nature or polymerization techniques, which can be a limiting factor in other particle fabrication techniques [14–17]. Ruhland et al. [12] synthesized polymeric Janus nanoparticles with different morphologies with the template-assisted technique. They studied the self-assembly of their nanoparticles at water/toluene interfaces by pendant drop tensiometry. They found that the interfacial tension decreased firstly by using Janus cylinders, followed by Janus spheres and Janus discs. Park et al. [18] synthesized and studied homogeneous polystyrene (PS) nanoparticles and gold-coated PS Janus nanoparticles at water/decane interfaces. Whereas the homogeneous PS nanoparticles exhibited a hexagonal lattice at the water/decane interface, the Janus nanoparticles aggregated in fractal structures. Furthermore, Nie et al. [19] found that amphiphilic polymeric JPs assembled into supermicelles. The Janus clusters seem to keep the asymmetry charge and Janus character, acting as larger Janus entities [20].

In this work, we used polymethylmethacrylate and poly-tert-butylmethacrylate as polymers because they exhibit a large contact angle difference (of water in a polymer-coated silicon wafer): $68°$ [21] and $108°$ [22], respectively. Thus, they are expected to have significant interfacial activity. We synthesized cationic homogeneous spherical nanoparticles made of the mentioned polymers and Janus nanoparticles with the polymers separated into two hemispheres by Electrohydrodynamic Co-Jetting. The morphology of such nanoparticles was characterized by SEM, DLS, and super-resolution imaging with Structured Illumination Microscopy (SIM). The interfacial activity at water/decane interfaces and interfacial dilatational rheology was studied with pendant drop tensiometry.

10.2 Materials and Methods

10.2.1 Materials

Polymethylmethacrylate (PMMA) with a molecular weight of $20\,kDa$, hexadecyltrimethylammonium bromide (CTAB), chloroform, dimethylformamide (DMF), poly(9,9-dioctylfluorene-alt-benzothiadiazole) (green dye) and decane HPLC were purchased from Sigma Aldrich, USA. Poly-tert-butylmethacrylate (PtBMA) was purchased from Polysciences, USA, and ADS306PT (red dye) was purchased from American Dye Source, Canada. ProLong Gold antifade reagent was provided by Life Technologies.

10.2.2 Janus and homogeneous nanoparticles fabrication and characterization

Nanoparticles were fabricated through the Electrohydrodynamic Co-Jetting process by flowing multiple polymeric solutions through metal capillaries in a side-by-side configuration [6, 13]. The flows are reproduced under a laminar regime and at the tip of the capillaries the solutions come together to form a drop, to which an electric voltage is applied. The application of the electric field causes the solutions to form a Taylor cone, which creates a spray of individual droplets that accelerate towards the counter electrode. During this process, the surface area to volume ratio of the nanoparticles decreases rapidly and the solvents used evaporate quickly resulting in polymeric nanoparticles deposited on the counter electrode. Due to the rapid evaporation of the solvents and the laminar regime used, the solvents do not have sufficient time to mix and the resulting nanoparticles have individual compartments made of each polymer solution instead of a mixture of all solutions used. In this work, Janus nanoparticles were fabricated by using two laminar flows, each of which contained a different polymer (one flow contained PMMA and the other contained PtBMA). For the PMMA flow, a polymer concentration of 5% w/v, a hexadecyltrimethylammonium bromide (CTAB) concentration of 2.5% w/v, and a solvent ratio of $70:30$ chloroform:DMF was used. For the PtBMA flow, a polymer concentration of 5% w/v, a CTAB concentration of 2.5% w/v, and a solvent ratio of $85:15$ was used. For homogeneous nanoparticles composed of each neat polymer the same solvent ratios were used, respectively. The flow rate used for all nanoparticles was $0.1\,ml/h$ with a distance of 35 cm between the needles and the counter electrode. Once fabricated, the nanoparticles were analyzed with Scanning Electron Microscopy (SEM) to determine their size and shape and ImageJ analysis to determine their size distribution.

10.2.3 Structured Illumination Microscopy (SIM) of Janus Nanoparticles

Janus nanoparticles with a separate dye in each domain (red and green) were fabricated as described above. The nanoparticles were directly jetted onto glass cover slips and were incubated in ProLong Gold antifade reagents overnight before imaging with a Zeiss Structured Illumination Microscope to demonstrate their bicompartmental nature.

10.2.4 Nanoparticle Isolation and Characterization

The nanoparticles were dispersed in DI water and separated via centrifugation at $3220\,RCF$ for 6 hours to isolate the desired fraction. The particle size distribution was analyzed via Dynamic Light Scattering (DLS) and their concentration was determined by Nanoparticle Tracking Analysis (NTA) with a Nanosight equipment. The electrophoretic mobility was measured using a Malvern Zetasizer. Before particle analysis measurements, the nanoparticles were repeatedly washed with DI water in glass containers to remove any trace of CTAB present in the solutions to eliminate the impact of this molecule in the experiments.

10.2.5 Pendant drop tensiometry

Pendant drop tensiometry is an extensively employed method to measure surface and interfacial tensions of liquids [23]. The pendant drop experiments are performed in a similar way as previous work with gold Janus nanoparticles [24]: first we deposit a given amount of particle dispersion with a microsyringe on an initial $20\,\mu L$ MilliQ water pendant drop in air. Next the pendant drop is shrunk down to $10\,\mu L$ to immerse the capillary in decane (see Fig. 10.5a and 10.5b). The immersion in decane provides a lower bare interfacial tension and thus a better adsorption of the particles at the interface [25]. Next, the pendant drop is grown up to $45\,\mu L$ inside the decane phase (see Fig. 10.5c) and the interfacial tension is monitored during 1h up to reach a stable value. This interfacial tension stabilization was measured for three initial concentrations of nanoparticles deposited at the pendant drop interface in separate experiments. The concentrations were calculated to get the same area covered by the different nanoparticles if all of them were arranged at the pendant drop interface with close-packing. Finally, for the intermediate concentration of nanoparticles, we performed growing and shrinking experiments in which the interfacial pressure $\Pi = \gamma_0 - \gamma$ (where γ_0 is the interfacial tension of pure water/decane, $52.3\,mN/m$, and γ is the interfacial tension) is plotted against the pendant drop area. Additionally, interfacial dilatational rheology is performed by growing and shrinking the pendant drop at different periods with an amplitude of $1\,\mu L$. From the phase and amplitude differences between the sinusoidal excitation and the oscillating interfacial tension we are able to estimate an interfacial dilatational elastic modulus E_d and viscosity η_d as in previous works [26]. These measurements were made at the water/air interface because the behavior is the same in both water/air and water/decane interfaces but the signal-to-noise ratio was higher at water/air interfaces.

10.3 Results and Discussion

The homogeneous nanoparticles made of PMMA, PtBMA and the Janus nanoparticles with PMMA in one hemisphere and PtBMA in the second hemisphere (labeled as JPs) were synthesized by Electrohydrodynamic Co-Jetting [6, 13]. This technique is represented in Fig. 10.2a. To create the nanoparticles by Electrohydrodynamic Co-Jetting, the solution parameters were changed in order to increase the dielectric constant of the jetted material. Specifically, a higher ratio of dimethylformamide (dielectric constant of 38) than chloroform (dielectric constant of 4.81) and a charged surfactant (CTAB) were employed to change the solution parameters, resulting in cationic nanoparticles as shown by the positive electrophoretic mobility in table in Fig. 10.3. Based on these changes, the nanoparticles obtained had significantly monodisperse populations as it can be observed by SEM imaging (Fig. 10.2b-d). The following average sizes were obtained: (i) PMMA homogenous nanoparticles: $100.8 \pm 51.3\,nm$; (ii) PtBMA homogenous nanoparticles: $82.2 \pm 33.1\,nm$; (iii) Janus nanoparticles: $90.2 \pm 39.5\,nm$.

To demonstrate the compartmental nature of the Janus particles, super-resolution imaging with Structured Illumination Microscopy (SIM) was used. These particles contained a green dye in the PtBMA compartment and a red dye in the PMMA compartment.

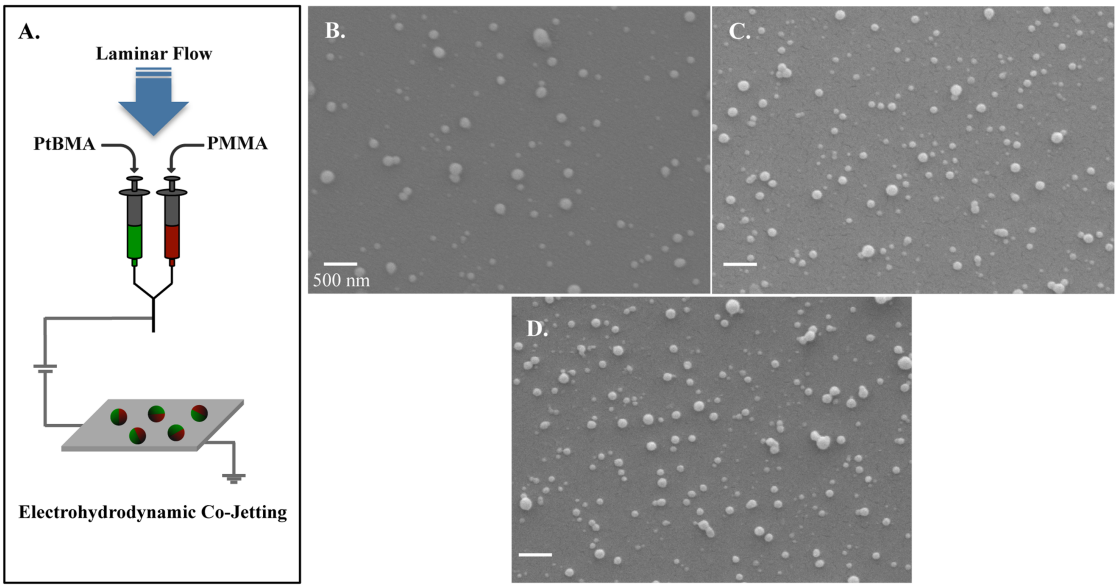

Figure 10.2: Fabrication of nanoparticles and their size characterization. (A) Schematic of Electrohydrodynamic Co-Jetting of Janus Nanoparticles. (B-D) SEM images of the as-fabricated PMMA, PtBMA, and Janus nanoparticles respectively. All scale bars are $500\,nm$.

As demonstrated in Fig. 10.4, the dyes are in two distinct regions of these particles, signifying the two separate domains.

To create a more monodispersed solution of particles and remove any potential aggregates, fractionation via centrifugation was used. In this technique, the larger particles are removed at lower centrifugation times/durations, while the smaller sized particles are isolated at longer durations and higher speeds. The average size after fractionation is similar for each nanoparticle and in the range of $200\,nm$ in diameter, as measured by DLS (see Fig. 10.3) and NTA (table in Fig. 10.3). Specifically, based on NTA measurements the nanoparticles averaged at $163 \pm 39.2\,nm$ for PMMA nanoparticles, $217 \pm 39.6\,nm$ for PtBMA nanoparticles, and $172 \pm 27.8\,nm$ for the Janus nanoparticles. The total concentration of the nanoparticle, which was then used to determine the surface area of each sample, was measured via NTA analysis. Also, all nanoparticles had high electrophoretic mobility values $(3.1 - 3.5 \cdot 10^8\,m^2/(V \cdot s))$, which is expected to stabilize and prevent aggregation in the water dispersion and at the water/decane interface.

The interfacial activity of the nanoparticles was characterized by pendant drop tensiometry (see Fig. 10.5). The interfacial tension of different concentrations of nanoparticles is represented in Fig. 10.6. In all experiments, the pendant drop was maintained to a constant drop volume of $45\,\mu L$. Many curves showed a first increase over time, this might be due to aggregation or reconfiguration of the nanoparticles at the water/decane interface during the first minutes. The measurements with PMMA nanoparticles showed an erratic behavior (see Fig. 10.6a) in which no trend was observed. PtBMA nanoparticles

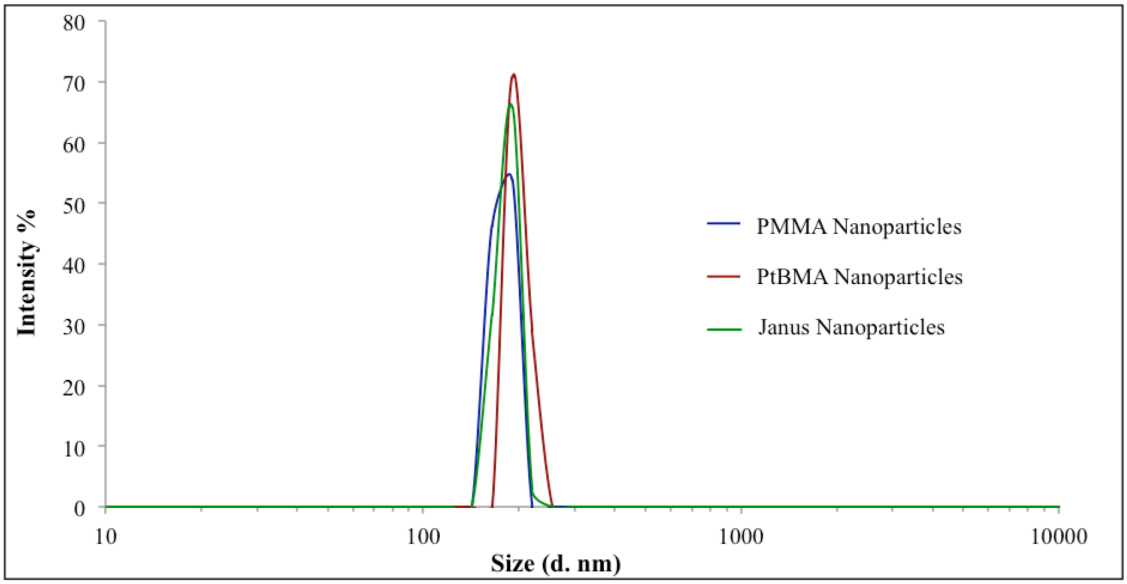

Nanoparticle	Average size (d. nm)	μ_e (10^{-8} $m^2/(V \cdot s)$)
PMMA	163± 39	3.2±0.1
PtBMA	217± 40	3.1 ± 0.1
Janus Nanoparticles	172± 28	3.5 ± 0.3

Figure 10.3: Particle analysis after fractionation into a specific size range via centrifugation. Top: Size distribution of each set of nanoparticles based on Dynamic Light Scattering analysis. Bottom: Table with the average sizes based on Nanoparticle Tracking Analysis and electrophoretic mobilities (μ_e) for each particle set.

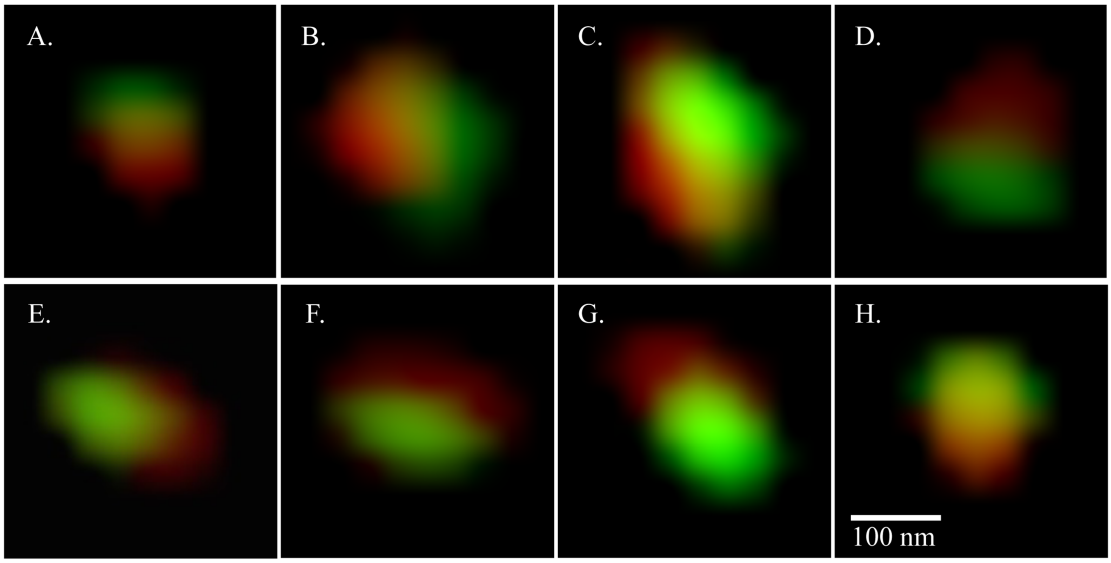

Figure 10.4: Super-resolution imaging of Janus nanoparticles with Structured Illumination Microscopy. (A-H) Images of specific Janus nanoparticles demonstrating their Janus nature.

showed a clear trend and reproducibility showing lower interfacial tension for increasing nanoparticle concentration (see Fig. 10.6b). Janus nanoparticles showed no trend with the particle concentration but for higher particle concentration the reproducibility seems to improve (see Fig. 10.6c). This erratic behavior can be explained with the cationic nature of the nanoparticles. As Ramos et al. [27] showed that cationic nanoparticles tend to be easily polluted by the media and especially with the negative silicates of glass flasks. Finally, for the majority of the measurements it seems that after 1 hour, the interfacial tension still is evolving. This may be caused because the spreading solvent is water, as well as the pendant drop. We can expect a Gibbs monolayer in which the nanoparticles are placed in the bulk and have to reach the interface in a slow process compared to laboratory timescales [28]. However, in the laboratory timescale, many of the growing and shrinking experiments show closed hysteresis cycles (see Fig. 10.7). Thus, the interfacial tension evolves in such a slow pace that for the entire experiment this change is not very significant. In Fig. 10.7, we plot the interfacial pressure Π against the normalized area (the area of the pendant drop divided by the area of all particles if they were forming an hexagonal compact monolayer). The fact that the x-values are far above from the unity (i.e. very low number of nanoparticles) and we obtain a high interfacial pressure reinforces our hypothesis of the pollution associated with cationic nanoparticles. Moreover, different color correspond to different kind of nanoparticle and cycles in the same x-range correspond to same number of nanoparticles deposited. Thus, it is clear that different runs with the same particle concentration lead to irreproducible cycles. One is attempted to extract some order from the chaos, but it is impossible to state anything from these irreproducible results. The only fact visible to the naked eye is a general trend of

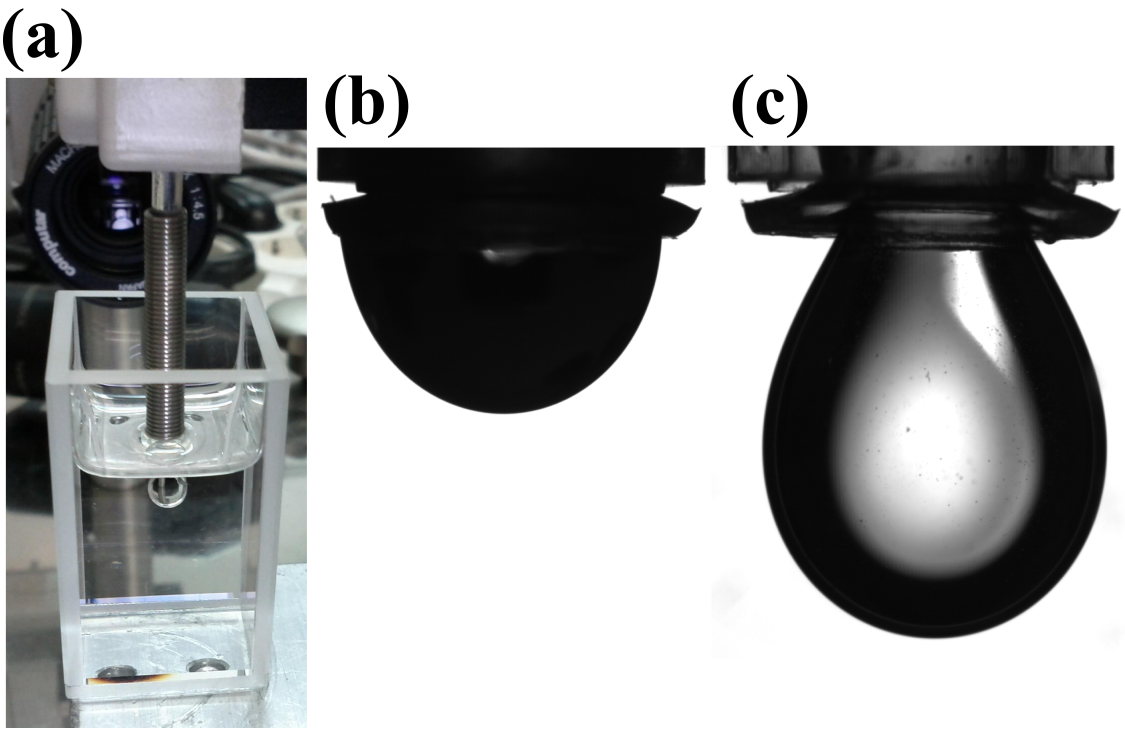

Figure 10.5: (a) Experimental setup. (b) A $10\,\mu L$ water pendant drop with Janus nanoparticles just before immersion in decane. (c) The same pendant drop illustrated in (b) grown up to $45\,\mu L$ in decane.

higher interfacial pressure values for Janus nanoparticles (red curves) compared to PMMA (green) and PtBMA (blue) nanoparticles. This would be in agreement with the theoretical prediction that a Janus nanoparticle with equal hydrophilic and hydrophobic areas present three times more surface activity than the corresponding homogeneous particles at a water/oil interface and previous experimental results in which Janus nanoparticles presented higher interfacial activity than homogeneous nanoparticles [5, 24]. If we take this idea further, the PMMA/PtBMA Janus nanoparticles would be better emulsifiers than the PtBMA or PMMA nanoparticles because of the interfacial activity. In any case, these results are a good example of the difficulties regarding the characterization of cationic nanoparticles that become polluted very easily.

Given the quantity of studies devoted to PMMA and PtBMA laden interfaces, we were interested in developing a deeper characterization of the PMMA/PtBMA Janus behavior at interfaces. As explained in the Materials section, the interfacial dilatational rheology was performed for different area per particle (i.e. different monolayer compression states) at water/air interfaces after testing that the behavior was the same at both water/decane and water/air interfaces but with lower signal-to-noise ratio at water/decane interfaces. The results of interfacial dilatational elastic modulus E_d and viscosity η_d are plotted in Fig. 10.8 against different periods for different areas per particle. It can be seen that E_d decreases and η_d increases with increasing periods. This can be explained in terms of the

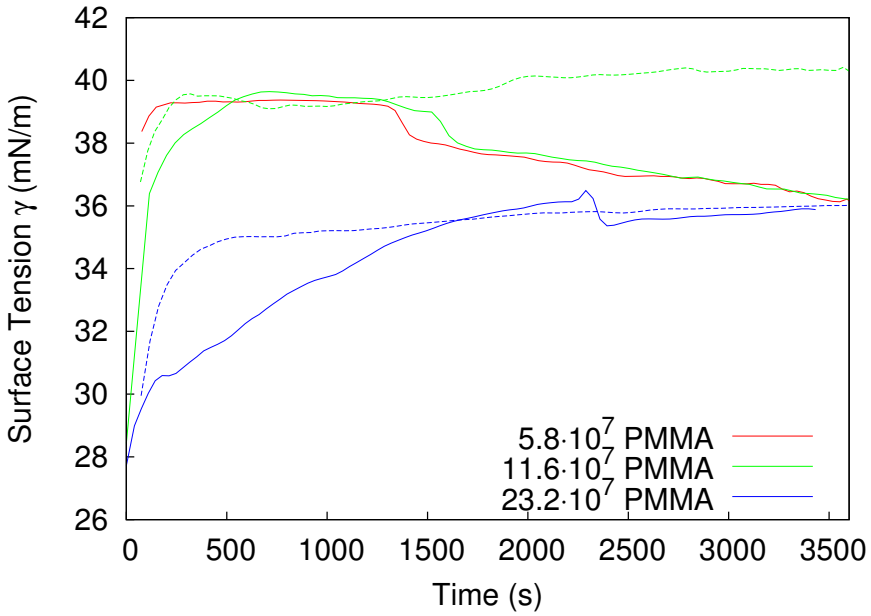

(a) PMMA nanoparticles

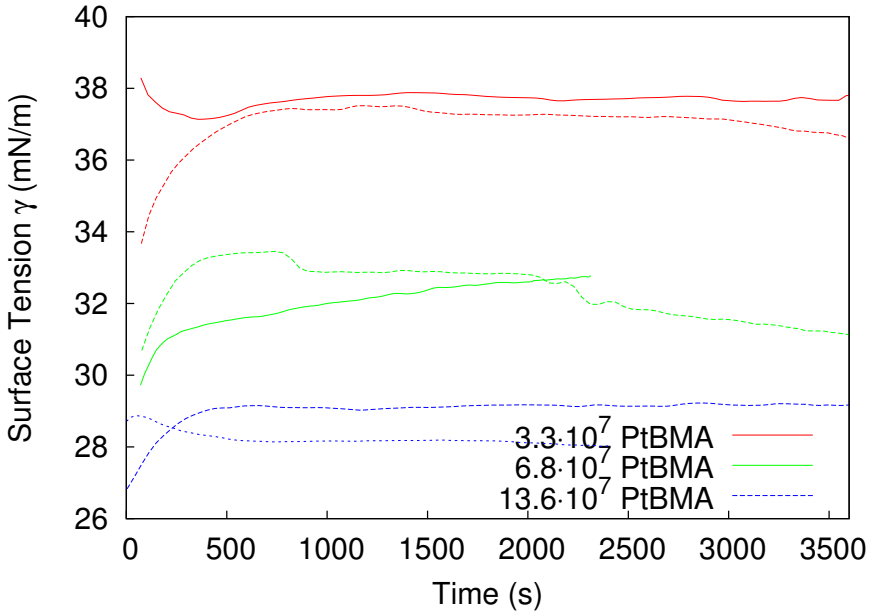

(b) PtBMA nanoparticles

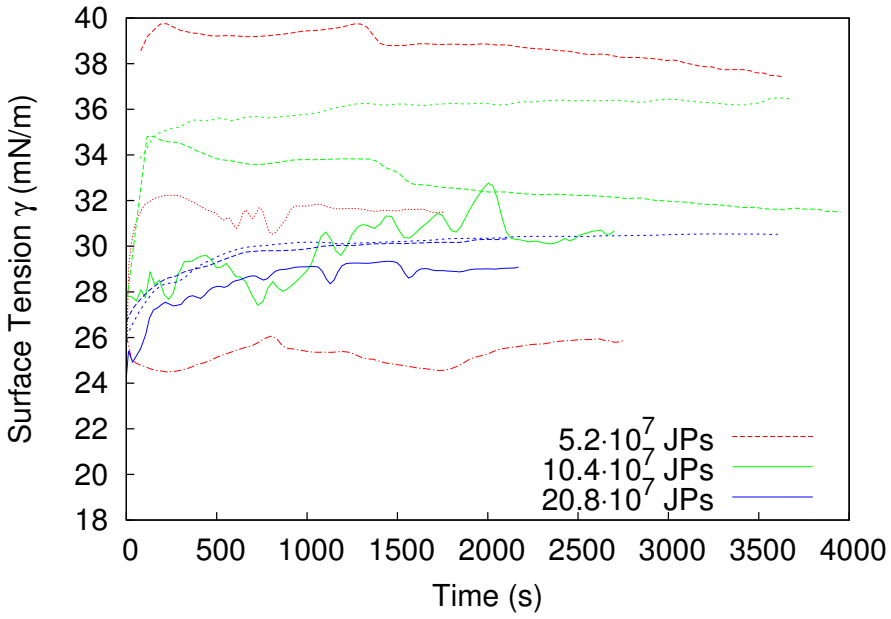

(c) Janus nanoparticles

Figure 10.6: Evolution of the interfacial tension γ over time of a $45\,\mu L$ water pendant drop immersed in decane with different number of deposited PMMA (a), PtBMA (b) and Janus nanoparticles (c). Curves with equal color correspond to equal particle concentration and different runs (i.e. different drops with different depositions).

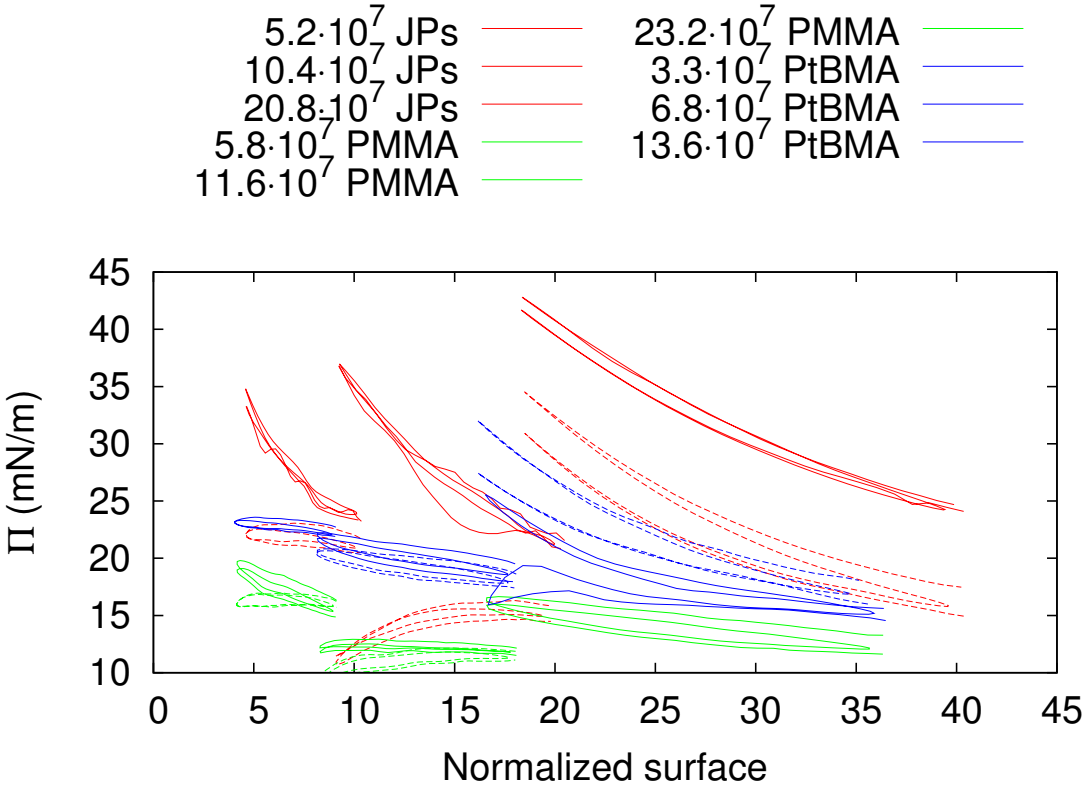

Figure 10.7: Growing and shrinking pendant drop experiments after the interfacial tension γ evolution over time. The interfacial pressure Π is plotted against the normalized area (area of the pendant drop divided by the area of the deposited particles as if they were forming an hexagonal compact monolayer). Each color stand for a different kind of nanoparticle. The curves of same color and same x-range correspond to different runs with same number of deposited nanoparticles (i.e. different drops with different depositions). The runs with equal color in the same x-range are plotted to show the irreproducibility of the measurements.

perturbations, where higher periods produce slower perturbations that result in less elastic and more viscous interfaces. Moreover, upon compression (i.e. lower area per particle) E_d and η_d increases clearly, pointing out an elastic shell behavior of the particle-laden interface. This elastic shell behavior points out the ability of these particles as emulsifiers as they are strongly adsorbed at the interfaces. However, further studies have to be taken to clarify that the elastic shell is not due to pollution, but because of the Janus nature of the nanoparticles as founded in previous works [26].

10.4 Conclusions

Polymethylmethacrylate/Polytert-butylmethacrylate (PMMA/PtBMA) Janus nanoparticles were fabricated by Electrohydrodynamic Co-Jetting. The Janus character was demonstrated by super-resolution imaging with Structured Illumination Microscopy, in which the two domains are revealed to be separated. The Janus nanoparticles and homogeneous nanoparticles of PMMA and PtBMA were characterized by SEM, NTA and DLS, revealing relative monodisperse nanoparticle dispersions with diameters in the range of $160 - 200\,nm$. All nanoparticles had high positive electrophoretic mobility values. The interfacial activity was studied by pendant drop tensiometry depositing different amounts of nanoparticles at water pendant drops and subsequent immersion in decane. All pendant drop experiments showed irreproducibility due to the cationic nature of the nanoparticles. Nevertheless, as general behavior, the Janus nanoparticles reach higher interfacial pressures in growing and shrinking pendant drop experiments, pointing out to their capability as emulsifiers. Moreover, the interfacial dilatational rheology showed an interfacial elastic shell.

Acknowledgements

This work was supported by the Spanish MINECO (projects MAT2013-44429-R and MAT2014-60615R), by "Junta de Andalucía" and FEDER (projects P10-FQM-5977 and P12-FQM-1443), Multidisciplinary University Research Initiative of the Department of Defense and the Army Research Office (W911NF-10-1-0518), the DOD through an idea award (W81XWH-11-1-0111), the Tissue Engineering and Regenerative Medicine Training Grant (DE00007057-36), and the European Community's Seventh Framework Programme (FP7/2007-2013) under grant agreement n° 310445 (SAVVY). The authors thank J.A. Holgado-Terriza and J.L. Muros-Cobos for the software Dinaten© used for the interfacial tension measurements.

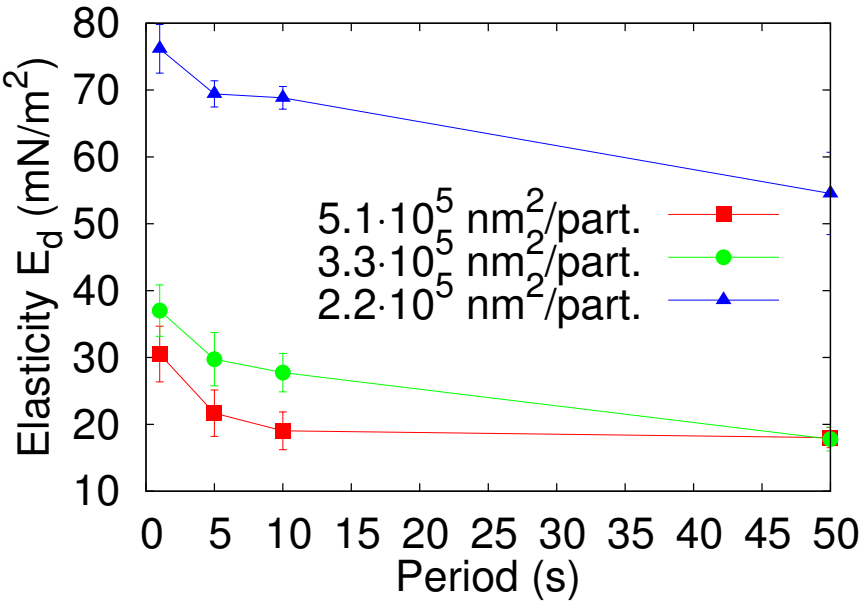

(a)

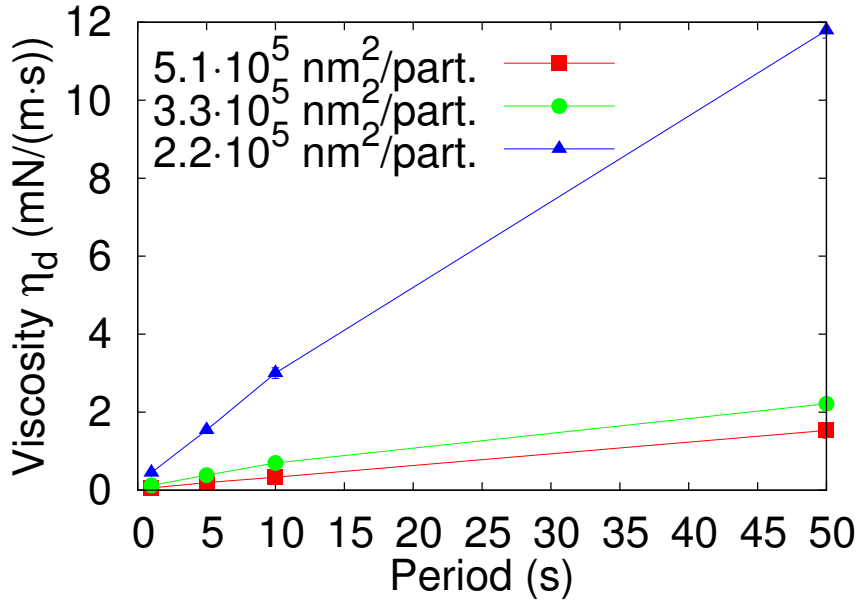

(b)

Figure 10.8: (a) Interfacial dilatational (a) elastic modulus E_d and (b) viscosity η_d against different periods ($1\,\mu L$ amplitude) for different areas per PMMA/PtBMA Janus nanoparticle at the water/air interface.

References

[1] Bradley, M.; Rowe, J. Cluster formation of Janus polymer microgels. *Soft Matter* **2009**, *5*, 3114–3119, DOI: 10.1039/B904316K.

[2] Kaewsaneha, C.; Tangboriboonrat, P.; Polpanich, D.; Eissa, M.; Elaissari, A. Facile method for preparation of anisotropic submicron magnetic Janus particles using miniemulsion. *J. Colloid Interface Sci.* **2013**, *409*, 66–71, DOI: 10.1016/j.jcis.2013.07.067.

[3] Faita, F.; Trindade, A.; Godinho, M.; Bechtold, I. Luminescent elastomeric Janus particles. *J. Colloid Interface Sci.* **2013**, *410*, 124–130, DOI: 10.1016/j.jcis.2013.07.073.

[4] Kaewsaneha, C.; Bitar, A.; Tangboriboonrat, P.; Polpanich, D.; Elaissari, A. Fluorescent-magnetic Janus particles prepared via seed emulsion polymerization. *J. Colloid Interface Sci.* **2014**, *424*, 98–103, DOI: 10.1016/j.jcis.2014.03.011.

[5] Binks, B. P.; Fletcher, P. D. I. Particles Adsorbed at the Oil-Water Interface: A Theoretical Comparison between Spheres of Uniform Wettability and "Janus" Particles. *Langmuir* **2001**, *17*, 4708–4710, DOI: 10.1021/la0103315.

[6] Walther, A.; Müller, A. H. E. Janus Particles: Synthesis, Self-Assembly, Physical Properties, and Applications. *Chem. Rev.* **2013**, *113*, 5194–5261, DOI: 10.1021/cr300089t.

[7] Sashuk, V.; Hołyst, R.; Wojciechowski, T.; Fiałkowski, M. Close-packed monolayers of charged Janus-type nanoparticles at the air-water interface. *J. Colloid Interface Sci.* **2012**, *375*, 180–186, DOI: 10.1016/j.jcis.2012.02.057.

[8] Qiang, W.; Wang, Y.; He, P.; Xu, H.; Gu, H.; Shi, D. Synthesis of Asymmetric Inorganic/Polymer Nanocomposite Particles via Localized Substrate Surface Modification and Miniemulsion Polymerization. *Langmuir* **2008**, *24*, 606–608, DOI: 10.1021/la703607s.

[9] Liu, L.; Ren, M.; Yang, W. Preparation of Polymeric Janus Particles by Directional UV-Induced Reactions. *Langmuir* **2009**, *25*, 11048–11053, DOI: 10.1021/la901364a.

[10] Ge, X.; Wang, M.; Yuan, Q.; Wang, H.; Ge, X. The morphological control of anisotropic polystyrene/silica hybrid particles prepared by radiation miniemulsion polymerization. *Chem. Commun.* **2009**, 2765–2767, DOI: 10.1039/B901094G.

[11] Li, C.; Wu, Z.; He, Y.-F.; Song, P.-F.; Zhai, W.; Wang, R.-M. A facile fabrication of amphiphilic Janus and hollow latex particles by controlling multistage emulsion polymerization. *J. Colloid Interface Sci.* **2014**, *426*, 39–43, DOI: 10.1016/j.jcis.2014.03.061.

[12] Ruhland, T. M.; Gröschel, A. H.; Ballard, N.; Skelhon, T. S.; Walther, A.; Müller, A. H. E.; Bon, S. A. F. Influence of Janus Particle Shape on Their Interfacial Behavior at Liquid-Liquid Interfaces. *Langmuir* **2013**, *29*, 1388–1394, DOI: 10.1021/la3048642.

[13] Roh, K.-H.; Martin, D. C.; Lahann, J. Biphasic Janus particles with nanoscale anisotropy. *Nat. Mater.* **2005**, *4*, 759–763, DOI: 10.1038/nmat1486.

[14] Sokolovskaya, E.; Rahmani, S.; Misra, A. C.; Bräse, S.; Lahann, J. Dual-Stimuli-Responsive Microparticles. *ACS Appl. Mater. Interfaces* **2015**, *7*, 9744–9751, DOI: 10.1021/acsami.5b01592.

[15] Rahmani, S.; Lahann, J. Recent progress with multicompartmental nanoparticles. *MRS Bull.* **Mar. 2014**, *39*, 251–257, DOI: 10.1557/mrs.2014.10.

[16] Yoon, J.; Kota, A.; Bhaskar, S.; Tuteja, A.; Lahann, J. Amphiphilic Colloidal Surfactants Based on Electrohydrodynamic Co-jetting. *ACS Appl. Mater. Interfaces* **2013**, *5*, 11281–11287, DOI: 10.1021/am403516h.

[17] Lee, K. J.; Yoon, J.; Rahmani, S.; Hwang, S.; Bhaskar, S.; Mitragotri, S.; Lahann, J. Spontaneous shape reconfigurations in multicompartmental microcylinders. *Proc. Natl. Acad. Sci. USA* **2012**, *109*, 16057–16062, DOI: 10.1073/pnas.1213669109.

[18] Park, B. J.; Brugarolas, T.; Lee, D. Janus particles at an oil-water interface. *Soft Matter* **2011**, *7*, 6413–6417, DOI: 10.1039/C1SM05460K.

[19] Nie, L.; Liu, S.; Shen, W.; Chen, D.; Jiang, M. One-Pot Synthesis of Amphiphilic Polymeric Janus Particles and Their Self-Assembly into Supermicelles with a Narrow Size Distribution. *Angew. Chem. Int. Ed. Engl.* **2007**, *46*, 6321–6324, DOI: 10.1002/anie.200700209.

[20] Hong, L.; Cacciuto, A.; Luijten, E.; Granick, S. Clusters of Charged Janus Spheres. *Nano Lett.* **2006**, *6*, 2510–2514, DOI: 10.1021/nl061857i.

[21] Ma, Y.; Cao, X.; Feng, X.; Ma, Y.; Zou, H. Fabrication of super-hydrophobic film from PMMA with intrinsic water contact angle below 90°. *Polymer* **2007**, *48*, 7455–7460, DOI: 10.1016/j.polymer.2007.10.038.

[22] Grundke, K. In *Molecular Interfacial Phenomena of Polymers and Biopolymers*, Chen, P., Ed.; Woodhead Publishing Series in Biomaterials; Woodhead Publishing: 2005, pp 323–374, DOI: 10.1533/9781845690830.2.323.

[23] Rotenberg, Y.; Boruvka, L.; Neumann, A. Determination of surface tension and contact angle from the shapes of axisymmetric fluid interfaces. *J. Colloid Interface Sci.* **1983**, *93*, 169–183, DOI: 10.1016/0021-9797(83)90396-X.

[24] Fernandez-Rodriguez, M. A.; Song, Y.; Rodríguez-Valverde, M. Á.; Chen, S.; Cabrerizo-Vilchez, M. A.; Hidalgo-Alvarez, R. Comparison of the Interfacial Activity between Homogeneous and Janus Gold Nanoparticles by Pendant Drop Tensiometry. *Langmuir* **2014**, *30*, 1799–1804, DOI: 10.1021/la404194e.

[25] Chi, L., *Nanotechnology: Volume 8: Nanostructured Surfaces*, 1st ed.; Wiley-VCH Verlag GmbH: 2010.

[26] Fernandez-Rodriguez, M. A.; Rodriguez-Valverde, M. A.; Cabrerizo-Vilchez, M.; Hidalgo-Alvarez, R. Surface activity and collective behaviour of colloidally stable Janus-like particles at the air-water interface. *Soft Matter* **2014**, *10*, 3471–3476, DOI: 10.1039/C3SM52624K.

[27] Ramos, J.; Forcada, J.; Hidalgo-Alvarez, R. Cationic Polymer Nanoparticles and Nanogels: From Synthesis to Biotechnological Applications. *Chemical Reviews* **2014**, *114*, 367–428, DOI: 10.1021/cr3002643.

[28] Garbin, V.; Crocker, J. C.; Stebe, K. J. Nanoparticles at fluid interfaces: Exploiting capping ligands to control adsorption, stability and dynamics. *J. Colloid Interface Sci.* **2012**, *387*, 1–11, DOI: 10.1016/j.jcis.2012.07.047.

From my close observation of writers they fall into two groups:
1) those who bleed copiously and visibly at any bad review, and
2) those who bleed copiously and secretly at any bad review.

Isaac Asimov

Comment on the Compression and Structure of Monolayers of Charged Latex Particles at Air/Water and Octane/Water Interfaces

M.A. Fernandez-Rodriguez[1], M.A. Rodriguez-Valverde[1], M.A. Cabrerizo-Vilchez[1], and R. Hidalgo-Alvarez[1,*]

[1] *Biocolloid and Fluid Physics Group, Applied Physics Department, Faculty of Sciences, University of Granada, 18071 Granada, Spain.*

[*] *rhidalgo@ugr.es*

In the work published by Aveyard and coworkers[1] it is proposed a model for the compression isotherm of micrometric polystyrene (PS) particles adsorbed at a water/octane interface. This model takes into account the partial screening of the electric charge of the PS particles in the water phase respect to the part submerged in the octane phase. Thus, each particle behaves like an effective dipole and the dipole-dipole interaction between particles has to be considered. The model results in Equation 6 of the cited work, reproduced in Eq. 11.1 here:

$$\Pi(x) = \frac{q^2}{2\sqrt{3}\varepsilon_{oil}R^3x^{3/2}}\left[1 - \frac{1}{(1+4\beta/x)^{1/2}} + \ln\frac{1+(1+4\beta/x)^{1/2}}{2}\right] \qquad (11.1)$$

where x is the ratio between the measured area of the water/octane interface with adsorbed PS particles and the area corresponding to the close packing of the monolayer, $\Pi(x)$ is the surface pressure at each compression state of the interface with PS particles, q is the effective charge of the dipole (the part submerged in the oil phase, not screened, and the corresponding mirror charge through the water/octane interface), ε_{oil} is the dielectric constant of the polar phase, R is the radius of the PS particles and β is a factor that takes into account the ratio between the effective length of each dipole (corresponding to a single PS particle) and the radius of the particle. Eq. 1 is written in the CGSE system. In Table 1 of the cited work, the surface charge density of the PS particles with a diameter of $(2.60 \pm 0.12)\,\mu m$ is reported to be $7.7\,\mu C/cm^2$. This results in a net electric charge of $(1.64 \pm 0.01)\cdot 10^{-12}\,C$ per particle. Furthermore, combining Eqs. A.3 and 5 from

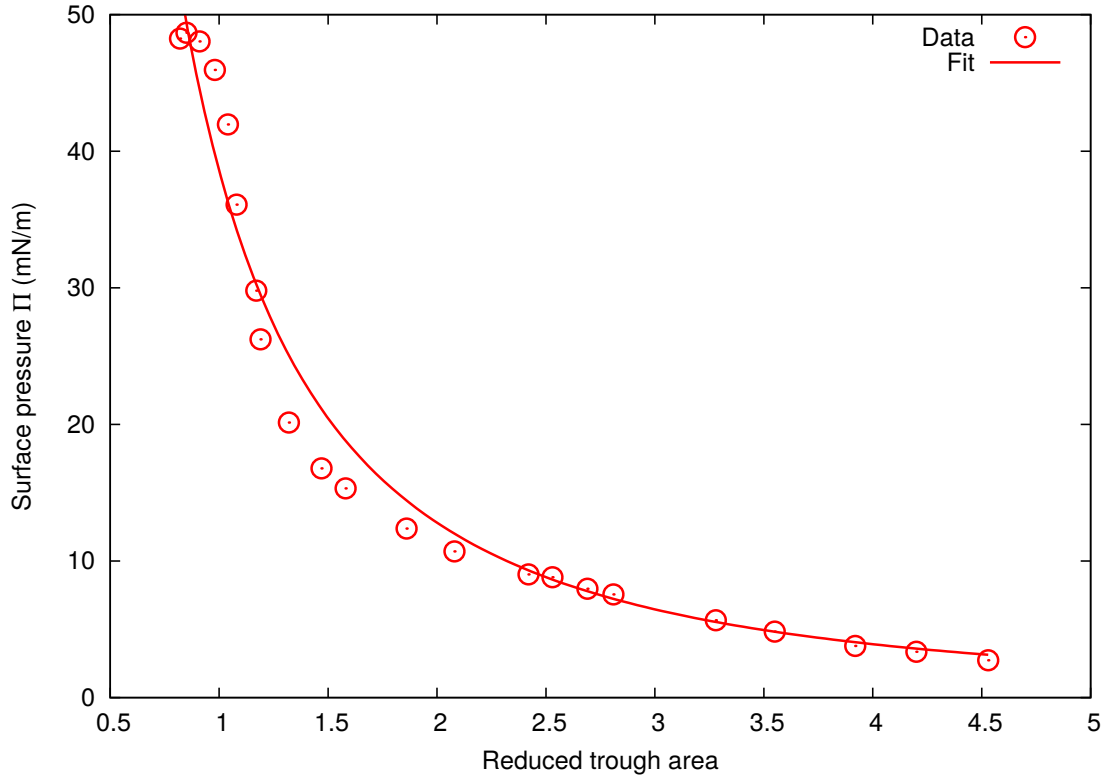

Figure 11.1: Data reproduced from Figure 16 in the R. Aveyard and coworkers work[1] of a compression isotherm of polystyrene particles ($(2.60 \pm 0.12)\,\mu m$-diameter) in a water/octane interface. The line correspond to a fit of the experimental data made using the Eq. 1.

the cited work, $\beta = (3 + cos(\theta))^2/4$, where θ is the contact angle of the particle at the water/octane interface. If we assume $\theta = 90°$ for a particle placed half in the water phase and half in the oil phase, it results in $\beta = 0.56$. We used Eq. 1 with the following input parameters: $R = 1.3 \cdot 10^{-4}\,cm$, $\varepsilon_{octane} = 2$, $\beta = 0.56$, and the CGSE to SI conversion factor: $\frac{q^2}{\varepsilon_{oil}} = \frac{q_{SI}^2}{4\pi\varepsilon_0\varepsilon_{oil}}$. Our result of the fitting of the data reported by Aveyard et al. (see Figure 16 in the cited work) is plotted in Fig. 11.1 with a particle charge of $q = (2.89 \pm 0.03) \cdot 10^{-10}\,C$.

The particle charge resulting from our fitting is two orders of magnitude higher than the net charge calculated from the value collected in Table 1 of the cited work, although it should be much lower because of the screening in the water phase and the low degree of ionization of the surface groups in the oil phase due to its low dielectric constant. In our opinion, these deficiencies should be known by the scientific community.

Acknowledgements

This work was supported by the Spanish MINECO (projects MAT2013-44429-R and MAT2014-60615R), by "Junta de Andalucía" and FEDER (projects P10-FQM-5977 and P12-FQM-1443).

References

[1] Aveyard, R.; Clint, J.; Nees, D.; Paunov, V. Compression and Structure of Monolayers of Charged Latex Particles at Air/Water and Octane/Water Interfaces. *Langmuir* **2000**, *16*, 1969–1979, DOI: 10.1021/la990887g.

IV Conclusions

One never notices what has been done; one can only see what remains to be done.

Maria Skłodowska-Curie

12 Conclusions

The term Janus particle was coined by de Gennes in 1992, since then multiple synthesis routes have been developed to create a vast collection of different Janus nanoparticles (JPs). In particular, JPs in which there is a wettability contrast between the two hemispheres of the JP have the potential to stabilize Pickering emulsions. All theoretical and simulation works point out to an improved ability of JPs to stabilize Pickering emulsions rather than the corresponding homogeneous nanoparticles (HPs). Some authors state that the desorption energy of JPs at interfaces is three times greater than for HPs. Nevertheless, there was a lack of knowledge on the characterization of the interfacial activity of JPs. Thus, in this work we have studied a collection of HPs and JPs thank to several collaborations with international research groups to try to answer the simple arising question: Are JPs better than HPs regarding the interfacial activity at water/air and water/oil interfaces? Or in other words, do JPs worth the effort of intrincate synthesis processes? We compile here the main conclusions of this work:

- The presence of surfactants hinder the role of the HPs and JPs at the interface. Thus, we studied nanoparticles without surfactants in bulk and synthesis routes in surfactant-free conditions were required.
- The pendant drop technique is a good compromise to characterize the interfacial activity of JPs from small amounts synthesized in laboratory. These samples are not enough to perform Langmuir balance experiments or emulsion characterization.
- The deposition of JPs from outside with a spreading solvent requires even lower number of JPs and the evaporation of the spreading solvent provides enough energy to place the JPs at the interface faster than the diffusion-driven adsorption of JPs from the bulk of the pendant drop.
- The pendant drop technique successfully enables to characterize the interfacial activity of nanoparticles by three ways:

1. Monitoring the direct deposition of HPs or JPs at the water/air interface with a spreading solvent from the surface tension evolution over time.
2. Building of a piecewise compression isotherm by performing cycles of growing and shrinking of the pendant drop for water/air and water/decane interfaces.
3. Interfacial dilatational rheology by periodic volume oscillations of the pendant drop, obtaining an interfacial dilatational elasticity and viscosity. This enables to characterize the collective behavior of the JPs at the interface of the pendant drop under stress conditions.

- There are multiple parameters that rule the interfacial activity of the JPs: shape, morphology and distribution of the spatial domains which confer the Janus character to the particle, spreading solvent, colloidal stability, charge and composition of the JP. In particular, the synthesis of JPs by one-pot methods lead to Janus-like nanoparticles rather than true JPs obtained by immobilization of HPs and functionalization of one side of the nanoparticle or by other synthesis routes as the Electrohydrodynamic Co-Jetting process that enables to produce nanoparticles with two halves with different polymers.

- The Freeze Fracture Shadow Casting Cryo-SEM (FreSCa cryo-SEM) technique allows to measure in a direct way the microscopic contact angle of HPs and JPs at the water/decane interface. Thus, it is possible to explore the microstructure of the nanoparticles at the water/decane interface, complementing the macroscopic interfacial activity characterization obtained by pendant drop tensiometry.

- 2 nm-diameter gold HPs functionalized by hexanethiol and dispersed in tetrahydrofurane (THF) were characterized at the water/air and water/decane interfaces. The results were in agreement with the simply scaled particle theory of hard disks.

- 3.5 nm-diameter gold HPs capped with hexanethiol and true JPs capped half with hexanethiol and half with 2-(2-mercapto-ethoxy)ethanol (MEE), both dispersed in THF, were characterized at water/air and water/decane interfaces. The HPs showed lower interfacial activity than the JPs. A hard disk model could fit the experimental results for the HPs, but it underestimated the interaction between the JPs at the interface.

- 100 nm-diameter Janus-like silver nanoparticles functionalized by 11-mercaptoundecanoic acid and 1-undecanthiol ligands and dispersed in methanol were studied at the water/air interface. They revealed a surface activity similar to the amphiphilic molecules but with much larger area per particle. We demonstrated the interplay between bulk colloidal stability and

surface activity of Janus-like particles. The interfacial dilatational rheology elasticity and viscosity depended on the lateral interactions between particles and were closely related to the monolayer microstructure. The monolayer microstructure was modeled through the Frumkin model that is an extension of the hard disk model in which the lateral interactions are included.

- The interfacial activity of PMMA-HPs (119 nm-diameter) dispersed in water, silica functionalized nanoparticles (silica-FPs) with methacryloxypropyltrimethoxysilane (181 nm-diameter) dispersed in water, and the aforementioned silver JPs (Ag-JPs) were characterized at the water/decane interface by pendant drop tensiometry and the direct contact angle (CA) was obtained by FreSCa cryo-SEM. The highest CA was obtained for the silica-FPs and Ag-JPs, and the lowest CA was obtained for the PMMA-HPs. The interfacial activity of Ag-JPs was significantly higher compared to silica-FPs and PMMA-HPs at equivalent particle concentrations. Although the silica-FPs and PMMA-HPs did not show a strong effect in reducing the water/decane interfacial tension, they were certainly adsorbed as reflected by FreSCA cryo-SEM measurements. A 100-fold higher concentration of silica-FPs and PMMA-HPs was necessary to obtain a similar reduction of the interfacial tension at the water/decane interface to the Ag-JPs. At higher concentrations, the silica-FPs exhibited fractal-like structures as a result of attractive interactions, unlike PMMA-HPs. Despite the fact that the CAs of silica-FPs and Ag-JPs were similar within errors, only the latter ones led to a significant reduction of the interfacial tension with the same surface coverage, probably as a result of its particular surface chemistry and Janus character.

- The aforementioned gold true JPs half functionalized by MEE were compared with similar JPs but functionalized by a shorter and more hydrophilic capping ligand than MEE, the 1,2-mercaptopropanediol (MPD), where both JPs were dispersed in THF. The two JPs were similar in fabrication process, hydrophobic capping ligand, wettability contrast, size and charge, but were functionalized with different hydrophilic capping ligand. The JPs-MPD exhibited a significantly higher interfacial activity at water/air and water/decane interfaces. Moreover, the interfacial dilatational rheology suggests an elastic shell-like behaviour of the pendant drop when the JPs-MPD are deposited at water/air and water/decane interfaces. This points out the importance of the chemical structure of the capping ligands in JPs to predict the interfacial activity and therefore their ability as emulsifiers. Shorter hydrocarbon chain and more hydroxyl terminal groups in the hydrophilic capping ligands seems to be a route to obtain enhanced interfacial activity of this type of JPs via enhanced hydration of the hydrophilic hemisphere of the JPs.

- The interfacial activity of gold HPs functionalized by polyethylene glycol (PEG) and JPs half covered by polystyrene (PS) and half by PEG (of 13 and 23 nm-diameter) were systematically studied by varying the spreading solvent from water to a water/chloroform ($CHCl_3$) and pure $CHCl_3$. The HPs exhibited no interfacial activity compared to the JPs, pointing out the ability of the later JPs as foam stabilizers. The better spreading agent was pure $CHCl_3$. In these conditions, the water/air interface behaved as an elastic shell which pointed out also the ability of these JPs as foam stabilizers. Finally, the interfacial activity was near zero when the pendant drops were immersed in decane, which might be due to a detachment of the nanoparticles during immersion in decane. Finally, the interfacial activity was near zero when the pendant drops were immersed in decane, which might be due to an irreversibly aggregation of the nanoparticles during immersion in decane. Thus, the roles of the polymers of the polymer shell and spreading agent are revealed to be very important when JPs with high interfacial activity in a specific interface are intended.

- Polymethylmethacrylate/Polytert-butylmethacrylate (PMMA/PtBMA) JPs and their corresponding HPs (in the range of 160-200 nm-diameter) were fabricated by Electrohydrodynamic Co-Jetting and dispersed in water. The true Janus character was demonstrated by super-resolution imaging with Structured Illumination Microscopy, in which the two domains appear separated. All nanoparticles had high positive electrophoretic mobility values. The interfacial activity was studied at the water/decane interface but there was irreproducibility due to the cationic nature of the nanoparticles. Nevertheless, as general behavior, the JPs are more interfacial active than the HPs. Moreover, the interfacial dilatational rheology showed an interfacial elastic shell.

Finally, after all these conclusions, the initial question appears to be answered: Regardless of the synthesis and characterization methods, the JPs show an enhanced interfacial activity compared to the corresponding HPs. From our point of view, the current scientific challenge is the scale-up of the synthesis processes of true Janus nanoparticles to be widely applied as emulsifiers in the industry.

List of Figures

List of Tables

Curriculum Vitae

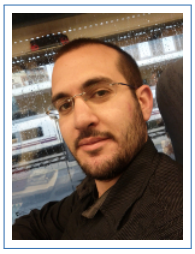

Miguel Ángel Fernández Rodríguez

Curriculum Vitae

Google Scholar Profile: tyhBrxsAAAAJ.
Orcid Profile: 0000-0002-9540-1979.
Researcher ID: J-2923-2015.

Academic Qualifications

2012-present **PhD grant in Excellence Projects 2010: Physicochemical characterization of the interfacial behaviour of Janus nanoparticles (code FQM 5977)**,
University of Granada,
Directors: Prof. Roque Hidalgo Álvarez and Prof. Miguel Ángel Rodríguez Valverde, 79644.36 €.
Award date: 1 Feb 2012.

2010-2011 **Master's degree in Colloids and Interfaces Science and Technology**, *University of Granada and Vigo*, Final evaluation: 3.000/4.
Award date: 10 Oct 2011.

2005-2010 **Bachelor's degree in Physics**, *Correspondence with Degree in Physics plus Master (level 7 of the European Qualifications Framework)*, University of Granada, Final evaluation: 2.603/4.
Award date: 9 Jul 2010.

Applied Physics Department, Faculty of Science, University of Granada
Campus de Fuentenueva s/n, 18071, Granada (Spain)
+34 619928750 • ☎ +34 958246175
FAX +34 958243214 • ✉ mafernandez@ugr.es

Grants

2013 **Short Term Scientific Mission for three months in ETH Zürich (Switzerland): *Synthesis and characterization of 2D particle arrays of Janus nanoparticles with interfacial activity***,
COST Action MP1106 under supervision of Prof. Lucio Isa,
3500 €.
From 23 Sep 2013 to 23 Dic 2013.

2009-2010 **Collaboration grant from the Ministry of Education: *Design and construction of device for Direct Laser Patterning (DLP) biochemically functionalized surfaces using self-assembled monolayers***,
University of Granada,
Director: Prof. Miguel Ángel Cabrerizo Vílchez, 2700 €.
Award date: 17 Nov 2009.

Published papers (18 citations + 5 self-citations)

2015 M.A. Fernandez-Rodriguez, L. Chen, C.P. Deming, M.A. Rodriguez-Valverde, S. Chen, M.A. Cabrerizo-Vilchez, and R. Hidalgo-Alvarez, **A simple strategy to improve the interfacial activity of true Janus gold nanoparticles: a shorter hydrophilic capping ligand**, Soft Matter, Accepted Manuscript, 2015, ISSN 1744-683X, DOI: 10.1039/C5SM01908G.

2015 M.A. Fernandez-Rodriguez, J. Ramos, L. Isa, M.A. Rodriguez-Valverde, M.A. Cabrerizo-Vilchez and R. Hidalgo-Alvarez, **Interfacial Activity and Contact Angle of Homogeneous, Functionalized, and Janus Nanoparticles at the Water/Decane Interface**, Langmuir, Volume 31, Issue 32, 2015, Pages 8818-8823, ISSN 0743-7463, DOI: 10.1016/acs.langmuir.5b02137.

2015 M.A. Fernandez-Rodriguez, M.A. Rodriguez-Valverde, M.A. Cabrerizo-Vilchez and R. Hidalgo-Alvarez, **Surface activity of Janus particles adsorbed at fluid-fluid interfaces: Theoretical and experimental aspects**, Advances in Colloid and Interface Science, In Press, 2015, ISSN 0001-8686, DOI: 10.1016/j.cis.2015.06.002.

Applied Physics Department, Faculty of Science, University of Granada
Campus de Fuentenueva s/n, 18071, Granada (Spain)
+34 619928750 • ☎ +34 958246175
FAX +34 958243214 • ✉ mafernandez@ugr.es

2014 M.A. Fernandez-Rodriguez, M.A. Rodriguez-Valverde, M.A. Cabrerizo-Vilchez and R. Hidalgo-Alvarez, **Surface activity and collective behaviour of colloidally stable Janus-like particles at the air-water interface**, Soft Matter, Volume 10, Issue 19, 2014, Pages 3471-3476, ISSN 1744-683X, DOI: 10.1039/C3SM52624K. Cited by 5.

2014 M.A. Fernandez-Rodriguez, Y. Song, M.A. Rodriguez-Valverde, S. Chen, M.A. Cabrerizo-Vilchez and R. Hidalgo-Alvarez, **Comparison of the Interfacial Activity between Homogeneous and Janus Gold Nanoparticles by Pendant Drop Tensiometry**, Langmuir, Volume 30, Issue 7, 2014, Pages 1799-1804, ISSN 0743-7463, DOI: 10.1021/la404194e. Cited by 7.

2014 M.A. Fernandez-Rodriguez, Y. Song, M.A. Rodriguez-Valverde, S. Chen, M.A. Cabrerizo-Vilchez and R. Hidalgo-Alvarez, **Interfacial Activity of AuC6 Nanoparticles Using the Pendant Drop Technique**, Journal of Colloid Science and Biotechnology, Volume 3, Number 2, 2014, Pages 184-187, ISSN 2164-9634, DOI: 10.1166/jcsb.2014.1084.

2014 M.A. Fernandez-Rodriguez, A.Y. Sanchez-Treviño, E. De Luna-Bertos, J. Ramos-Torrecillas, O. Garcia-Martinez, C. Ruiz, M.A. Rodriguez-Valverde and M.A. Cabrerizo-Vilchez, **Wettability and osteoblastic cell adhesion on ultrapolished commercially pure titanium surfaces: the role of the oxidation and pollution states**, Journal of Adhesion Science and Technology, Volume 28, Issue 12, 2014, Pages 1207-1218, ISSN 0169-4243, DOI: 10.1080/01694243.2014.893815. Cited by 2.

2014 M. Toledano, I. Cabello, M.A. Cabrerizo-Vilchez, M.A. Fernandez and R. Osorio, **Surface Microanalysis and Chemical Imaging of Early Dentin Remineralization**, Microscopy and Microanalysis, Volume 20, Issue 01, 2014, Pages 245-256, ISSN 1431-9276, DOI: 10.1017/S1431927613013639. Cited by 8.

2014 M.A. Fernandez-Rodriguez, M.A. Rodriguez-Valverde and M.A. Cabrerizo-Vilchez, **Selective desorption of organophosphonates on chemically functionalized titanium by Direct Laser Patterning**, Colloids and Surfaces A: Physicochemical and Engineering Aspects, Volume 441, 2014, Pages 899-904, ISSN 0927-7757, DOI: 10.1016/j.colsurfa.2013.02.047.

Applied Physics Department, Faculty of Science, University of Granada
Campus de Fuentenueva s/n, 18071, Granada (Spain)
+34 619928750 • ☎ +34 958246175
FAX +34 958243214 • ✉ mafernandez@ugr.es

Participation in peer-review activities

2014 Referee of Current Opinion in Colloid & Interface Science, ISSN: 1359-0294.

Participation in Research Projects

2010-2011 **Participation in excellence project reference P08-FQM-04325: *Adhesion of colloidal binders for paints***,
Contract at the University of Granada. *Selected in public call, B.O.J.A. number 125 28 June 2010 (Resolution of 2 June 2010, annex 5)*,
Duration: one year,
Project manager: Prof. Miguel Ángel Cabrerizo Vílchez,
29665.9 €.

2010-2011 **Participation in excellence project with reference P07-FQM-02517: *Complex fluids confined in curved interfaces***,
University of Granada,
Duration: one year,
Project manager: Prof. Miguel Ángel Rodríguez Valverde.

2008-2009 **Participation in the teaching innovation project with reference 08-222: *The ten most beautiful experiments in Physics. Laboratory of scientific outreach***,
University of Granada,
Duration: one year,
Project manager: Prof. Miguel Ángel Cabrerizo Vílchez.

Teaching

2015 **Teacher in "Numeric Methods", course of Physics Grade, 6 ECTS**,
University of Granada.

2015 **Summer National Scientific Campus 2015, 50h**,
University of Granada.

2015 **Introduction to 3D printing with Blender. "Course of modelling and animation 3D in Blender (5^{th} edition)", 3h (of 5.2 ECTS)**,
University of Granada.

Applied Physics Department, Faculty of Science, University of Granada
Campus de Fuentenueva s/n, 18071, Granada (Spain)
+34 619928750 • ☎ +34 958246175
FAX +34 958243214 • ✉ mafernandez@ugr.es

2014 **Teacher in "Numeric Methods", course of Physics Grade, 4.8 ECTS**,
University of Granada.

2014 **Teacher in "Thermodynamics Laboratory", course of Physics Grade, 1.2 ECTS**,
University of Granada.

2014 **Introduction to 3D printing with Blender. "Advanced course of modelling and 3D animation with Blender oriented to teaching", 2h**,
University of Granada.

2014 **Introduction to 3D printing with Blender. "Image and 3D printing applied to sculpture and sculptural restoration", 12h**,
University of Granada.

2014 **Summer National Scientific Campus 2014, 50h**,
University of Granada.

2014 **Introduction to 3D printing with Blender. "Course of modelling and animation 3D in Blender (4^{th} edition)", 2h (of 5.2 ECTS)**,
University of Granada.

2014 **Introduction to Linux course, 10h**,
University of Granada.

2013 **Linux course, 20h**,
University of Granada.

2013 **Interfacial phenomena in the operation of oilfields course (Third edition)**,
University of Granada and INTEVEP, S.A.

2013 **Permanent class of open education: Physics for Entertaiment (Second edition), 5h**,
University of Granada.

2012 **Permanent class of open education: Physics for Entertaiment (First edition), 4h**,
University of Granada.

Applied Physics Department, Faculty of Science, University of Granada
Campus de Fuentenueva s/n, 18071, Granada (Spain)
+34 619928750 • ☎ +34 958246175
FAX +34 958243214 • ✉ mafernandez@ugr.es

Participation in international advanced schools

2015 ***46th IFF Spring School "Functional Soft Matter".***,
Jülich (Germany).

2014 **COST Actions MP1106 & CM1101 Joint Training School: *Particles at liquid interfaces. Fundamental and Applications***,
Bonassola (Italy).

Participation in conferences

2015 ***Smart and green interfaces: Fundamentals and diagnostics (SGI-FunD).*** **Enhanced interfacial activity of Janus gold nanoparticles with shorter hydrophilic capping ligand**,
Sofia (Bulgaria),
Oral presentation.

2015 ***6th International Workshop on Bubble and Drop Interfaces.*** **Interfacial activity and contact angle study of PMMA homogeneous, silica functionalized and silver Janus nanoparticles at the water/decane interface**,
Postdam-Berlin (Germany),
Oral presentation.

2014 ***XIV Inter-Biennial meeting of the Specialized Group of Thermodynamic.*** **Surface activity and collective behaviour of Janus particles at liquid interfaces**,
Vigo (Spain),
Oral presentation (presented by Prof. R. Hidalgo-Alvarez), ISBN: 9788481586527.

2014 ***XXIV Sitges Conference on Statistical Mechanics.*** **Surface activity and collective behaviour of Janus particles at liquid interfaces**,
Barcelona (Spain),
Plenary presentation (presented by Prof. R. Hidalgo-Alvarez).

2014 ***2nd Colloids and Interfaces Young Researchers Meeting.*** **Direct measurement of the contact angle of nanoparticles at the water/decane interface by FreSCa cryo-SEM technique**,
Granada (Spain),
Oral presentation, ISBN: 9788415814863.

Applied Physics Department, Faculty of Science, University of Granada
Campus de Fuentenueva s/n, 18071, Granada (Spain)
+34 619928750 • ☎ +34 958246175
FAX +34 958243214 • ✉ mafernandez@ugr.es

2014 ***10^{th} European Adhesion Conference.*** **Chemical Patterning of Commercially Pure Titanium Surfaces based on Organophosphonates**,
Alicante (Spain),
Oral presentation (presented by Prof. M.A. Cabrerizo-Vilchez).

2014 ***2014 Annual Meeting of the Adhesion Society.*** **Chemical Patterning of Commercially Pure Titanium Surfaces based on Organophosphonates**,
San Diego, California (USA),
Oral presentation (presented by Prof. M.A. Cabrerizo-Vilchez).

2013 ***Swiss Soft Days 2013.*** **Interfacial activity of colloidally stable Janus-like silver nanoparticles by pendant drop tensiometry and direct deposition**,
Bern (Switzerland),
Poster.

2013 ***European Society for Biomaterials 2013.*** **Chemical Patterning of Commercially Pure Titanium Surfaces based on Organophosphonates**,
Madrid (Spain),
Oral presentation (presented by Prof. M.A. Cabrerizo-Vilchez).

2013 ***European Society for Biomaterials 2013.*** **In-Situ Monitoring of Biomimetic Hydroxyapatite Growth on Functionalized Titanium Surfaces: An AFM Study**,
Madrid (Spain),
Poster (presented by A.Y. Sanchez-Treviño).

2013 ***COST Action MP1106 Workshop: Multiphase flows with/without phase change.*** **Pendant drop technique for the characterization of homogeneous and Janus gold 2-nm nanoparticles**,
Zaragoza (Spain),
Oral presentation (presented by Prof. M.A. Cabrerizo-Vilchez).

2013 ***International Soft Matter.*** **Interfacial activity of Janus-like silver nanoparticles**,
Rome (Italy),
Poster.

Applied Physics Department, Faculty of Science, University of Granada
Campus de Fuentenueva s/n, 18071, Granada (Spain)
+34 619928750 • ☎ +34 958246175
FAX +34 958243214 • ✉ mafernandez@ugr.es

2013 ***5th Iberian Meeting in Colloids and Interfaces.*** **Interfacial activity comparison between bare, homogeneous and Janus gold nanoparticles**,
San Sebastián (Spain),
Oral presentation.

2013 ***2013 Annual Meeting of the Adhesion Society.*** **Chemical patterning of smooth titanium surfaces**,
Daytona Beach, Florida (USA),
Oral presentation (presented by Prof. M.A. Cabrerizo-Vilchez, ISBN: 9781627481373).

2012 ***First meeting of Colloids and Interfaces young researchers.*** **Janus gold nanoparticles with interfacial activity**,
Benidorm (Spain),
Oral presentation.

2012 ***Jülich Soft Matter Days 2012.*** **Janus particles with interfacial activity**,
Bad Honnef (Germany),
Poster.

2012 ***Second Workshop on Advances in Colloidal Materials.*** **Janus Particles with Interfacial Activity**,
University of Granada (Spain),
Poster and Oral presentation.

2012 ***5th International Workshop Bubble and Drop Interfaces B&D 2012.*** **How to stabilize the wettability response of titanium surfaces for bioadhesive applications?**,
University of Krakow (Poland),
Oral presentation (presented by Prof. M.A. Cabrerizo-Vilchez, ISBN: 978-83-60514-16-0).

2011 ***Biocolloid and Fluid Physics Group 25th Anniversary: 1986-2011.*** **Direct Laser Patterning on smooth titanium surfaces: application for biomaterials**,
University of Granada (Spain),
Poster (ISBN: 978-84-338-5324-0).

Applied Physics Department, Faculty of Science, University of Granada
Campus de Fuentenueva s/n, 18071, Granada (Spain)
+34 619928750 • ☎ +34 958246175
FAX +34 958243214 • ✉ mafernandez@ugr.es

2011 ***4th Iberian Meeting on Colloids and Interfaces 2010.*** **Characterization of finely polished titanium: a wettability study**,
University of Oporto (Portugal),
Poster (ISBN: 978-989-97397-0-3) and Proceeding (ISBN: 978-989-97397-2-7).

2010 ***International Soft Matter 2010***,
University of Granada (Spain),
Attendee.

Participation in Public Engagement and outreach events

2015 **European Researchers' Night (H2020-MSCA-NIGHT 2015)**,
University of Granada.

2015 **Workshop: "Recreative Physics IV and V." Open doors day.**,
Granada Science Park.

2014 **Public workshop: "Tapas with Science 2."**,
Organized by the Association of Young Researchers of Granada..

2014 **Public workshop: "Tapas with Science."**,
Organized by the Association of Young Researchers of Granada..

2014 **Talk: "The movement of young researchers."**,
Excellence International Bio Tic Campus (University of Granada).

2013 **Workshop: "Recreative Physics: Laboratory of the ten most beautiful experiments in Physics." Open doors day.**,
Granada Science Park.

2012 **European Researchers' Night, ID 316618 (FP7-PEOPLE-2012-NIGHT)**,
University of Granada.

2010 **Science fair in Lorca: *Expostudy***,
Teaching and resources centre in Lorca.

2009 **Science fair in Salamanca**,
Organizing professor: M.A. Cabrerizo-Vilchez (XXL Physics).

2009 **Science fair in Miranda de Ebro**,
Organizing professor: M.A. Cabrerizo-Vilchez (XXL Physics).

Applied Physics Department, Faculty of Science, University of Granada
Campus de Fuentenueva s/n, 18071, Granada (Spain)
+34 619928750 • ☎ +34 958246175
FAX +34 958243214 • ✉ mafernandez@ugr.es

2009 **Open day at the Granada Science Park**,
Organizing professor: M.A. Cabrerizo-Vilchez (XXL Physics).

2008 **The ten most beautiful experiments in Physics: *VIII Science week***,
Faculty of Sciences, University of Granada.

2008 **Madrid x science**,
Organizing professor: M.A. Cabrerizo-Vilchez (XXL Physics).

2008 **Open day at the Granada Science Park**,
Organizing professor: M.A. Cabrerizo-Vilchez (XXL Physics).

2008 **Science fair in Lorca: *Students fair***,
Teaching and resources centre in Lorca.

2007 **Science fair in Sevilla**,
Organizing professor: M.A. Cabrerizo-Vilchez (XXL Physics).

2007 **Madrid x science**,
Organizing professor: M.A. Cabrerizo-Vilchez (XXL Physics).

2007 **Open day at the Granada Science Park**,
Organizing professor: M.A. Cabrerizo-Vilchez (XXL Physics).

2006 **Science Fair in Sevilla 2006**,
Organizing professor: M.A. Cabrerizo-Vilchez (XXL Physics).

2006 **Open day at the Granada Science Park**,
Organizing professor: M.A. Cabrerizo-Vilchez (XXL Physics).

2006 **Science fair in Lorca: *Students fair***,
Teaching and resources centre in Lorca.

Commitment to European Research Policies

March 2014 - Now **President of the Association of Young Researchers of Granada**,
Spain. Member of the Federation of Young Researchers/Precarious.

Feb 2012 - Dec 2013 **Spokesperson of the Federation of Young Researchers/Precarious**,
Spain. Member of The European Council of Doctoral Candidates and Junior Researchers (Eurodoc).

Useful skills

2013 **Construction of an open-source 3D printer model Prusa i2**,
Founding partner of www.granadaimprusa.org.

Applied Physics Department, Faculty of Science, University of Granada
Campus de Fuentenueva s/n, 18071, Granada (Spain)
+34 619928750 • ☎ +34 958246175
FAX +34 958243214 • ✉ mafernandez@ugr.es

2013 **Advanced Arduino course**,
Darwin Eventur (University of Granada).

2012 **PhD course: learning to innovate**,
University of Granada.

In the research work developed at the Surfaces and Interfaces laboratory in the University of Granada, University of Malaga and ETH-Zurich, I have worked with several techniques:

- Direct Laser Patterning that enables the design of topographically and chemically patterned surfaces.
- Confocal microscopy to obtain topographical profiles up to 0.1 μm feature size.
- Synthesis of self-assembled monolayers on metalic surfaces.
- Atomic force microscopy to obtain topgraphical profiles at nanometric scale.
- Contact angle and hysteresis measurements by ADSA-P and ADSA-D (*Axysimmetric Drop Shape Analysis Profile and Diameter*) of drops and captive bubbles.
- Contact angle and hysteresis measurements by *tilting* technique.
- Most stable contact angle measure by vibrated drop technique.
- Flow potential measurements with an Anton Paar device.
- Gas ashing/etching RF plasma device.
- Pendant drop tensiometer and rheology measurements.
- Self Assembly and deposition of nanoparticles at liquid-liquid interfaces in a Langmuir trough.
- Gold layer plasma sputtering.
- Gold quantum dots fabrication.

Languages

English **Upper-intermediate level. Currently studying advanced level**.

Software skills

Operative systems: Linux

Text editors: Libreoffice, Latex

Science software: Gnuplot, Octave, Maxima, Origin

Programming languages: c, c++, Fortran

Applied Physics Department, Faculty of Science, University of Granada
Campus de Fuentenueva s/n, 18071, Granada (Spain)
+34 619928750 • ☎ +34 958246175
FAX +34 958243214 • ✉ mafernandez@ugr.es